Kode Technology Modification of Nanofibres to Capture Particulates

Ankita Poudyal

2019

Centre for Kode Technology Innovation
School of Engineering, Mathematical and Computer Sciences
Faculty of Design & Creative Technologies
Auckland University of Technology

A thesis submitted to Auckland University of Technology
in fulfilment of the requirements for the degree of Doctor of Philosophy

Abstract

With the continual rise in the levels of urban and industrial pollution, there is increased contamination of air and water by small particulate matter. Most of the current filtration methods can capture such particles by trapping through size exclusion, that is by filtration through membranes, which have pores smaller than the particles. This approach is problematic because small pore dimensions block flow. If particles could be captured by surfaces with larger pores, it would be possible to achieve a membrane that could remove pollutants and have a good flow characteristic at the same time. Attempts to make such activated capture membranes have been done earlier but are limited. Nanofibre mats made up of fibres less than 1000 nanometres in diameter are one of the extensively used advanced materials for air and water filtration. However, surface functionalization of nanofibres is complicated. Most procedures are complex involving multiple steps that can damage surfaces.

Kode Technology is a surface engineering technology that has the potential to modify membranes in a single step without significantly changing the structure of the surface. The extension of this technology to modify nanofibre surfaces could potentially create high-efficiency filters capable of capturing air and water particulates with minimal compromise in flow characteristics. The main aim of this research was to establish whether coating nanofibres with Kode constructs could enhance the adsorption and filtration of air and water particles. The research included a study of the modification mechanism, comparison of various functional heads and construct designs, limitations and extension to capture cells such as red cells and bacteria. A variety of Kode constructs were applied to nanofibres made from various polymers. For water particle capture, in-house synthesised silver nanoparticles were used as surrogates of pollutants. UV-Vis spectroscopy was used as a main quantitative tool and SEM, EDS and FTIR were used for qualitative analysis. For air particle capture, aerosols were generated using sources such as diesel combustion, wood-burning and incense combustion. Laser particle counters were used for quantification and size distribution analysis and were further analysed by SEM and EDS for morphological and chemical signatures. Additionally, modification of nanofibres was studied by applying Kode constructs during fabrication (electrospinning) and after electrospinning.

It was observed that surface modification of nanofibres by Kode constructs can significantly enhance the adsorption and filtration efficiencies of nanofibres and that the technology has the potential to be utilised for the capture of nanoparticles as compared to aerosols. After the successful coating and capture of air and water particles, the research was proof-of-concept, extended to capture biological particles such as microbes and RBCs. The conclusions from this research are that Kode Technology has the potential to be used for actively capturing pollutants and other contaminants.

Table of Contents

List of Tables

List of Figures

List of Abbreviations

[-]Agnp	Negatively charged silver nanoparticles
[+]Agnp	Positively charged silver nanoparticles
Ad	Adipate, $-CO(CH_2)_4CO-$
AE	Adsorption Efficiency
CA	Contact Angle
CMG	Carboxymethylglycine, an oligomer of $-[N(CH_2COOH)CH_2CO-Gly-Gly]-$
CV	Crystal Violet
DLS	Dynamic Light Scattering
DOPE	Dioleoylphosphatidylethanolamine
EDS	Electron Dispersive X-ray Spectroscopy
EIA	Enzyme Immuno-Assay
FE	Filtration Efficiency
FSL	Function-Spacer-Lipid (Kode Technology construct)
FTIR	Fourier Transformed Infra-red Spectroscopy
MOF	Metallic Organic Framework
PAH	Polycyclic Aromatic Hydrocarbons
PAN	Polyacrylonitrile
PCL	Polycaprolactone
PEI	Polyethyleneimine
PMMA	Poly (Methyl Methacrylate)
PVB	Poly Vinyl Butyrate
PVP	Polyvinylpyrrolidone
RBC	Red Blood Cells
RE	Rare Earth
RT	Room Temperature
SEM	Scanning Electron Microscopy
TLC	Thin Layer Chromatography
TPU	Thermoplastic Polyurethane
VOC	Volatile Organic Compounds

Attestation of Authorship

"I hereby declare that this submission is my own work and that, to the best of my knowledge and belief, it contains no material previously published or written by another person (except where explicitly defined by acknowledgement), nor material which to a substantial extent has been submitted for the award of any other degree or diploma of a university or other institution of higher learning."

Ankita Poudyal

Auckland

2019

Intellectual Property Rights

Intellectual property rights comprising all aspects of the projects reported in this thesis belong to Kode Biotech Limited and shall not be passed on to a third party without explicit approval in writing from Kode Biotech Limited (www.kodebiotech.com).

Acknowledgments

Chapter 1: Introduction

Pollutant particles are diverse in size, ranging from large to nanoscale, which means that conventional filtration membranes which use size-exclusion must have small pores to capture most pollutant particles. However, small pores cause a high constriction in airflow. What is needed are membrane that are able to capture nanoparticle pollutants and have high air-flow characteristics and this can be potentially achieved using modified membranes with large pores that actively capture pollutants. This research focuses on this mechanism by modifying the surface of nanofibre membrane (with large pores) so that the modified membranes actively capture nanoparticles while maintaining high flow through characteristics. Because traditional surface functionalisation techniques are complicated and use harsh chemicals, this study explored the use of Kode Technology to modify nanofibres to capture pollutants. The approach taken was to use charged Kode constructs applied on surface as a thin-film coating and measure their ability to capture charged particles. Charged nanoparticles were synthesised as pollution surrogates because in contrast to the various air pollutants generated using combustion methods, the performance of the modified membranes to capture charged nanoparticles could be validated and characterised. A high level of capture of nanoparticles and combustion generated particles was achieved using Kode-modified nanofibres. The conclusions of this thesis were positive and can be used as a basis to explore more varieties of Kode constructs to capture a wider range of environmental pollutants including toxic gases and viruses.

1.1   Nanofibres

Nanofibres are defined as fibres with diameters less than 1000 nanometres. Diameters of 50-500 nanometres are typical for most nanofibres [1]. They are notable for their characteristic features such as large surface-area-to-volume ratio, extremely small pore dimensions and superior mechanical properties. Due to these features, nanofibres have a wide range of applications in areas such as high-performance filtration, battery separators, wound dressing, vascular grafts, enzyme immobilisation, electrochemical sensing, composite materials, reinforcements, blood vessel engineering and tissue engineering [2]. A comparison of a nanofibre mat with a single strand of human hair and a pollen grain is shown in Figure 1.
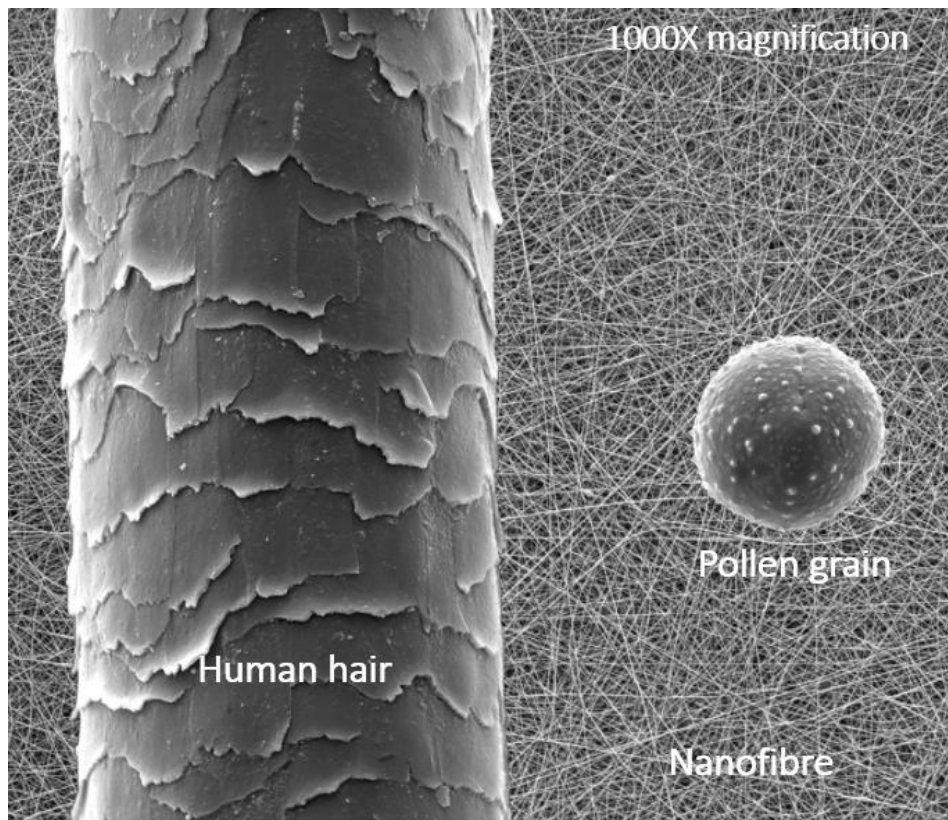
Figure 1: Comparison of nanofibre with pollen grain and a single strand of human hair [3].

Several methods are used to fabricate nanofibres such as self-assembly, phase separation, template-based methods and electrospinning. In most of these processes, the fibres are collected as nonwoven random fibre mats known as nanowebs, consisting of fibres having diameters from several nanometers to hundreds of nanometers [4].

Different methods for fabrication are described below:

1) Self-assembly
2) Phase separation
3) Template method
4) Electrospinning

1.1.1 Self-assembly method

Self-assembly is a bottom-up technique where individual molecules arrange themselves in certain patterns to form, for instance, macromolecular nanofibres. Several intermolecular forces and the structure of smaller units determines the shape of nanofibres. The building blocks of nanofibres can assemble into ordered structures such as superlattices, monolayers, honeycomb or tubes. The self-assembly method is used in

nano-structuring and nano-fabrication because of its simplicity, versatility, spontaneity, low cost and high yielding [5].

The self-assembly process involves various driving forces such as electrostatic force, hydrogen bonding, hydrophobic interactions, pi (π) interactions, π–π interactions and van der Waals force. Additionally, it can also be affected by different conditions such as pH and ionic strength [6]. Self-assembly requires the components to be mobile and often the building block molecules in the fluid carrier medium move randomly under Brownian motion. Therefore, there is less precise control over the transport and contact of the building blocks on the molecular scale. In attempts to achieve control, the solution of building blocks is often agitated with changes in temperature and viscosity [7].

The self-assembly process is most commonly used to generate peptide nanofibres and peptide amphiphiles. Specific peptide amphiphiles can self-assemble into nanostructure under certain physiological conditions. The resultant structures are highly bioactive and used for biomedical applications such as tissue engineering, regenerative medicine and drug delivery [8].

1.1.2 Phase separation method

In the phase separation method, the nanofibres are formed due to the instability of the polymer within the solvent. Two different phases are formed due to physical inconsistency of the components used and nano-matrices form by precipitation of polymer-poor phase and polymer-rich phase [9]. Important steps involved in this technique are polymer dissolution, gelation, solvent extraction, freezing and freeze-drying. Firstly, the polymer is dissolved in solution and the phase separation is induced, either thermally or through the addition of a non-solvent to the polymer solution, to create a gel. The polymer solution under this condition becomes thermodynamically unstable and tends to separate into two phases. Water is then used to extract the solvent from the gel. The polymer-rich phase then solidifies on reducing the temperature to a 3-D microporous structure. The process of a general phase separation method for fabrication of nanofibres is shown in Figure 2. The advantage of this method is that it does not require specialized equipment with consistency in batches. Moreover, constructs can be produced in a mould to achieve a specific geometry. However, this method is effective with only a select number of polymers and with a low yield [10].
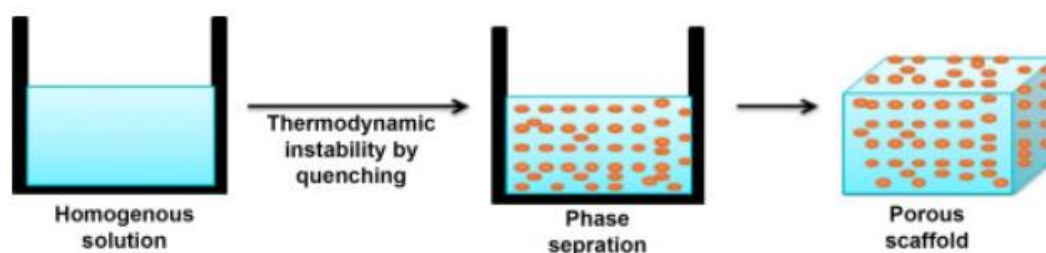
Figure 2: Process of phase separation for the fabrication of nanofibres [11]. The thermodynamic instability of the homogenous solution can be introduced either thermally or by addition of a non-solvent.

Various polymers have been used to fabricate nanofibres using phase separation. Among the various scaffold fabrication techniques, thermally induced phase separation (TIPS) is one of the most versatile methods to produce porous polymeric scaffold and it has been largely used for its capability to produce highly porous and interconnected nanofibre membranes [12]. Polymers such as poly-L-lactide acid (PLLA), poly-lactic-co-glycolic acid (PLGA), and poly-DL-lactic acid (PDLLA) can form fibre diameters from 50–500 nm, and porosities up to 98.5% [13]. PLLA is a widely used biodegradable scaffolding material. A series of biodegradable amphiphilic poly(hydroxyalkyl(meth)acrylate)-graft-poly(L-lactic acid) (PHAA-g-PLLA) copolymers have been synthesised and fabricated into nano-fibrous scaffolds using thermally induced phase separation. For example, PLLA-based macromonomers were first prepared using functional hydroxyalkyl (meth)acrylates (HAA). The PHAA-g-PLLA copolymers were then synthesised using free-radical copolymerization of PLLA-based macromonomers and HAA [14]. The resulting nanofibrous scaffold showed great potential to be applied for biomedical applications. Recently, fabrication of chitosan membranes was done by low temperature-induced phase separation that produced very thin nanofibres in the range of 40-60 nm [15]. In the research work, phase separation was used to overcome the shortcomings of other methods such as electrospinning and freeze-drying that required the use of organic acids such as concentrated acetic acid or trifluoroacetic acid to fabricate chitosan. Such solvents are highly corrosive, toxic and have an unpleasant odour. The resultant fibres demonstrated high adsorption of copper ions with possibility to be applied for heavy metal removal.

1.1.3   Template-based method

In template-based synthesis, firstly a nanostructured ceramic or polymeric membrane is prepared to serve as the template. Then the targeting material is added in contact with

the nanostructure to form nanofibres and finally, the template is removed to leave free nanofibres. The other fabrication methods are generally dependent on low-temperature chemical or physical processes. Therefore, the template-based technique can be a good alternative to fabricate nanofibres without the dependency on temperature. Templates can be derived from synthetic as well as natural substances and based on the structure of the template, the process can be divided into hard and soft template methods [16].

Anodized aluminium oxide (AAO) is a popular ceramic hard template that has been widely used [16,17]. Anodic aluminium oxide (AAO) template is fabricated by aluminium anodizing in given electrolytes (oxalic, sulphuric or phosphoric acid) solution. It has a hexagonally ordered pore array that is considered ideal for fabrication. However, it is limited by the difficulty to monitor the pore size [18].

Soft templates do not have rigid structures. Surfactants, polymers and biopolymers are some commonly used soft templates. It is mainly based on the micellar action that can form organic and inorganic templates during the reactions and is comparatively easier to build and remove. Polyaniline (PANI) nanostructures were obtained by oxidative polymerization in the presence of sucrose octaacetate as a soft template, and ammonium peroxydisulfate (APS) acting as an oxidizing agent [19]. The resultant nanofibre showed more thermal stability and electrical conductivity due to its higher crystallinity and highly ordered structure. The use of zinc oxide as a soft template to synthesise PANI nanofibres to make gas sensors was also reported [20]. The results showed that the fabricated fibres had a significant enhancement in sensing of ammonia gas at room temperature and was least affected by humidity.

1.1.4 Electrospinning

Electrospinning is the most commonly used method to fabricate nanofibres because of its simplicity and suitability for a variety of polymers and ceramics [21,22]. In comparison to conventional methods, it has advantages of low cost, more capability, and high speed. In the electrospinning process, a polymer solution held by its surface tension at the end of a capillary tube is subjected to an electric field. A charge is induced on the liquid surface by an electric field. Mutual charge repulsion causes a force directly opposite to the surface tension. As the intensity of the electric field is increased, the hemispherical surface of the solution at the tip of the capillary tube elongates to form a conical shape known as the Taylor cone [23]. When the electric field reaches a critical value at which the

repulsive electric force overcomes the surface tension force, a charged jet of the solution is ejected from the tip of the Taylor cone. Since this jet is charged, its trajectory can be controlled by an electric field. As the jet travels in air, the solvent evaporates, leaving behind a charged polymer fibre, which lays itself randomly on a collecting metal screen. Thus, continuous fibres are laid to form a non-woven fabric. Figure 3 illustrates the electrospinning process.
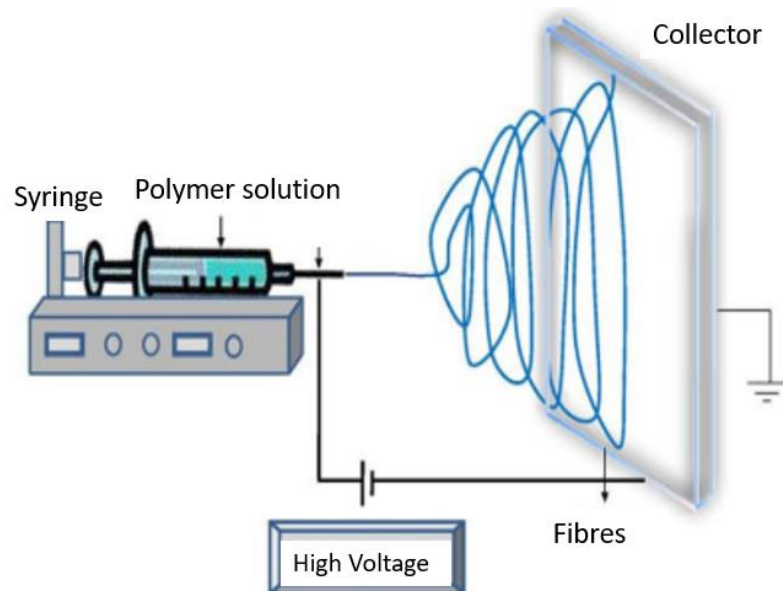
Figure 3: Process of electrospinning [24]. A charge is induced on a polymer solution using a high voltage and a jet of polymer is ejected as fibres.

The parameters affecting the process can be described as solution properties including viscosity, conductivity, and surface tension; controlled variables including hydrostatic pressure in the capillary, electric potential at the tip, and the distance between the tip and the collection screen; and ambient parameters including temperature, humidity, and air velocity in the electrospinning chamber [23].

Electrospun nanofibres can have various applications. Research on biomedical applications has focused on (i) the generation of fibrous scaffolds for tissue engineering, (ii) wound dressing, (iii) drug delivery mechanisms and (iv) enzyme immobilisation to achieve faster reaction rates in biological reactions [25,26]. In addition to biomedical applications, they have been widely studied as a potential filter material in the environmental protection field [27]. The properties of some commonly used polymer types for nanofibres fabrication and their uses in filtration are discussed in the following section.

PCL (Polycaprolactone)

PCL is generally used for low-temperature filtration [28]. It has a low melting point of 60°C and is cohesive. The main benefits of PCL are its biodegradability and insolubility so that it can be used for both filtration and biomedical applications.

PA66 (Nylon 6, 6)

PA66 is generally used for high-temperature air and liquid filtration because it has a high melting point of around 248-258°C and is extremely cohesive [29]. It is insoluble in water due to which it can achieve a high filtration efficiency with relatively low depositions.

PMMA (Poly Methyl Methacrylate)

PMMA is used for high flow air and liquid filtration. It is readily scalable and is insoluble in water making it applicable for air and water filtration. It is more suitable for low-pressure applications such as antipollution facemasks that require maximum breathability. The main limitation is its relatively low durability [30].

PVOH (Polyvinyl Alcohol)

PVOH is commonly used for both air and water filtration but is generally cross-linked with other polymers [31]. It is cohesive in nature and melts at 200°C. It is soluble in water and thus proposes a challenge in filtration scale up, as suitability for filtration is limited to dry and non-humid air. However, it can be readily cross-linked by maleic acid and sulphuric acid as catalyst [32].

PEO (Polyethylene Oxide)

PEO is also used for low-temperature air filtration [30]. It is slightly lofty and melts at 65°C. It is also soluble in water, which means its usage, and scalability is limited. It is commonly used in combination with other polymers.

PVDF (Polyvinylidene fluoride)

PVDF is an extremely cohesive polymer and it melts at 177°C. The PEO electrospun nanofibres are scalable and commonly utilised as water filters due to their insolubility, inertness and porosity. It can also be used with corrosive solutions and in relatively high temperatures [33].

7

TPU (Thermoplastic Polyurethane)

TPU is highly elastic and the melting temperature ranges from 55°C to 220°C. It is currently used in some commercial facemasks. However, it requires the use of toxic solvents for electrospinning. Therefore, it is hard to produce the polymer on an industrial scale. TPU has a moderate pressure drop and is extremely elastic and durable. The limitation of TPU includes its unsuitability in high-pressure applications due to air/liquid overcoming the elastic forces that result in an increase of pore size [33,34].

PVAc (Polyvinyl Acetate)

PVAc is generally used for low-temperature air filtration due to its low melting temperature of 60°C. It is often used in combination with other polymers for nanofibre fabrication [35].

PES (Polyethersulfone)

PES has a melting temperature of 220°C and is slightly resilient in nature. It is effective for high-temperature filtration and is resistant to most of the solvents [36].

PAN (Polyacrylonitrile)

PAN is highly cohesive and has a melting temperature of greater than 300°C, which makes it very suitable for high-temperature air and liquid filtration. The fabrication of PAN nanofibres is highly scalable. It is commonly used within membrane filters for biomedical purifications [37,38].

1.2 Polymer surface modification techniques

Polymers have diverse applications in areas such as adhesion, printing, food packaging, membrane separations and ion exchange including medical uses such as cell culture, biosensors, diagnostic assays, drug delivery and many more [39]. Synthetic polymers can be designed and fabricated to have suitable mechanical properties and functionalities. Some materials have excellent bulk chemical and physical properties. However, they do not have suitable surface properties required for specific applications.

Surface modification or functionalisation is a technique that can be used to introduce modifying agents on polymer surfaces to enhance their surface properties or specificity towards a desired molecule [40]. They are usually modified to increase or decrease hydrophilicity, ionic charge, adsorption, roughness, and other electrical and optical

properties. A well-engineered surface modification process allows for optimizing functionality, chemical interactions with ligands and biocompatibility without changing the mechanical features of polymers [41].

Generally, there are three ways to modify a surface: remove material from the surface, add material to the surface or change the material of the surface. As reviewed in Ratner's paper [41], the main considerations for choosing a modification technique are surface chemistry, structure and chemical properties of modifying agent and the ability of the modifying agents to remain denatured. Reproducibility, cost and difficulty of the immobilisation process also need to be considered.

As reviewed by various authors [26,42,43], depending on the nature of modification techniques, they can be broadly categorized into the following.

a) Pre-treatment by physiochemical methods

b) Modification by immobilisation of molecule

1.2.1 Pre-treatment by physicochemical methods

Physicochemical treatment of surface constitutes treatment using active gases, vapours or radiation or solution treatments to improve the surface properties. It is usually done prior to modification by immobilising active agents [41]. It provides active sites on the otherwise inactive surface by introducing functional groups, chemically reactive ions or free radicals. It is commonly done to achieve improved hydrophilicity and adhesion [44]. Physical treatments include active gas treatments such as ion beam, corona discharge, crosslinking surface molecules by ionising radiation, UV, radio-frequency gas discharge (RFGD) etching, etc. Solution or chemical treatments include polymer coatings and oxidization, sulfonation, chlorination, acetylation and salination using various reagents. Similar treatment protocols have been used for nanofibre modification. However, some common techniques are listed below.

Plasma treatment

Plasma treatment improves the wettability and adhesion by introducing polar groups on the nanofibre surface. It can be done using air or typical gases including hydrogen or other gases such as nitrogen and oxygen that produce functional groups such as carbonyl ($>C=O$), carboxyl ($-COOH$), hydroxyl ($-OH$), hydroperoxides ($HOO-$), and amines ($-NH_2$) that depend on the nature of plasma. Such functional groups are crucial for the further

physisorption and chemical interaction of active molecules [45]. Plasma treatment based on non-thermal methods is a convenient and cost-effective way to tailor the surface properties of polymers such as PCL [46]. PCL is a polymer that has good chemical stability and is biocompatible which makes it usable for applications such as tissue generation and particulate filtrations. However, it lacks adhesion due to high hydrophobicity. Polymers such as chitosan, gelatin and collagen are blended with PCL to improve wettability but it deteriorates the excellent mechanical properties of PCL. Poly(methyl methacrylate) (PMMA) electrospun fibres have also been treated with O_2 plasma to introduce polar functional groups such as hydroxyl and carboxylic acid groups, resulting in improved hydrophilicity [47]. The advantage of plasma treatment is that it serves the purpose without significant change in the scaffold morphology and mechanical properties. However, the requirement of a vacuum system is a major disadvantage of this method as it increases the cost of operation.

UV treatment

It provides similar effects of plasma but the process is dependent on the UV absorption coefficients of surfaces at specific wavelengths. Therefore, it is limited in the number of surfaces it can be used to modify. However, UV treatment can process wide areas as well as small spots, unlike plasma treatments. Nanofibres treated with UV have been proved to achieve change in polarity, chemistry, charge, roughness and morphology of nanofibres [48]. UV irradiation in the presence of a reactive gas has also been mentioned by a study [49]. The enhancement of adhesion of surfaces induced by UV irradiation has been reported in many studies [50,51].

Surface graft polymerization

Surface graft polymerization is a chemical modification method where the modification is achieved by grafting monomer on the surface of materials. The key advantage of these techniques is that the surface of the materials can be modified uniquely with different grafting monomers while maintaining the intrinsic properties [52]. As reviewed in the paper, this technique is easy and more stable due to the strong attachment of graft to the surface. It also offers controlled introduction of grafts with high density without changing the bulk properties. It includes two steps: a) surface activation and b) graft polymerization. Because of the absence of chemically reactive functional groups on most substrate surfaces, a surface activation process is needed to create reactive sites on them

that can generate further grafting processes. Reactive groups can be generated through chemical reactions, plasma treatment, ozone exposure or irradiations. This method has been used to prepare nanofibre surfaces for inducing antibacterial properties. For example, polyurethane (PU) nanofibres were modified with poly(4-vinyl-N-hexyl pyridinium bromide) after treatment with argon plasma to produce surface oxide and peroxide groups on surface [53]. Then the nanofibres were immersed in 4-vinylpyridine monomer solution with exposure of UV irradiation. Hexylbromide was further used for of grafted pyridine groups for antibacterial activity. This technique has also been utilized for improving water solubility of surface. Graft polymerization of acrylic acid (AA) was done on chitin nanofibre and the resultant nanofibre showed improved dispersibility in basic water [54]. Similarly, various other kinds of monomers have been attached to nanofibres for different applications [55,56]

1.2.2   Modification by immobilisation methods

The recent developments on surface modification through the attachment of biologicals and non-biologicals to solid surfaces has advanced it's application in medical and environmental sectors [57,58]. The choice of surface or support matrix is also an important criterion to achieve optimum immobilisation because the morphological and physicochemical properties of a surface can affect the activity of immobilized molecules. One of the desired properties of support matrix is mesoporous structure where the large surface area can permit higher loading of molecules [42]. Since the pore dimensions and total surface area can critically affect the binding capacity, nanofibre surfaces are considered as excellent candidates for immobilisation as they have high surface area to volume ratio with highly macroporous morphology.

 A properly oriented molecule can help in proper exposure of active sites. Therefore, consideration should also be made while choosing the spacer arm between the surface and the immobilised or modifying molecule. Longer and flexible spacers can provide more mobility to the immobilised molecule resulting in better sensitivity of the technique [59]. High efficacy immobilisation must also fulfil requirements such as easy and rapid modification, stable and high-density attachment of molecules and no significant change in structure of molecules as well as the modified surfaces. As reviewed by Mohamad et al., the main techniques of immobilisation on nanofibres can be categorised as the following [42]

1) Non-covalent bonding

2) Covalent bonding

3) Entrapment

Figure 4 represents the schematics of the immobilisation techniques as reviewed by Mohammad et al. Although comprehensive, the list is not definitive as they have been classified differently by various authors [59,60].
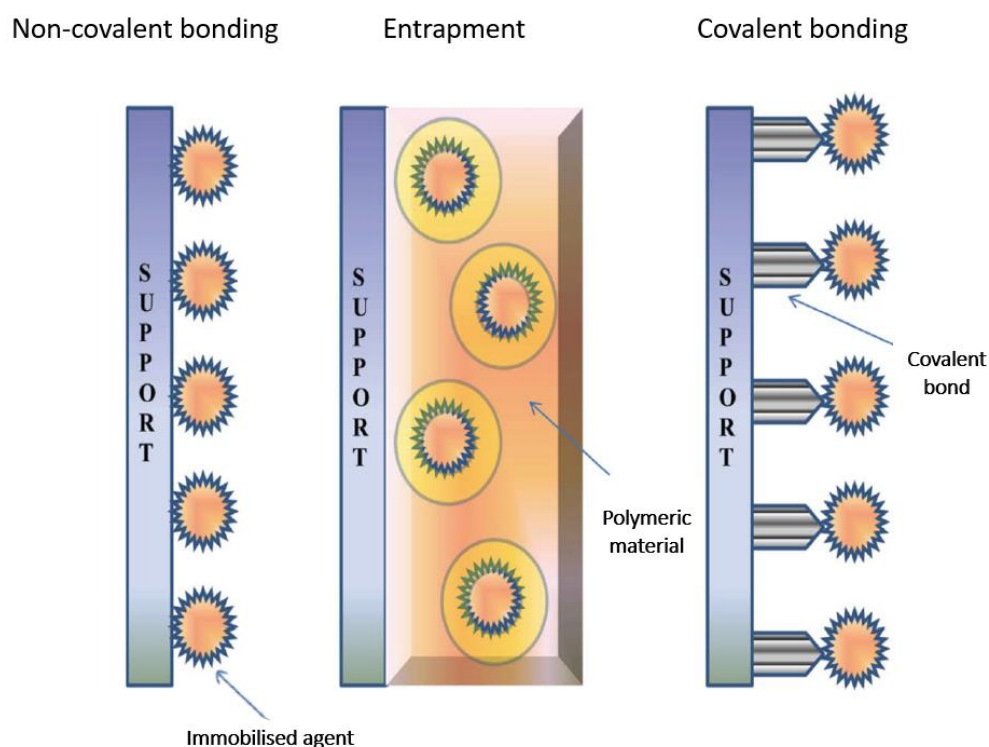
Figure 4: Schematic representation of different methods of immobilisation of molecules. Non-covalent bonding is formed without any chemical bond between the support or surface, entrapment is the process where the modifying agent is trapped inside a 3D polymeric material and covalent bonding involves the process of forming an irreversible bond between the immobilised agent and the surface [42].

Non-covalent bonding

Non-covalent bonding is a process of physical attachment to the surface through different mechanisms such as hydrogen bonding, van der Waals interactions, ionic and electrostatic interactions [61]. Adsorption was one of the first immobilisation methods that were used for non-covalent attachment of biomolecules such as enzymes, antibodies and glycans [41]. It can be simply carried out by mixing the molecule with suitable adsorbent surface under appropriate conditions of ionic strength, pH, temperature and incubation period. The excess of loosely bound molecules can then be washed off and the adsorbents can be directly used. However, due to weak binding, the adsorbed molecules

can desorb, resulting in lower stability of modification. The surfaces are also susceptible to non-specific binding and therefore the technique can be difficult to control. Some commonly immobilised agents through non-covalent interactions are discussed below.

a) Drugs and biomolecules

Nanofibre surface is used for release of drugs for controlled dosage of therapeutic agents. Drugs such as peptides, proteins (including antibodies) can be loaded on the surface using simple physical adsorption. Hydrophobic drugs are mixed with the polymer solution before electrospinning. However, due to harsh conditions of electrospinning some drugs can be less effective after the release [62]. Therefore, modification can be done by simply attaching drugs post-fabrication. Heparin is a glycosaminoglycan that has a strong affinity towards growth factors. Nanofibres such as PEO and PLGA have been immobilised with low molecular weight heparin [62]. These modified surfaces have potential applications in local delivery of growth factors with enhanced therapeutic efficacy. Cancer therapy is a common application of drug-loading technique. Drugs such as fluorouracil and oxaliplatin have been loaded onto polylactide (PLA) nanofibres to suppress tumour growth [63]. Chitosan/PEO nanofibres have been loaded with paclitaxel (PTX) which is a well-known mitotic inhibitor and a radio sensitising agent by simple adsorption and the resultant fibres showed chemotherapeutic activity [64]. Drug-loaded nanoparticles with unique drug-releasing profile have also attracted attention lately. Nanoparticles are used to enhance the solubility of hydrophobic drugs, increase stability, provide controlled release and deliver higher concentrations through enhanced permeation [65,66]. Such nanoparticles can be embedded during electrospinning [67] or after electrospinning [68]. Nanoparticle decorated fibres have been explored for wound care, regenerative medicine and dental engineering [68].

b) Self-assembled monolayers (SAM)

Self-assembled monolayers (SAM) are formed by spontaneous adsorption of highly ordered molecular assemblies on the surfaces of various substrates. The process is initially driven by physical adsorption through van der Waals or hydrophobic interactions but stable monolayers are formed by chemical interaction between the adsorbate and the surface [69]. The molecules are attached to the surface by strong covalent-like interactions that are extremely stable. The weakly attached molecules can then be washed out easily after SAM formation. One of the common classes of SAMs is based on

strong adsorption of compounds such as thiols, sulphides and related moieties on elements such as gold, silver, copper and platinum [70]. According to the paper, the self-assembly of alkanethiols on gold is a commonly studied self-assembly process. The interaction is reversible and is simply formed by dipping gold into a solution of corresponding alkanethiols. Monolayers of fatty acids on silver surfaces and alkylchlorosilanes, alkylaminosilanes on hydroxylated surfaces have also been studied. SAMs have been widely applied to biosensors, neural prosthetic devices, protein microarrays and microfluidics [71].

Covalent bonding

The covalent bond is a strong molecular bond made by sharing of electrons in the atoms. It includes interactions such as metal-to-metal bonding, σ-bonding, π-bonding, bent bonds and can be simply divided into two types of bonding - polar bond and non-polar bond [42,72]. Chemical groups such as carboxyl, hydroxyl, thiol and amino groups are commonly utilised for binding of modifying molecule to the surface. However, such groups are not required for the functional activity of the molecule. Covalent methods provide more stable immobilisation with very less chance of desorption from the surface but due to harsh conditions required for the process, the structure and activity of the molecule can be affected. Some examples of the functionalities that can be utilised are epoxides, amines, aldehydes, thiols, maleimides, azides, hydrazides and N-hydroxysuccinimide (NHS) esters [73]. Some common techniques of covalent modification are listed below.

a) Cross-linking

Crosslinking is the process of chemically joining two or more molecules through a covalent bond. It is a frequently used technique, which provides a more stable attachment than adsorption. Functional groups such as primary amines ($-NH_2$), carboxyls ($-COOH$) sulfhydryls ($-SH$), carbonyls ($-CHO$) and hydroxyls ($-OH$) can be utilised for cross-linking of modifying agent with the surface [74]. Various synthetic and natural molecules have been used for functionalisation to improve the chemical and mechanical features of nanofibres and other surfaces. Some of these are discussed below.

Laminin is a component of extracellular matrix protein that helps in differentiation of neural cells. Covalent modification of nanofibre using laminin through series of chemical reactions has been widely studied. For example, the proliferation of Schwann cells on the

laminin-modified PCL-chitosan nanofibre substrate was investigated where cross-linked laminin showed better activity than adsorbed laminin [75]. Covalent cross-linking was also explored for modifying silica by surface grafting of (3-aminopropyl) trimethoxysilane, which was subsequently reacted with 4-(N-maleimidomethyl) cyclohexane-1-carboxylic acid 3-sulfo-N-hydroxysuccinimide ester sodium salt (sulfo-SMCC) [76]. The resulting surface was finally cross-linked with laminin with covalent thiol-maleimide linkage of laminin to silica nanofibre.

Gelatin and collagen are good candidates to create tissue-engineered scaffolds as they are biocompatible. However, they dissolve in aqueous media making them unsuitable. By cross-linking the carbonyl groups on the glutaraldehyde and the amine groups of the gelatin, the nanofibres can be made water-stable [77]. Insolubility is also an important requirement for filtration applications. As reviewed by various authors, water-soluble nanofibres can be modified by cross-linking to improve hydrophobicity and glutaraldehyde is predominantly used for stabilising water-soluble nanofibres because it offers a simple, low cost and effective technique for modification. Many studies show successful modification of polyvinyl alcohol (PVA) nanofibres with glutaraldehyde resulting in improved water stability along with enhanced mechanical properties [78–80].

Genipin is one of the newly studied cross-linking agents for polymers such as chitosan, gelatin, PVP and PEO [81,82]. The papers reported improved chemical and mechanical stability of chitosan nanofibres by spontaneous reaction of genipin with the NH_2 group chitosan or a protein with a reactive amino-group.

An epoxide is a cyclic ether composed of a three-atom ring. This ring makes it highly reactive. Ethylene glycol diglycidyl ether (EGDE) is a diepoxy cross-linker with two epoxide groups on either end. It has been used to react with an amino group on the amino acid at the end or in the middle of the keratin to improve the water-resistance [83]. The study also reports improved crystallinity and thermal stability after cross-linking. It has also been cross-linked on chitin beads to enhance adsorption of copper ions by improving stability on acidic and basic solutions [84]. This technique can be extended to modify chitin nanofibres in a similar way.

The isocyanate groups on cross-linking agents can react with hydroxyl groups on the surface to improve the mechanical properties of nanofibres. Diisocyanate is a commonly used agent for such cross-linking reactions. It has been used for the modification of silica

aerogel with subsequent incorporation of carbon nanofibres. It was found to increase the stability of the product without changing the density and porosity [85].

b) Click chemistry

The click chemistry concept was introduced by Sharpless and colleagues in 2001 [86]. Ever since the relevance of this concept and its applications has been widely increasing [87–89]. Click reactions offer advantages such as the ease in conducting a reaction with no side products and its broad applicability in modular approaches [90]. The reactions can be conducted in mild conditions.

The copper (I)-catalyzed 1,3-dipolar cycloaddition of azides and alkynes has been extensively used as "click" reactions for various applications. A promising and efficient way of obtaining clickable nanofibrous scaffolds was explored using commercially available PCL nanofibre. It was reported that this method was high yielding and non-destructive as compared to other commonly used techniques such as saponification or aminolysis [91]. Introduction of antimicrobial properties using click chemistry has also been explored. For example, Polyacrylonitrile (PAN) nanofibre was modified using sodium azide (NaN_3) and silver nitrate ($AgNO_3$) as a catalyst to yield antibacterial activity. The resultant product was also found to exhibit excellent stability [92]. Nitrile click (i.e. −CN + alkyne) chemistry was used to modify PAN nanofibres with silver ions with the assistance of microwave radiation. It was also successful in producing an excellent antibacterial material [93].

The copper initiated click chemistry has potential drawbacks of toxicity. Therefore, metal-free click chemistry has also been explored. Strain-promoted azide-alkyne cycloaddition (SPAAC) has been used to modify biomolecules for use in living systems [94]. It works on the concept of ring strain, which provides dramatic rate acceleration between azide and cyclooctynes compared to normal unstrained alkynes.

The series of thiol-based reactions that meet the "click" criteria, particularly, radical-mediated reactions are the most commonly used metal-free modification technique used for tissue engineering applications. However, they require UV source that could induce damage [95]. Therefore, base/nucleophiles–mediated thiol-X reactions including thiol-Michael, thiol-isocyanate, thiol-epoxide and thiol-halide reactions have gained increasing attention.

Entrapment

Entrapment is a common technique of immobilising biomolecules inside a 3D structure by polymerising material network around it. It is the most effective way of immobilising active agents such as vitamins, biocatalysts due to the stabilising and protective effect. The retention and release of entrapped molecules can also be controlled with ease, making it suitable for therapeutic purpose. One of the desired properties of polymers for entrapment is a mesoporous structure with large surface area. Therefore, nanofibres are considered an excellent support matrix for this technique.

Coaxial electrospinning is one of the commonly used methods for entrapment, which is a modified form of electrospinning that involves an arrangement of multiple concentric spinnerets to co-spin compound fibres. It offers an advantage of duo-phase production of nanofibres by blending their properties while allowing their individual identities to be maintained. This technique has been used to produce core-shell fibres useful in many applications including drug delivery and material encapsulation. Molecules such as genes, proteins and growth factors have been entrapped in core-shell fibres [96].

Healing agents such as dicyclopentadiene (DCPD) and isophorone diisocyanate (IPDI) were encapsulated in PAN nanofibres using co-axial electrospinning. Results showed excellent recovery of agents. Lee and co-workers also used a similar method to produce self-healing composites by encapsulating dimethylsiloxane in PAN [97,98]. Several groups have reported the entrapments of biological organisms/cells into electrospun nanofibres. Encapsulation of bacterial viruses as an alternative to antibacterial antibiotics and gene delivery vectors has been reported [99,100]. The entrapment of eukaryotic cells is also used for the delivery of therapeutic molecules to diseased sites. Human umbilical vein endothelial cells (HUVECs) were entrapped in PEO/PCL shell nanofibres. The modified nanofibres were found to exhibit improved cell viability [101].

1.3 Pollutants

1.3.1 Air pollutants

Air pollution is the presence of excessive quantities of harmful substances in the atmosphere that is detrimental to human health and the whole planet. Such substances could be released by various sources such as described below [102–105].

a) Man-made sources: fossil fuel power stations, manufacturing facilities, biomass combustion, waste deposition, vehicles, aircraft and nuclear weapons etc.

b) Natural sources: dust, methane production by animals, radioactive decay, wildfires and volcanic activity etc.

Some common contaminants found in the air are listed below.

Particulate matters

Particulate matter or PM is a mixture of solids and liquid matter found in the atmosphere. Some particles are released directly from a specific source, while others form in complicated chemical reactions. Particles come in a wide range of sizes and chemical composition. The size of the particle is an important parameter as it controls the dynamic behaviour of particles as well as their chemical and physical impacts upon the environment. It is also certainly an important parameter for the health consequences of the respective human exposure as particle size determines: (i) the deposition of particles within the human respiratory system; (ii) the amount of surface area that can contact tissues; and (iii) the rate of particle clearance from lungs [106]. Based on size, PMs can be divided into:

a) PM of size 2.5-10 µm (PM10)
b) PM of size 2.5 µm or less (PM2.5)

Figure 5 shows the comparison of PM10 and PM2.5 with human hair and fine beach sand. Different sources of PMs are farming, mining, and dust storms, pollen, mould, and combustion processes, such as petrol and diesel vehicles, wood burning, coal burning for power generation, and industrial activities [107].
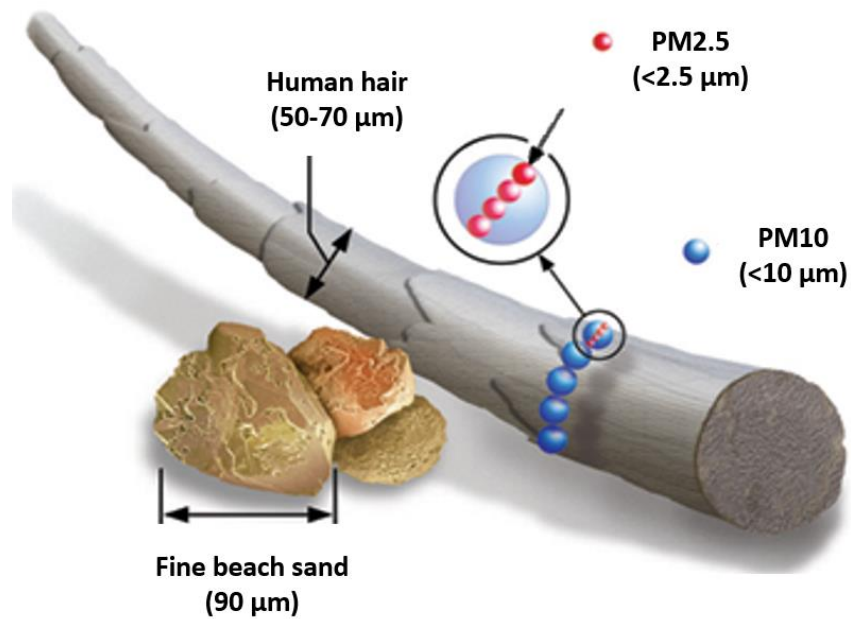
Figure 5: Comparison of particulate matter with human hair and beach sand [108].

The health effects of inhalable PM are well documented [109]. They are due to exposure over both the acute short term (hours, days) and chronic long term (months, years). A huge spike in the occurrence of diseases such as asthma, cancer, high blood pressure, birth defects and many other cardiovascular and respiratory problems in the past couple of decades is directly proportionate to the increased PM level all over the world [110,111]. Ambient (outdoor) air pollution in both cities and rural areas was estimated to cause 4.2 million premature deaths worldwide per year in 2016. This mortality is due to exposure to small particulate matter PM2.5 [112,113]. Recent studies have also associated PM2.5 with skin damage and aging [114,115].

Based on their transport to different regions of our respiratory system, they can be divided into a) inhalable fraction, which is less than 100 μm and can enter our throat b) thoracic fraction, which is less than 10 μm and can enter our bronchi c) respirable fraction, which is less than 4 μm and can reach our alveoli [116]. They have different health impacts depending on what part of the respiratory organ they can reach. Figure 6 describes these fractions and their health effects.
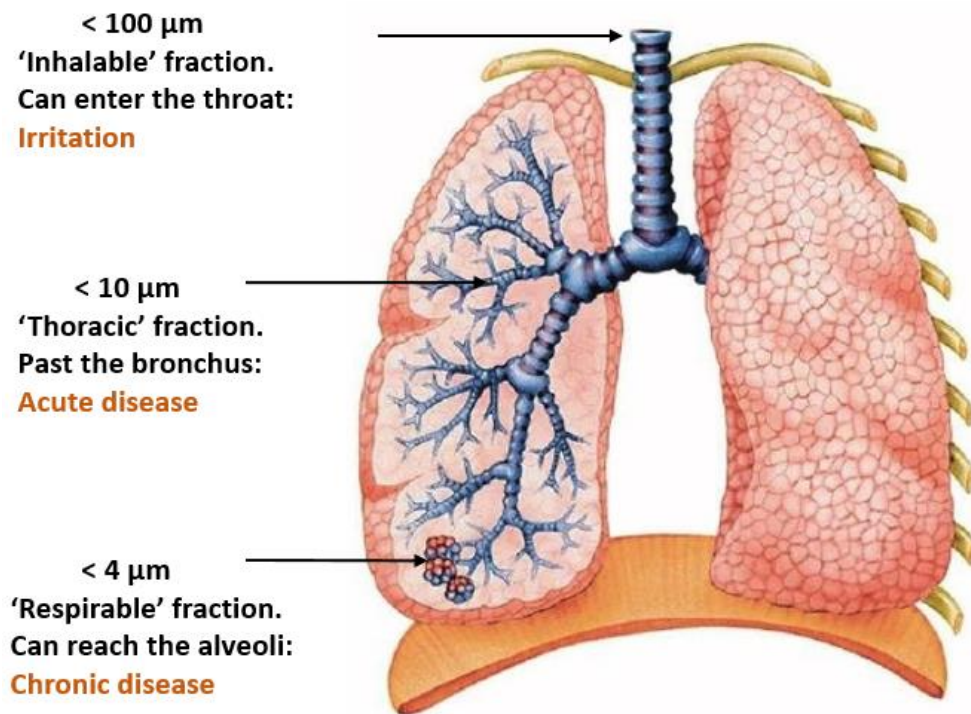
Figure 6: Health effects of different fractions of PM based on size [117].

Volatile organic compounds and toxic gases

Volatile organic compounds (VOCs) are a wide-ranging group of organic molecules that are considered as major contributors to air pollution. They have high vapour pressure, which contributes to their volatile nature. They can cause acute symptoms such as irritations of the nose, eyes, throat, headache, nausea, allergic skin reactions and serious damage of internal organs such as kidney and liver [118]. Sources such as industrial plants, vehicles and aircraft emit these pollutants into the atmosphere causing harm to human health and the ecosystem [119]. International concerns regarding VOCs arise due to their toxic nature, their ability to travel great distances and their tendencies to accumulate and distribute in the environment. Polycyclic aromatic hydrocarbons (PAH) such as anthracene, phenanthrene and pyrene are considered as the most dangerous VOCs, posing multiple threats. They are produced by incomplete combustion of organic matter. They can originate from natural processes such as biomass combustion and volcanic eruptions. However, anthropogenic activities like wood burning, petrol and diesel combustion and industrialisation release large amounts of PAH into the atmosphere [120]. VOC such as methane is considered to be less harmful but can contribute to global warming, whereas, more harmful VOCs such as benzene can lead to photochemical smog

when combined with other gases such as nitrogen oxides (NOx) [121,122]. Photochemical smog is the chemical reaction of sunlight, NOx and volatile organic compounds (VOCs) in the atmosphere, which results in the formation of airborne particles (particulate matter) and ground-level ozone.

1.3.2 Water pollutants

Water pollution is the introduction of contaminants into water sources. Water pollutants can come from many different sources such as industry, waste treatment plants, pesticides, rainwater runoff. The pollutants can be organic, inorganic, radioactive or acidic/basic in nature, which can have severe health impacts [123]. For example, the World Health Organization (WHO) has reported that 842,000 deaths occur every year due to diarrhoea [124]. Water pollution can be considered a major factor in the realisation of these grim statistics. Water contaminants can be categorised as:

Particulate matter

Suspended particulate matter are heterogeneous aggregates of organic matter, microbiological particles and mineral fragments. They can interact with other pollutants in water and induce more harmful effects. The atmospheric PM is one of the major sources of water PM. When the insoluble particulate matter are exposed to water, they cannot readily dissolve and later settle under the water bodies [125]. Particulate contaminant filtration is dependent on factors such physicochemical properties of particles and particle size.

Nano contaminants

There is a huge surge in the use of nanoproducts (1-100 nm) for various applications. The unique physiochemical properties of nanomaterials such as larger surface to mass ratio and greater surface reactivity make them ideal to be used as components of any commercial product [126]. For example, titanium dioxide nanoparticles are being extensively used for better UV protection utilising their enhanced light absorption and scattering properties [127]. Silver nanoparticles are used in clothing and detergent manufacturing due to their antimicrobial properties [128,129]. The use of nanomaterials can also be found in food packaging, processing and development of food additives as they can increase the stability and enhance the delivery and bioavailability of nutrients [126]. Nanoparticles from these sources can enter air, soil or water affecting the aquatic

ecosystem. Most particles are released as domestic waste during cleaning and contaminate the surface waters. Apart from harming aquatic organisms, they also cause human health hazards when those surface waters are used for drinking water [130]. The conventional treatment technologies such as activated sludge, reverse osmosis and nanofiltration are not very efficient in removing complex nano pollutants released as pharmaceutical products, industrial additives and other personal products [131]. Moreover, there is a lack of knowledge of toxic effects and behaviour of nanoparticles and there are no adequate analytical techniques for the measurement of nanoparticles. Therefore, there is a need for efficient removal of nanoparticles.

Nutrients

Nitrates and nitrites are major sources of nutrient pollution of water sources. Mostly, commercial fertilisers and animal manure contribute to nitrogen and phosphorus contamination [132]. The increase in levels of nutrients could encourage algae and weed growth, which further deteriorates the quality of water.

Pesticides and chemicals

Pesticides are used to protect crops against insects, weeds, fungi, and other pests. They also help in increasing the food yield. Some commonly used pesticides are fungicides and insecticides. However, some are toxic to humans and can have both acute and chronic health effects [133]. Pesticides can remain in the soil and water for years. Farmlands are the major source of pesticide contamination. The water from rainfall and irrigation is transported to the groundwater and freshwater, resulting in their contamination. Other chemicals such as oils and spills from agricultural and horticultural industries also contaminate water sources.

Heavy metals

Heavy metals are naturally occurring elements that have high atomic weights and densities. They are important constituents of several key enzymes and play important roles in various oxidation-reduction reactions. However, they carry major health risks if found in excess. Some toxic heavy metals include arsenic, lead, mercury, cadmium and chromium [134,135].

1.4 Application of nanofibres in filtration applications

Filtration is traditionally the leading, and today the most developed industrial sector involved in the application of polymer nanofibres [136]. Nanotechnologists have discovered new filtering media for effective filtrations. Nanofibrous media have low basis weight, high permeability and small pore size that make them appropriate for a wide range of filtration applications. In addition, nanofibre membrane offers unique properties like high specific surface area, good interconnectivity of pores and potential to incorporate active chemistry or functionality on nanoscale. Therefore, nanofibrous membranes are extensively being studied for air and liquid filtration where high-performance purification is needed such as in hospitals, healthcare facilities, research labs, electronic component manufacturers, military and government agencies, food, pharmaceutical and biotechnology companies.

The first sub-micron sized fibre filtration media was commercialized in the USA by Donaldson co., in the 1980s. The technique has since been adopted by many industries and research groups and has undergone massive improvements to suit different filtration markets [137]. The increasing number of warnings from health organisations and agencies combined with increasingly stringent government regulations and health and safety concerns from the public are pushing the development of next-generation filter media with more efficient filtration capabilities. Modified or functionalised nanofibres are being widely studied as such advanced filter media [137]. Some examples of their applications are discussed below.

1.4.1 Use of modified nanofibres in air filtration applications

Air pollutants are comprised of volatile organic compounds (VOCs), sulphur dioxides, nitrogen dioxides, ozone, viruses, dust and smoke, etc. Polycyclic aromatic hydrocarbons (PAHs) are other commonly occurring toxic airborne pollutants, and are produced by the incomplete combustion of organic matter [138,139]. Dust particles or pathogens typically occur as liquids, solids, or combinations. For example, dust particles and pathogens develop a liquid outer phase when they hit the surface of filtration media that has been humidified by atmospheric moisture or from the moisture from human respiration. An interfacial tension, therefore, develops between the particle and the filter media.

These complexities of the composition of airborne pollutants have led to increases in demand for high-efficiency filtration media consisting of multiple layers for capturing

particulates of different sizes, forms and compositions. Unfortunately, multilayers filter media is often hindered by poor breathability and high-pressure drop, which is undesirable for filters. Thus, researchers are trying to develop single layer multi-functional nanofibre filtration media to address the issues of poor breathability and poor filtration efficiency. It is also possible to utilise the inherently large surface areas of the nanofibres and to chemically modify and functionalise the nanofibre surfaces so that they are able to adsorb larger amounts. Moreover, nanofibre fabrication process often allows for the incorporation of functional molecules within the fibres to better capture target particulates, viruses and hazardous gases with greater efficiency.

The use of modified nanofibres to remove different kinds of air pollutants are discussed below.

Particulate matter removal

Many variables influence the efficiency of filter media in capturing particulates, including duct size, fan strength, air velocity and environmental conditions such as humidity. However, PM filtration is dependent on two important mechanisms: surface filtration and depth filtration. Simply put, surface filtration occurs when particles are too large to pass through the pores of a filter and are trapped on the surface of the filter media. The general mechanisms for the surface filtration of PMs include diffusion, interception, intermolecular interaction, straining, inertial impaction, gravitation and electrostatic interaction of particles on the filter surface [140].

Diffusion and interception can be the most important particle capture mechanisms of nanofibres. Diffusion results in the capture of fine particles below 0.5 µm on the fibre surface due to Brownian motion whereas particle interception occurs, when the distance between fibre surface and the particle centre is equal to or less than the radius of the particle [141].

If particles contaminants are not removed efficiently through these mechanisms, they tend to clog filter media and significantly reduce airflow. In addition to these attributes, nanofibre membranes exhibit strong van der Waals forces, which enable them to attract sub-micron sized particles. The good interconnectivity of the pores also results in improvements in inertial impact and interception of particles. In addition, there is great

potential to modify the nanofibre filtration media by incorporating additional functionality on the nanofibre surfaces that could enhance the chemical interaction and electrostatic attraction with particle contaminants. In general, such functional filter membranes work on the principle of creating an affinity for a molecule based on its physical/chemical or biological properties. Relying on the specific ligands immobilised at the surface, the nanofibres capture and separate molecules selectively. On the other hand, depth filtration occurs when particles are small enough to fit into the pores of the filtration media but are trapped during their journey through the material. Consequently, the particle size distribution and the pore size of the filtration media determines whether surface or depth filtration occurs. Thus, in both surface filtration and depth filtration situations, the particles that are small enough to enter the filter structure are collected by chance interactions with the fibres of the filter. The selection of the ideal filter material for surface and depth filtration requires knowledge of the interfacial energies at the surface between the fibres and the particulates as well as surface interaction mechanisms.

In the case of nanofibre air filters, dust particles and airborne pathogens can have relatively wet surfaces when compared to the dry nanofibre material. Thus, when airborne pollutants touch the surface of the nanofibre, an interfacial tension will arise at the solid-liquid or solid-solid boundary/interface from the polarity disparity of the solid phase of the fibre and moisture-containing pollutant particles. Due to this interfacial tension, the adherence between solid nanofibres and relatively wet particles are increased. It is possible to enhance such interactions and adherence between the nanofibres and the particulates by introducing polar molecules to the nanofibre polymer backbones. A polar nanofibre, owing to the unevenly distributed charge on its molecular backbone, experiences high interfacial tension when in contact with another polar or non-polar surface of a different phase (when compared to non-polar fibres). This phenomenon makes polar nanofibres particularly suitable for surface and depth filtration.

Polyacrylonitrile (PAN) is a polar polymer that is commonly used in nanofibre air filters. The polar nature and small fibre diameters make PAN nanofibres highly suitable for use in facemasks that are required to remove PM2.5 particles. Electrospun nanofibres made from PAN are also strong and can withstand conversion into filters [142]. Liu et al. have

mentioned that PM2.5 particles are often electrically charged, thus enabling bonding between the particles and the nanofibres by means of dipole interactions. The PM2.5 particles typically have sticky amorphous carbon-like morphologies with cores containing condensed solid matter and outer surfaces containing light organic matter with polar functional groups (C-O, C=O and C-N)[143]. In such situations, filtration materials that have high dipole moments are more efficient at attracting particulate pollutants.

Figure 7 shows the functionalised PAN filter with high adhesion of particles as compared to commercial filters. According to Liu et al.[143], such surface-modified filters can be made very thin, almost transparent, allowing for maximum air and light to pass through.
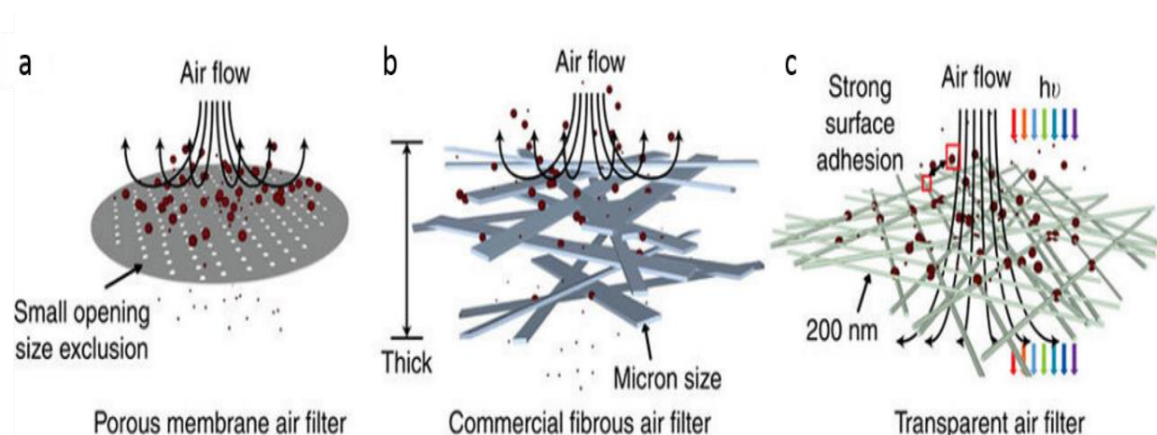
Figure 7: Comparison of different air filters [143]. a) Schematic of a porous air filter capturing PM particles by size exclusion. b) Schematic of a bulky fibrous air filter capturing PM particles by constraint. c) Schematic of an air filter that captures PM particles by strong surface adhesion whilst allowing high light and air penetration. Red boxes in c) indicate surface adhesion.

It has also been proved that high dipole moments can be created on the surface of PAN nanofibres with the addition of an ionic liquid in the form of diethyl ammonium dihydrogen phosphate (DEAP) [144]. The resultant PAN nanofibre was found to be more hydrophilic with greatly enhanced particle capturing efficiency due to the enhanced surface roughness and the associated increase in the number of adsorption sites. Moreover, the filters showed high levels of air permeability. Since PAN nanofibres are currently being electrospun for air filtration applications on a commercial scale, this simple modification technique has great potential to be translated into commercial products.

In addition to high filtration efficiency, an ideal filter should manifest high breathability. The packing density of the nanofibres greatly influences the breathability of the filtration media. Packing density is often referred to as solidity, which is the volume of solids in the

medium per unit volume. A high nanofibre packing density results in smaller pore sizes and lower breathability, but higher filtration efficiency. Inversely, a low nanofibre packing density results in larger pore sizes and higher breathability, but lower filtration efficiency. It is, therefore, possible to engineer the nanofibre component to best suit the filter performance requirements. Another important consideration for the design of nanofibres air filters is thermal stability. Some filter applications involve the filtration of hot air or gases (e.g. vehicle exhausts) or even exposure to steam. Zhang et al. recently developed polyimide (PI) nanofibre filters that are able to withstand temperatures of up to 370°C [145]. These filters were shown to have a 99.98% removal efficiency of 0.3 μm sized particles and achieved the standard requirements of high-efficiency particulate air (HEPA) filters [145]. Similarly, incorporation of SiO_2 particles into PI nanofibre membranes resulted in filtration media with high porosity, excellent electrolyte wettability, enhanced ionic conductivity and outstanding thermal stability [146].

Volatile organic component removal

Activated carbon has traditionally been the material of choice for capturing volatile organic component (VOC) and photochemical smog. Most of the commercially available VOC filtration materials contain activated carbon. In recent times, cyclodextrins have been utilised by researchers to modify electrospun nanofibre materials to enhance the capture of VOCs. Cyclodextrins are produced from starch and are naturally occurring non-toxic cyclic oligosaccharides. Cyclodextrins are a family consisting of three major compounds: α-cyclodextrin (α-CD), β-cyclodextrin (β-CD) and γ-cyclodextrin (γ-CD). Each of the cyclodextrins is crystalline and homogenous substances which consist of torus-like macro-rings built up from glucopyranose units α-CD is comprised of six glucopyranose units, β-CD is comprised of seven such units, and γ-CD is comprised of eight such units. Because of their specific conformation, cyclodextrins are able to become hydrophobic hosts for intermolecular interactions and therefore are able to form non-covalent inclusion complexes with various other molecules. They are recognized for their complexation capacities with hazardous chemicals and are used in many industrial applications [147,148]. Kayaci et al., have incorporated all three major forms of cyclodextrins into polyester (PET) nanofibres for entrapment of aniline vapour. They showed that electrospinning PET with cyclodextrins also improved the mechanical properties and

produced bead-free nanofibres. γ-CD functionalised PET nanofibres exhibited the greatest aniline capture efficiency when compared to those functionalised with α-CD and β-CD [149]. Previously, the researchers had successfully functionalised poly (methyl methacrylate) PMMA nanofibres with different concentrations of β-CD to entrap aniline, styrene and toluene volatiles [150].

Celebiogl and Uyar were the first to report the electrospinning of cyclodextrin inclusion complexes (CD-IC) without using a carrier polymer matrix and were successful in electrospinning hydroxypropyl-β-cyclodextrin (HPβCD) and its inclusion complexes with triclosan (HPβCD/triclosan-IC) [151]. Further tests were performed to compare the molecular entrapment of volatile organic compounds (aniline and benzene) by HPβCD and HPγCD [152]. It was found that HPβCD was more successful at encapsulating the VOCs than HPγCD, and both compounds showed a higher affinity for the encapsulation of aniline over that of benzene.

Another emerging and commercially scalable technology for the removal of VOCs involves the use of Metal Organic Framework (MOF) particles. MOFs have incredibly high surface areas and their properties can be modified to enable them to capture different VOCs. While traditionally used activated carbon can efficiently capture VOCs, one shortcoming is the difficulty in attaching functional molecules to the carbon to enable broad-spectrum protection. Since MOFs allow for the covalent anchoring of functional groups, they can be extensively used in the capture of various classes of chemicals.

Functionalisation of nanofibre with MOF could result in a new generation of functionalised air filter materials that can remove particulate matter as well as VOCs. It has been shown that the surface area of nanofibre can be increased by incorporating MOF's into the material, thus enhancing the filtration efficiency and active surface area of the nanofibres. The performance of PAN nanofibres was analysed after modification with ZIF-8 MOFs. The BET surface area of the PAN nanofibre was improved from 115 m^2/g to 1024 m^2/g with the incorporation of ZIF-8 nanoparticles at a mass ratio of 60% [153]. The authors predicted that the defects and unbalanced metal ions on the surfaces of the MOFs offer positive charges that can polarise airborne particles. This results in increased electrostatic interactions that can enhance the capture of SO_2 and particulate matter. When tested in hazy environments in Beijing, the composite nanofibres outperformed unmodified nanofibre filters in terms of PM2.5 and PM10 particle removal efficiency. The

ZIF-8/PAN composite filter layer was shown to selectively adsorb toxic gases such as SO_2 when exposed to a SO_2/N_2 mixture. After SO_2 adsorption, the modified filter was regenerated by exposing it to a stream of N_2 gas, thus showing that MOF modified filters can also be re-used and recycled.

Other kinds of MOF particles that have been proven to capture VOCs and other toxic gases are MOF-199, Mg-MOF-74 and UiO-66-NH2. Recent research involves synthesis of indium-based MOFs and their ability to adsorb CO_2 [154]. Such MOFs are structurally rigid and stable with open metal sites and have great potential to provide active gas adsorption sites in electrospun nanofibre materials. Furthermore, Vellingiri et al., analysed three MOFs (MOF-5, Eu-MOF, and MOF-199) to determine the adsorption capacities of a mixture of 14 volatile and semi-volatile organic gaseous species [155]. The results showed that MOF-199 had highest equilibrium adsorption capacity of the three MOFs and showed the presence of strong π-π interactions. It was also noted that the polarity of the guest molecule greatly affected the absorption behaviour of the MOFs [155].

Rare earth metal oxides (RE) are also evolving as active materials that are suitable for the removal of VOC's. Some of these oxides include Ce_2O_3, CeO_2, La_2O_3, Pr_2O_3, Nd_2O_3, Sm_2O_3 and Er_2O [156] recently utilised rare earth oxide powders to modify nanofibre. The authors showed that the addition of RE powders increased the tensile strength of the nanofibre mats, and more importantly, increased the adsorption efficiency of several different VOCs.

Bioremediation is another interesting technology that can be utilized for VOC removal. It involves the biodegradation of organic contaminants into carbon dioxide, water, inorganic compounds and cell proteins and includes the transformation of complex organic contaminants to other simpler organic compounds by microbial activity [157]. Fungal strains, mostly members of the dematiaceous fungi group, were tested to determine whether or not the fungi could utilise VOCs as the sole carbon and energy source for growth [158]. The results were promising, but this research is still in its infancy and has yet to be fully explored. Bacterial species such as *Pseudomonas spp.*, *Sphingomonas* spp., *Flavobacterium* spp., *Burkholderia* spp. (Gram-negative), and *Rhodococcus* spp., *Mycobacterium* spp., and *Bacillus* spp. (Gram-positive) have successfully been used to degrade polycyclic aromatic hydrocarbons (PAHs) and VOCs, including naphthalene, phenanthrene, pyrene, anthracene and benzopyrene [157].

However, bioremediation processes have yet to be combined with nanofibres for active filtration applications, and there appears to be great scope for further work in this field.

1.4.2 Use of modified nanofibres in water filtration applications

The large surface area to volume ratio of the nanofibrous scaffolds offers a great capacity to adsorb toxins, such as viruses, dyes, heavy metals and other micro and nano particulates from liquids. In addition, the high porosity of electrospun nanofibres provides a good permeation flux as water molecules can transport through the membrane with low hydraulic resistance. Electrospun nanofibres can serve the dual purpose of adsorption and filtration due to such advantageous physical properties. Filtration of particulates is a pressure-driven process. The pore size distribution of membranes can be controlled during fabrication. A good porosity results in high hydraulic permeability. Such feature makes the nanofibre membranes suitable for filtration technologies such as microfiltration, ultrafiltration, nanofiltration, reverse osmosis, forward osmosis and membrane fabrication [159].

Different polymer materials can be used for liquid filtration. However, based on the properties of the polymer, they can be broadly divided into hydrophobic and hydrophilic. Membrane distillation (MD) is one of the low cost and energy-saving microfiltration technologies that are widely being investigated. It is a thermally driven process where vapour is transported through hydrophobic membranes. The partial vapour pressure across the two sides of the membrane acts as the driving force [160]. Since, the membrane acts as the barrier between the two phases, the productivity and energy efficiency of the process is highly depended on the properties of membrane. Various hydrophobic nanofibre membranes fabricated through electrospinning are being studied for this purpose [161,162]. Such membranes have been used for desalination of seawater and brackish water. Some common examples of hydrophobic membranes include PVDF, PS and PES. They are suitable for MD as well as other conventional microfiltration. On the other hand, hydrophilicity of membranes is reported to exhibit anti-fouling properties. A hydrophilic polymer such as cellulose acetate (CA) is often blended with hydrophobic polymers to enhance their wettability property [161].

Various modification methods such as physical coating or chemical grafting have been applied to enhance adsorption of various pollutants as well as their antifouling properties. Some of them are discussed below.

Dye removal

Treatment methods for dye removal from water include adsorption, coagulation and biological treatments [163]. However, dye removal can be challenging due to their complex molecular structures and slow degradation rates [164]. Electrospun nanofibre membranes have the potential to be used in alternative methods of dye removal. Despite having pores that are too large for the size exclusion of dye particles, the large surface areas of the nanofibres and the ability to functionalise the nanofibre surfaces can be utilised for dye removal.

Nanofibres synthesised from biopolymers are increasingly gaining favour as adsorbents for dye removal due to their environmental and sustainability benefits [165–168]. Cellulose nanofibres have been successfully used in the removal of dye particles from the water as they contain reactive hydroxyl (−OH) functional groups on their surfaces that adhere to dye molecules [169]. A commonly used method for cellulose membrane modification involves an oxidative surface treatment using (2,2,6,6-tetramethyl-piperidin-1-yl)oxyl (TEMPO). However, TEMPO is a toxic substance and thus it has a limited suitability for large scale use [170]. Recently, a more environmentally friendly solvent-free method has been reported using Meldrum's acid to modify cellulose-based polyvinylidene fluoride (PVDF) membranes. This treatment resulted in the enhanced adsorption of crystal violet, a positively charged (cationic) dye, from contaminated water [171]. Furthermore, Aziz et al. reported the removal of negatively charged (anionic) dyes, using silk fibroin (SF)/polyacrylonitrile (PAN) double-layer nanofilters with the addition of polyaniline (PANI)/TiO_2 nanoparticles as modifying agents [172]. The nanoparticles were also found to increase the strength and elasticity of the fibres in the nanofilters.

Amine-functionalisation is also an effective modification treatment for nanofibres due to the pollutant-chelating capacity of the amine functional groups [173]. For example, cobalt-ferrite nanofibres (Co-ferrite NF) were recently modified by L-arginine to complex with both anionic and cationic dyes. It was shown that the adsorption of the anionic dye decreased as the pH was increased due to reductions in electrostatic attractive forces. Alkaline conditions also encouraged the adsorption of a cationic dye due to the negative charge of the adsorbent surface. Cyclodextrins have also been utilized for dye removal.

For example, a simple filtration method for the functionalization of carbonaceous nanofibres with β-CD has proven to remove fuchsine acid [148].

Heavy metals removal

Molecular imprinted polymers (MIPs) are polymer particles that are being utilised for the removal of heavy metals. MIPs can be created to have a "memory" of the shape and the functional groups of a template molecule. Therefore, they can be designed to have high selectivity and affinity for a target molecule. They are synthesised by complex formations between template molecules and functional monomers by either covalent or non-covalent interactions [174] and provide the advantage of high selectivity and specificity towards a given analyte [175]. However, the presence of significant hydrophobic interactions between the MIPs and the template molecules lead to being driven by hydrophobic interactions with nonspecific bindings in pure aqueous media. To solve this problem, G. Pan et al., synthesised MIPS with ultrathin hydrophilic shells that showed greater water compatibility [176]. Luo et al. have reported the preparation of Pb (II) ion-imprinted polymers with hydrophilic bi-component polymer brushes. The polymer showed high Pb (II) specificity as well as anti-clogging properties [177]. Arsenic and selenium removal have also been reported with the use of MIPs [178]. Not many studies have been performed to date to investigate the functionalization of electrospun nanofibres with MIPs, especially for the removal of heavy metals from wastewater. This is seen as an emerging technology with great potential, and further research in this area is anticipated.

Charge modification is another common technique to prevent heavy metal particles from binding to membranes. For example, amines have been used to modify TiO_2 nanoparticles to carry a positive charge. The resultant modified nanoparticles have been used to functionalise PAN/CNT for chromium removal from wastewater. Chromium exists in two oxidation states, namely Cr (VI) and Cr (III). Cr (VI) is more toxic, carcinogenic and mutagenic to living organisms when compared to Cr (III) [179,180]. Such charge modified PAN/CNT shows a remarkable removal proficiency for Cr (VI) [181]. In the paper, the removal was predicted to be based on both mechanisms of adsorption and reduction, which is noteworthy as the reduction of Cr (VI) to Cr (III) can decrease the toxicity largely. In addition, the paper also showed that the adsorption capacity remained at 80% even after 5 times usage, indicating a good reusability factor. The researchers have achieved further

success in using the same membrane for arsenic As (III) and As (V) removal [182]. However, SEM imaging showed that the pores of the membrane were largely blocked after modification, indicating that despite the good heavy metal affinity, they would have poor permeability if used as filtration membranes.
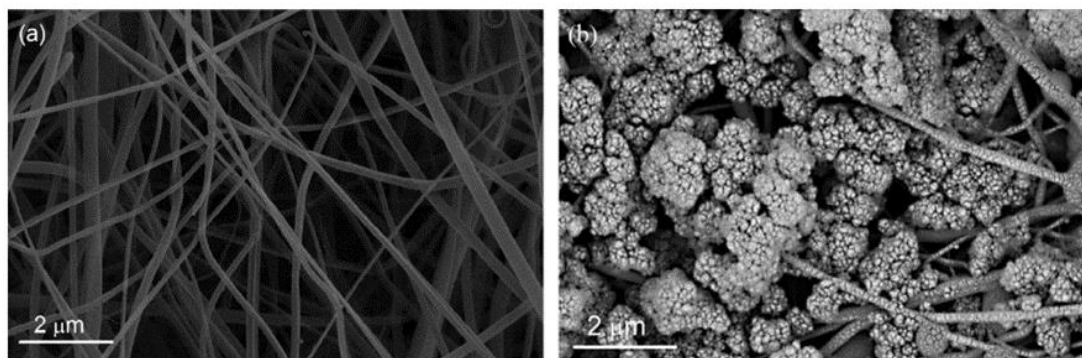
Figure 8: SEM images of (a) PAN nanofibres and (b) PAN-CNT/TiO$_2$-NH$_2$

Furthermore, Kumar et al. have applied a simple oxidation modification technique to polyaniline/g-C$_3$N$_4$ (graphitic carbon nitride)nanofibres using a ternary mixture of H$_2$SO$_4$, HNO$_3$ and H$_2$O$_2$ [183]. The nanofibres developed a net positive charge on their surfaces, which provided the resultant nanofibre composite with selective binding capacity for Cr (VI). Oxidation with TEMPO can also enhance the absorption affinity of Copper (II), as the introduced carboxylate groups have an affinity for Cu^{++} ions. The authors further demonstrated that these oxidized membranes could also be used for other metals such as Ni (II), Cr (III) and Zn (II). However, as stated previously, the toxicity of TEMPO should be taken into consideration.

In summary, current methods for purifying heavy metal ions are based on methods that are typically expensive and toxic and there is a great need for new cost-effective and bio-compatible approaches.

Antimicrobial removal and antifouling effects

Various pre-functionalised membranes are used for the detection and removal of pathogens, where the modification agents are either simply immobilised or covalently bonded to the membranes [184]. Different kinds of nanofibres have been electrospun and studied for the purpose of pathogen removal. Some active agents that have been used

to modify nanofibre surfaces include metal nanoparticles, antibiotics, triclosan, chlorhexidine and biguanides [185].

The incorporation of silver nanoparticles into filtration membranes can result in good antibacterial properties. The use of silver nanoparticles has been gaining a lot of recent attention as they are very effective antimicrobial agents, even when used at lower concentrations. They are also considered to be non-toxic, have FDA approval, are widely accepted in filtration products, and are easy and inexpensive to synthesise [185]. Dubey et al. encapsulated silver nanoparticles into a hydrophilic-hydrophobic polymer blend of poly(ethylene oxide) and polycaprolactone (PCL) [186]. Apart from the antibacterial resistance by *E. coli*, the addition of silver nanoparticles also reduced the fibre diameter from an average of 150-300 nm to an average of 70-150 nm and enhanced the surface roughness. A recent study is worth a mention because of the use of a low-cost iron (Fe) powder to supplement the use of the more expensive silver (Ag) particles. β-cyclodextrin and cellulose nanofibres were used in the ratio of 1:1 polymer concentration to achieve bead-free nanofibres to which they added Fe and Ag particles [187]. The particle modified nanofibre membrane showed antibacterial activity against 12 pathogenic bacterial strains, showing the greatest antibacterial activity against *E. faecalis* and *P. mirabilis*.

Membrane fouling can cause severe reductions in the flux and quality of filtered water. Cyclodextrins are often used as antifouling agents in membranes as they have the ability to provide hydrophilisation [151,188]. Hydrophilicity is a desired property of a filtration membrane that increases permeation and provides an anti-fouling effect. However, methods to make membranes more hydrophilic can be complex. Yu et al. reported a simple method of dip coating PVDF membranes in a boron-cadmium solution to make them more hydrophilic [189]. The resultants membranes showed an increase in water flux and as well as remarkable antifouling properties.

1.5 Kode Technology modification

Kode Technology is a surface engineering technology that enables modification of various biological and non-biological surfaces [190,191]. The modification is achieved by Function-Spacer-Lipid (FSL) or Kode constructs that are amphiphilic molecules able to disperse in water and then self-assemble into biological membranes or onto solid surfaces. Modification by these constructs is very easy and is achieved by simple contact of the surface with an appropriately buffered solution containing one or more FSLs. FSLs have

already been used in a variety of techniques including antibody specificity mapping, antibody/toxin neutralization, diagnostic assays, immune system manipulation, and animal modelling of transfusion reactions [191].

As reviewed in the papers by Barr and Williams et al., FSL constructs are made of three parts that play different roles in surface functionalisation [192,193]. The hydrophobic lipid structure (L) helps in anchoring the constructs to the membrane or surfaces. The spacer (S) provides the distance between the functional head surface, providing optimised orientation. It also imparts solubility to the construct. The functional head group (F) can be comprised of any functional moiety that can actively modify surface properties.

The most commonly used lipid for FSL construct is dioleoylphosphatidylethanolamine (DOPE). It is a membrane phospholipid that works efficiently with biological assays. Sterol and ceramide are examples of few other lipids that have been used. The spacers are either short adipate linker (1 nm) or a longer carboxymethylglycine (CMG) motif (7 nm). They help in increasing the distance of the functional group from the surface providing flexibility to the construct [191]. The functional head groups can include different molecules such as polyamine, carbohydrates, peptides, fluorescent markers and antimicrobial agents. The three distinct parts of FSL constructs can be compared to a Lego structure (a building block toy figure) where 'F' is comparable to head that gives functionality, 'S' is similar to the body that separates head from the leg and provides some flexibility in the body and L is comparable to leg that helps in firm attachment. Figure 9 illustrates the schematic of different FSL constructs, compared with Lego toy figures.
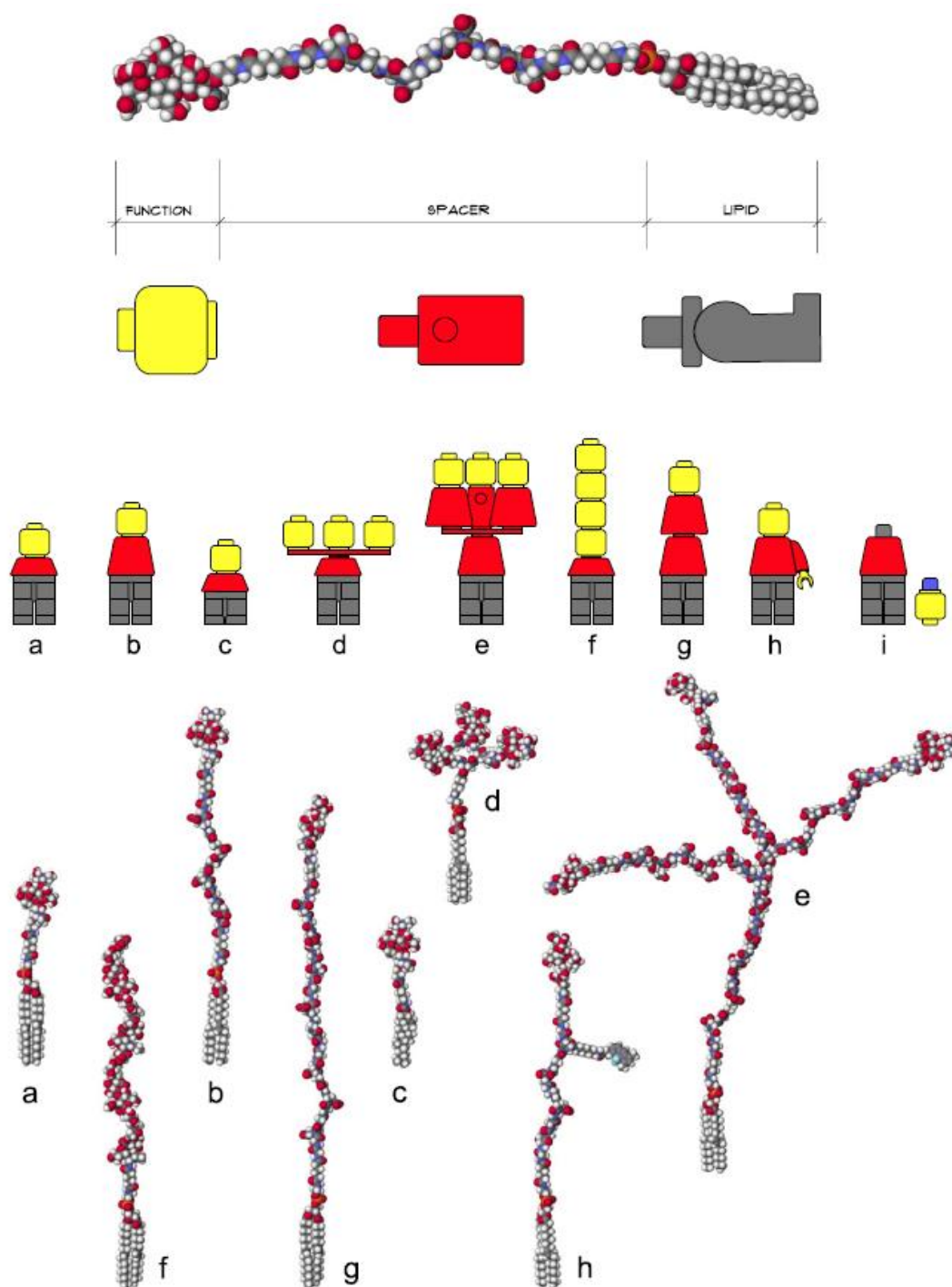
Figure 9: Schematic representation of different FSL constructs. The upper image shows a generic Kodeconstruct based on a carboxymethylglycine (CMG) spacer linked to a DOPE lipid tail. The 'building block toy figure' representations beneath show a yellow head representative of a single type of functional head, the red body represents a spacer, and the grey legs represent a lipid tail. The 9 structures shown at the bottom of the figure are space-filling molecular models of the building block toy figures with each having the same tetrasaccharide blood group A functional head except model which has an (8-mer) hyaluronic acid functional head. Variation representations shown are (a) short 1 nm adipate spacer, (b) CMG 7 nm spacer, (c) sterol lipid instead of DOPE, (d) clustered head, (e) trimeric CMG template, (f) linear repeating functional heads, (g) double length linear CMG spacer and (h) functionalised CMG spacer where the spacer can undertake a secondary function, in this example, the fluorophore BODIPY is attached, secondarily attached functional head. Figure copyright of Kode Biotech and reproduced with permission[190].

Initially, Kode Technology was mostly used to modify surfaces with glycans [191]. Regarding surface modification of nanofibre, Barr et al. reported the first application of glycan-based Kode constructs to functionalise different nanofibre surfaces including PA66, CA and PVB [192]. The blood group glycans were printed on a nanofibre surface in alphanumeric form using a bioprinting method. Then, enzyme immunoassay was done by adding antibodies, followed by a phosphate labelled anti-immunoglobulin conjugate and a chromogenic substrate. The glycans were then easily detected with monoclonal antibodies, identified by the appearance of alphanumeric codes. Figure 10 represents an enzyme immunoassay (EIA) done on blood group antigen A printed on nanofibres with 16 different monoclonal anti-A reagents.

Other non-glycan functional moieties have also been explored over the years [194,195]. However, this thesis reports the first example of modification of nanofibres with charged constructs such as FSL-SPM that has polyamine functional head and FSL-Z that has a simple functional head and the charge is provided by its spacer. Unlike blood groups containing FSLs, the constructs used in this thesis do not have the ability to be bound with a chromogenic substrate to be identified through EIA methods. Therefore, other detection methods have been attempted. It is also the first time that the FSL modified nanofibres have been used for adsorption or filtration of particulate matter.
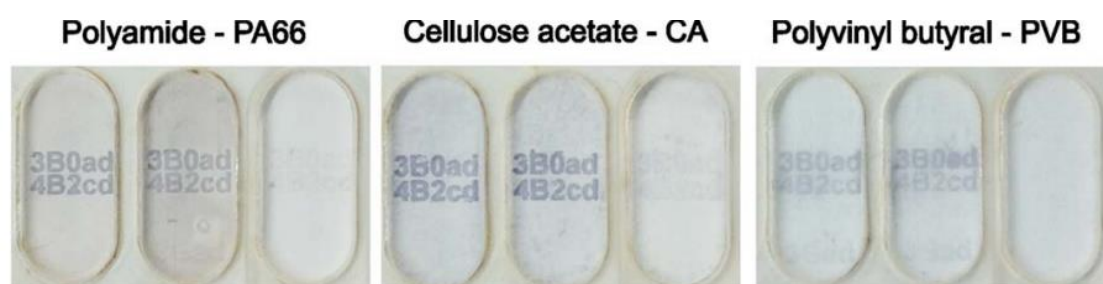
Figure 10: Anti-A enzyme immunoassay on nanofibres. Result of a printed FSL enzyme immunoassay on the three different nanofibre membranes and tested against different monoclonal anti-A reagents [196]. Different FSL glycan constructs were printed as unique codes onto nanofibre membranes, which were then constructed into microplates. Different antibodies were then added to each well, followed by a phosphatase labelled anti-immunoglobulin conjugate and a precipitating chromogenic substrate (with appropriate washing steps). Printed FSL codes only become visible if they have reacted with the primary antibody.

There are some limitations of Kode Technology that should be considered. Although, Kode constructs are known to coat all biological and non-biological surfaces [193,197], the exact mechanism(s) that allows these constructs to modify surfaces is variable and

depends on the variable properties of the surface being modified. Almost certainly a variety of different mechanisms must occur on the same surface including formation of bilayers, multi-layers, aggregation and self-association, all driven by the amphipathic design of the Kode construct and the unique properties of the surface being coated. Therefore, being able to measure or describe the coating mechanism is complicated, and further compounded by many factors including the diversity in functional heads, spacer and lipid components of Kode constructs. Methods such as NMR, AFM and other tools have been applied to try and quantify the amount of Kode constructs on the surfaces and have been used for characterisation of surface modification. However, no firm conclusions have been able to be derived as to the mechanisms of coating. However coating procedures are usually followed by a washing step, where it is believed that only the surface bound layer is reasonably firmly attached, while the additional coating layers are less firmly bound and are easily lost during washing, with the consequence that washed surfaces probably only have a monolayer coating. Unfortunately, monolayers are very difficult to directly measure, or even detect, and therefore most methods of detection are through secondary measurements, such as EIA or binding assay. Additionally, as Kode Technology is based on non-covalent modification of surfaces it is not as robust as covalent attachment modification. Non-covalent coatings can usually be reversed with changes in environmental parameters such as temperature, moisture or pH, and the Kode compounds are more susceptible to degradation due to their partial biological composition (i.e. lipids tails, amino-acid spacers, biological bonds). Further, in this study, the coating methods and potential impacts on stability of Kode constructs on surfaces were done with very little optimisation. Previously, stability studies have been done using various Kode constructs on different surfaces, showing that Kode constructs are stable on nanofibre surfaces for up to 8 months [192]. Having in this research established the proof-of-concepts relating to coating, further development is still needed to optimise the coating parameters in conjunction with developing appropriate storage conditions for potential products. All the same the stability achieved without optimisation is compatible with product design, and following optimization, it is anticipated product appropriately package and stored would be stable for at least 6-12 months, if not much longer.

1.6   Rationale and significance of the study

The rationale and significance of this research can be justified from the following aspects:

1. ### The need for modified membranes

   Fine particulate matter in air and water cause various health hazards and detrimental environmental impacts. Conventional filters capture pollutants based on size exclusion. Such filters have a small pore size and do not provide good flow rate. Surface modification techniques can be used to functionalise membranes so that filtration does not only depend on the pore-size but also on the active functions of the filters. This could potentially help to develop efficient filters where good capture and good flow rate are not mutually exclusive. Nanofibres are thin non-woven fibres with diameters less than 1000 nm. They are considered as advanced materials for use as filtration media. The surface properties of nanofibres can be greatly enhanced due to their advantageous property of large surface area. Modifying these nanostructures can help to trap pollutants based on an active capture mechanism with maximization of functions. The growing need for advanced material filters capable of filtering diverse kinds of pollutants without having to compromise in the flow rate calls for the need to functionalise filtration membranes.

2. ### The challenges of modification:

   Not many technologies have been recognized to date as being able to coat surfaces without prior treatment of the surface. Functionalisation of membranes can be done using various techniques but most modifying procedures are complex and depend on harsh conditions. Regarding nanofibres, modifications have been done in the past using various molecules and techniques [137,198,199]. However, they come with several limitations such as introduction of multistep processes, bio-incompatibility, denaturation of the bioactive compounds, entrapment of biomaterials inside the fibres, corruption of fibre integrity and poor anchoring of active compounds [196]. Electrospinning is the most commonly used method for nanofibre manufacture and depends on various parameters one of which is charge. Therefore, functionalising them with charged molecules still stands as a challenge. Moreover, there is possible loss of functions during

production as described by studies of Lockwood and Ding [200], where adsorption capacity of nanofibre membranes were lost or reduced after surface modification. Additionally, in most cases where functional groups cannot be grafted directly onto any polymer surface, a linker molecule along with the desired exposed functional groups have to be tethered to the fibre. However, the involved procedures are complicated. Therefore, more research has to be done on such standardized designs so that functionalisation procedure can be more effective yet simple.

3. An alternative approach to modification:

KodeTechnology is a rapid surface engineering technology that is used to modify or functionalise any biological and synthetic surface. It is based on Function-Spacer-Lipid (FSL) constructs. As implicit in the name, the constructs consist of a functional head supported by a spacer and a lipid tail which serve to make the construct amphipathic. It is a simple procedure where the constructs spontaneously self-assemble onto the surfaces without the need for pre-treatment. It could be an effective approach to actively capture pollutants without the need for complex modification strategies.

1.7   Aim

The aims of this research are:

1. To investigate the suitability of Kode Technology in functionalising nanofibres to create surface-modified filters.
2. To synthesise and characterise micro and nano-sized pollutants or surrogates in air and water.
3. To assess the ability of modified nanofibres to capture synthesised pollutants by process of adsorption and filtration.
4. To analyse the potential of modified nanofibres to capture biological particles.

Chapter 2: Liquid particulates capture – methods and results

One of the aspects of this research was to address whether FSL modification of nanofibres could be applied to capture nanoparticles in liquid phase through two different processes of adsorption and filtration. This chapter will firstly concentrate on characterisation of different nanofibre surfaces and FSL or Kode constructs and the success and limitations of surface modification using the constructs. Secondly, the application of Kode modified surfaces to capture contaminants will be shown. This chapter will also compare and analyse the process of adsorption or filtration using parameters such as types of nanofibre surface, types of Kode constructs, types of nanoparticles, types of contaminants, concentrations of constructs and contaminants, solvents for construct dilution and other physiological conditions such as time and pH.

2.1   Nanofibre characterisation

Electrospun nanofibres were supplied by Revolution Fibres Ltd, NZ. Different polymer-based nanofibre mats were received and were modified using Kode constructs in the lab. Polycaprolactone (PCL), polyamide 6,6 (PA66) or nylon, poly (methyl methacrylate) (PMMA) and polyvinyl butyrate (PVB) are some examples of polymers that have been used for this study. Scanning electron microscopy was used for characterisation of fibre thickness, morphology and Kode modification. Contact angle measurement was done for the analysis of hydrophobicity of surfaces.

2.1.1   Scanning electron microscopy (SEM) analysis

Method overview

Hitachi SU-70 was used for SEM. Figure 11 shows SEM images of different nanofibres at different magnifications observed at 5.0 kV voltage of an electron beam. Platinum sputter coating was done for 40s to improve the conductivity of fibres that aided in better visualisation.
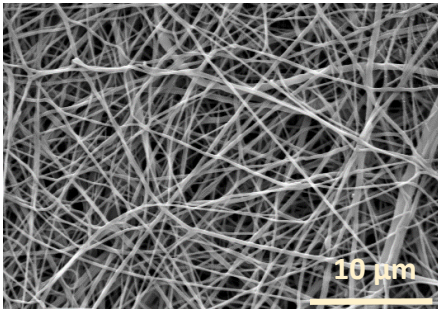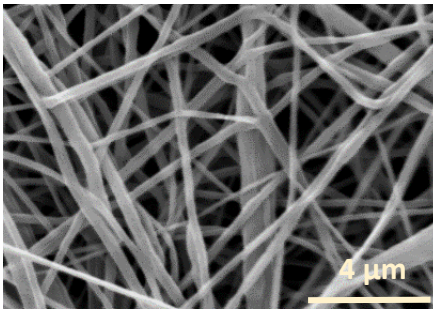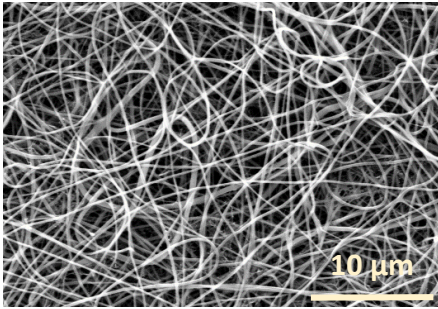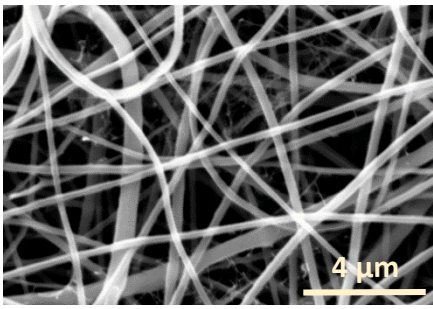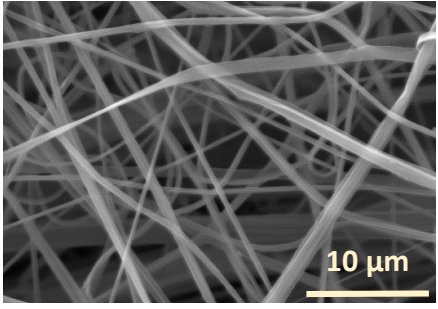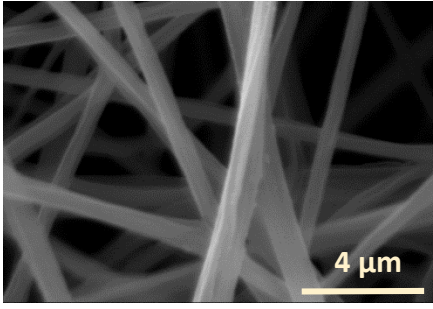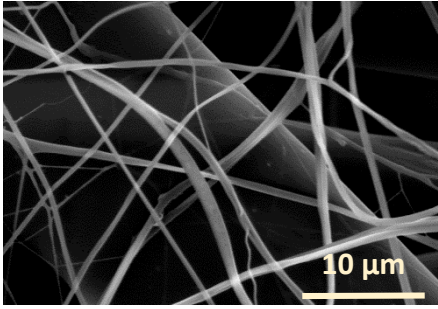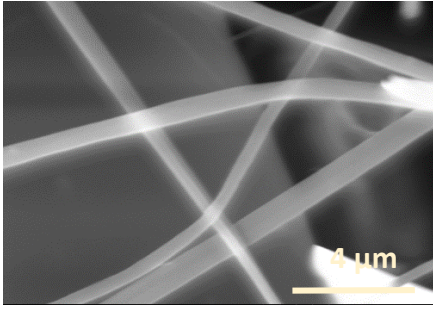
Nanofibre	Magnification	
	x3.5k	x12.0k

Figure 11: SEM characterisation of different nanofibres.

Results and interpretations

The fibre diameter was observed to be less than 1000 nm for all samples analysed. Morphologies of all fibres were found to be similar to each other. There was no significant difference in structures or surface roughness. The fibres were smooth and uniform throughout the area of sample analysed. However, we can observe the difference in fibre diameter among different types of fibres, which is a result of differences in polymer type and its effect during electrospinning.

2.1.2   Contact angle measurement

The wetting behaviour of materials is an important surface property that depends on the chemical composition and microstructure of the surface. Adhesive forces between a liquid and solid cause the liquid to spread effectively while the cohesive forces are responsible for the liquid to ball up. These forces can be analysed by recording the contact angles (CA) of the probing liquids on the sample surface. A contact angle higher than 90° indicates hydrophobicity of the surface [201].

Optical tensiometer (Attention Theta) was used to measure water contact angles. Two microliters of MilliQ water was dropped on the surface of different nanofibres and CA was recorded by a high-speed camera at a different time in milliseconds of contact time. Values were averaged to get mean contact angles. Surface roughness affects the measurement of contact angles, which should also be accounted. For this study, it was assumed that water coats the microstructure of nanofibres equally and only static contact angle was recorded. However, it should be noted that a dynamic contact angle measurement that can be calculated by wetting and de-wetting methods could give results that are more reliable [202].

Results and interpretations

Figure 12 shows that CA for all surfaces was measured to be above 90°, indicating that these surfaces are hydrophobic. Such surfaces are resistant to contact with liquid and therefore difficult to coat by modifying agents. A good surface modification technique requires a balance between the hydrophobic and hydrophilic aspects so that a wider range of modifying molecules can be utilised. If a surface were too hydrophobic, modifying solutions that are hydrophilic in nature would not be capable to spread evenly,

resulting in a non-uniformly modified surface. On the other hand, if a surface were too hydrophilic, there could be reduced interaction with hydrophobic modifying agents. The study did not focus on a specific range or value of contact angles of the surfaces used. However, the contact angle investigation was done to better understand how the water-wetting property affected the coating process.
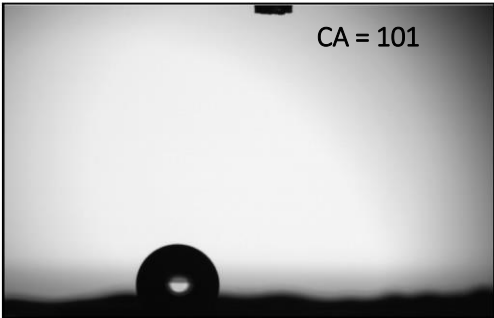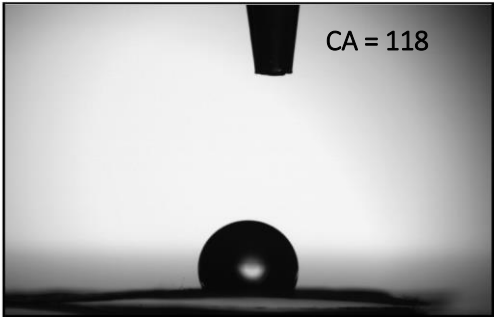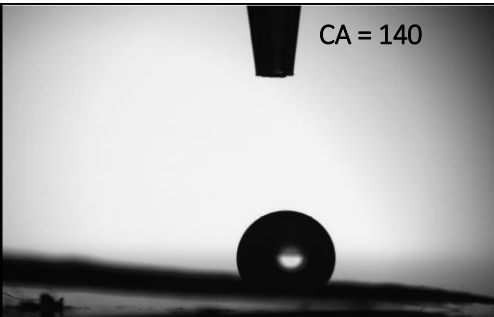
Nanofibre	Waterdrop
PCL	CA = 101
Nylon	CA = 118
PMMA	CA = 140

Figure 12: Images of a water droplet on different nanofibres and their average contact angles. PMMA is observed to be more hydrophobic, followed by PA66 and PCL.

2.2 Kode Technology modification of nanofibres

2.2.1 Analysis of Kode constructs

For this study, FSL with charged functional groups were used as major surface modifying agents. Charge plays an important role in adhesion of particles to filter surface. Based on the electrostatic forces, charge modified filters could potentially adsorb particles that possess charge on their surface. Harmful particulate matters usually exhibit highly polar functional groups that could interact with polar surface [203]. Therefore, surface coating by polar molecules could potentially create filters that could actively attract more contaminants into the surface. Polyamines are good examples of such charged compounds that could be utilized for modification. They are organic compounds bearing more than two amino groups (primary and secondary, i.e. $-NH_2$ and $-NH-$) and can be positively charged and therefore interact with negatively charged particles.

All Kode constructs were obtained in a powdered form and were synthesised for this project by the laboratory of Carbohydrates, Shemyakin-Ovchinnikov Institute of Bioorganic Chemistry, Russian Academy of Sciences in Moscow by standardised procedures [191,197]. Quality control of these compounds was primarily NMR, mass spectroscopy and thin layer chromatography as described elsewhere [191,197]. All compounds were verified to as being >95% pure (results not shown). Firstly, a biogenic polyamine called spermine was analysed as a potential functional head. Spermine has two primary and two secondary amino groups. It is present in most organisms as an essential growth factor [204]. Generally, it exists as a polycation at pH <7. It functions to stabilize the helical structure of nucleic acids, particularly in viruses. It also plays role in cellular metabolism and proliferation and has previously been utilized for modification of bio surfaces and proteins through covalent and non-covalent interactions for medical applications [204–206].

Spermine was used as an active functional head the Kode construct and the molecule was called FSL-spermine (FSL-SPM). It constitutes an adipate (Ad) as a spacer to connect spermine residue with a dioleoylphosphatidylethanolamine (DOPE) lipid tail (Figure 13). It was expected that spermine would provide an overall positive charge to the construct and that FSL-SPM could modify nanofibre surfaces by adding a positive charge to the surface. This way, the surfaces could actively capture negatively charged particles. Additional physical forces acting between spermine and negatively charged particles

were assumed: 1) hydrogen bonding and 2) point-like hydrophobic interactions due to the $-(CH_2)_3-$ and $-(CH_2)_4-$ bridges between nitrogen atoms of spermine.

FSL-SPM was utilised as a primary modifying agent against which all other constructs were analysed and tested for their ability to coat and capture particles. Although spermine has been used to coat surfaces for medical applications previously, this thesis presents the first example of its use in filtration applications. This is also the first time that any Kode construct has been used to modify nanofibre surfaces for pollutants removal.
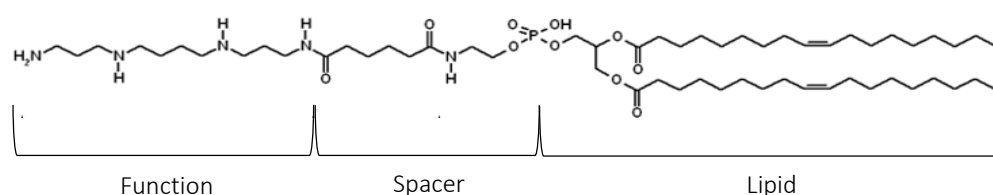
Figure 13: Structure of FSL-SPM illustrating three different parts of the construct. Spermine is the functional head; the spacer is made up of adipate and the lipid is made up of DOPE.

Fourier-transform infrared spectroscopy (FTIR) characterisation of powdered form of FSL-SPM was done to confirm the presence of expected functional groups (Figure 14). The characteristic amide and amine stretch for N-H and C=O are observed as peaks in the regions of in 3700-3500, 3500-3300 and 1690-1630 regions as mentioned in the literature [207]. The presence of peaks in these regions confirmed the presence of polyamine in the sample. Other peaks correspond to several C=O, O-H and C-H groups present in the construct. FTIR analysis has been further discussed in detail in section 2.2.5.
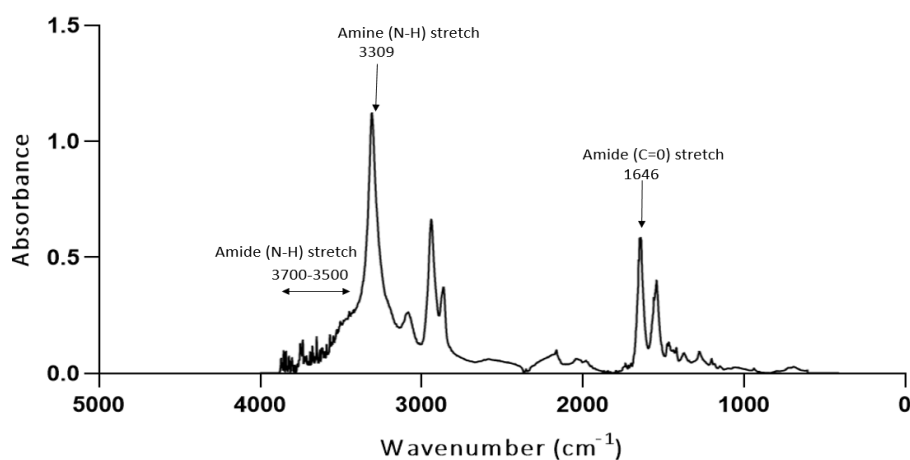
Figure 14: FTIR characterisation of FSL-SPM. The polyamine spermine in FSL-SPM contributes to N-H stretches resulting in the appearance of their characteristics peaks. Amide stretch is attributed to two CO groups of adipate spacer.

Apart from FSL-SPM, a variety of other FSLs derived from FSL-polyamines were tested for their ability to capture negatively charged particles. The FSL-polyamines have been listed below in Table 1.

Table 1: FSL-polyamines used for nanoparticle capture study.

Polyamine code	Chemical name
31-1	DOPE-Ad-Triethylenetetraamine
32-1	DOPE-Ad-1,2-Bis(3-aminopropylamine)ethane
33-1	DOPE-Ad-pentaethylenehexamine
36-1	DOPE-Ad-N,N'-Bis(3-aminopropyl)-1,3-propanediamine

A thin layer chromatography (TLC) assay was further done to characterise all polyamines including spermine and FSL-SPM and their signatures were compared on a TLC plate. TLC solvent was prepared using ethyl acetate, pyridine, acetic acid and water in the ratio of 3:1:1:1. After the TLC was run, ninhydrin (0.35%) was used to visualise polyamines on the plate. The principle behind using ninhydrin has been discussed in detail in section 2.2.4. In Figure 15, it is observed that spermine and FSL-SPM have only one spot which shows that they are pure compounds whereas other FSL-polyamines have separated into more than one spot, indicating they are made up of mixture of starting polyamine, aim FSL and isomeric FSLs where FS part is attached to an inner nitrogen atom of the amine.
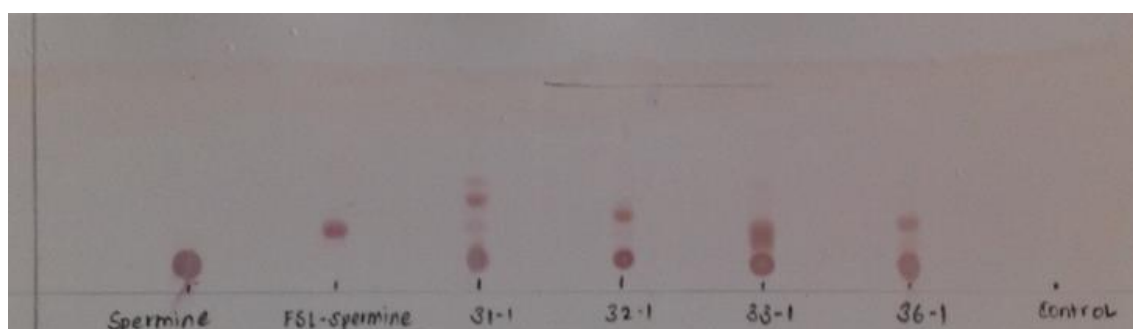
Figure 15: TLC characterisation of spermine and other FSL-polyamines. Spermine and FSL-SPM have only one spot, indicating their purity. Other polyamines have more than one spot, indicating presence of side product of chemical synthesis.

Another Kode Technology construct known as FSL-Z was also tested for the opposite effect, that is to adsorb positively charged particles. It is a family of FSL constructs each with a methyl molecule replacing the regular functional head. A variety of FSL-Z has been

engineered but the construct used for this study was made of two units of carboxymethylglycine (CMG) spacers linked with an adipate (Ad) group which is linked to a DOPE lipid tail (Figure 16a). Due to the presence of negatively charged carboxyl groups in the spacer, it was expected to provide an overall negative charge to the construct. FSL-biotin is another FSL-construct that was compared with FSL-Z for its efficiency in capturing positively charged particles. FSL-biotin has a similar structure to FSL-Z with respect to the spacer and lipid group but with an additional small functional head called biotin. Biotin is a neutrally charged hydrophobic molecule. Therefore, it was expected that FSL-biotin would carry a charge similar to that of FSL-Z (Figure 16 b) and as large quantities of it were available and it had some unique characteristics, it was studied in parallel with FSL-Z compounds.

a)
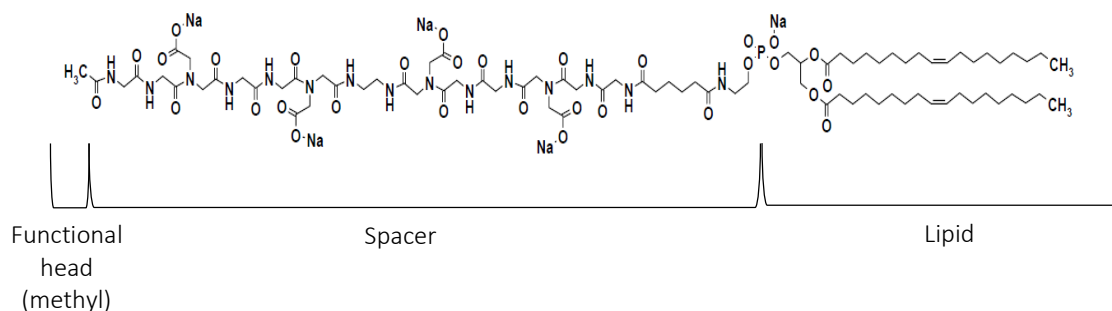
b)
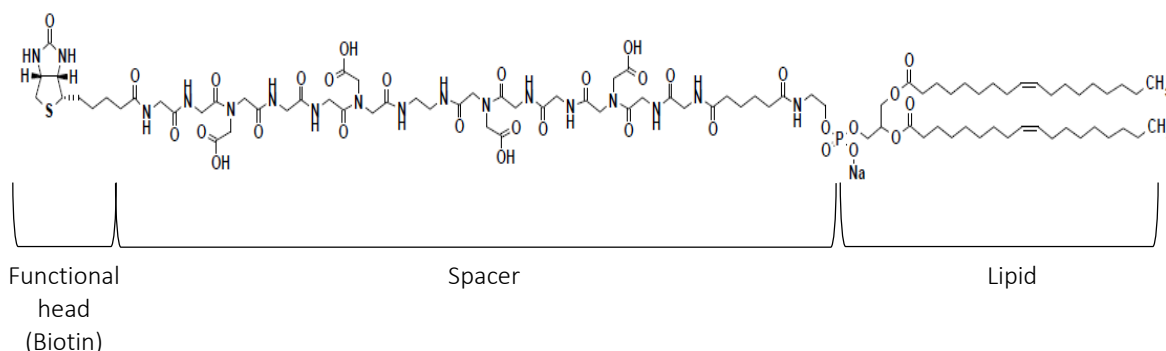
Figure 16: Structures of FSL constructs used to capture positively charged particles. a) structure of FSL-Z b) structure of FSL-biotin.

Malvern zeta sizer was used to confirm the charge of FSL-SPM and FSL-Z. It was predicted that FSL-SPM would have an overall positive charge due to the presence of positively charged spermine. FSL-Z and FSL-biotin were predicted to have a negative charge due to absence of a positively charged functional head and presence of a large negatively

charged spacer and several COOH groups. Zeta potential measurements validated these expectations (Figure 17). The charge of FSL-SPM was found to be 20 mV whereas the charge of FSL-biotin and FSL-Z was observed to be minus 25 and minus 30 respectively.
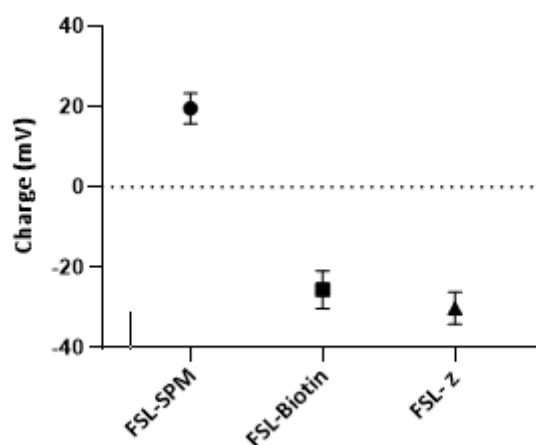
Figure 17: Comparison of charge of FSL constructs. FSL-SPM has a positive charge of 20mV. FSL-biotin and FSL-Z have negative charge of -25 and -30 mV respectively.

Table 2: List of FSL constructs used for the study.

FSL construct	Active (charged) group	Charge
FSL-SPM	Functional head	positive
FSL-Z	Spacer	negative
FSL-biotin	Functional head and spacer	negative
FSL polyamine 31-1	Functional head	positive
FSL polyamine 32-1	Functional head	positive
FSL polyamine 33-1	Functional head	positive
FSL polyamine 36-1	Functional head	positive

2.2.2 Immobilisation of Kode constructs onto nanofibre

The immobilisation or insertion of Kode constructs onto nanofibre surface was done by a standard coating method. A standard protocol was developed (referred to as Protocol 2.2.2 hereafter) that has been described below:

Protocol 2.2.2: Standard coating method

1. Nanofibre surface was washed with MilliQ water to remove any particles or contaminants on the surface and was allowed to dry at room temperature (RT).

2. The dried surface was cut into strips of desired area by outlining finely with a pencil and cutting with scissors.

3. Kode construct was diluted to desired concentrations (mg/mL) using a suitable solvent.

4. 100 µL of Kode construct was then dropped to a glass slide using a micropipette. 100 µL of solvent used to dilute the respective construct was also dropped alongside as control.

5. The desired area or cut strip of nanofibre was immediately dipped into the drop and allowed to sit. Each strip was incubated for a total of 2 minutes with turning the strip over after 1 minute to ensure even coating.

6. The coated strip was washed 3 times in MilliQ water to remove unbound Kode construct (potentially leaving a monolayer to remain on the surface). Washing was done by plating 2 mL of MilliQ water in 24 well plates and dipping the strip in different wells for 3 times.

7. The washed surface was allowed to dry at RT before using for assays.

Polycaprolactone (PCL) was chosen as a model polymer nanofibre to study the effect of FSL modification on fibre diameter and morphology. PCL is a biodegradable polymer commonly used in both air and water filtration. The thickness of the nanofibre mat was measured by weighing a meter square of the surface to be used. Considering even and smooth fabrication of nanofibres as determined by SEM, thickness was assumed to be same throughout the mat. A thickness of 4 gsm has been used for most assays in this study. Regarding FSL construct, FSL-SPM has been used to coat PCL surface for preliminary analysis of Kode Technology modification.

2.2.3 SEM and fibre diameter analysis

Morphological properties such as fibre diameter, uniformity, orientation and surface roughness are important characteristics of electrospun nanofibre. Most conventional techniques use harsh chemicals to modify surfaces resulting in damaged surfaces, drastic change in fibre diameters and blocked pores. Therefore, it is necessary to assess the impact of Kode modification on the morphology of nanofibres.

Measurement of mean fibre diameter and diameter distribution can provide information about how Kode constructs modify nanofibre surfaces. The most commonly used method for characterisation of nanofibre morphology has been manual measurement using SEM images and analysis tools such as Image J. However, it is time-consuming and systemically biased. Several imaging software has been developed in the past to get more precise data [208] but due to non-uniformity in fibre structures even along the length of a single fibre, an advanced software capable of measuring at multiple points is required.   Diameter J is an added plugin or algorithm to Image J software that can run automated analysis on multiple images within 60 seconds [209]. It can determine the fibre diameter at every pixel along the fibre to produce histogram diameters and therefore has been used in this study.

Method overview

SEM was used to visualize any change in fibre diameter of PCL after coating at different concentrations of FSL-SPM. PCL nanofibre strips of 52 mm^2 (5 mm x 10.5 mm) were coated with 0.01, 0.05, 0.5 and 1 mg/mL concentrations of FSL-SPM each, washed and dried using Protocol 2.2.2. Diameter J was used to analyse the change in fibre morphology after modification using the SEM images. Nanofibres were sputter-coated with platinum for 40s and visualised at 10kV voltage.

Results and interpretations

Increased mean fibre diameters after FSL-SPM coating confirmed the modification of surfaces. There was no significant change in fibre diameter up to 0.05 mg/mL but at 0.5 mg/mL and 1 mg/mL of coating, the mean fibre diameter was increased from 186 nm to 230 nm and 273 respectively (Refer to Table 3). The SEM images in Figure 18 show the change in morphology of the fibre mats at different concentrations of coating along with their respective diameter distribution graphs. The fibres remain intact and non-degraded

at all concentrations. However, at higher concentrations (0.5 mg/mL and 1 mg/mL), the pore sizes have decreased because of the coating layer. Fibre diameter distribution is consistent with the average diameter values obtained in Table 3.
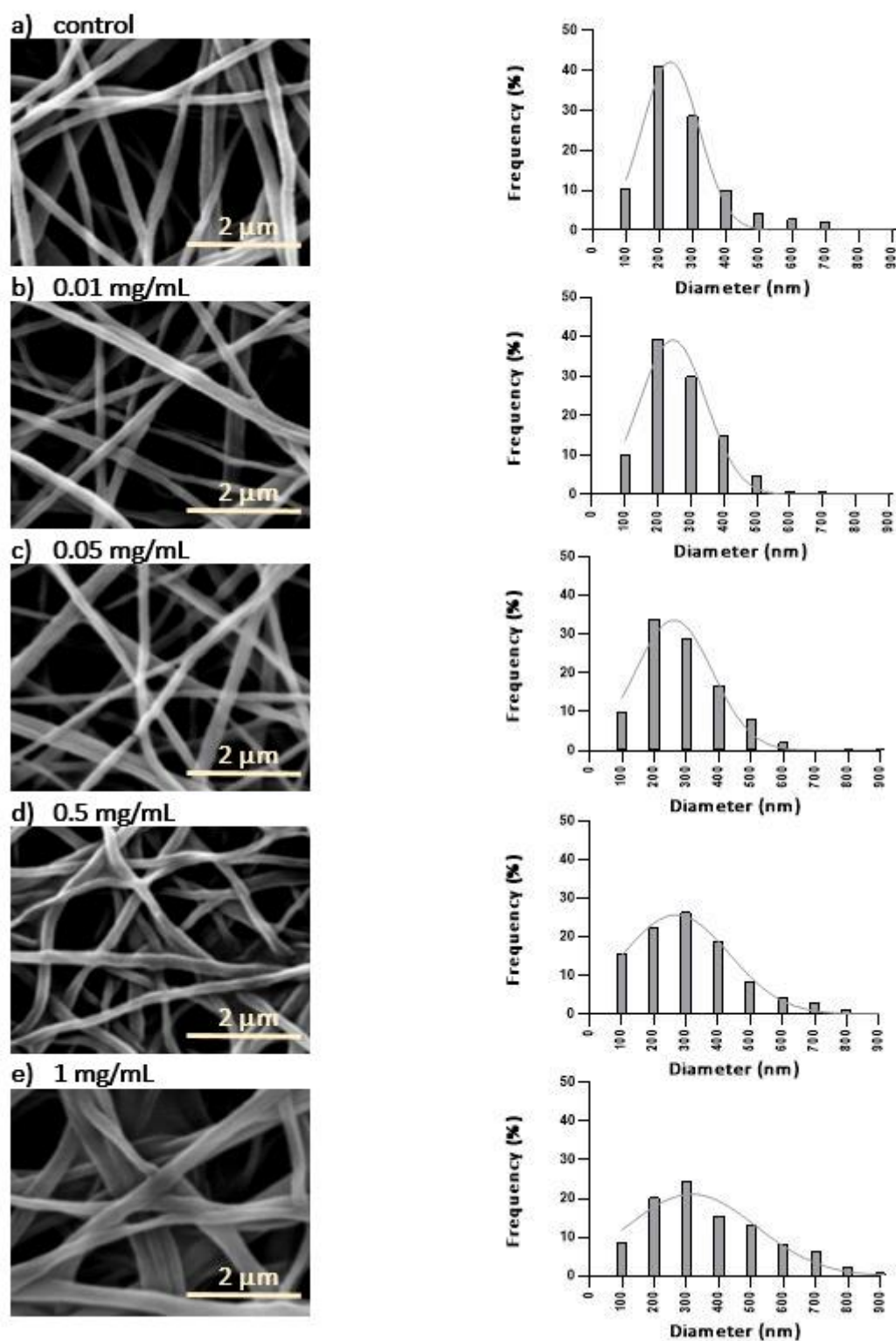
Figure 18: Effect of different concentrations of FSL-SPM coating on fibre diameter of PCL nanofibre a) control PCL nanofibre with no FSL-SPM coating, b) PCL nanofibre at 0.01 mg/mL FSL-SPM coating, c) at 0.05 mg/mL FSL-SPM coating, d) at 0.5 mg/mL FSL-SPM coating and e) at 1 mg/mL of FSL-SPM coating.

Table 3: Summary of fibre diameter of control and FSL-SPM coated PCL nanofibres.

FSL concentration (mg/mL)	Fibre diameter (nm)	Diameter SD ± (nm)	Skewness
0 (Control)	186	79	1.38
0.01	199	86	0.79
0.05	202	95	0.70
0.5	230	170	0.70
1	273	179	0.81

Table 3 summarises the diameter analysis results. The possible reason for an increase in fibre diameter at higher concentrations of 0.5 and 1 mg/mL could be that a web-like coating is seen on the fibre surface that has covered the distinct edges of fibres. This could have resulted in the discrepancies in the automated software analysis where multiple fibres might have been analysed as a single fibre.

However, for the lower concentration, the fibres are well separated from one another and there is no interference of the coating layer and thus it is interpreted that the fibre diameter calculations are valid and thus no significant increase in diameter is observed for coatings below 0.5 mg/mL.

To further investigate whether the coating layer could be a result of insufficient drying of the fibres before SEM visualisation two conditions were compared

1. The fibres were dried at room temperature and SEM analysis was done the next day.
2. The coated fibres were dried at room temperature and further kept in a petri-dish filled with desiccators for one week before analysis.

The fibres showed similar morphologies at 0.5 mg/mL and 1 mg/mL for both conditions as seen in Figure 19.

FSL-SPM coating	Dried at RT for one day	Dried at RT with desiccators for 1 week
0.5 mg/mL		
1 mg/mL		
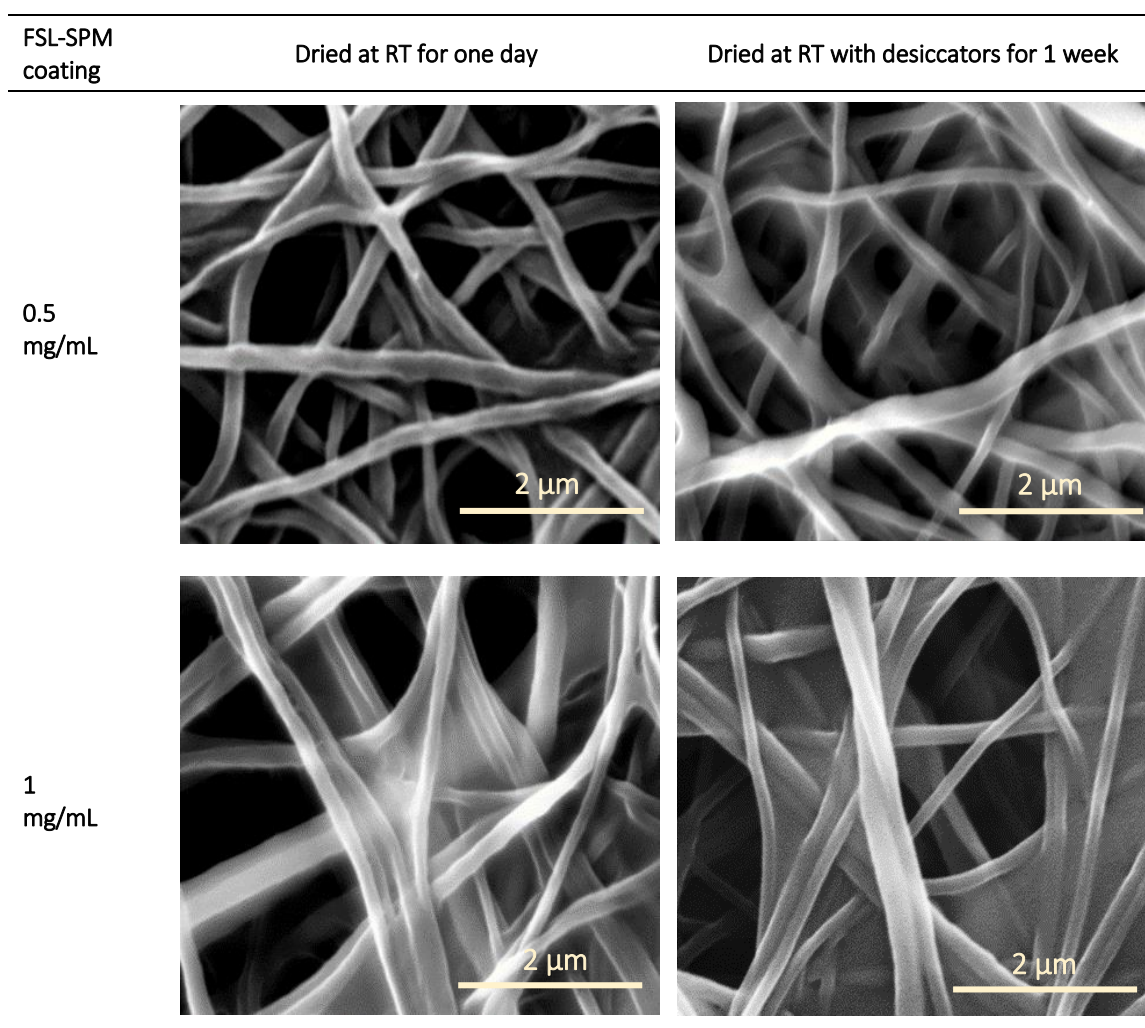
Figure 19: PCL nanofibre at two different drying conditions. At high concentrations of 0.5 and 1 mg/mL, the fibres appear to be thick with webbing even after extensively drying for one week, in the presence of desiccators.

While it is desired to have thin fibres with maximum pore size for filtration applications where usually good flow rate is required, fibres with increased diameter can be as effective for adsorption applications that are not flow rate dependent. Therefore, an increase in diameter or reduction in pore size at higher concentrations is not a disadvantage, when it comes to adsorption. Thus, hereafter, experiments have been designed to include all of these concentrations as parameters.

2.2.4 Ninhydrin derivatisation of FSL-SPM immobilised on nanofibres

Quantification of Kode constructs on modified nanofibres is necessary to understand the coating mechanism of constructs and to assess the true amount of construct required to capture or remove pollutants. Based on the coating method (Protocol 2.2.2), 100 μL volume of a particular construct is required to coat a nanofibre surface. However, there is a possibility that the entire volume used during coating is not immobilised on the

surface. Therefore, FSL-SPM was taken as a model construct to assess how much construct is adsorbed on the surface during the coating process. For this purpose, ninhydrin was used to quantify FSL-SPM based on the principle of chemical derivatisation. Ninhydrin is generally used to derivatise compounds with primary amino groups, forming a purple coloured product called Rheumann's purple [210]. The use of ninhydrin to measure polyamines such as putrescine, spermidine and spermine has been described by many authors in the past [211,212].

Method overview

Two molecules of ninhydrin are required to interact with polyamine. Therefore, an increasing concentration of FSL-SPM (made up in 100 μL of 95% ethanol) was mixed with 300 μL of 0.35% ninhydrin (also made up in 95% ethanol) to achieve the ratio of FSL-SPM: ninhydrin equivalent to 1:3. Ethanol was used at 95%, keeping in consideration that the extraction of FSL-SPM would be done using the same solvent. The mixture was then heated to 100°C for 5 minutes until the purple colour was developed. 100 μL of the purple complexed solution from each concentration of FSL-SPM was transferred to a 96-well plate and absorbance was measured at 570 nm. The calibration curve generated by this method is shown in Figure 20.

PCL nanofibre of area 100 mm² (10 mm x 10 mm) was coated with 0.5 mg/mL, 1 mg/mL and 2 mg/mL FSL-SPM using Protocol 2.2.2. The FSL-SPM adsorbed on the surfaces was extracted using 200 μL of 95% ethanol. 100 μL of the volume of the extracted solution was then transferred to a 96-well plate for absorbance analysis at 570 nm. The generated calibration curve was then used to quantify the amount of FSL-SPM present on respectively coated surfaces.
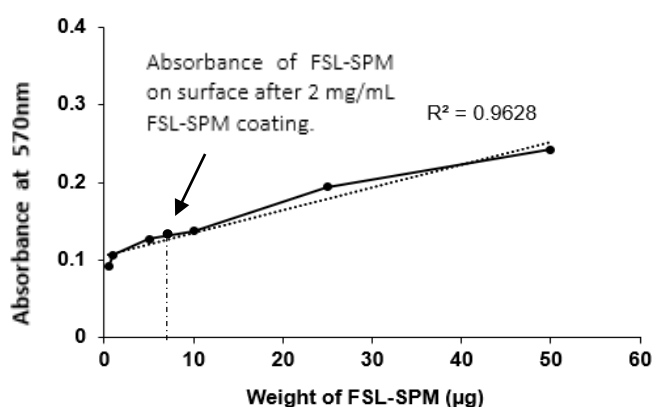
Figure 20: Calibration curve generated by ninhydrin derivatisation with FSL-SPM.

Results and interpretation

The method was not sensitive enough to quantify the amount of FSL-SPM extracted from the nanofibres coated with 0.5 and 1 mg/mL FSL-SPM, as the extracted concentration fell outside of the calibration curve. However, at 2 mg/mL of coating, 7 μg of FSL-SPM was quantified using the calibration curve. Since only 100 μL of 2 mg/mL was used to coat the surface (Protocol 2.2.2), a total amount of 200 μg was applied on the surface during the coating process and the results indicated that only 3.5% (7 μg) of the applied construct remained on the surface after washing. This finding is important in determining the true capacity of FSL-SPM in the removal of nanoparticles.

2.2.5 FTIR characterisation of FSL-SPM modified nanofibre

FTIR provides information about the structure of chemical groups in a substance. The technique works on the fact that bonds and groups of bonds vibrate at certain frequencies which can be used to get the molecular signatures of materials [213,214]. Spermine in FSL-SPM contains amine and amide groups giving rise to certain characteristic peaks in the region of 3700-3300 cm^{-1} of infrared radiation. Amide N-H stretching is observed in 3700-3500, amine N-H stretching is observed in 3500-3300 and amide C=O stretching is observed in 1690-1630 [215]. Those peaks could be used as a molecular signature of FSL-SPM on a nanofibre made up of a material having none of these specific peaks.

Method overview

PCL nanofibre was coated with 1 mg/mL FSL-SPM following Protocol 2.2.2. The surface was dried before analysing. The FTIR spectra of coated PCL was then compared with PCL with no FSL-SPM and pure FSL-SPM powder.

Results and interpretation

According to Figure 21a and b, it was observed that new peaks appeared in the FTIR spectra of modified PCL that corresponded with the characteristic amide and amine peaks present in the spectra of FSL-SPM powder. The FTIR results indicated the presence of FSL-SPM on the coated surface of PCL nanofibre.

a) 3700-3500 cm $^{-1}$

b) 3500-3300 cm $^{-1}$
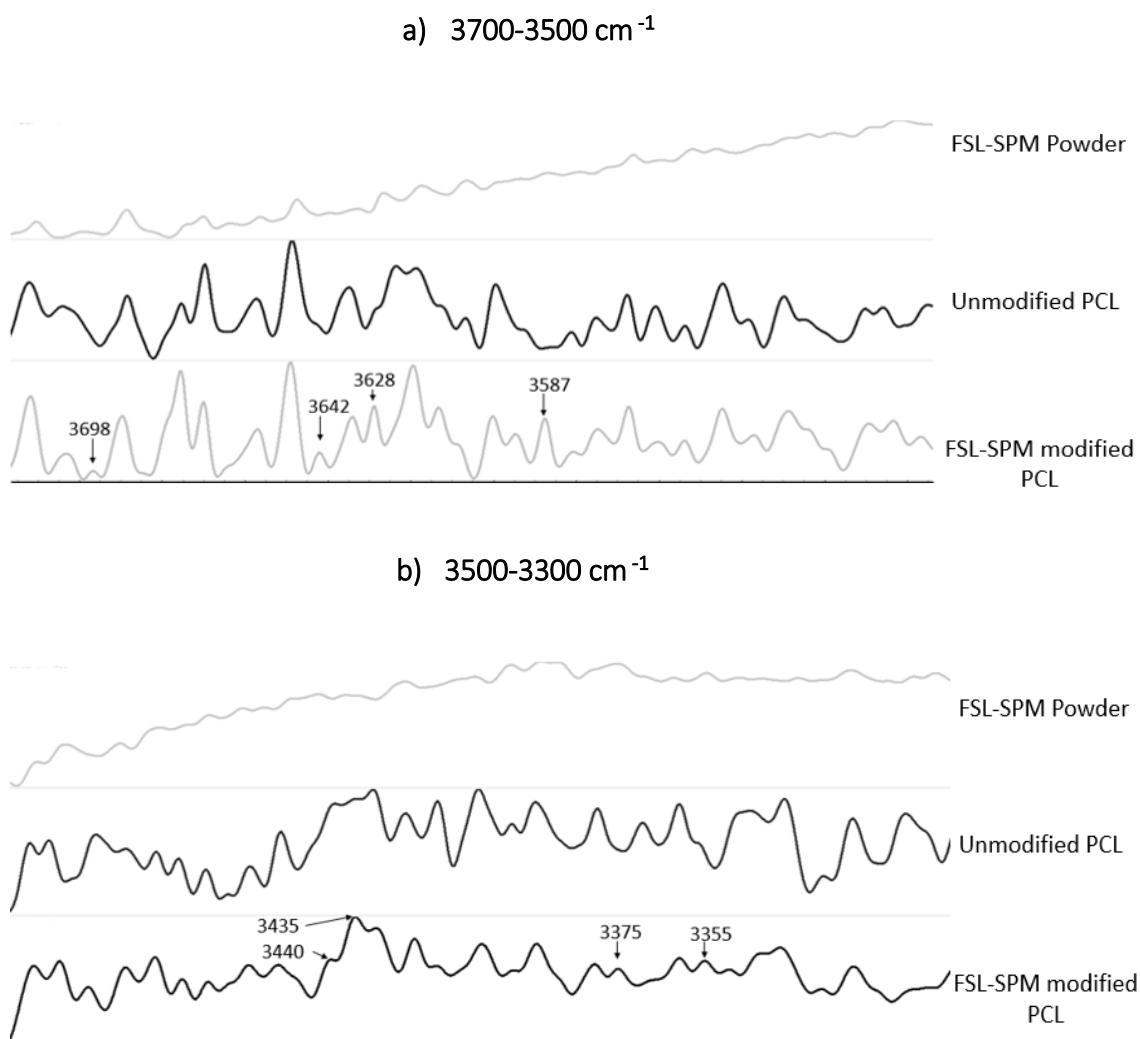
Figure 21: FTIR analysis of FSL-SPM modification of PCL nanofibre. a) shows the appearance of peaks on the FSL-SPM modified PCL that correspond with the peaks of FSL-SPM powder, which is not observed in the unmodified PCL surface. The peaks in this region (3700-3500 cm^{-1}) are caused by the amide (N-H) stretching. b) shows similar appearance of peaks on the modified surface corresponding to the peaks of FSL-SPM powder but in the region of 3500-3300 cm^{-1}. These peaks are caused by amine (N-H) stretching.

2.3   Synthesis and characterisation of nanoparticles

In house synthesised silver nanoparticles (Agnps) with negative and positive charge were used as surrogates for pollutant particles because of the feasibility of their characterisation, standardisation and quantification. Agnps were synthesised using different precursors and were characterised using ultra-violet visible spectroscopy (UV-Vis), scanning electron microscopy (SEM) and electron dispersive x-ray spectroscopy (EDS) for size, morphology and elemental analysis. A zeta-sizer (Malvern Zetasizer Nano

ZS) was further used to confirm the size and charge of the particles. pH of the Agnp solutions were analysed using a pH meter.

[-]Agnps were synthesised using the following protocol [216]

1. 2 g of glucose and 1 g of polyvinylpyrrolidone (PVP) (40,000 $gmol^{-1}$) was dissolved in 40 mL of MilliQ water and heated to 90°C. Glucose was used as a stabilising agent.

2. 0.5 g of silver nitrate ($AgNO_3$, >99.9% pure) was dissolved in 1 mL MilliQ water and was quickly added to the heated mixture. The appearance of brown colour indicated the formation of [-]Agnp.

3. The dispersion was held at 90°C for 1 hour and then left to cool at room temperature.

4. The particles were collected by centrifugation at 7200 rpm for 90 minutes for three times to remove excess glucose, NO_3^- oxidation products, excess PVP and Ag^+(Ultracentrifugation at 30,000 rpm for 30 minutes is preferred but this alternative was chosen in the absence of ultracentrifuge).

[+]Agnps were synthesised using the following protocol [216].

1. 1 g of polyethyleneimine (PEI) (25000 $gmol^{-1}$) was dissolved in 40 mL of water and heated to 90°C.

2. 0.5 g $AgNO_3$ was quickly added to the mixture and the dispersion was held at 90°C for 1 hour and left to cool at room temperature.

3. Since the particles did not settle down as quickly as [-]Agnp, the suspension was centrifuged at 7200 rpm for 120 minutes for three times to remove excess oxidation products and PEI.

Using these protocols, 35 batches of [-]Agnp and [+]Agnps each were synthesised the same day and mixed to get final suspensions of [-]Agnp and [+]Agnp separately. The multi-batch approach was done to maintain the consistency of characteristics of particles for all experiments as each batch of particles have difference in shape, size and charge as all these parameters are difficult to control in each synthesis experiment. Therefore, a large volume was synthesised the same day to prepare stock solutions. Final suspensions were kept at 4°C, covered with aluminium foil to protect from light. The stock solutions of both Agnps were then used for characterisation and other assays. UV-vis spectrophotometry was used to generate the standard absorbance graph for silver ions. A calibration curve

was then developed for quantitative analysis, using the maximum absorption peak based on the principle of Beer-Lamberts law [217]. The Agnp solutions were characterised by UV-Vis, SEM and EDS each time the nanoparticles experiments were conducted to confirm the stability of nanoparticles throughout all experiments. Moreover, controls were included in all the adsorption and filtration experiments to further access and confirm the stability of the particles.

2.3.1 UV-Vis spectroscopy

Method overview

Silver ions have a standard peak in the absorbance vs wavelength curve at 400-500 nm. UV-Visible spectra were used to confirm the presence of silver and find the λ_{max} (wavelength at which absorbance is maximum). Using the λ_{max}, a calibration curve was generated. Stock solutions (X) were diluted to different concentrations starting at 0.001% (v/v) of X to 0.3%(v/v) of X. 1 mL each of these dilutions were plated in 24 well plates for absorbance analysis.

Results and interpretation

As illustrated in Figure 22, the absorbance scan of both Agnp solutions was in agreement with the standard absorbance curve of silver found in literature [218]. It confirmed the successful synthesis of nanoparticles, giving the characteristic peak in between 400-500 nm. The wavelength of highest absorbance (λ_{max}) was noted to be 430 nm for [-]Agnp and 416 nm for [+]Agnp. Since the two values are not significantly different, 430 nm was used for generation of calibration curves for both Agnps. It was also calculated that for 1 mL volume of nanoparticle solutions, 80 μL:920 μL of [-]Agnp: H_2O solution gave similar absorbance value (≈0.5 at 430nm) as given by 65 μL:935 μL of [+]Agnp:H_2O.

Negatively charged silver nanoparticle or [-]Agnp

a)

b)
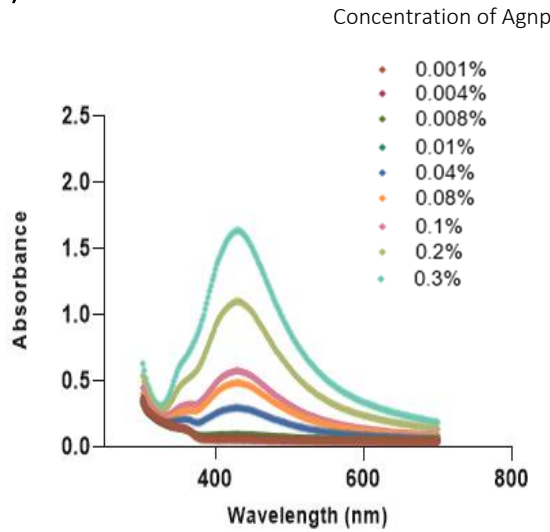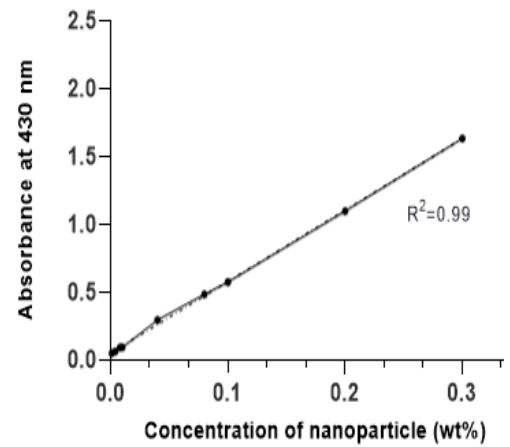
Positively charged silver nanoparticle or [+]Agnp

c)
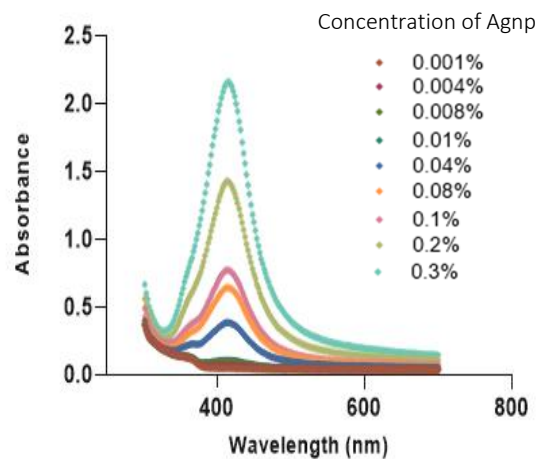
d)
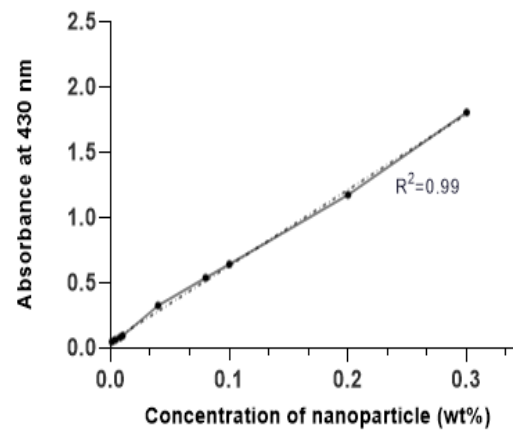
Figure 22: UV-vis characterisation of Agnps. a) and c) show the absorbance scan of different concentrations of [-]Agnp and [+]Agnp respectively, at wavelengths 300-700nm. Both absorbance curves are complementary with the characteristic absorbance curves of silver, cited in the literature, thus confirming the synthesis of silver nanoparticles. b) and d) are calibration curves of [-]Agnp and [+]Agnp respectively at 430nm. 430nm was chosen as the standard wavelength (λ_{max}) because at this wavelength, maximum absorbance value was achieved for all concentrations of [-]Agnp.

2.3.2 pH measurement

The pH of the nanoparticle suspension plays an important role in determining the size and charge of nanoparticles. Since the adsorption and filtration of nanoparticles by FSL constructs is largely charge-dependent, it is important to analyse the pH of the suspension because the charge on the surface of nanoparticles is highly dependent on the presence of H^+ and OH^- ions present in the suspension. The standard working solution

of both Agnps was named 1×, based on the results and interpretation of 2.3.1. The volumes of Agnp and water to make 1 mL of 1× of each Agnp are summarized in Table 4. The pH of Agnp suspensions was measured before each experiment repeatedly and mean values were calculated which can also be found in Table 4. It is worth noting that the pH valued of [-]Agnp and [+]Agnp were comparable (6.2 and 6.5 respectively). The solutions were desired to be of neutral charge, near pH 7 and comparable with each other which aligned with the pH measurements obtained.

Table 4: Volume of Agnps used to prepare 1 mL of 1× concentration and pH of respective Agnps.

Agnp	Volume of original Agnp	Volume of MillQ water	Absorbance reading at 430 nm	pH	SD (±) of pH
[-]Agnp	80μL	920μL	≈0.5	6.2	0.1
[+]Agnp	65μL	935μL	≈0.5	6.5	0.1

2.3.3 SEM and EDS analysis

Silver nanoparticles were visualized with a scanning electron microscope (Hitachi SU-70) on the surface of mica. 5 μL each of stock solutions of [-]Agnp and [+]Agnp was dropped on a mica surface and was dried at ambient temperature. Platinum sputter coating was done for 40s using a sputter coater. In addition, chemical characterisation was done by using the elemental analysis feature of electron dispersive x-ray connected to the microscope. For normal SEM observations, 5kV was set as voltage of electron beam and was changed to 10kV for all EDS analysis. SEM images were used for diameter calculations and size distribution analysis using Image J.

Results and interpretation

Figure 23 shows the difference in the size of [-]Agnp and [+]Agnps. The average diameter of [-]and [+]Agnp were calculated to be 80 nm and 150 nm by using Image J. Histograms of particle diameter distribution indicated that the particles were mostly poly-dispersed for [+]Agnp whereas for [-]Agnp, the particles size was relatively uniform. Figure 24 represents the EDS analysis of Agnps. The analysis was done at two points- Point 1) on

empty space of mica surface, where no particle was present and Point 2) directly on the surface of nanoparticles. The EDS graph showed the presence of Ag element at Point 1 but not at Point 2. Therefore, it further validates that EDS can be used in qualitative characterisation of silver.

SEM image	Diameter distribution
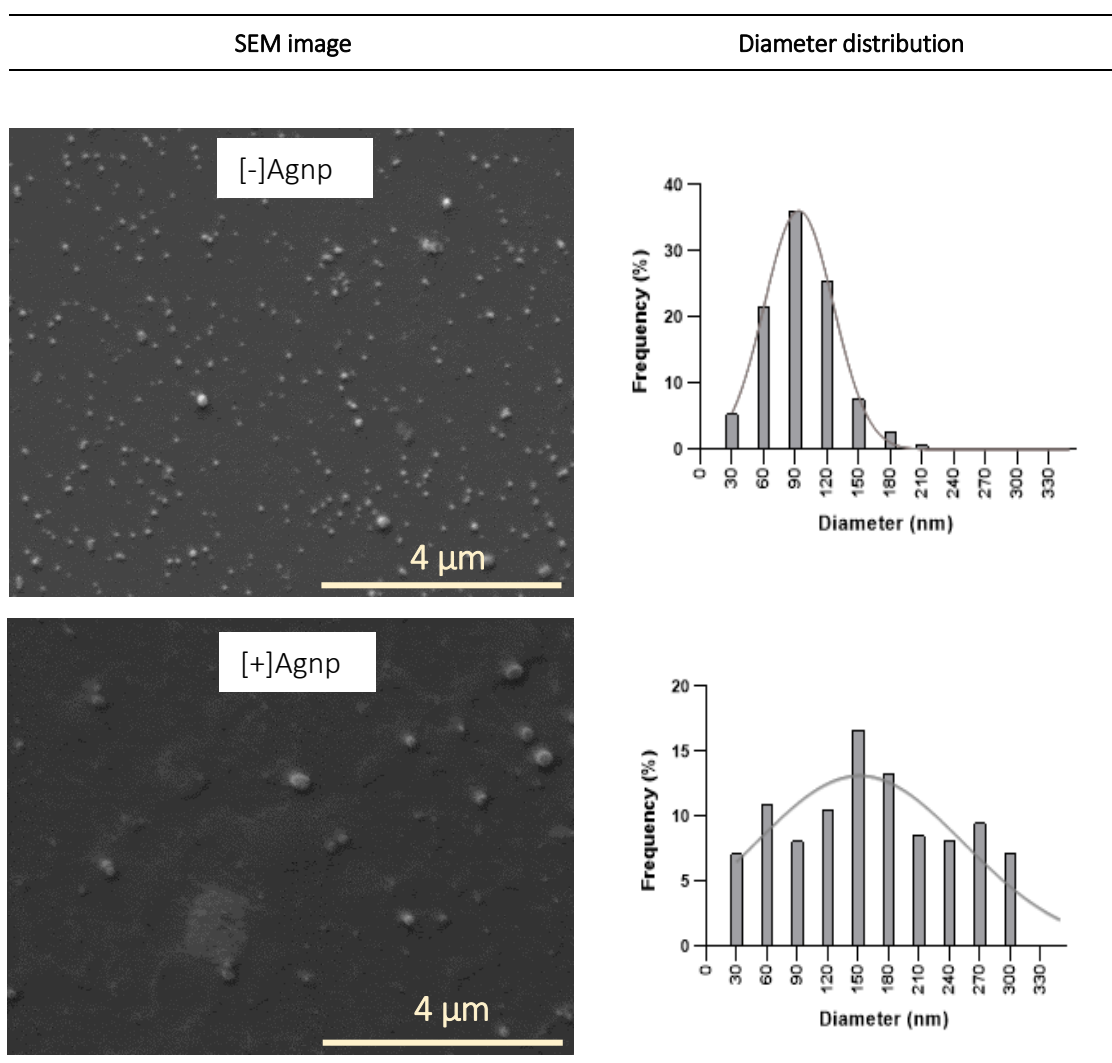
Figure 23: SEM images and size distributions of [-]Agnp and [+]Agnp. The deviation from bell-curve or normal distribution indicates that the particle diameters are not ideally symmetric. However, in comparison with [+]Agnp, the diameter distribution of [-]Agnp is fitting the curve better, indicating that the particles had a relatively more uniform size.
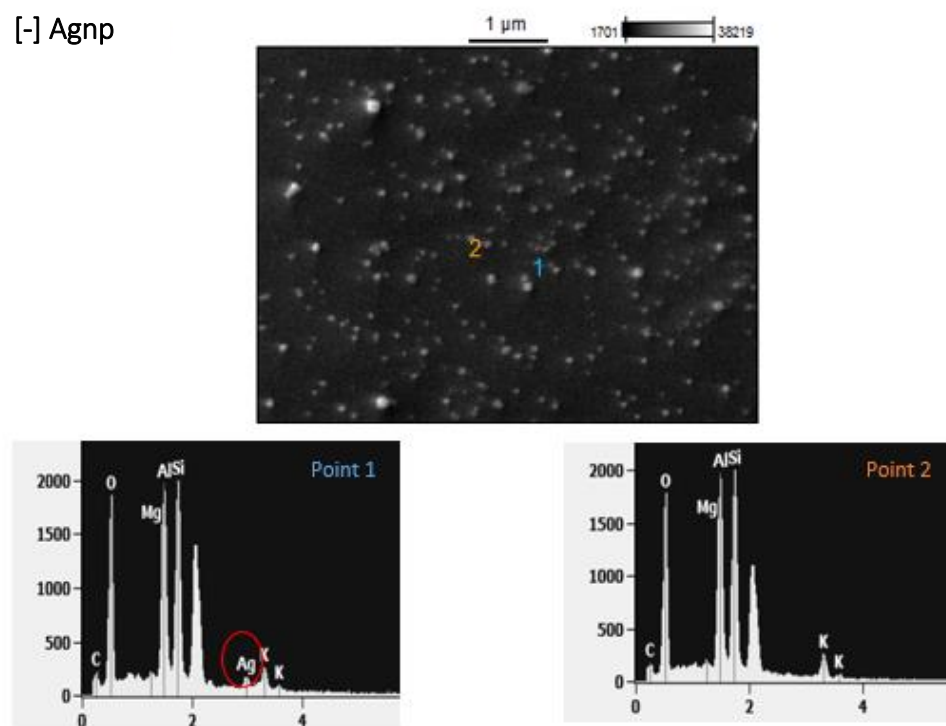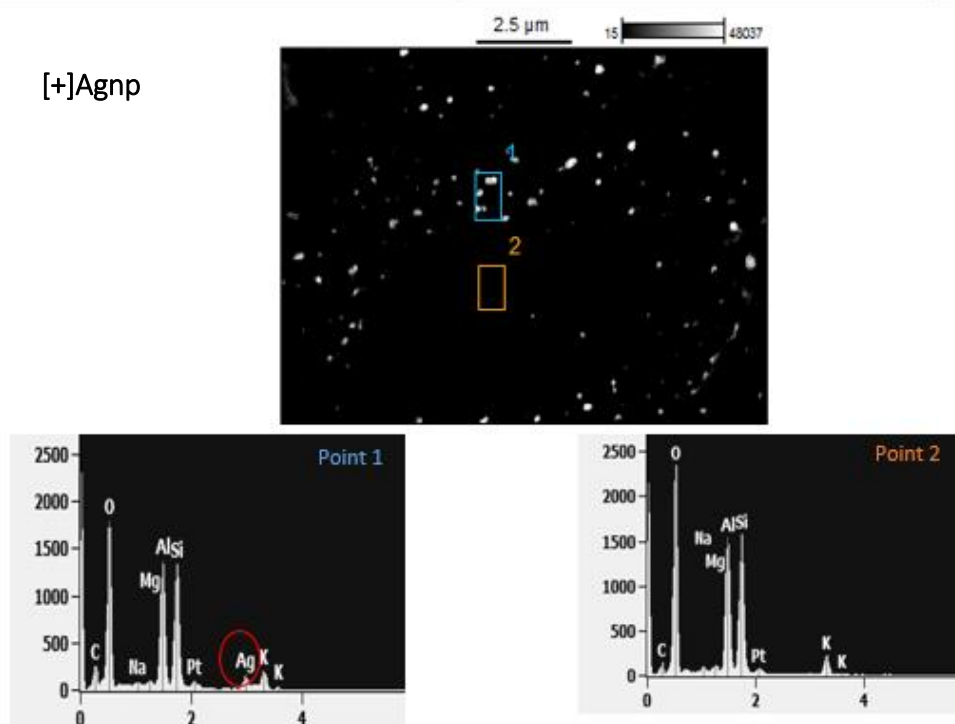
Figure 24: EDS analysis of [-] and [+] silver nanoparticles. a) shows EDS of [-]Agnp and b) shows EDS of [+]Agnp. Point 1 was analysed directly on the particle whereas point 2 was analysed on an empty area of mica with no nanoparticle. As expected, in EDS graph, point 1 shows the presence of Ag (indicated by red circles) but point 2 shows no presence of Ag. Other elements except Ag are the inherent components of the mica surface.

2.3.4   Zeta-sizer analysis

Zeta potential (ζ-potential) is the electrokinetic potential in colloidal suspensions. In presence of an electric field, charged particles exhibit different effects, such as electrophoresis, electro-osmosis and sedimentation potential. For nanoparticles, in practice, electric potential is determined at a location away from the surface which is at the diffusion layer [219]. A zeta-sizer was used to measure the size and zeta potential of Agnps by using the principle of Dynamic Light Scattering (DLS) and electrophoresis.

Method overview

Measurement of zeta potential was done by varying the pH of nanoparticle suspensions at 3, 5, 7, 9 and 11. Sodium hydroxide (NaOH, 0.01M) and hydrochloric acid (HCL, 0.01M) were used as base and acid to adjust pH. In addition, sodium chloride solution (NaCl, 100mM) was maintain stable pH values. Firstly, 6mL of NaCl solution was prepared and adjusted for the desired pH, using NaOH/HCL. Then the pH adjusted NaCl was mixed with 6mL of (1×) nanoparticle suspensions (Refer to Table 4 for preparation of 1× solution of Agnps). Total 12 mL volume of each sample was prepared for zeta-sizer analysis. For zeta measurement at original pH, 1× solutions of each Agnps was directly diluted in water to make up 12 mL of total volume. 1× solutions could not be directly analysed because the concentration was too high. If the sample concentration becomes too high, the laser beam of zeta sizer will become attenuated by the particles decreasing the scattered light that is being detected, producing error. Generally, the sample should be optically clear for accurate measurement. Finally, average values were calculated from three measurements of each sample.

Results and interpretations

For original pH (non-adjusted) solutions, the size of [-]Agnp and [+]Agnp was measured to be 80 (±1) nm and 175 (± 17) nm respectively and the charge was calculated to be -14 (±3) mV and 33 (±2) mV respectively. A summary of size and charge analysis is shown in Table 5. The table also compares the size obtained by zeta-sizer with that calculated using ImageJ in 2.3.2.

Both size and charge were found to be dependent on the pH of the nanoparticle solutions as observed in Figure 25, where the orange spots correspond to the original pH values. The size of [-]Agnps increased at lower and higher pH and remained closer to the size at original pH when pH was adjusted at 7 and 9. The increase in size can be interpreted as agglomeration of particles due to the effect of acid and base. The phenomenon has been reported in literature in the past [220]. In original suspension, all nanoparticles have either negative charge (in case of [-]Agnp) or positive charge (in case of [+]Agnp). Due to similar charge of nanoparticles, there is an electrostatic repulsion. The H^+ and OH^- ions can coat nanoparticle surface in different ways and result in attraction between particles thus resulting in agglomeration. In case of [+] Agnp, there is no significant change in size with the variation of pH. This could be due to better stability of [+]Agnp as compared to that of [-]Agnp.

The diameter of the particles was observed to be affected by change in pH. Regarding the change in charge with respect to pH, charge decreases at higher pH values due to the presence of excess OH^- and at lower pH, it shifts towards positive side due to the presence of excess H^+. In conclusion, it was observed that pH is critical in zeta potential analysis and it affects the charge of the whole system of nanoparticle suspensions. This, in turn also affects the diameter of nanoparticles.

Table 5: Summary of size and charge analysis of Agnps. The sizes obtained by ImageJ analysis and DLS of zeta-sizer are compared.

Sample	Diameter (nm)		Charge (mV)
	SEM	DLS	
[-]Agnp	80 ± 6	80 ± 1	-14 ± 3
[+]Agnp	153 ± 9	175 ± 17	33 ± 2

[-]Agnp
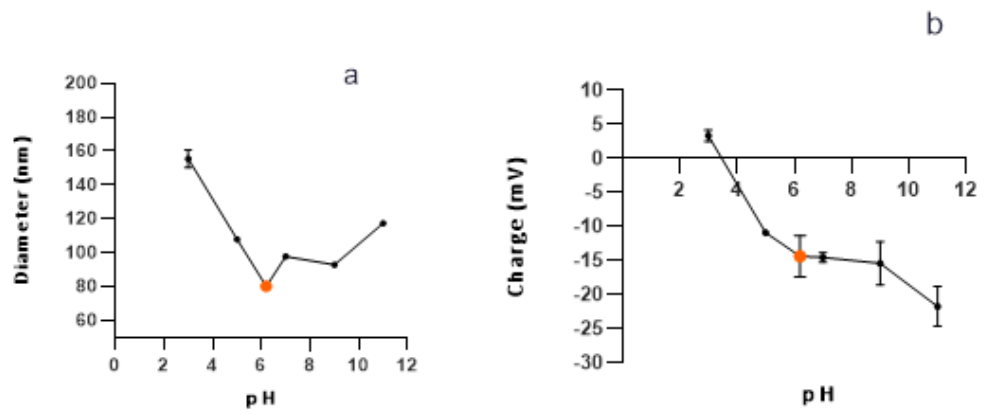
[+]Agnp
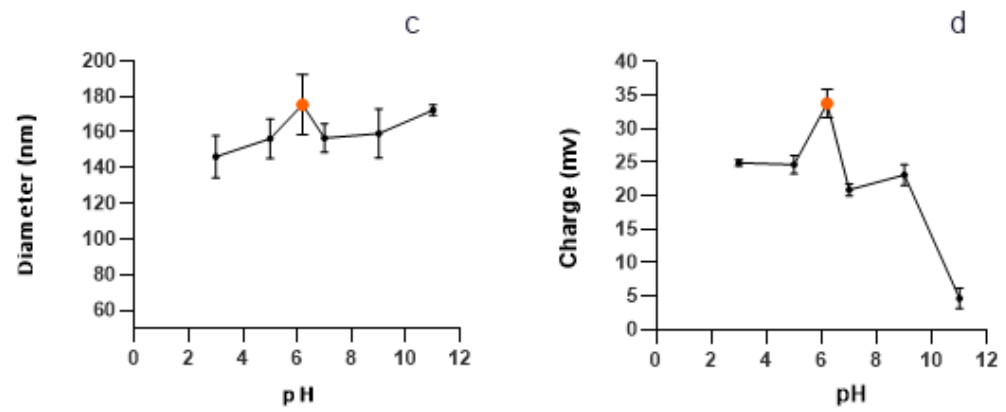
Figure 25: Diameter and charge analysis of Agnps at different pH. a) and b) show a change in diameter and charge of [-]Agnp whereas c) and d) show change in diameter and charge of [+]Agnp. The orange dot refers to values at original pH of each nanoparticle solution.

2.4　Nanoparticle capture

The atoms on the surface of adsorbent material (especially porous surface structure) are free to attract absorbable solutes, as they are not completely bonded with other adsorbent atoms. There can be different mechanisms of adsorption generally classified as physisorption mediated by weak van der Waals forces or chemisorption by covalent bonding, or also may occur due to electrostatic attraction [221]. We have utilized the mechanism of electrostatic attraction to capture charged nanoparticles in both processes of adsorption and filtration in our study.

After coating of the nanofibre surface (Refer to Protocol 2.2.2), the synthesised Agnps were tested for capture using various parameters such as the concentration of FSLs, the concentration of Agnp, pH of Agnp suspension, time of adsorption, the process of capture (adsorption vs filtration), type of nanofibres and FSL molecules. Additionally, the stability of FSL molecules on the coated surface was also tested.

2.4.1　Nanoparticle capture - adsorption

Adsorption was first used to test whether Kode or FSL constructs had an affinity towards the charged particles. Conclusions obtained from the assay were utilised to test the capture of particles through filtration.

At first, a general adsorption protocol was developed to compare various other parameters by keeping a few parameters constant such as nanofibre polymer type, the packing density of nanofibres, concentration of nanoparticle solution and time of adsorption.

Protocol 2.4.1: Standard adsorption protocol

1. 5 mm x 10.5 mm coated PCL nanofibres of 4 gsm (coated using Protocol 2.2.2) were immersed in 1 mL of 1× Agnp solution. The adsorption was done in a 24-well plate for robustness.

2. Two sets of controls 1) control nanofibre (with no FSL construct) and 2) control solution (1× Agnp solution without any nanofibre) were included in all assays.

3. 24-well plate was then kept in an orbital shaker to aid adsorption process for 1 hour.

4. Initial analysis of capture was done by noting the change of typical brown colour of Agnp solutions after adsorption. Successful adsorption was indicated by the

shift of brown colour of solution to transparency while the white surface of nanofibre turned brown.

5. For quantitative analysis, the absorbance of control solution was measured at the beginning of the experiment. After adsorption, nanofibres were taken out of the wells and absorbance was measured again with a UV-Vis spectrophotometer at wavelength of 430 nm.

6. The difference between absorbance of Agnp solution before and after the assay was used to calculate the amount of silver adsorbed onto nanofibre surfaces employing calibration curve in 2.3.1. The following formula was used to calculate the adsorption efficiency.

$$AE\ (\%) = \left(\frac{Cb - Ca}{Cb}\right) * 100$$

Where,

AE = Adsorption efficiency expressed in (%)

Cb = Concentration of Agnp before adsorption

Ca = Concentration of Agnp after adsorption

Various parameters (Table 6) were tested using the same standard protocol and SEM and EDS were further used to confirm adsorption.

Table 6: Various parameters used in Agnp adsorption and filtration experiments.

Parameter	Data points
Types of FSL constructs	FSL-SPM, FSL-Z, FSL-Biotin and FSL-HA
Concentration of FSL's	0.01 mg/mL to 2 mg/mL
Concentration of Agnp	1×, 3×, 6×
Time of adsorption	1, 3, 6, 9 and 12 hours
pH of Agnp solution	Original, 3, 5, 7, 9 and 11
Types of nanofibres	PCL, PVB, Nylon
Packing density of PCL nanofibre	0.5 gsm, 1.5 gsm, 4 gsm

Establishment of model experiments

Model experiments were conducted to test the adsorption efficiency of two differently charged constructs (FSL-SPM and FSL-Z) to capture two differently charged nanoparticles ([-]Agnp and [+]Agnp). These experiments were then taken as a base to conduct other experiments. For an example of the experiment, the capture of [-]Agnp by FSL-SPM can be observed in Figure 26, where two parameters have been compared 1) solvent for FSL-SPM dilution (70% methanol and water) and 2) different concentrations of FSL-SPM. A similar experiment was done to capture [+]Agnp by using FSL-SPM. FSL-Z was also tested to capture both [-] and [+]Agnp. In all these model experiments, the concentration of Agnp solution was always kept at 1× and four concentrations of constructs (0.01, 0.05, 0.5 and 1 mg/mL) were always included along with the control nanofibre and control solutions. Various other constructs (Table 6) were tested, based on the same method. All results are interpreted and discussed in the following section.
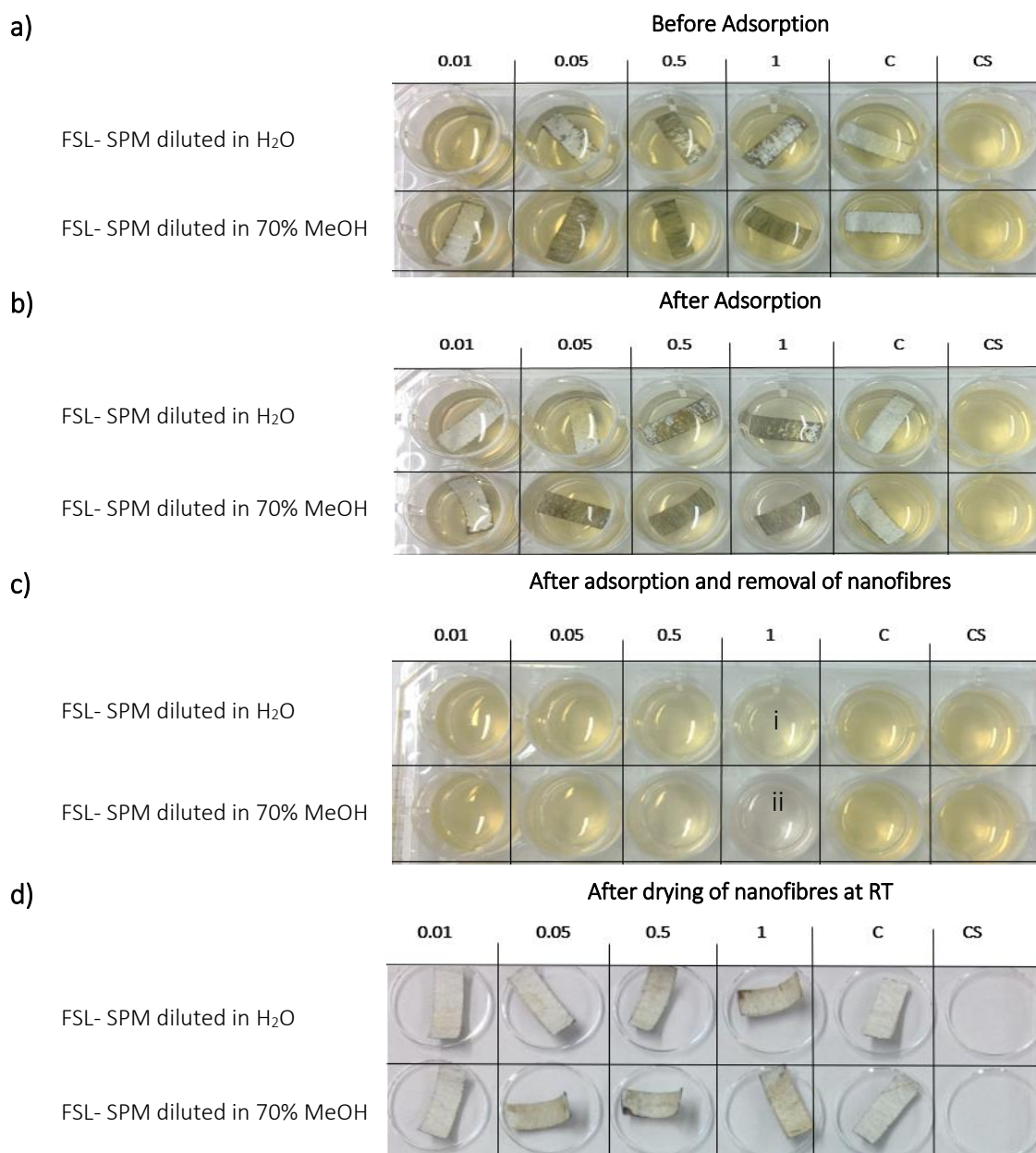
Figure 26: An example of adsorption assay using standard protocol. In a) four different concentrations of FSL-SPM (0.01, 0.05, 0.5 and 1 mg/mL) were coated on PCL nanofibre surface. The coated fibres were immersed in 1mL of [-]Agnp solution in each well. The first four wells consist of coated nanofibres. 'C' stands for control where the wells were filled with uncoated nanofibres and 'CS' stands for control solution where the wells were only filled with Agnp. The first row had nanofibres coated with FSL-SPM made up in water whereas the second row had nanofibres coated with FSL-SPM made up in 70% methanol. b) and c) show the plate after 1 hour of adsorption with and without nanofibre respectively. In c), it was observed that the colour of NP solution was visually changed as indicated by i) and ii), at 1 mg/mL of FSL-SPM coating. The change is significant for ii), indicating that at 1 mg/mL coating, FSL-SPM diluted 70% methanol works better in adsorbing particles as compared to FSL-SPM diluted in H_2O.

Results and Interpretations

Agnp adsorption by FSL-SPM coated nanofibres
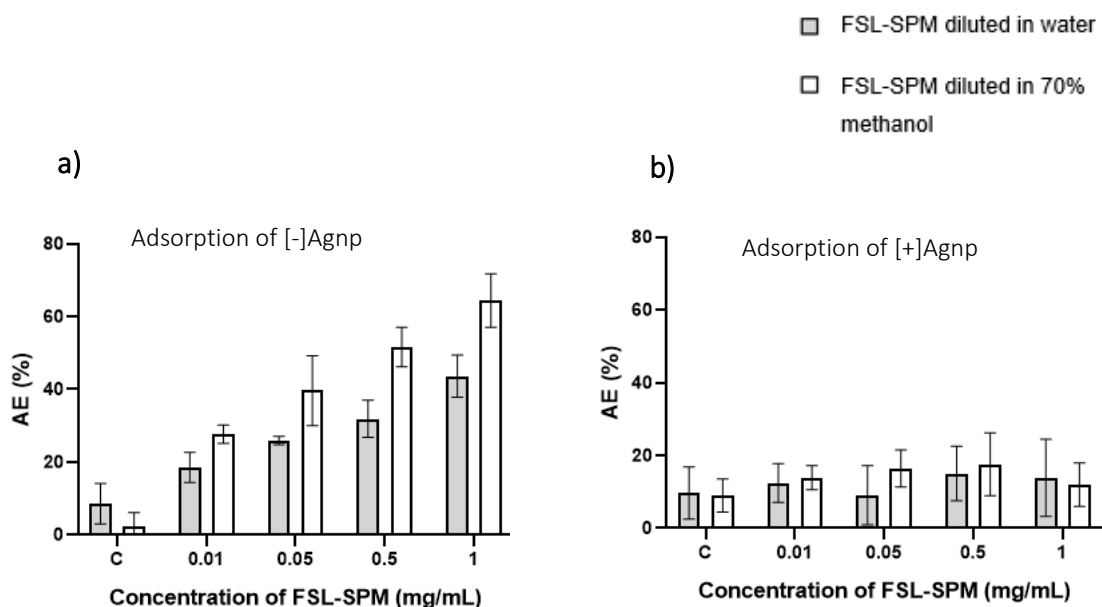
Figure 27: Adsorption efficiency (AE) of FSL-SPM for [-] and [+]Agnp. a) The AE of FSL-SPM is observed to increase for [-]Agnp with increasing concentration of FSL-SPM as expected. Application of FSL-SPM in methanol is found to work better than in water. b) The AE of FSL-SPM is observed to remain below 20% at all concentrations of FSL-SPM. This was also expected due to the presence of [+] charge on the Agnp that has no electrostatic attraction with the positively charged functional groups of FSL-SPM.

Figure 27 demonstrates that FSL-SPM adsorbed an increasing amount of [-]Agnp with its increasing concentration when applied in water or 70% methanol during coating. However, it was not capable of adsorbing [+]Agnp even at high concentrations for both solvents. This was expected because the mechanism of adsorption was predicted to be dependent on the electrostatic attraction caused by the presence of oppositely charged functional groups at the surface of nanoparticles and the coated nanofibres. It was observed that application of FSL-SPM in 70% methanol worked better than application in water for [-]Agnp adsorption and remained consistent at all concentrations of FSL-SPM. It was noticed that while immersing nanofibres in FSL-SPM diluted in water while coating, the FSL solution remained as a bubble and was hard to penetrate due to which the surfaces were not coated evenly. This represented hydrophobicity of PCL nanofibre. However, while nanofibres were immersed in FSL-SPM diluted with 70% methanol, the entire surface was instantly coated. The phenomenon was easier to observe due to an interesting property of PCL surface i.e., it turns transparent from white, when completely

wet, exposing the black coloured polypropylene (PP) support beneath. Additionally, it was observed that FSL coating alone can enhance the hydrophilicity of the nanofibre surfaces. In Figure 26a, it can be noticed that control nanofibres and the fibres coated with 0.01 mg/mL FSL-SPM are white, possibly indicating that they are still hydrophobic and thus resist wetting by Agnp solution. However, at higher concentrations (0.05, 0.5 and 1 mg/mL), they have turned transparent indicating that the higher amount of FSL-SPM on their surface has helped to increase their hydrophilicity. It is also worth noting that the wetting of nanofibres by Agnp has also greatly increased for nanofibres coated with FSL-SPM in 70% methanol than with water(represented again by the turning of the white colour to transparent). The difference in wetting property of methanol and water could be an important factor resulting in better efficiency of coating with 70% methanol-diluted FSL-SPM.

A similar experiment was conducted using FSL-Z coated nanofibres. As expected, the adsorption efficiency was enhanced for [+]Agnp and no successful adsorption was observed in the case of [-]Agnp (Figure 28). However, the adsorption efficiency of FSL-Z for [+]Agnp was lower than that of FSL-SPM for [-]Agnp. From zeta analysis, it was found that FSL-Z has a negative charge of -30 mV as compared to FSL-SPM that has a positive charge of +20 mV. On the other hand, [+]Agnp has a charge of +33mV and [-]Agnp has a charge of -14 mV. Based on this, it was predicted that FSL-Z would show better adsorption of [+]Agnp due to higher charge present on the construct as well as nanoparticles. However, results were not congruent with the prediction. FSL-Z showed lower adsorption efficiency than expected. In FSL-Z, the negative charge is provided by CMG spacer that is responsible for attracting the positive particles, unlike FSL-SPM where the positive charge is the functional head.

The experiment further proved that coating FSL-SPM in 70% methanol works better than water, indicated by higher adsorption efficiencies for nanofibres coated with methanol-diluted FSL-Z as compared to water-diluted (Figure 28). FSL constructs were diluted in 70% methanol for all future experiments.

Agnp adsorption by FSL-Z coated nanofibres
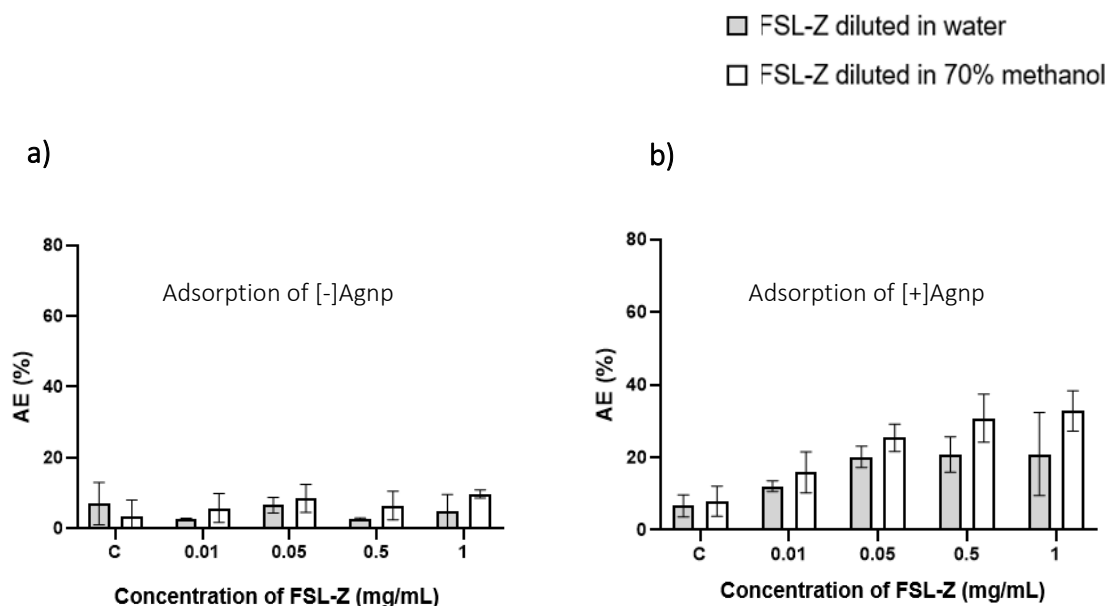
Figure 28: Adsorption efficiency (AE) of FSL-Z. a) shows unsuccessful adsorption of [-]Agnp by FSL-Z at all concentrations. b) shows increased adsorption of [+]Agnp with increasing concentrations of FSL-Z. 70% methanol is observed to be the better solvent for coating than water.

The adsorption of nanoparticles was visually analysed and confirmed by using SEM and EDS. Figure 29 and Figure 30 show the successful adsorption of [-]Agnp by FSL-SPM at various concentrations of FSL-SPM. The EDS result in Figure 30 validates the presence of silver on the surface. The green dots represent silver elements on the surface as determined by EDS. The overlaid image in Figure 30c proves successful capture of Agnp on the FSL-SPM coated nanofibre surface.

a) Control (No FSL-SPM)

b) 0.01 mg/mL FSL-SPM

4 μm

4 μm

c) 0.05 mg/mL FSL-SPM

d) 0.5 mg/mL FSL-SPM

4 μm

4 μm

e) 1 mg/mL FSL-SPM

4 μm
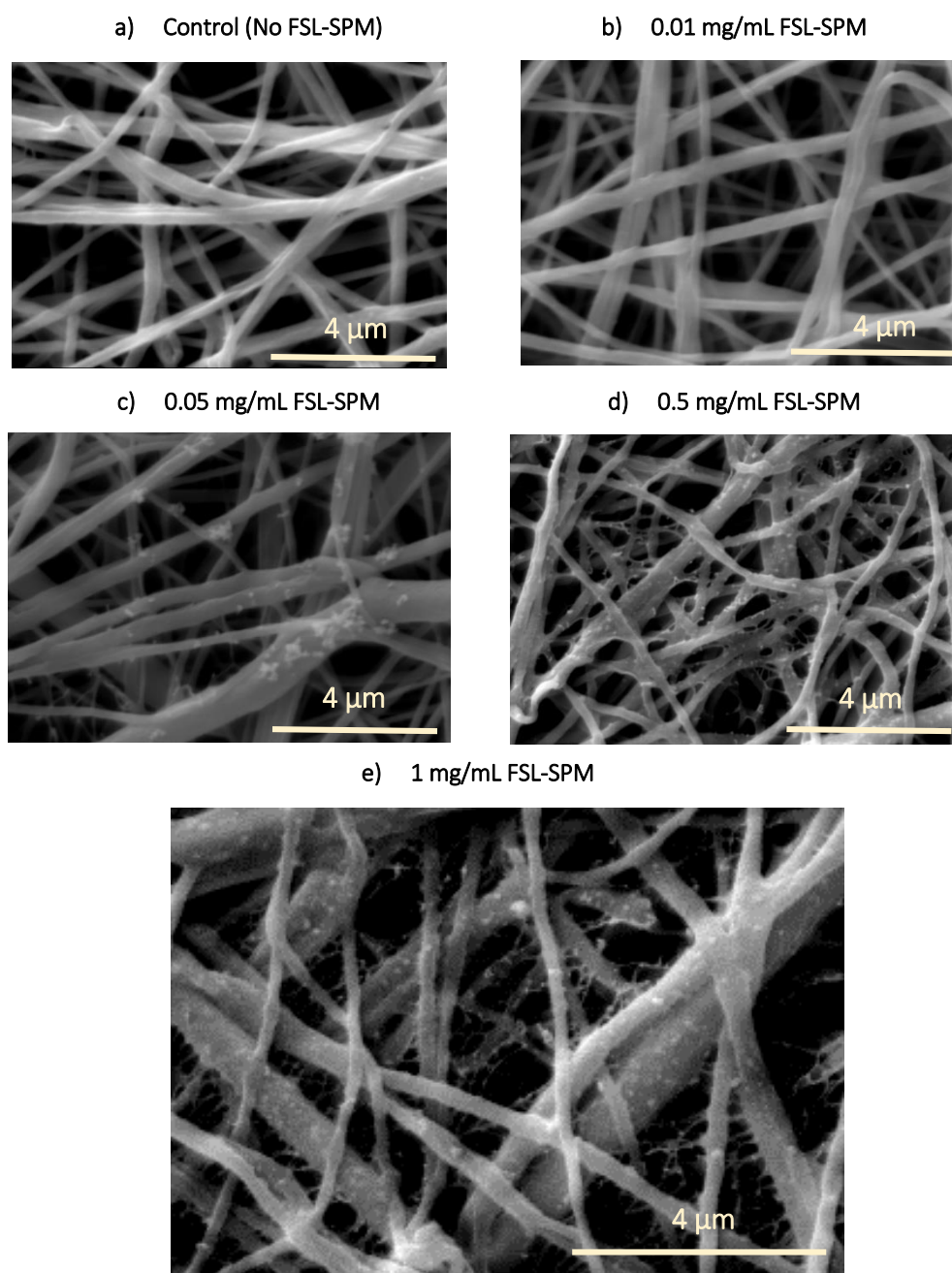
Figure 29: SEM images illustrating adsorption of [-]Agnp with increasing coating concentration of FSL-SPM. a) shows control nanofibre with no FSL-SPM. No Agnp is visible on the surface indicating that there was no significant adsorption. b), c) d) and e) show an increasing amount of particles on the surface with increasing FSL-SPM coating concentration.

74

a)   b)

2.5 μm   2.5 μm

c)

2.5 μm
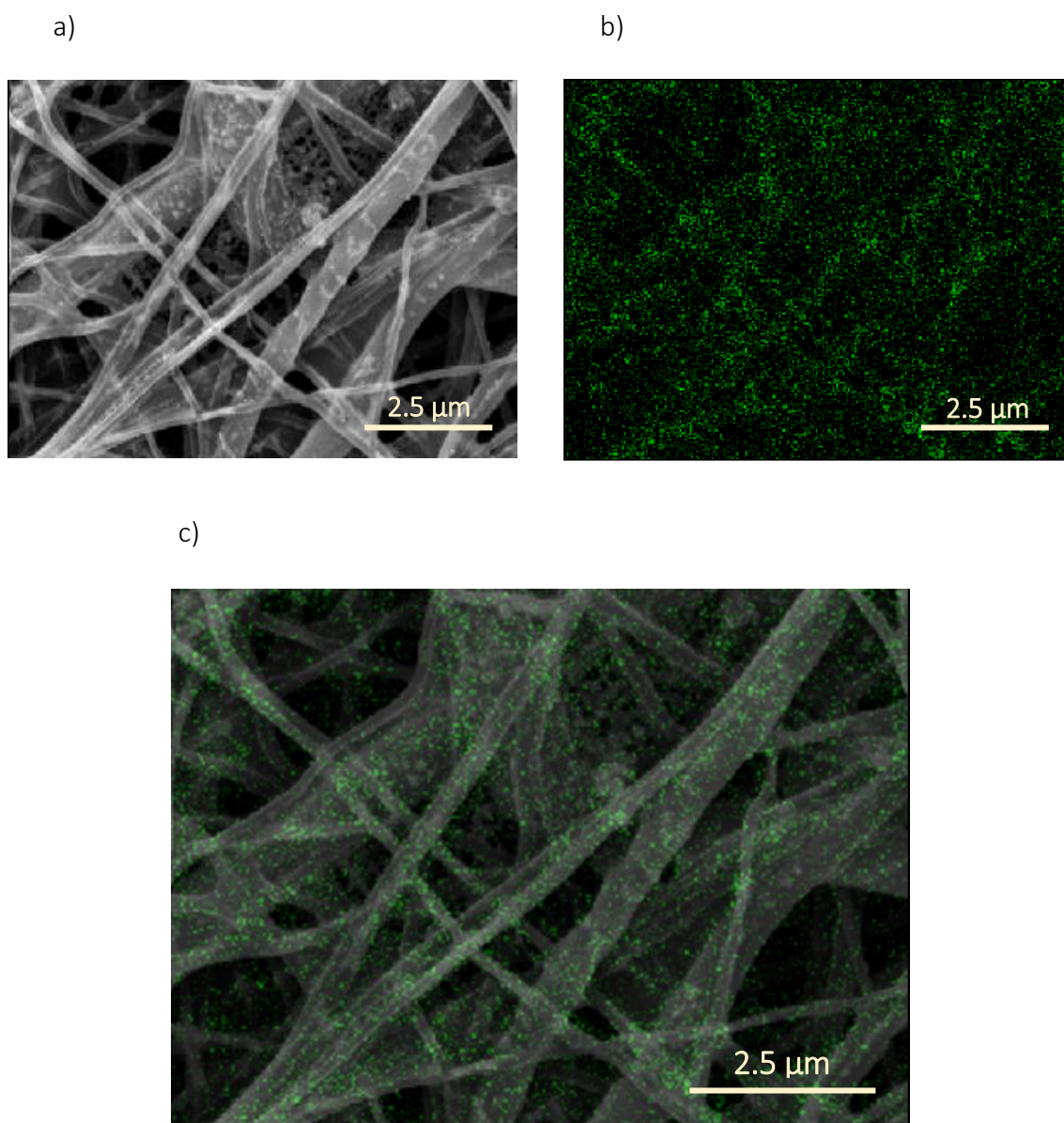
Figure 30: EDS analysis of 1 mg/mL coated nanofibre. a) SEM image of an area of PCL nanofibre used for EDS analysis. b) The EDS characterisation of silver particles on the area indicated by green dots. The green dots make up a complementary image with the SEM images. c) shows the overlaid image of a and b further indicating that the position of green dots (nanoparticles) matched (higher density) with the position of fibres on the surface.

Comparison of different constructs with FSL-SPM and FSL-Z

After the establishment of model experiments, it was necessary to analyse various other constructs for their ability to adsorb charged nanoparticles. Firstly, it was important to validate that FSL-SPM construct shows better activity than spermine alone. It is known that FSL-constructs coat most biological and non-biological more efficiently than others. Based on the model experiments, the adsorption efficiency of spermine was compared with that of FSL-SPM. Further, other negatively charged constructs such as FSL-biotin and FSL-HA were also compared with FSL-Z.
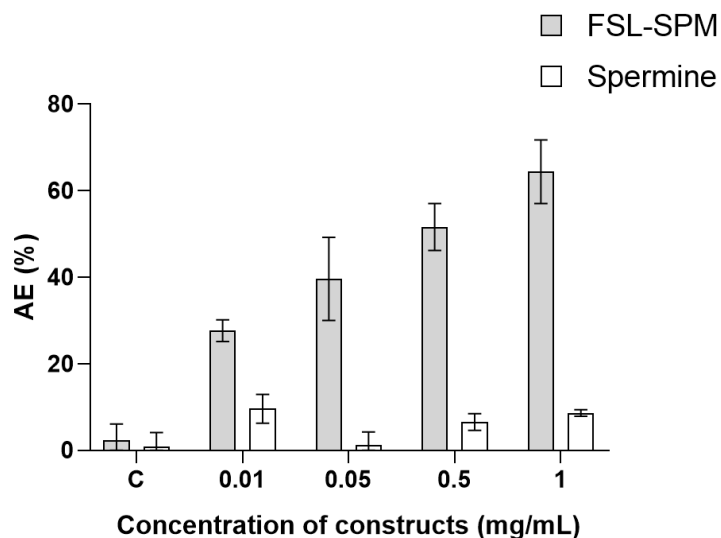
Figure 31: Comparison of adsorption of [-]Agnp by FSL-SPM and spermine. It was observed that FSL-SPM showed very high adsorption efficiency as compared to spermine at all concentrations.

It was successfully demonstrated that FSL-SPM was able to adsorb [-]Agnp much more efficiently than spermine (Figure 31), as expected due to hydrophobic interaction of DOPE tails with the fibre material and each other, probably forming self-assembled membrane-like layers and multiple layers. It further proves that FSL-SPM adheres to surfaces strongly and remains stable even after washing, unlike spermine. A comparison between SEM images of FSL-SPM and spermine coated nanofibres after adsorption is shown in Figure 32.
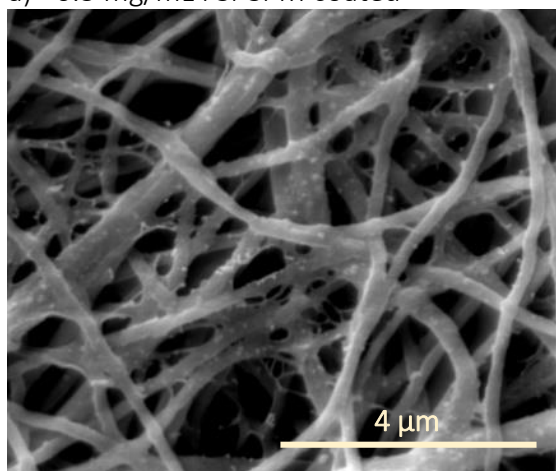
a)   0.5 mg/mL FSl-SPM coated   b)   0.5 mg/mL spermine coated
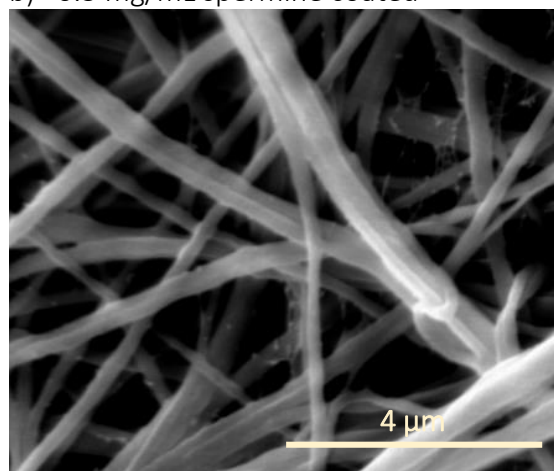
Figure 32: Adsorption of [-]Agnp by FSL-SPM and spermine coated nanofibres. a) shows efficient adsorption of [-}Agnp particles by at 0.5 mg/mL (0.4 µM) FSL-SPM coating. b) shows no [-]Agnp particles at 0.5 mg/mL (2.5 µM) of spermine coating.

Further, the adsorption efficiency of FSL-SPM was also compared with other FSL polyamines mentioned in Table 1. The comparison of the efficiencies for different concentrations has been shown in Figure 33. FSL-SPM is observed to work better than 36-1 at all concentrations. 31-1 works similar to FSL-SPM at 0.5and 0.5 and 1 mg/mL but its efficiency decreases at 0.01 and 0.05 mg/mL. In case of 32-1 and 33-,1, the efficiency of FSL-SPM is greater only at 0.01 mg/mL but at higher concentrations, the efficiency is either comparable or lower and the difference is not dramatic.
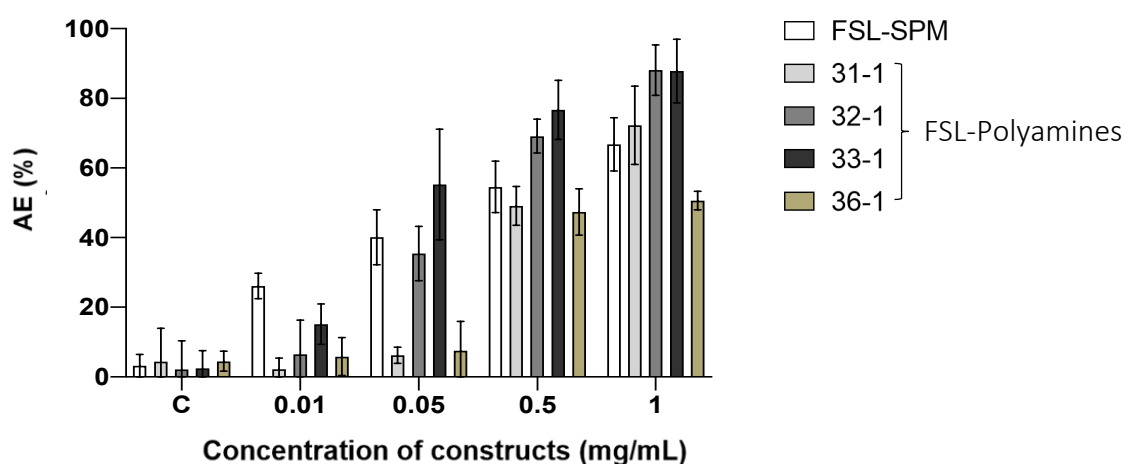
Figure 33: Comparison of adsorption of FSL-SPM with other FSL-polyamines.

FSL-Z was compared with other negatively charged FSL constructs such as FSL-HA and FSL-biotin as shown in Figure 34 and it was observed that the adsorption capacities of FSL-HA and FSL-biotin at all concentrations were less than those of FSL-Z. Although FSL-HA has a larger negatively charged functional group (Hyaluronic acid, HA) than the negatively charged spacer (CMG) of FSL-Z, it is poor in adsorbing [+]Agnp which suggests the dependence of adsorption on various other factors than just the charge. Another possible reason could be better adherence of FSL-Z in nanofibres than other constructs, which needs to be investigated.
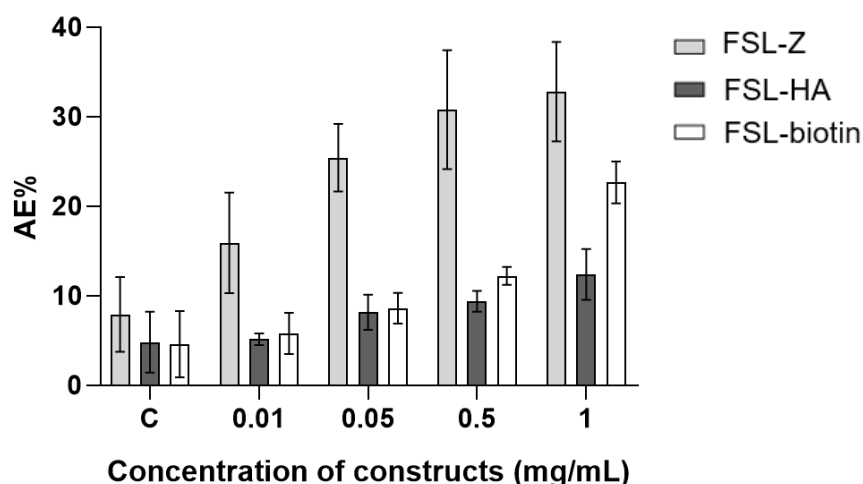
Figure 34: Comparison of adsorption of FSL-Z with FSL-HA and FSL-biotin. FSL-Z is observed to be more efficient in adsorption of [+]Agnp as compared to other constructs.

Effect of pH on adsorption

The aqueous environment affects the physical and chemical characteristics of colloidal nanoparticles. Changes in ionic strength and pH of suspension can result in dissolution, aggregation along with a change in surface chemistry, zeta potential and shape of the nanoparticles [222,223]. This can greatly affect the adsorption of nanoparticles. As discussed previously, the adsorption mechanism in this study is dependent on the electrostatic attraction between charged silver nanoparticles with charge-modified nanofibre surfaces.

Method overview

To assess the effect of pH on Agnp adsorption by FSL modified nanofibre surface, the standard adsorption experiment (Refer to Protocol 2.4.1) was conducted using FSL-SPM coating on PCL nanofibre. NaCl (100 mM) was used as a buffering agent for adjustment of pH of nanoparticle suspensions, similarly as in 2.3.3. The pH of NaCl solution was adjusted at 3, 5, 7, 9 and 11 using NaOH and HCL. 1× of silver nanoparticle solution was made according to volumes used in Table 4. However, instead of using only water for suspension, the particles were suspended in a pH adjusted NaCl solution (H_2O and NaCl used in ratio 1:1).

Results and interpretation

It was observed that at lower pH values of 3 and 5, the colour of [-]Agnp solution changed slightly pinkish and at pH 11, the colour was dramatically changed to dark brown colour (Figure 35). However, near pH values of 7 and 9, the colour of the Agnp suspension stayed similar to that of original suspension. This indicated possible agglomeration of nanoparticles at the high and low end of the pH range and a shift in the surface plasmon peak resulting in change of colour. The pH-dependent change in optical properties of nanoparticles has been previously discussed by various authors [224–226].

| original | 3 | 5 | 7 | 9 | 11 |
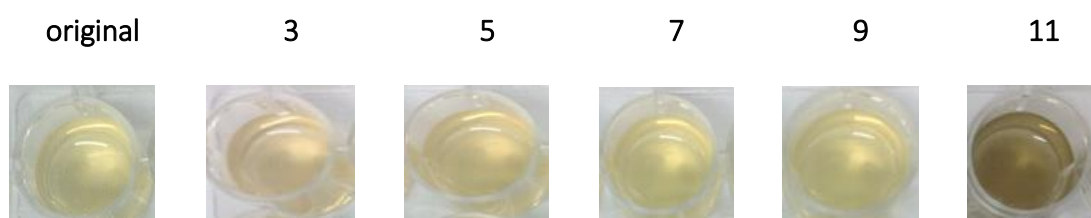
Figure 35: Change in colour of [-]Agnp suspensions at different pH. At lower pH values of 3 and 5, the colour has changed to slightly pink colour and at pH 11, the colour has changed to dark brown colour, indicating change in charge and size of particles and potential agglomeration. However, for pH values 7 and 9, the colour is similar to that of original suspension, indicating relative stability of charge and size at these values.

The change in particle size with pH has also been evidenced in section 2.3.3. The charge and size analysis of [-]Agnp at different pH is shown again in Figure 36. Therefore, the colour change of suspension highlighted the effect of pH in determining the charge and size of particles and indicated that adsorption efficiency could be affected by changing pH.
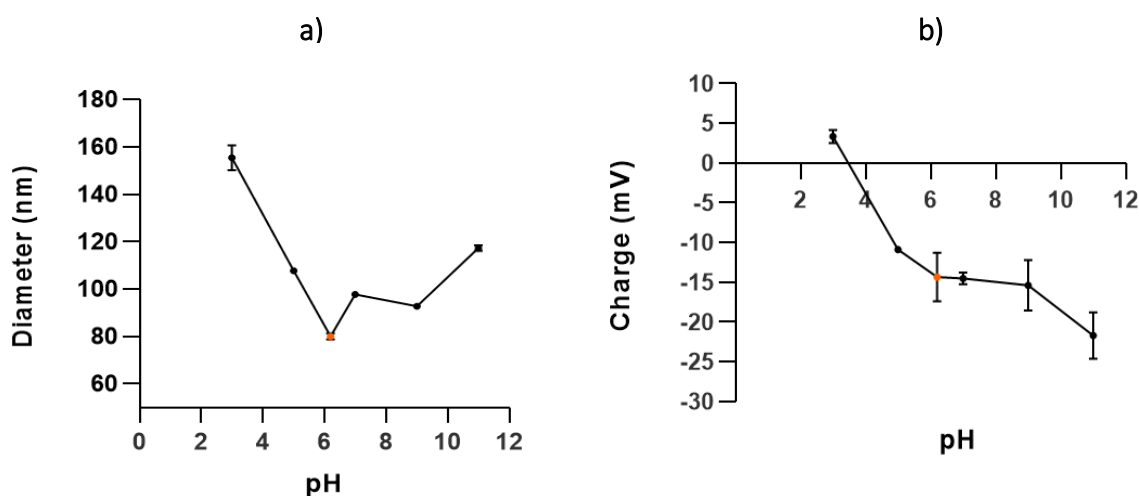
Figure 36: The charge and size analysis of [-]Agnp at different pH. This figure is also discussed in detail in section 2.3.3, Figure 26.

In section 2.3.3, it was shown that the surface charge of Agnps varied with pH of the suspensions. It was found that the positive charge on the surface increased with decreasing pH and vice versa. Based on this, it was hypothesised that adsorption of negative silver nanoparticles would decrease at lower pH due to decreased electrostatic attraction between the H^+ coated nanoparticles and positively charged, FSL-SPM modified the surface. Similarly, it was predicted that enhanced adsorption would be observed at higher pH due to OH^- coating of nanoparticles. However, the opposite trend was observed experimentally (Figure 37).
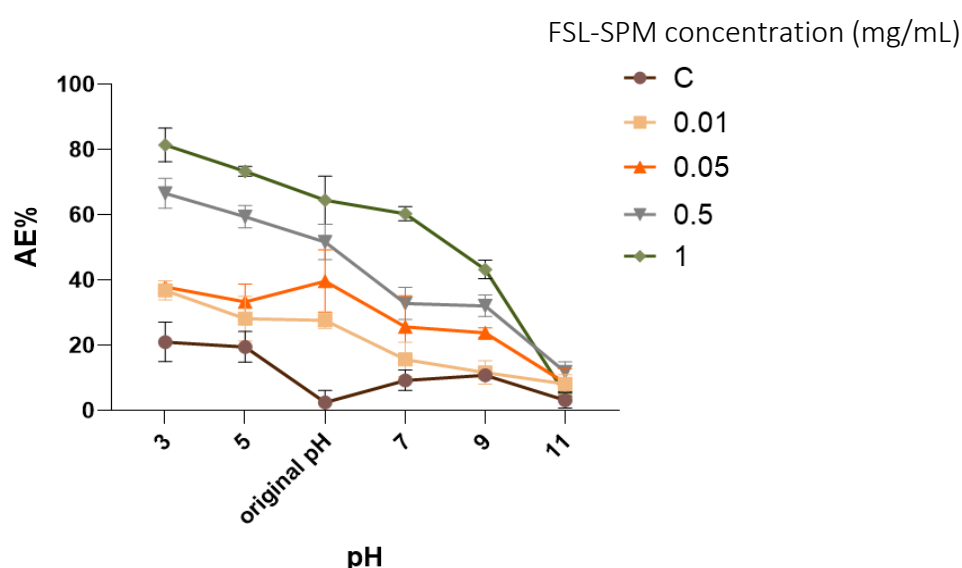
Figure 37: Change in adsorption efficiency (AE) at different pH of [-]Agnp suspensions. The adsorption efficiency is enhanced for lower pH value of 3 and 5 as compared to the original pH (approximately 6) and follows a decreasing trend with increasing pH.

A similar phenomenon in adsorption of Agnps was observed by Kang et al., [227] for negatively charged polystyrene particles and they have discussed the potential reasons for this adsorption behaviour. One of the reasons could be the competition of OH^- with negatively charged nanoparticles. At higher pH values, the excess OH^- could compete with the Agnps for adsorption at positive sites on nanofibres, resulting in a decrease of adsorption efficiency. The lower adsorption efficiencies at all pH values (7, 9 and 11) validate the interpretation.

At lower pH, the increase in adsorption efficiency can be interpreted to be due to the coating of nanofibre surfaces with excess H^+ ions, imparting a higher positive charge to the surface. This could help in attracting negatively charged particles. A similar explanation has been put forward by Banerjee et al. [228]. The fact is also supported by the

increase in adsorption capacity of control nanofibre for [-]Agnp at pH 3 as compared to [-]Agnp at original pH, indicating that control nanofibres might have also gained some positive charge from H^+ ions. Interestingly, in Figure 38, SEM image of 0.5 mg/mL FSL-SPM coated after adsorption of [-]Agnp at pH 3, shows agglomeration of nanoparticles which could also have helped in enhancement of adsorption. Instead of attaching each nanoparticle on an active site, only a few active sites on nanofibres were enough to attach the already agglomerated bulk of nanoparticles in the suspension, resulting in removal of large number of nanoparticles at once. Another possible mechanism could be that at lower pH, the available negatively charged nanoparticles could be adsorbed by FSL-SPM on nanofibre surface. Then the adsorbed particles could have attracted oppositely charged particles in the suspension (caused by H^+ ion coating of [-]Agnp) such that the adsorption was taking place on the nanoparticle surface rather than the nanofibre surface.

It should also be considered that the increased AE at pH 3 means that interaction of the nanoparticles with fibres was mediated not only because of charge but could have also resulted from the interaction of silver with polyamines due to co-ordination forces, like in case of chelators. For silver, it is well discussed in literature [229,230]. When Ag particle is charged, this interaction is reduced because, at pH 3, particles become neutral, as seen in Figure 36b and thus is able to switch on the co-ordination interactions.
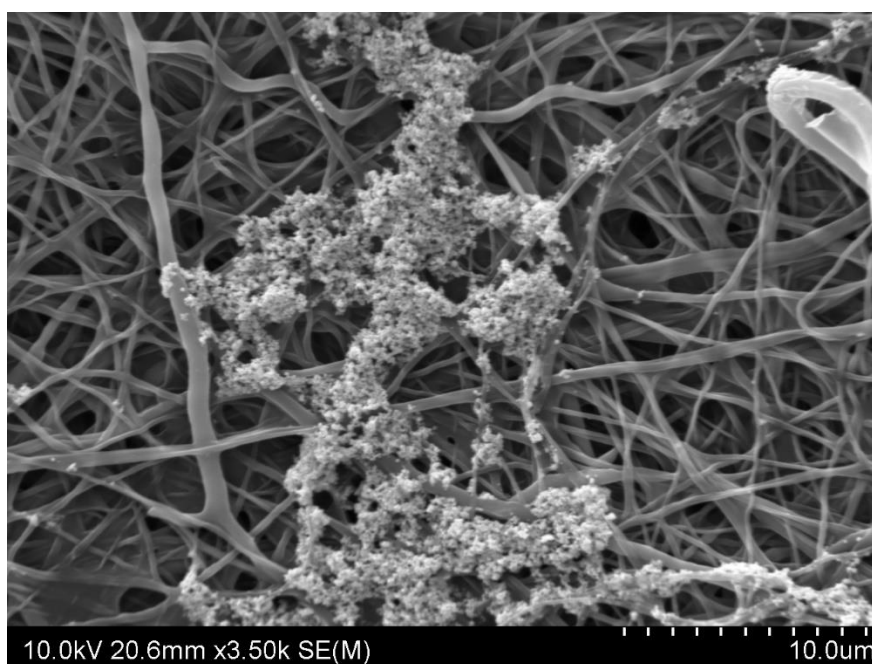
Figure 38: The adsorption of [-]Agnp (at pH 3) on 0.5mg/mL FSL-SPM coated PCL nanofibre. The particles are agglomerated and have attached in bulk instead of even attachment throughout the surface.

Effect of initial nanoparticle concentration

The initial concentration of adsorbate is an important parameter in the adsorption process. The effect of initial concentration on the removal of various pollutants has been extensively studied [228,231–233].

Method overview

Three initial concentrations, 1x, 3x and 6x of [-]Agnp and [+]Agnp were used for adsorption by FSL-SPM and FSL-Z respectively. The volumes of Agnps and H_2O used to make up 1 mL each concentration were calculated based on Table 4. The standard adsorption experiment (Protocol 2.4.1) was conducted using four concentrations of constructs 0.01, 0.05, 0.5 and 1 mg/mL for 1 hour.

Results and interpretation

Regarding FSL-SPM, there was no significant difference in adsorption efficiencies for all initial concentrations used in Figure 39a. However, for FSL-Z, the adsorption efficiency was greater for 1x [+]Agnp as compared to 3x and 6x Figure 39b.
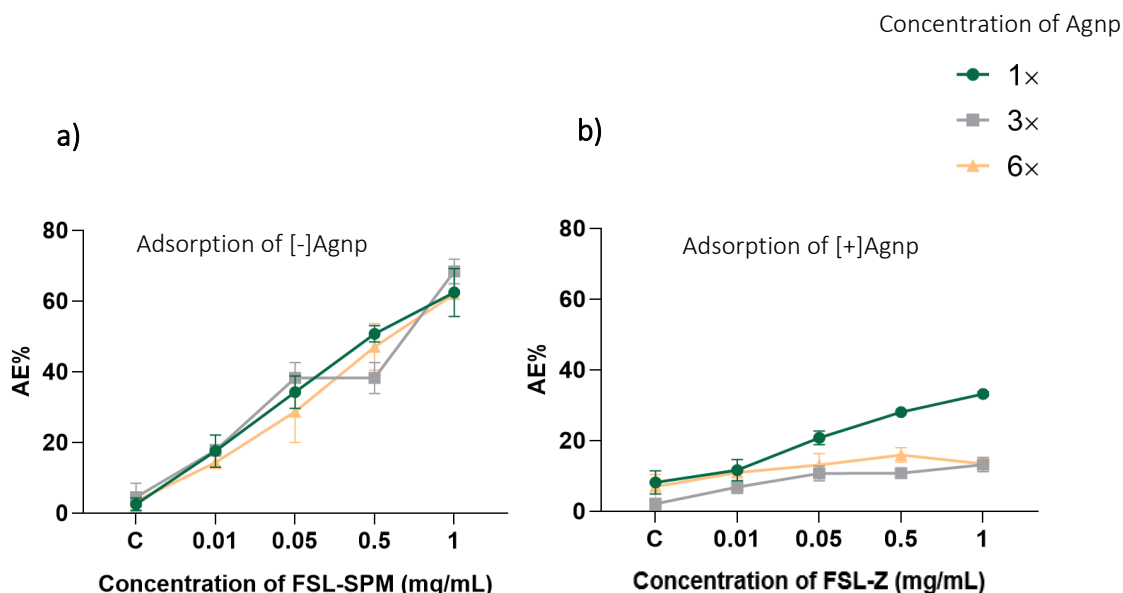
Figure 39: Adsorption by FSL-SPM and FSL-Z at a different initial concentration of Agnps. a) Adsorption of 1x, 3x and 6x concentrations of [-]Agnp by FSL-SPM. b) Adsorption of 1x, 3x and 6x of [+]Agnp by FSL-Z.

The results indicate that the change in the initial concentration of Agnp does not affect the adsorption capacity of FSL-SPM for up to 6x. However, higher concentrations than

that could affect the adsorption efficiency that needs to be investigated. On the other hand, FSL-Z shows poor adsorption with increasing initial concentration so the initial concentration should be maintained low to achieve optimum adsorption.

Effect of contact time

Method overview

The contact time used for standard adsorption protocol was 1 hour. However, adsorption behaviours of FSL-SPM for [-]Agnp was monitored at different contact times of 1, 3, 6, 9 and 12 hours. After adsorption at each given contact time, nanofibres were removed from the reacting wells and the solution left behind in the well was measured for absorbance values. The nanofibres were then put back in their respective reacting wells to continue for the next time point. The experiment was performed in triplicate to assess the effect of contact time.

Results and interpretation

In Figure 40, the adsorption of [-]Agnp by different concentrations of FSL-SPM at different contact times is shown. The adsorption efficiencies expressed are subtracted from the control to represent a true change in adsorption behaviour with respect to contact time and concentration of FSL-SPM coating.
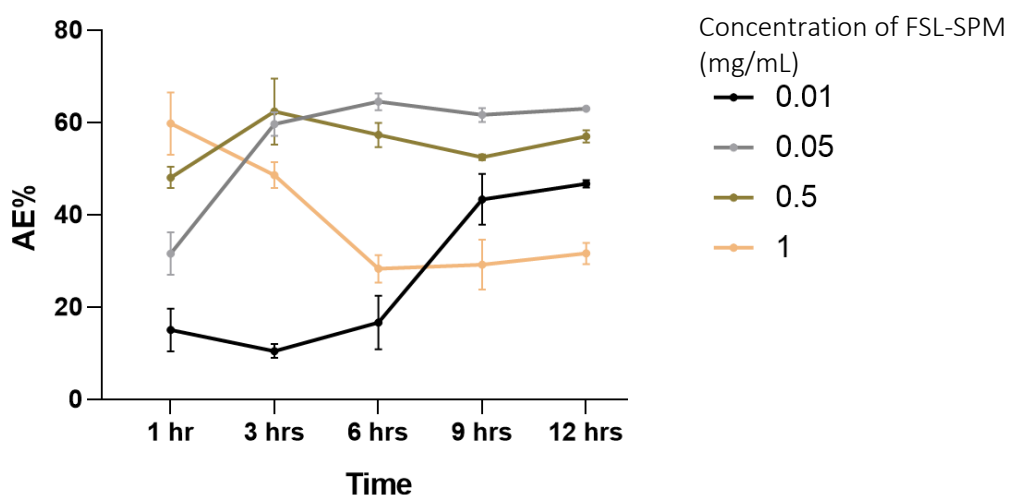
Figure 40: Adsorption of 1x [-]Agnp by different concentrations of FSL-SPM at different contact times. For, 0.01 mg/mL, the adsorption sharply increases at 9 hrs and for 0.05 and 0.5 mg/mL, adsorption is sharply increased at 3 hrs. However, for 1 mg/mL, the adsorption efficiency is observed to decrease with increasing contact time up to 6 hrs and approaches towards equilibrium after that.

The trend of adsorption at different time points varied with the concentration of FSL-SPM used. It was observed that 0.05 mg/mL had the most ideal trend where the adsorption kept increasing up to 6 hrs and achieved an equilibrium state. For, 0.01 mg/mL the adsorption only sharply increased at 9 hours but overall adsorption efficiency was lower than that of 0.05 mg/mL, even at 12 hrs contact time. For 0.5 mg/mL the adsorption trend is similar to that of 0.05 mg/mL for up to 3 hrs but after that AE decreases as compared to that of 0.05 mg/mL coated fibres. However, for 1 mg/mL, the adsorption efficiency was higher as compared to other coating concentrations in the beginning but gradually decreased with increasing contact time. It was hypothesised that at higher concentration of FSL-SPM coating, the construct could have desorbed from the surface with time. This phenomenon is also validated by the change in colour of nanoparticle solution at these concentration and contact times. For example, Figure 41 shows the reacting wells with nanoparticle solution left behind after removal of nanofibres coated with 1mg/mL FSL-SPM at different time points.

FSL-SPM	Contact time (hrs)					
(mg/mL)	0	1	3	6	9	12
0.01						
1						
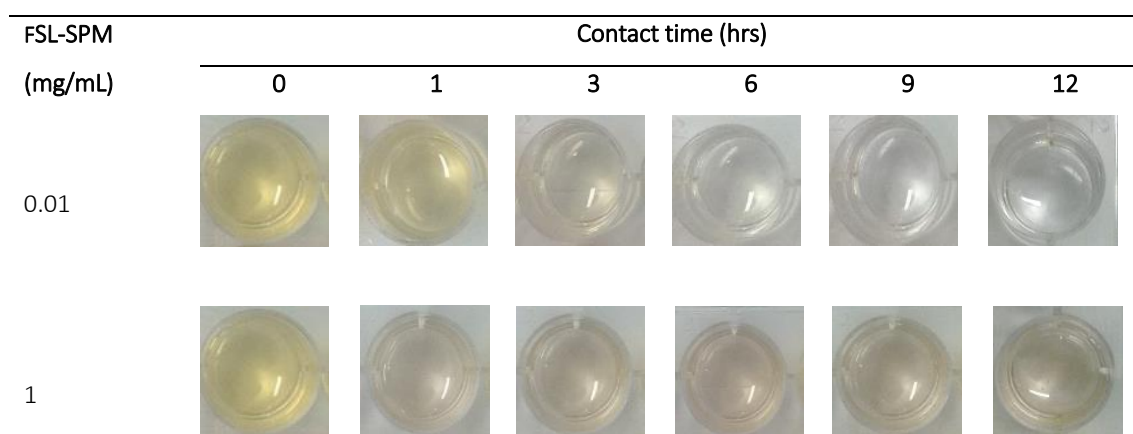
Figure 41: The change in colour of [-]Agnp after adsorption by FSL-SPM at different contact times. At 0.01 mg/mL FSL-SPM coating, the yellow colour of the nanoparticle solution turns more transparent with increasing contact time. It indicates transfer of nanoparticles from the solution to the coated surface. However, at 1 mg/mL, the nanoparticles solution turns brown in colour, indicating that nanoparticles have not been completely transferred and possibly physio-chemical characteristic of the nanoparticles has been changed, resulting in the colour change.

The increasing transparency of the nanoparticle solution with increasing contact time shows successful adsorption of nanoparticles on 0.01 mg/mL FSL-SPM coated surface. However, in the case of 1 mg/mL coating, the colour of nanoparticle turns brownish with increasing contact time. This illustrates that the nanoparticles are still present in the solution but due to the change in size of the particles, optical properties of the

nanoparticle solution could have changed. It is possible that desorbed FSL-SPM could have played a role in changing the charge and size of nanoparticles, resulting in the change of colour.

To further validate the desorption of FSL-SPM, the nanoparticle solutions of different colours (yellow, transparent and brown) achieved after adsorption of 12 hours were observed under SEM (Figure 42). 5 µL of each kind was dropped on a surface of mica, dried and sputter coated for 40 seconds for SEM visualisation.
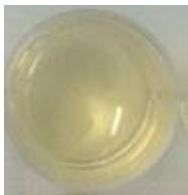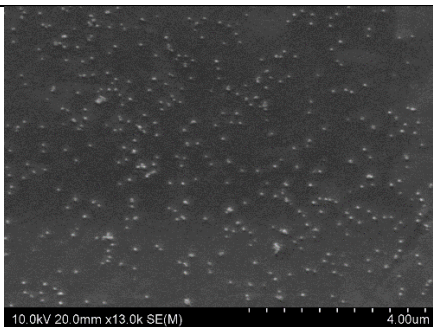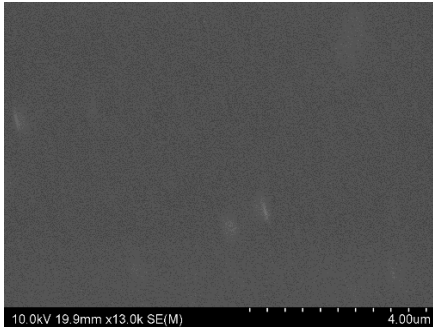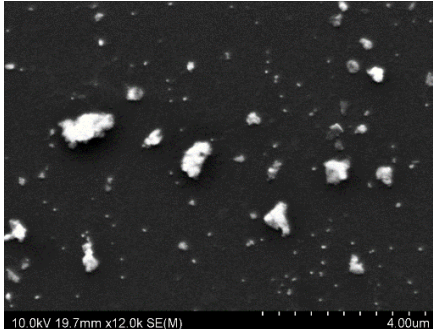
		Nanofibre	Agnp solution	SEM image of Agnp solution
a)	After adsorption by control nanofibre			
b)	After adsorption by 0.01 mg/mL FSL-SPM coated nanofibre			
c)	After adsorption by 1 mg/mL FSL-SPM coated nanofibre			

Figure 42: Nanofibres and [-]Agnp solutions after adsorption by FSL-SPM coated nanofibres. a) SEM image shows evenly dispersed Agnp solution when it is in its original state and the colour of the solution is yellow. b) After adsorption, the colour of Agnp turns transparent as all nanoparticles are stuck on to the fibres, which is why no particles are observed in the SEM image of the solution. c) SEM image shows agglomeration of particles and the Agnp solution is observed to turn brown, possibly indicating the effect of agglomeration of particles.

Complementary with the desorption hypothesis, it was observed that when the solution is yellow (original colour), the nanoparticles are dispersed, distinctly separated and uniform in size and the transparent solution showed no presence of nanoparticle. However, the brownish solution showed agglomeration of nanoparticles as observed in Figure 42. It supports the interpretation that the possible desorption of FSL-SPM into the nanoparticle solution could have disturbed the ionic composition of the solution or disrupted the [-] charge of particles by coating the surface of nanoparticles with a positive charge in FSL-SPM, thus resulting in agglomeration.

Similar comparison (as in Figure 43) was done for spermine coated nanofibres and adsorption was analysed after 12 hours contact time. Results are shown in Figure 44.

		Nanofibre	Agnp solution	SEM image of Agnp solution
a)	After adsorption by control nanofibre			
b)	After adsorption by 0.01 mg/mL spermine coated nanofibre			
c)	After adsorption by 1 mg/mL spermine coated nanofibre			
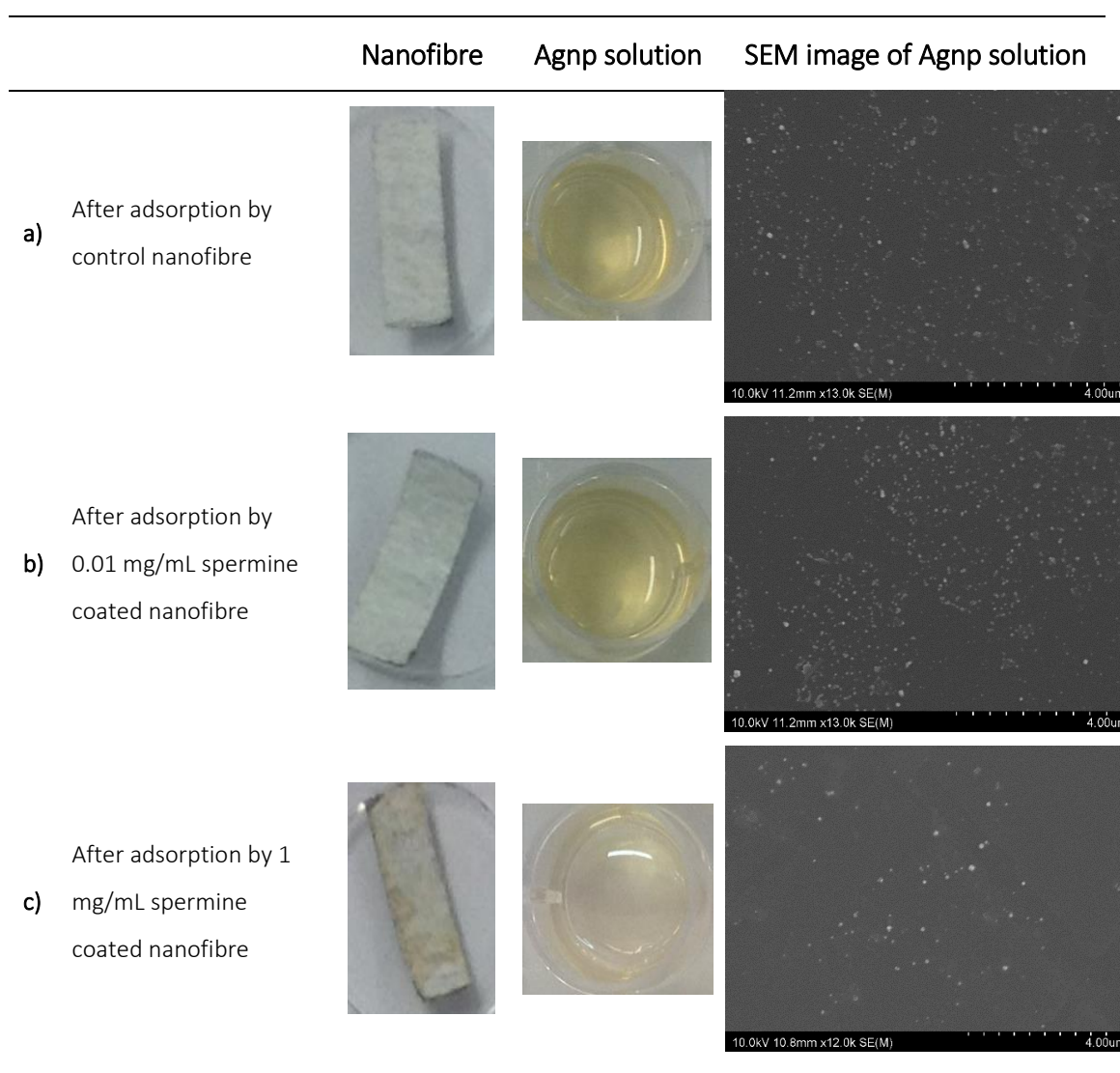
Figure 43: Nanofibres and [-]Agnp solutions after adsorption by spermine coated nanofibres. Spermine does not result in a change of Agnp solution even at 1mg/mL of coating and no agglomeration is observed.

In Figure 43b, 0.01 mg/mL concentration of spermine is not enough to cause efficient adsorption of nanoparticles. Therefore, the Agnp solution is still yellow, unlike FSL-SPM effect as seen in Figure 42b. However, at 1 mg/mL spermine coating, nanoparticles are adsorbed to some extent on the nanofibres after 12 hours of contact time (Figure 43c) and interestingly, agglomeration is not observed as shown by the SEM image of the Agnp solution

The difference in the agglomeration effects of FSL-SPM and spermine at 1 mg/mL of coating could possibly indicate that FSL-SPM is adsorbed on the fibres at higher amounts as compared to spermine. It has also been discussed in the previous section where it was interpreted that spermine washes away during the coating process whereas FSL-SPM adheres to the surface strongly. The presence of higher amount of FSL-SPM on the nanofibres could mean that a higher concentration of molecule desorbs from the surface that is enough to cause the agglomeration effect whereas for spermine, not enough molecule remains on the surface after coating, even at 1 mg/mL concentration and thus minimum desorption occurs.

To further prove the desorption of FSL-SPM into Agnp solution and its induced agglomeration of nanoparticles, an increasing concentration of FSL-SPM was directly added to 1 mL [-]Agnp solutions. Similarly, an increasing concentration of spermine was also added to a different set of 1 mL [-]Agnp solutions. The mixtures of solutions were observed for colour change after 12 hours.

 It was observed that FSL-SPM in solution produced the same effect of colour change in Agnp solutions as described in Figure 42 but only at certain concentrations. Similarly, spermine in solution also caused the effect but at different concentrations as compared to FSL-SPM. The colour change at different concentrations for FSL-SPM and spermine is shown in Figure 44.
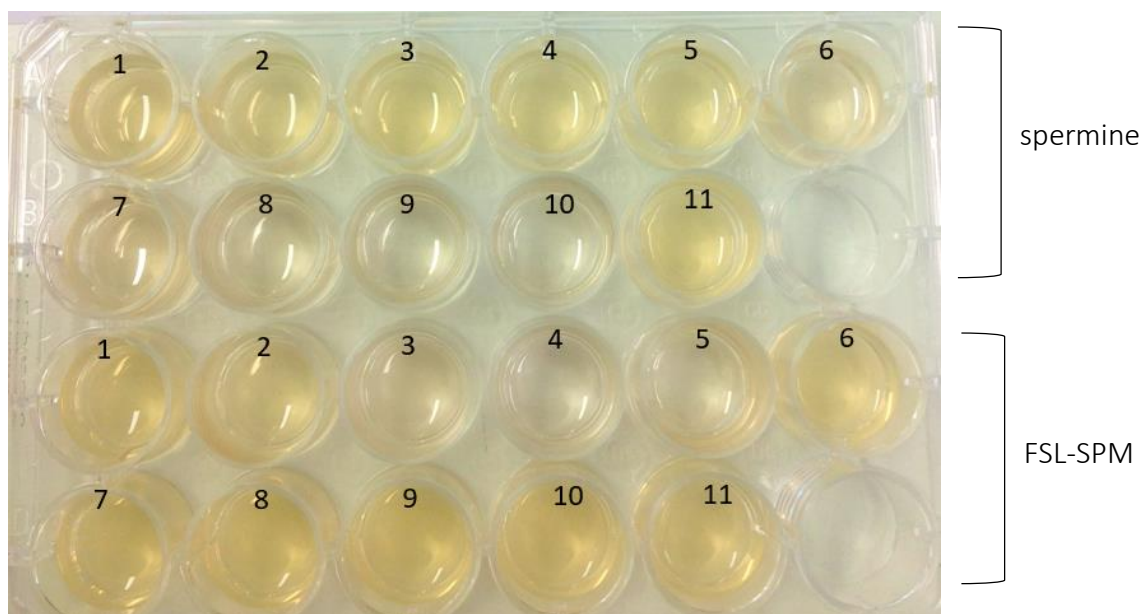
Figure 44: The colour change in [-]Agnp solution after the direct addition of FSL-SPM and spermine. 1-10 are increasing concentrations of FSL-SPM and spermine in mg/mL added to [-]Agnp solutions; 1: 0.0002, 2: 0.0005, 3: 0.001, 4: 0.005, 5: 0.01, 6: 0.05, 7: 0.1, 8: 0.25, 9: 0.5, 10: 0.1, and 11 is 0 mg/mL of FSL-SPM (control). Spermine induces colour change starting at 0.05 mg/mL to 1mg/mL. However, FSL-SPM induces colour change at lower concentrations of 0.001, 0.005 and 0.01 mg/mL.

It was further interpreted that the change of Agnp solution only at certain concentrations could possibly indicate the requirement for a balance of spermine molecules and the nanoparticles. Too low or too high concentration could result in a hook or prozone effect that has been previously described in the literature in terms of antibody-antigen agglutination reactions [234,235]. Therefore, an equivalence reaction with optimal nanoparticle and charged molecules could have only occurred at certain concentrations. Further, this also possibly indicates the importance of lipid (DOPE-DOPE interactions) and spacer groups in FSL-SPM in helping to bring two nanoparticles together by forming a bridge between the particles as compared to just the spermine. This could have resulted in lower concentration of FSL-SPM being enough to produce the effect.

Some of the concentrations from Figure 44 were visualised under SEM to assess whether agglomeration has occurred in the solutions. Solution (vii) of spermine and solution (iii) of FSL-SPM were compared against solution (xi)-control Agnp solution. The SEM images are compared in Figure 45.
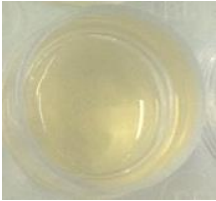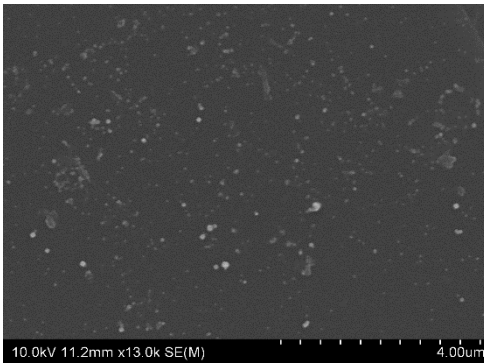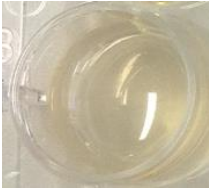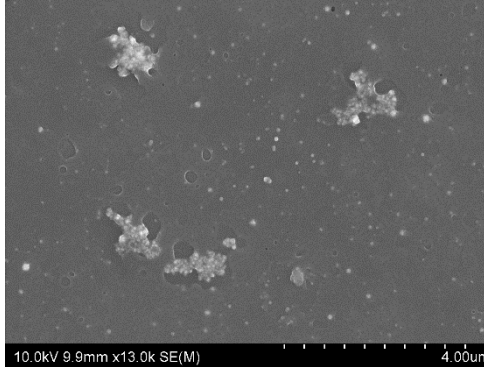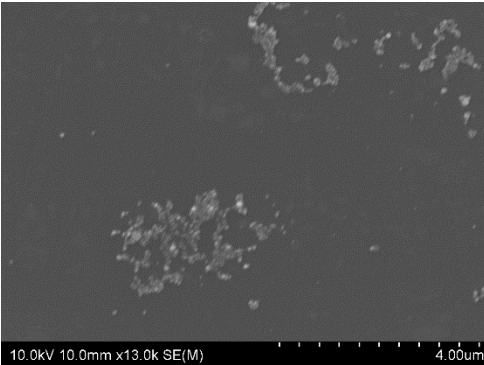
Agnp solutions (refer to Figure 45)	Photo image	SEM image of solution
a) Control solution (11)		
b) Solution (7) of spermine (0.01 mg/mL spermine added to Agnp solution)		
c) Solution (3) of FSL-SPM (0.001 mg/mL FSL-SPM added to Agnp solution)		

Figure 45: Comparison of a mixture of [-]Agnp solutions with FSL-SPM and spermine. The mixture solutions from Figure 45 were visualised under SEM and it was observed that the colour change induced by direct addition of 0.01 mg/mL spermine or 0.001 mg/mL FSL-SPM is accompanied by agglomeration of the particles.

It was observed that both the solutions in Figure 45b and c showed agglomeration of nanoparticles when visualised under SEM but in the control solution in Figure 45a, nanoparticles were evenly dispersed with no sign of agglomeration. Therefore, with all the supporting evidence, it was concluded that when nanofibres are coated with higher concentrations of FSL-SPM, there is a chance of desorption of FSL-SPM into Agnp solution, especially with increasing contact times that can result in agglomeration of particles and lower adsorption capacity.

Effect of nanofibre thickness

The thickness of the fibre, usually expressed in gram per square meter (gsm) affects the adsorption capacity of nanofibre surfaces. For a given average diameter of the fibre in an electrospun mat, a higher gsm nanofibre has a greater number of fibres and are densely packed. This provides a larger surface area for modification and thus produces more active sites for adsorption. However, for effective filtration, higher permeability is desired along with capture of particles [236,237]. In such case, a high packing density or greater thickness introduces higher pressure drop and the performance of the filter decreases whereas for adsorption it is an advantageous feature because the performance of adsorbate is not dependent on the flow rate. Many study show increase in adsorption efficiency with increase in mass and thickness of adsorbent [238–240].

Method overview

Nanofibre thickness of increasing order (0.5, 1 and 4 gsm) was compared against each other for their adsorption efficiency of [-]Agnp after coating with 0.5 mg/mL FSL-SPM. These values of thickness were chosen because they were standard samples manufactured by Revolution Fibres. Thickness higher than 4gsm could also be investigated but has not been included in this study.

Results and interpretation

From Figure 46, it is apparent that 4 gsm thickness works better for all nanofibre types. The decrease in efficiency with decreasing gsm was expected because, with decreasing thickness of fibres, lesser area is available for FSL-SPM attachment and nanoparticle adsorption
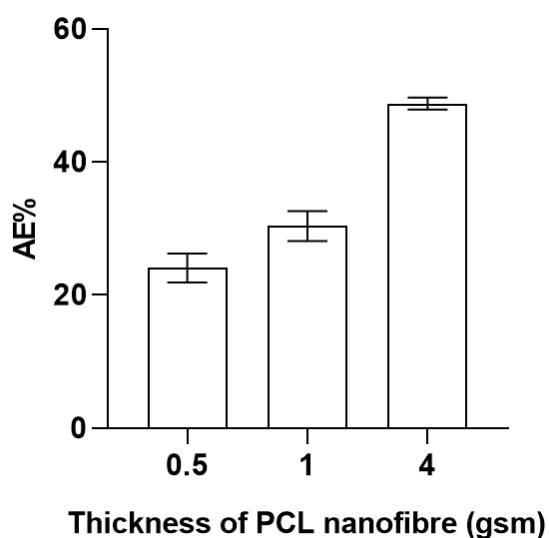
Figure 46: Comparison of [-]Agnp adsorption efficiency by PCL nanofibre of different thickness.

Stability test of FSL-SPM by using adsorption protocol

Stability of constructs at different times and conditions of storage is an important factor in understanding the strength of attachment of FSL constructs and viability of the functional groups. Various FSL-constructs have been found to be stable on modified surfaces for up to 8 months of storage at room temperature [241], where immunostaining was used to assess the functionality of the constructs. However, FSL-constructs used in this study do not contain functional groups that can be visualised through immunostaining. Therefore, the ability of FSL-SPM to adsorb negatively charged nanoparticles was utilised to understand the stability of charged constructs.

Method overview

PCL nanofibres were coated with 0.5 mg/mL FSL-SPM (Protocol 2.2.2) and divided into two groups for storage, in the fridge at 4°C and at room temperature (RT). Enough nanofibres were coated so that stability test could be conducted in triplicates and were kept in Petri-dishes properly sealed with paraffin. The nanofibres were tested for their stability at 2 and 4 months of storage by measuring their adsorption efficiency to remove [-]Agnp from the solution. The standard adsorption protocol (Protocol 2.4.1) was followed and the efficiency of stored nanofibres was compared with that of nanofibres coated on the same day of the experiment.

Figure 47 shows that FSL-SPM is stably attached to the nanofibre surface and the functionality of the construct does not deteriorate upon storage up to 2 months irrespective of the condition of storage. However, at 4 months, the adsorption efficiency of nanofibres stored at room temperature decreases, which could be possibly caused by either the loss of attachment of the lipid part of the construct from the surface or the loss of functionality of spermine in the construct. More investigation is required to assess the decrease in adsorption efficiency with time. On the other hand, the nanofibres stored in the fridge at 4°C showed comparable adsorption efficiency with the nanofibres coated on the same day. The points towards the importance of temperature in loss of activity of the construct.
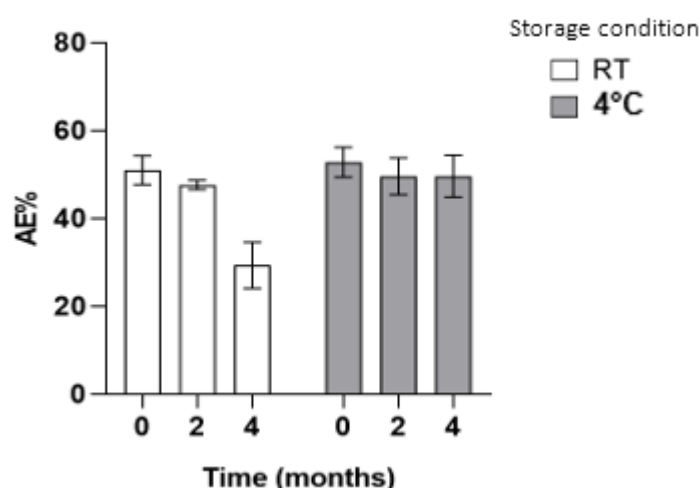
Figure 47: Stability test of FSL-SPM coated nanofibre.The adsorption efficiency deteriorates when stored at RT with time as compared to storage at 4°C.

Modification before electrospinning vs post-electrospinning

Electrospinning is dependent on many variables and therefore the introduction of a modifying agent into the polymer solution before electrospinning could influence the electrospinning process in an undesirable manner. It could also result in uncontrolled effects in pore-size, fibre diameter and morphology. For these reasons, post electrospinning modification of surface is the most preferred method. Specifically, in case of surface modification by charged molecules like FSL-SPM, there is high possibility that

electrospinning could be affected as the process is highly dependent on charge of the polymer solution. Nevertheless, the ability to co-electrospin modifying agents along with the polymer solution would help in scaling up the fabrication process and could produce evenly modified surfaces without an additional stage of post-manufacture modification. Therefore, it was necessary to compare the efficiency of modification by adding FSL-SPM during electrospinning vs modifying the fabricated nanofibres after electrospinning.

Method overview

Electrospinning was done at Revolution Fibres Ltd. using standard protocols. FSL-SPM was directly added to the prepared polymer solutions and mixed thoroughly before electrospinning. Firstly, electrospinning of PCL was by done by adding FSL-SPM to the polymer solution. The standard protocol for spinning of PCL required the use of acids. Therefore, it was predicted that acids could possibly denature FSL-SPM. A preliminary trial was conducted to assess the effect of the addition of FSL-SPM in the polymer solution and it was observed that the fibre morphology was greatly changed with dramatic increase in fibre diameter (Figure 48). The resultant modified fibre was not successful in capturing [-]Agnp. Thereafter, instead of PCL, PVB polymer solution was chosen for electrospinning with FSL-SPM, considering that no acid was involved in the process.

a)   b)
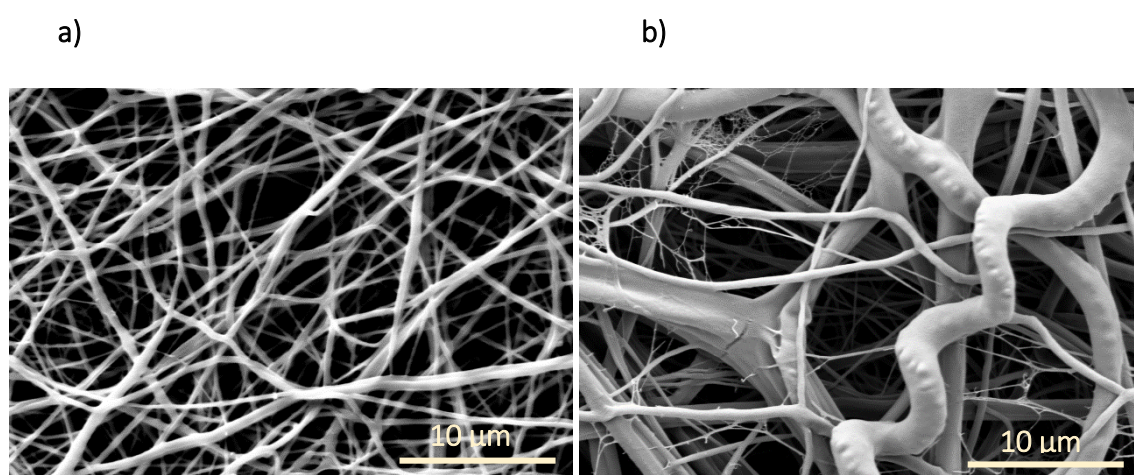
Figure 48: The effect of pre-electrospinning FSL-SPM modification of PCL nanofibre. a) shows control PCL nanofibre without FSL-SPM. b) shows PCL nanofibre electrospun after adding FSL-SPM to the polymer solution.

Referring to the standard coating protocol 2.2.2, to achieve 0.5 mg/mL FSL-SPM coated nanofibre, only 100 μL of 0.5 mg/mL is applied for coating, which means 0.05 mg of FSL-

SPM, would be in contact with the surface. Taking this fact into consideration, the pre-fabrication modified PVB nanofibres with 0.05 mg of FSL-SPM was compared with post-fabrication modified PVB coated with 0.5 mg/mL of FSL-SPM by using the standard adsorption protocol. The surface area of nanofibre was also kept consistent for both pre and post-fabrication samples. Then the surfaces were used to remove [-]Agnp using the standard adsorption protocol (Protocol 2.4.1). However, it should be noted that in the protocol, the entire volume of the construct applied to the surface does not come in contact with the surface and that the excess construct is always washed before using for all experiments. Therefore, investigation that is more sensitive is required to measure the true amount of FSL-SPM on the post electrospinning modified surfaces. Nevertheless, this experiment could provide valuable insights into the difference between adding FSL-SPM before and after electrospinning/fabrication.

Results and interpretation

The adsorption efficiency was observed to decrease for the fibre modified pre-fabrication as compared to fibres modified post-fabrication (Figure 49). The fibre diameter and morphology of PVB nanofibres remained unchanged even after the addition of FSL-SPM to the polymer solution, indicated by similar morphology in Figure 50b,c. SEM images in Figure 50 further validated better adsorption capacity of post-fabrication modified nanofibre, where more particles are adsorbed on Figure 50b and in an even manner as compared to Figure 50c.

The possible reason could be that when the fibres are coated after electrospinning, the lipid and spacer part is properly attached and oriented, ensuring optimum exposure of the functional head for removal of nanoparticles. However, when the constructs are mixed with the polymer solution during electrospinning, the mechanism of insertion of the constructs on the surface is not under control. It is possible that the constructs could have been buried or entrapped inside the fibres during electrospinning and there is loss in the number of constructs available on the surface for carrying out the function. However, more experiments need to be conducted using various polymer solutions and constructs to assess the best conditions for pre-fabrication modification.
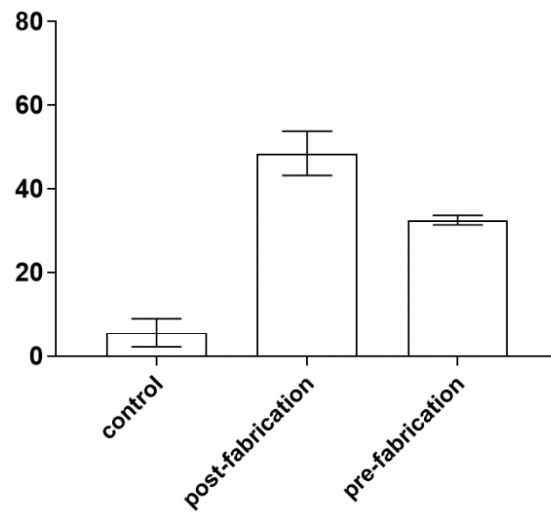
Figure 49: Comparison of [-]Agnp adsorption capacity of PVB nanofibre modified pre and post-fabrication.

a) Control PVB nanofibre
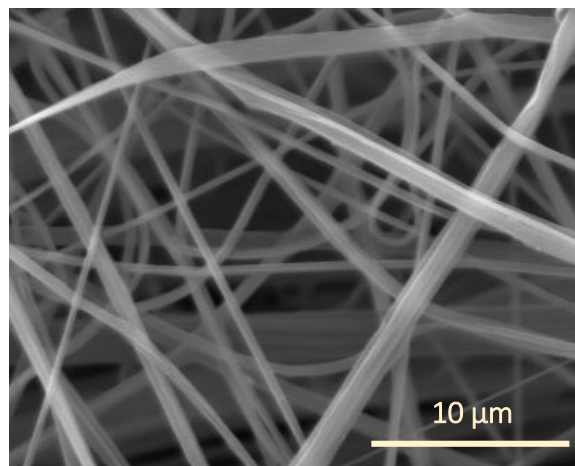
b) Post-fabrication modification
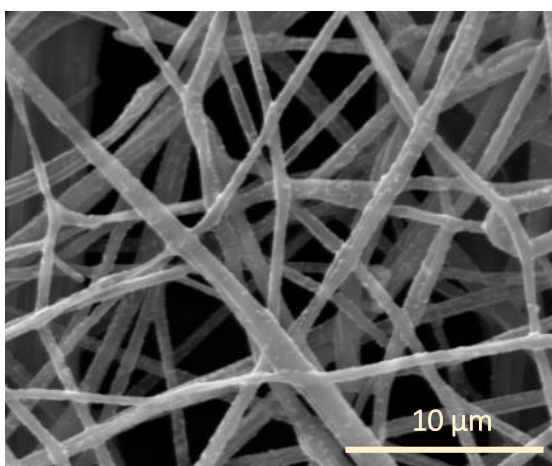
c) Pre-fabrication modification
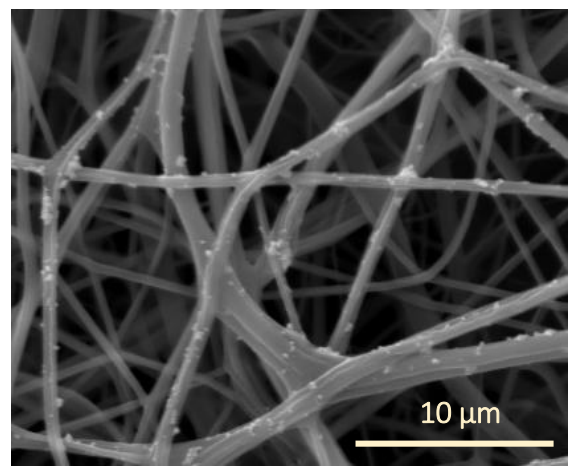
Figure 50: SEM images of PVB nanofibre after adsorption of [-]Agnp. a) shows control PVB nanofibre. b) shows PVB nanofibre modified with FSL-SPM post-fabrication and c) shows PVB nanofibre modified prefabrication. b) shows greater and even removal of nanoparticles as compared (c).

2.4.2 Nanoparticle capture - filtration

The results of the adsorption assays that proved the efficiency of FSL-SPM in capturing the [-]Agnps were further validated using a different set of protocol involving filtration of nanoparticles through the modified nanofibres. Adsorption assays were conducted in 24-well plates, allowing the nanoparticles to adsorb on to the coated fibres for a given time. However, filtration assays were conducted by passing the nanoparticle suspension through the coated fibres inserted in a filter holder connected to a syringe. Variables affecting the filtration process such as flow rate, initial concentration of nanoparticles, concentrations constructs were taken into consideration and the experiments were conducted based on a standard protocol designed for filtration.

Protocol 2.4.2: Standard filtration protocol

1. PCL nanofibres were coated with FSL-SPM by following the standard coating protocol described in section 2.4.1. However, the area of the surface coated was changed to 10 mm × 10 mm. It was done so that the fibre area would be enough to be properly inserted inside the filter holder.

2. A reusable filter holder was connected with a 1 mL syringe containing 1 mL of nanoparticle solution. The coated nanofibre was properly inserted inside the filter holder and sealed.

3. A syringe pump (Orion Sage Pump, Thermo Scientific) was used to control the flow rates of filtration.

4. The filtrate was collected in a microfuge tube and 100 µL of the filtrate was transferred to a 96-well plate for absorbance analysis using UV-Vis spectrophotometer.

5. A standard curve was generated for the volume to be analysed for absorbance similarly as in Protocol 2.4.1.

6. Filtration efficiency was calculated by measuring the difference between the absorbance of nanoparticle solution before and after filtration and employing the standard curve (Similar to adsorption efficiency calculation in 2.4.1).

Comparison of adsorption with filtration

Method overview

Using the standard filtration protocol (Protocol 2.4.2), the filtration efficiency was calculated for nanofibres coated with 0.01, 0.05, 0.5 and 1 mg/mL FSL-SPM and the efficiency was compared with adsorption efficiency of respectively coated nanofibres (discussed in 2.4.1). The flow rate of filtration was maintained at 6 mL/min. The adsorption efficiency (AE%) of FSL-SPM was then compared with filtration efficiency (FE%). The absorbance analysis for efficiency calculation was done at 430 nm for both assays. However, it should be noted that although the surface area used for filtration and adsorption is not the same but comparable. For adsorption, 52.5 mm^2 of PCL (4 gsm) nanofibre was used whereas 50.2 mm^2 was used for filtration. This 4% difference in surface area is small and thus ignored for comparisons.

Results and interpretation

Filtration assay was found to be more efficient in capturing nanoparticles as compared to adsorption assay for 0.05, 0.5 and 1 mg/mL (Figure 51). Images in Figure 52 further validate that filtration enhances the capturing capacity of the coated surface. Generally, filtration is dependent on mechanisms such as size exclusion, inertial impaction, diffusion and electrostatic interaction between the particle and the filter media [140]. Larger particles are usually removed by size exclusion. However, since the size of nanoparticles is very small, the increase in efficiency is predicted to be the result of two mechanisms working together a) inertial impaction that occurs when the suspending liquid passes through the filter, but the nanoparticles hit the fibres and get stuck b) electrostatic interaction between the nanoparticles and the FSL-SPM. In the case of adsorption, the capturing process is passive and only the outer surface of nanofibre in contact with nanoparticle solution is actively involved in attracting the particles towards the surface, whereas in filtration, the bulk structure of nanofibre is involved in active capturing of the particles. This could be a possible reason for significant increase in efficiency for filtration as compared to adsorption.
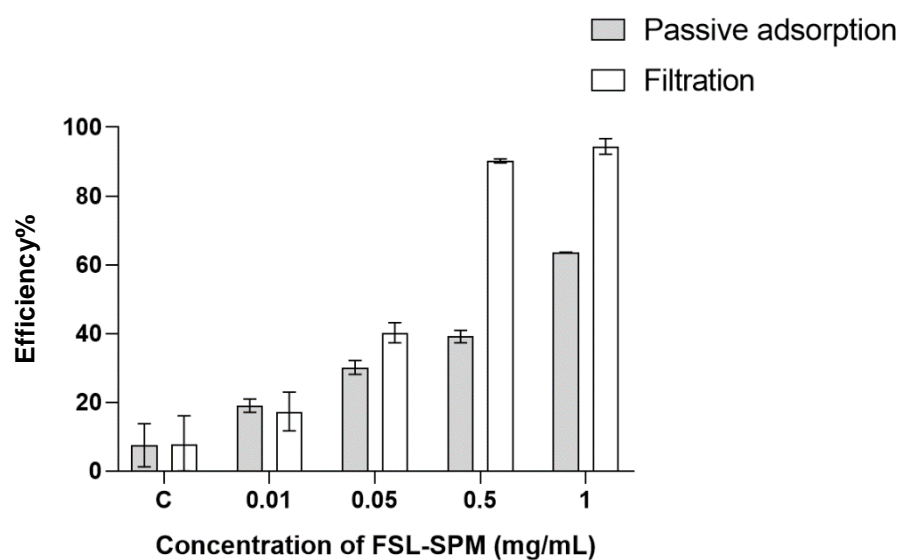
Figure 51: Comparison of adsorption and filtration efficiency of FSL-SPM for the capture of [-]Agnps.

.

a)

b)

Passive adsorption
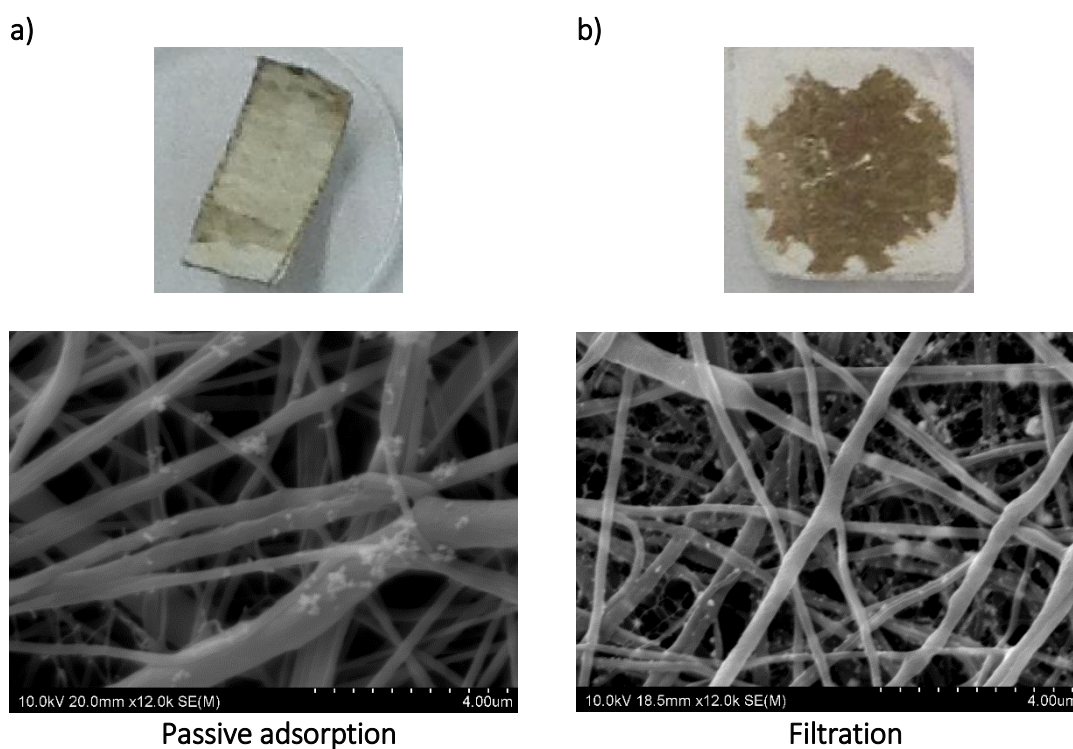
Filtration

Figure 52: Comparison of adsorption and filtration capacity of FSL-SPM coated nanofibre. Both a) and b) are coated with 0.5 mg/mL FSL-SPM a) shows camera image of coated nanofibre after adsorption along with its SEM image. b) shows coated nanofibre after filtration. The brown colour is from Agnp. In a), the whole surface area in the camera image was used for adsorption whereas in b), only the brown circular area was used for filtration.

Comparison of FSL-SPM with spermine

Complementing the adsorption results, filtration assay further validated that FSL-SPM is more efficient in the removal of [-]Agnp as compared to spermine alone (Figure 53). Moreover, the results showed that FSL-SPM was not washed away bypassing the nanoparticle solution through the fibres whereas spermine was probably washed away in the initial stage while washing after FSL-SPM coating. It further highlights the importance FSL immobilisation for proper attachment to the surface.
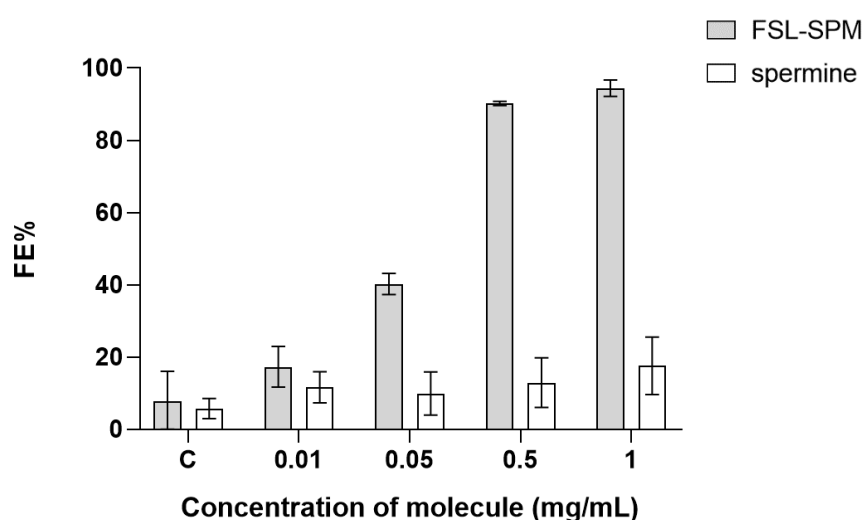
Figure 53: Comparison of filtration efficiency of FSL-SPM with spermine.

Effect of initial concentration

1× concentration of nanoparticles was observed to be filtered more efficiently as compared to 3× and 6× concentrations (Figure 54). Unlike adsorption where the efficiency of removal of 3× concentration was found to be greater at 1mg/mL FSL-SPM coating as compared to 1× and 6×, the filtration efficiency of 1× was observed to be higher than other concentrations at all concentrations except 0.01 mg/mL. At higher concentrations, it is generally observed that the binding sites on the nanofibres get saturated faster than at lower concentration [242]. It could be responsible for the loss of efficiency as the concentration of nanoparticle increases.

99
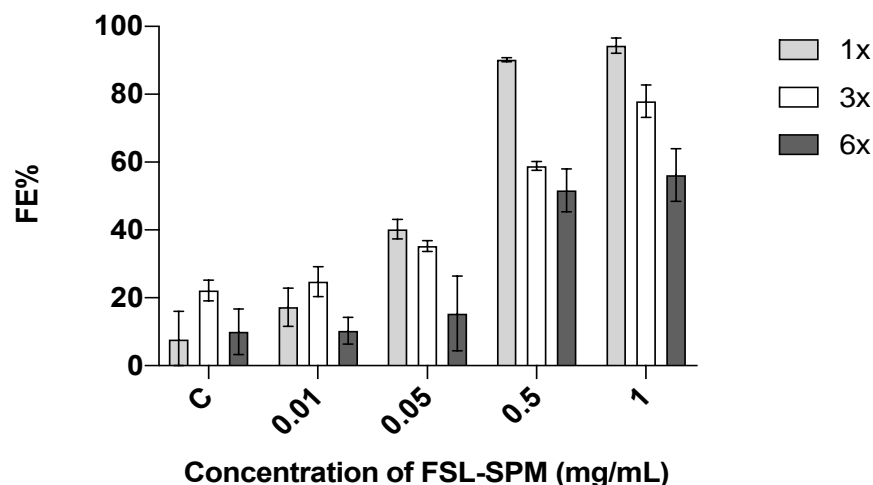
Figure 54: Filtration efficiency (FE) of FSL-SPM at different concentrations of FSL-SPM and [-]Agnp. 1× concentration of nanoparticle is observed to be filtered with greater efficiency as compared to other nanoparticle concentrations.

Effect of flow rate

Generally, adsorption efficiency decreases when the flow rate is increased [243–245]. According to the authors, increasing the flow rate causes a shorter retention time due to which particles do not get to be in contact for required period. On the other hand, slower flow rate provides enough time for the particles to diffuse properly onto the surface.

Since 1 mL of solution was filtered, the time required for 0.06 mL of Agnp solution to pass through the filter was 1000 seconds. Similarly, the time required for 0.6 and 6 mL of solution was 100 seconds and 10 seconds respectively. Figure 55 shows the effect of flow rate on adsorption efficiency of 0.5 mg/mL coated FSL-SPM for different concentrations of [-]Agnp. It is apparent that filtration is highly dependent on the flow rate of the solution. According to the figure, the filtration efficiency was observed to be the highest at 0.6 mL/min for all concentrations. However, at the lowest flow rate of 0.06 mL/min, the adsorption efficiency is observed to be the lowest in this study. The possible reason for this phenomenon could be desorption of FSL-SPM from the surface due to the longer contact time of surface with nanoparticle solution. It was observed that at 1× concentration of Agnp, adsorption efficiency did not reduce at higher flow rates but achieved an equilibrium after 0.6 mL/min. It indicates that for that concentration of particle, 0.6 L/min is sufficient to adsorb all the particles and increasing the flow rate does not affect the adsorption process. However, for 3× and 6× concentrations, the adsorption efficiency decreased at 6 mL/min. It could be a combined effect of unavailability of

binding sites and lower retention time for adsorption. Therefore, there must have been a balance of ideal retention time, availability of binding sites and favourable conditions for FSL-SPM to remain attached to the surface.
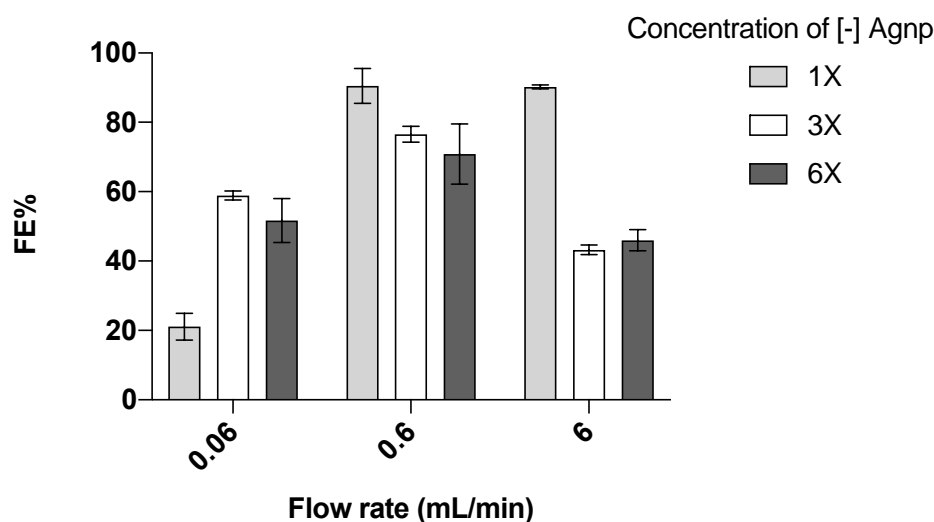
Figure 55: Effect of flow rate on adsorption efficiency of 0.5 mg/mL FSL-SPM coated filter. 0.6 mL/min is observed to be the ideal condition of flow rate, providing maximum adsorption efficiency.

It is also necessary to consider that this trend of adsorption efficiency change due to a change in flow rate could be different for different concentration of FSL-SPM analysed. More investigation is required to assess an ideal concentration of FSL-SPM and flow rate to achieve the maximum adsorption efficiency.

Conclusion

In this chapter, analysis of Kode constructs, nanofibres characterisation and assessment of nanofibre surface modification were done as a preliminary investigation. Silver nanoparticles (Agnp) with negative and positive charge were synthesised in the lab as surrogates of particulate matter. Various physical and chemical aspects such as charge, size and elemental composition of the nanoparticles were characterised. Different Kode constructs were trialled to modify nanofibres that were then used to capture nanoparticles through process of adsorption and filtration. A variety of parameters such as type of solvents, coating concentration, pH, contact time, and pre and post electrospinning modification were studied. Thus, the experiments conducted in this chapter were established as model experiments and the conclusions derived from the

study was utilised to analyse capture of air particulate matter using Kode modified nanofibres in the next chapter.

This chapter established some important conclusions as given below and air particle capture study (Chapter 3) was guided by these conclusions.

- o FSL-SPM can modify nanofibre without significant change in fibre morphology up to 0.05 mg/mL for PCL nanofibre. The pore size of nanofibres also remain unchanged up to 0.05mg/mL, indicating that the surface can be used for filtration without significant change in flux. However, concentrations up to 1 mg/mL can be utilised in capturing particles through adsorption process where flow rate is an affecting parameter. Such FSL-SPM modified filters can be used to efficiently capture negatively charged particles

- o Kode constructs such as FSL-Z can also capture positively charged particles. However, more investigation is required to optimise their application and possibility of their use along with FSL-SPM to capture a wider range of particles.

- o FSL-SPM capture particles better through filtration as compared to adsorption and that the filtration process depends on parameters such as flow rate and concentration of particles

- o Considering the coating effects and study of capturing efficiency, FSL-SPM coating works better at concentrations below 0.5 mg/mL for filtration applications.

- o Modification of nanofibres with FSL-SPM post electrospinning is more efficient that pre electrospinning

- o The activity of FSL-SPM coated nanofibres for capturing particles is retained for up to 4 months when stored at 4°C

Chapter 3: Air particulates capture – methods and results

3.1 Characterisation of nanofibre and FSL modification

PMMA (polymethyl methacrylate) nanofibre with a thickness of 0.5 gsm and a TPU (Thermoplastic polyurethane) support layer was used for air particulates capture. This particular polymer was chosen because of its wide use in air filtration applications. The thickness of 0.5 gsm is suitable for air particles capture because such thin filter media do not change the airflow rate significantly. The polymer was electrospun on a TPU support as it provides enough rigidity for ease of handling during experiments. Unlike liquid particulates capture where adsorption and filtration mechanisms were compared, for air particulate capture, only filtration was used.

An area of 60 mm x 60 mm nanofibre was used for this study. Since the area utilised for air particle filtration was much larger than for liquid filtration, the coating method was slightly modified from Protocol 2.2.2 as follows

1. Nanofibre strips were first washed in MilliQ water and dried at RT.
2. The washed surfaces were then flooded on one side (the surface of PMMA that would be exposed to the influent air) with 150 µL of FSL-SPM with the help of a micropipette.
3. The coated surfaces were then washed in MilliQ water for three times using separate beakers and dried at RT.

Ideally, FSL modification should not change the morphology of the nanofibre surface or decrease the pore size. Therefore, it was important to observe if the coatings result in blockage as it would result in decrease of airflow rate. For this, the coated surfaces were characterised using SEM. Additionally, Diameter J was used to analyse the fibre diameter distributions before and after coating. SEM observation showed that coatings above 0.4 mg/mL of FSL-SPM drastically changed the morphology of the surface, blocking almost all the pores (Figure 56).

Control (No FSL-SPM)   0.05 mg/mL

0.1 mg/mL   0.2 mg/mL
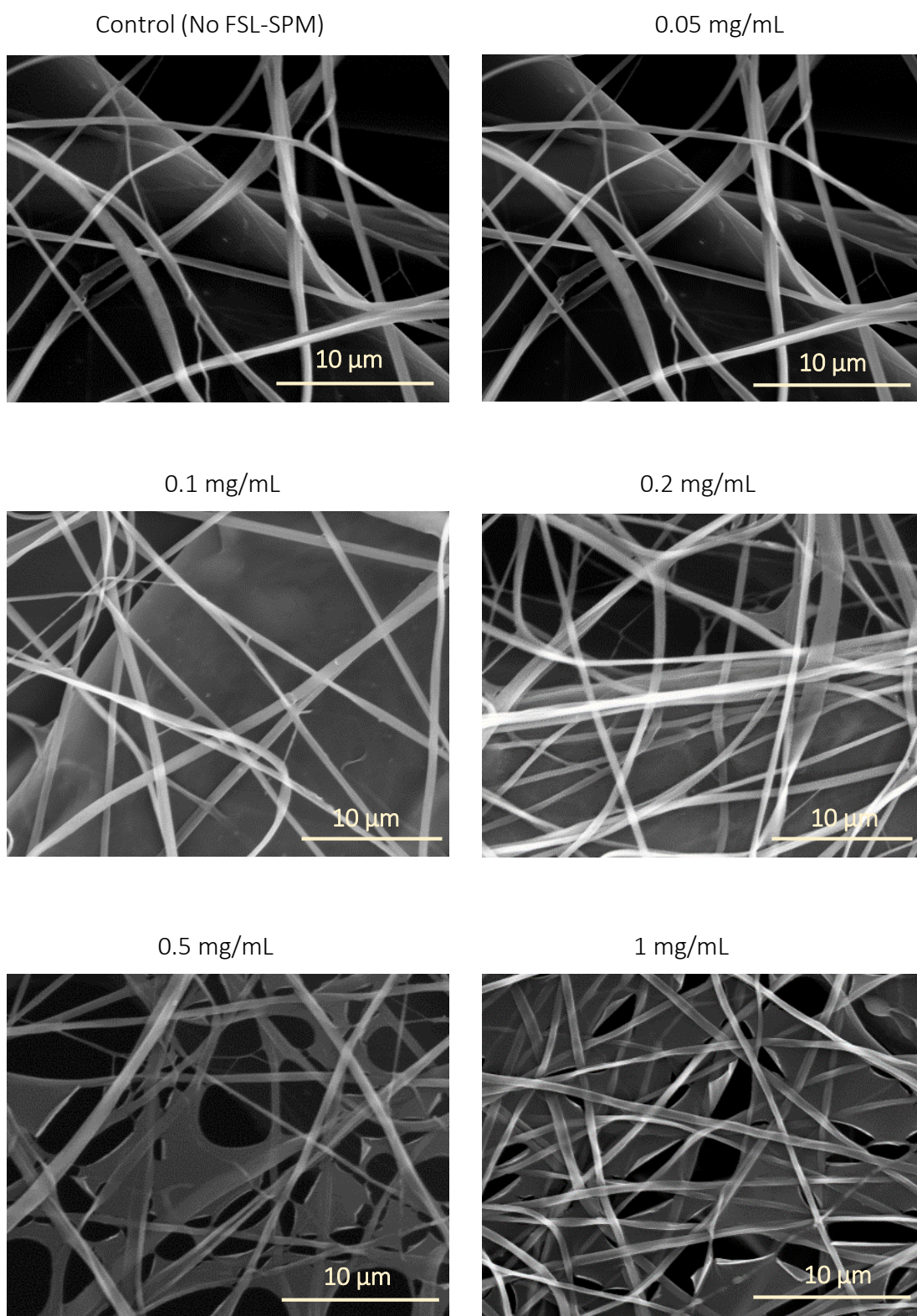
0.5 mg/mL   1 mg/mL

Figure 56: Change in the morphology of PMMA nanofibre with increasing FSL-SPM concentration. For up to 0.2mg/mL, FSL coating does not block pores. However, at higher concentration of 0.5mg/mL and 0.1mg/mL, after washing, the coating becomes visible as a thin film, almost blocking pores. The thick fibre-like structures behind the nanofibres in first four images represent the TPU backing layer that acts as support material for PMMA. It is not visible for last two images due to change in contrast of images.

When compared with fibre diameter analysis of PCL, at 0.5 mg/mL and 1 mg/mL the coating is more clearly visible as a thin film in case of PMMA as seen here in Figure 56 but not for PCL as seen in Figure 18. The possible reason for this difference in the coating is the difference in thickness of respective nanofibres used. PMMA has a lower thickness of 0.5 gsm as compared to PCL of 4 gsm used in the study. With lower thickness, a smaller number of fibres or surface area is available for coating due to which the excess FSL-SPM is visible in the form of a proper coating layer at higher concentrations for PMMA nanofibre.

It is also known that good quality filter is defined as a filter that can capture particulates while maintaining a good airflow across them. Since pore size is an important characteristic as it can change the airflow rate significantly, it is important to study the effect of FSL modification in terms of change in pore size.

To get an even coating layer without blocking the pores, 1mg/mL FSL-SPM was applied on PMMA surface using the same method as mentioned above but washing procedure was modified. Other solvents such as PBS and 70% methanol were used and washed for different times and compared with H_2O washing. It was predicted that these solvents would likely remove the excess coating on the surface. However, phosphate ions in PBS buffer reacted with FSL-SPM, causing precipitation of FSL-SPM to form crystalline structures on the coated surface after washing with PBS. On the other hand, 70% methanol seemed to remove more than desired. Figure 57 summarises the results.
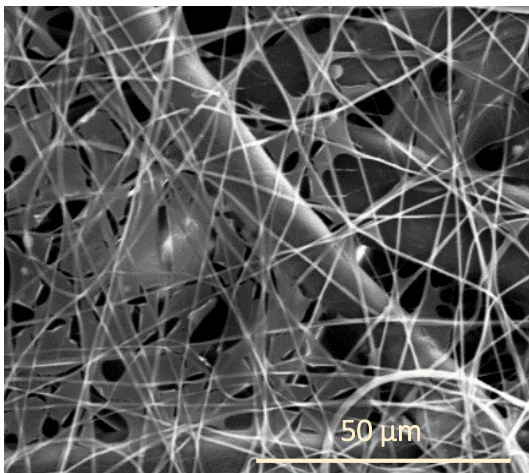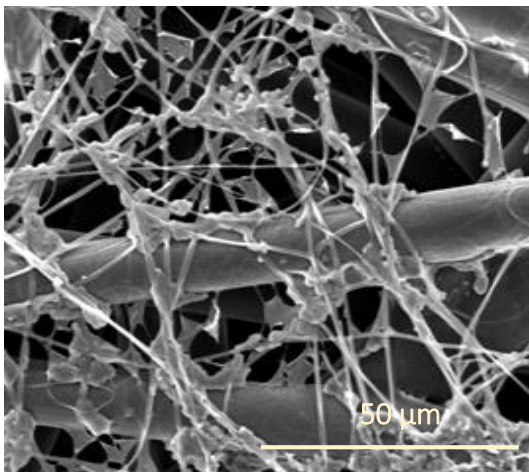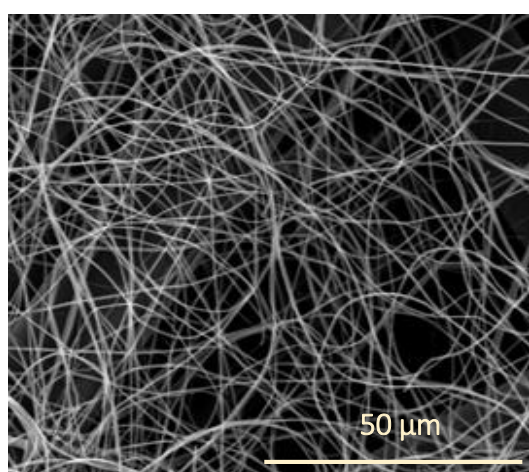
	Washing solvent	After washing
a)	H$_2$O	
b)	PBS	
c)	70% methanol	

Figure 57: SEM images of 1 mg/mL FSL-SPM coated PMMA nanofibres after washing with different solvents a) shows coated PMMA nanofibre after washing with water, b) show the nanofibre after washing with PBS and c) shows the nanofibre after washing with 70% methanol. PBS is observed to react with FSL-SPM to form precipitates, indicated by crystal formation. 70% methanol completely washed off the coating, indicating that it might be too harsh for washing as compared to water.

At 0.2 mg/mL, the pores dimensions and fibre diameter were not affected and there was no visible blocking of the pores. Since PMMA has been used only for filtration assays in this study unlike in Chapter 2, where adsorption by FSL-SPM coated PCL has also been analysed for adsorption assays. Therefore, the highest coating concentration was kept at 0.2 mg/mL of FSL-SPM. At 0.5 mg/mL and 1 mg/mL, there was an extensive blocking of pores and solvents such as methanol and PBS were not successful in removing the excess layer. It was observed that FSL-SPM was precipitated by PBS and methanol resulted in complete removal of FSL-SPM. Therefore, to ensure the best possible coating, 0.2 mg/mL was used set as the highest concentration to be tested for filtration applications. However, it should be noted that 0.3 and 0.4 mg/mL concentrations of coating could also be possibly analysed.

Therefore, PMMA was coated with FSL-SPM only up to 0.2 mg/mL and washed in water for the capture of air particles. Diameter J was used to calculate the change in fibre diameter after coating. Fibre diameter distribution was also analysed (Figure 58) that showed that for up to 0.2 mg/mL of FSL-SPM coating, there is no significant change in diameter. Table 7 summarises the fibre diameters along with the percentage increase in diameter as compared to control nanofibre.

Table 7: Average Fibre diameter at different concentrations of FSL-SPM. There is no significant change in diameter size for up to 0.2 mg/mL of FSL-SPM coating.

FSL concentration (mg/mL)	Fibre diameter (nm)	SD (±) of diameter	Skewness
0 (Control)	475	296	1.50
0.05	504	234	1.65
0.1	549	245	0.64
0.2	553	274	0.32

FSL-SPM coating (mg/mL)	SEM image of PMMA	Fibre diameter distribution
0		
0.05		
0.1		
0.2		
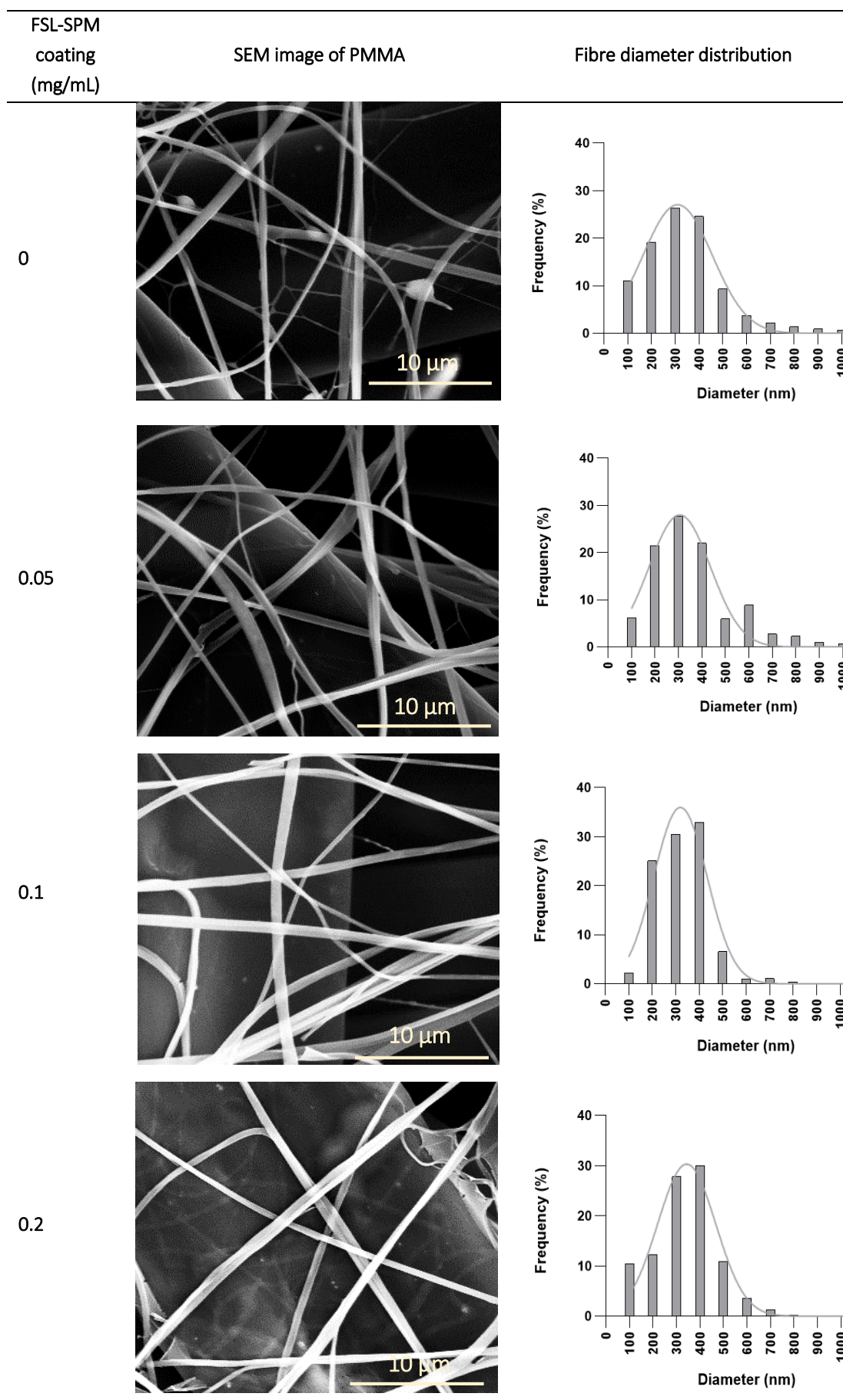
Figure 58: SEM image and fibre diameter distribution of PMMA nanofibre modified with different concentrations of FSL-SPM.

3.2 Synthesis and characterisation of particulates

Different sources were used for the synthesis of air particulates 1) diesel smoke 2) wood combustion and 3) incense burning.

Diesel smoke

For the production of diesel smoke, a diesel engine (Yanmar L40AE-D) was modified by adding a heat exchanger to the system (Figure 59). The engine was attached with a water pump and connected to a water tank for it to continuously pump water in and out, as the engine runs. It was designed so that the pumped water ran through the heat exchanger tube and cooled down the exhaust pipe, which was constituted inside the exchanger and a water trap was installed to get rid of moisture produced during diesel combustion. The heat exchanger system reduced the temperature of the exhaust gas so that particles could be obtained at ambient temperature.

1: water reservoir, 2: diesel engine, 3: water pump, 4: exhaust heat exchanger, 5: water trap, 6: particle outlet
Figure 59: Diesel engine set-up for production of diesel smoke

Further, an accumulator tank of 10 L was connected to the exhaust along with a pressure gauge as represented in Figure 60 to collect the smoke in a controlled manner and transferred to the lab for filtration experiments. Therefore, only a limited volume of diesel smoke could be collected in the accumulator tank and analysed at one time. For this reason, diesel smoke particles were only used in the preliminary phase of the project. The

research was then extended to study incense and wood particle filtration as these particles could be easily synthesised and tested inside the fume hood using those sources.
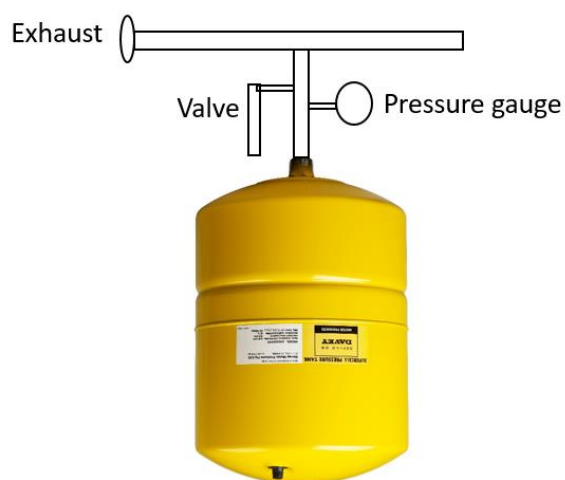
Figure 60: Schematic of connection of exhaust of the diesel engine system with the accumulator. The accumulator is connected by a valve before the exhaust outlet point and the smoke is directed into the accumulator by turning on the valve.

Incense smoke

Incense smoke was produced from commercially available incense sticks as shown in Figure 61. They were burnt inside a fume hood in the lab and the particles were collected.

Figure 61: Typical incense sticks used for air capture study

Wood smoke

Wood smoke was generated using a barbeque smoke generator (Smokai, NZ) that was used to combust pieces of wood. It was additionally connected to an air pump that helped in a steady production of smoke. Figure 62 shows the set-up of the wood smoke generator.
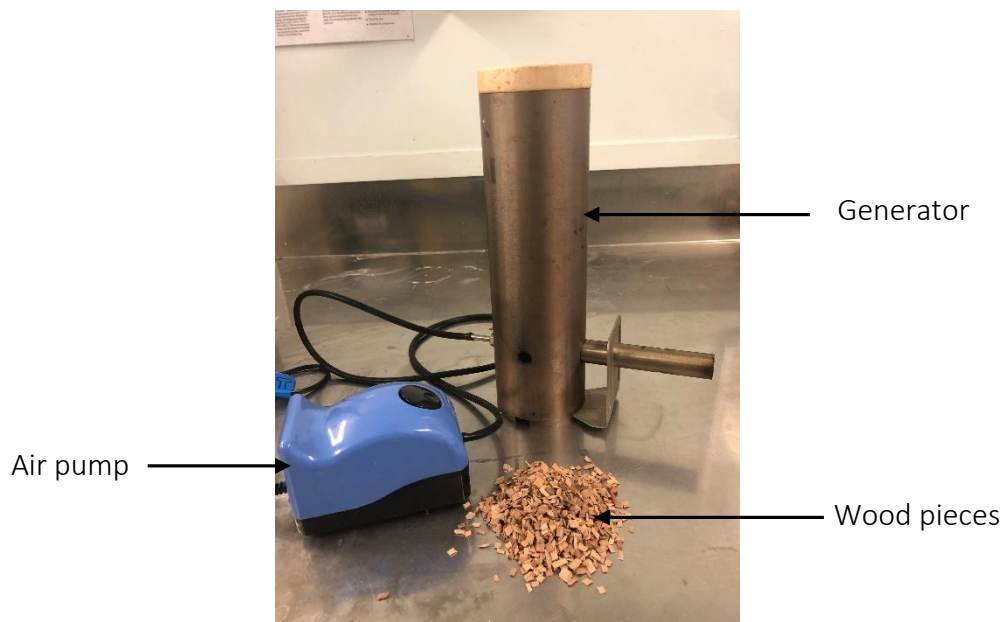
Figure 62: The set-up of the wood smoke generator

3.2.1 SEM and EDS characterisation

Characterisation of particulates was done using SEM (Hitachi S-70) and EDS to investigate particle size and morphology. Firstly, particles generated from different sources were collected on nanofibres or on mica surfaces placed directly in the path of the smoke. Manual SEM examinations choosing random fields were carried out at various magnifications up to 40,000 ×. EDS spectra of particles were obtained and for elemental analysis of samples. A laser particle counter (Graywolf Handheld 3016-IAQ) was used for size distribution analysis.

Results and Interpretations

SEM images showed the presence of both fine (<2.5 μm) and coarse particles (>2.5 μm) in smoke samples obtained using diesel, incense and wood combustion (Figure 63). A detailed scan of samples from all three sources detected more fine particles than the coarse ones. A very small number of particles greater than 10 μm was observed. Although characterisation was done for all particles less than 10 μm, considering that PM2.5 particles were present in a greater amount than particles bigger than 10 μm, filtration efficiency analysis was conducted only for PM2.5 particles in this study.

Coarse particles (observed at < 5k magnifications)	Fine particles (PM2.5) (observed at > 5K magnifications)
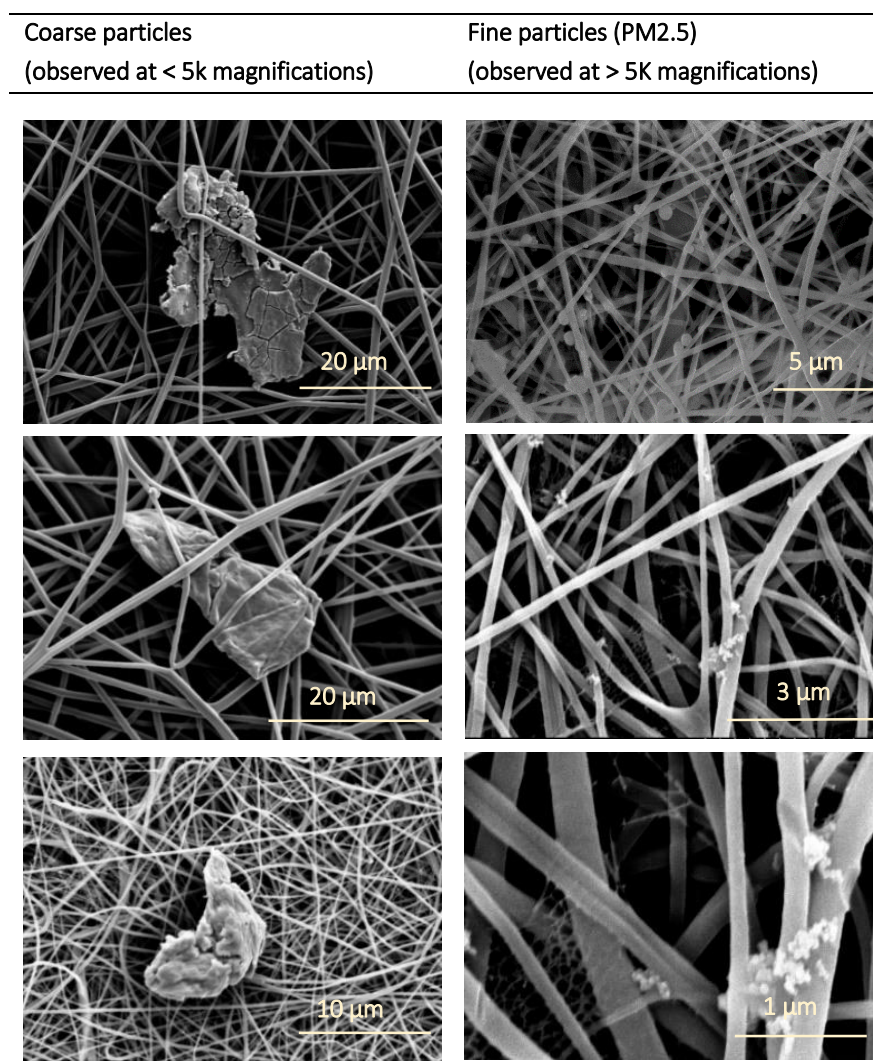
Figure 63: SEM images showing the presence of both coarse and fine particles in a smoke sample obtained from various sources such as diesel, incense and wood combustion.

Surface roughness of the particles was greatly varied even among the particles from the same source. Some had flat or smooth surfaces whereas some surfaces were rough and ridged (Figure 64). It is known that surface roughness can hugely affect the physical and mechanical properties of a body [246]. According to Figure 64, it was also observed that the flat surface particles had well-defined shape and were solid while the rough ones seemed to change their shapes to adapt to the shape of the filament in the filter easily, suggesting they were more liquid/gel-like. Such flexibility is an important property as it can increase the contact area between the particles and the surfaces they adhere. This enhances their adhesion forces and helps in strong attachment, mediating more harmful effects [246].

Smooth surface	Rough surface
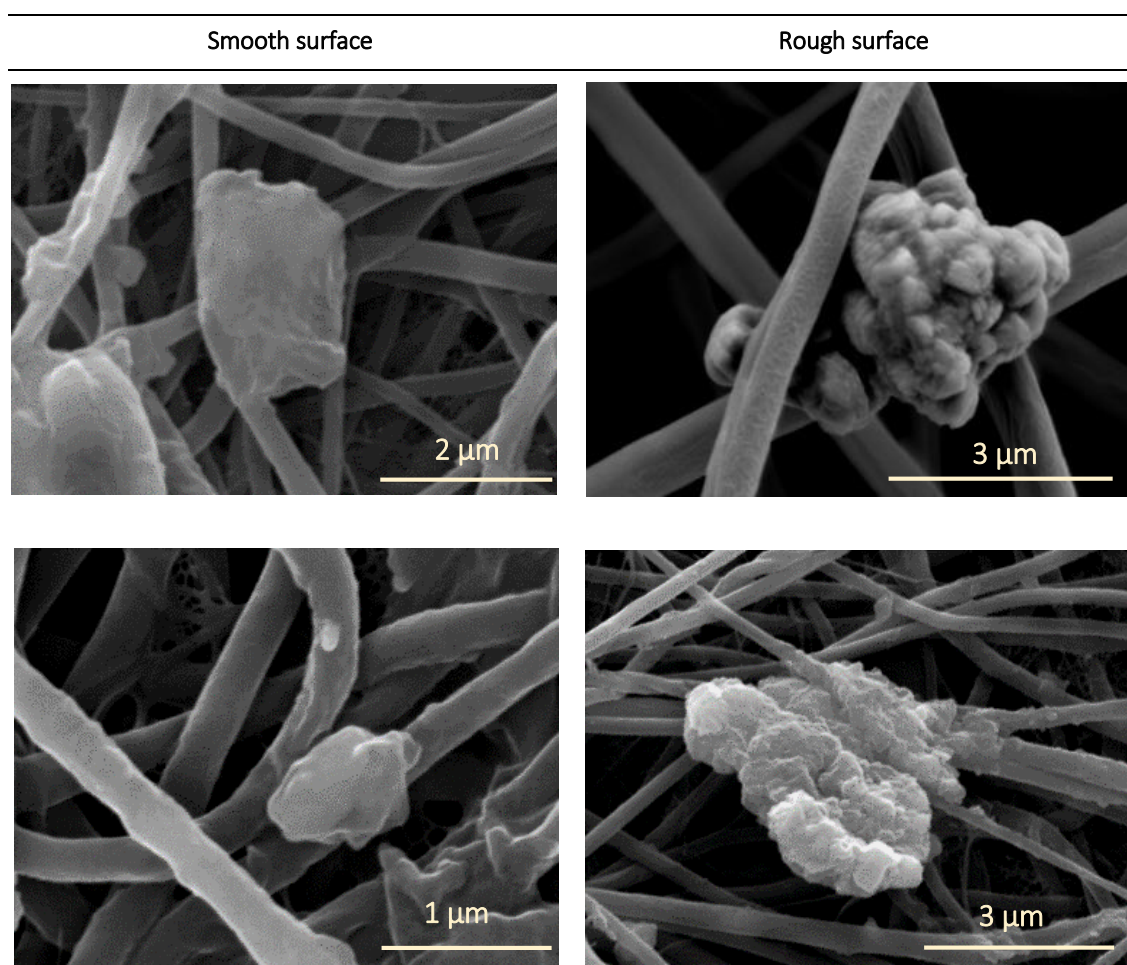
Figure 64: Different surface textures of particles. Smooth surface particles are flat with definite shapes whereas rough surface particles have irregular structure.

Regarding the morphological traits, the shapes of particles can provide important information about their chemical contents. Morphological analysis revealed mainly three categories of shapes a) fluffy aggregates b) elongated particles c) fly ash similar to those previously reported in literature [247,248]. They are illustrated in Figure 65.
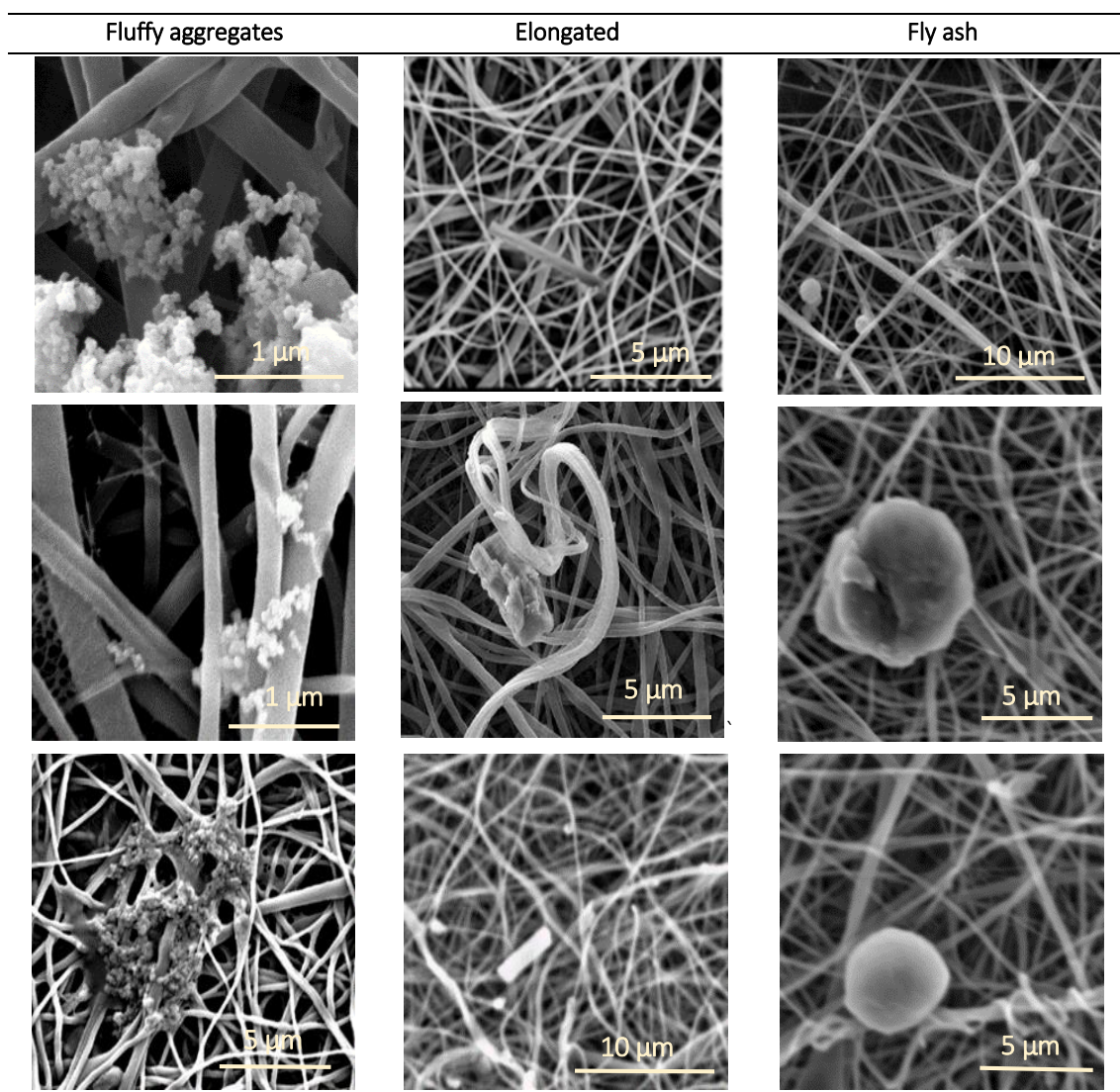
Figure 65: Different morphological features of particulate matter visualised by SEM. Fluffy aggregates are soot particles with high surface roughness. Elongated particles are crystalline with smooth surface and fly ash particles are spherical.

Fluffy aggregates are the agglomeration of soot particles forming a fuzzy structure that is considered as most notorious form of PM2.5s contributing to air contaminants in industrial and urban environments. Moreover, they have high surface roughness with highly adhesive capacity. They are usually observed to be carbonaceous with a very high carbon content as compared to oxygen and other inorganic elements [249]. The observation was consistent with EDS spectra in Figure 66.

Type	SEM image	EDX spectra

Fluffy aggregate
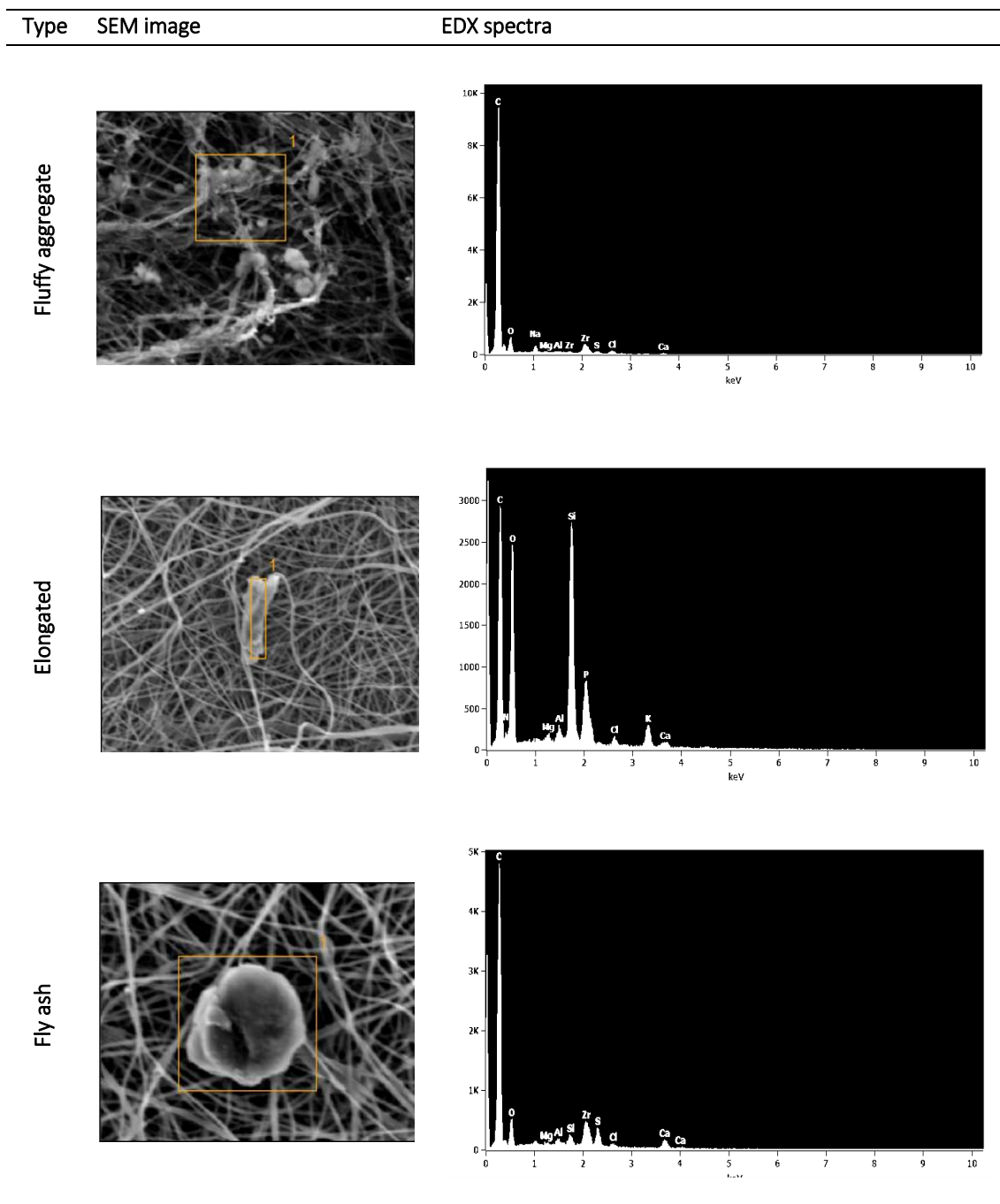
Elongated

Fly ash

Figure 66: EDS spectra of particles with different morphology. Fluffy soot aggregates have a higher carbon content as compared to other particles. Elongated particles have a higher content of inorganic elements such as Si, Al, Mg and P. Fly ash particles are usually a mixture of both organic and inorganic contents. However, their carbon content is lower than that of fluffy aggregates.

According to Figure 66, the elongated particles were found to be mainly composed of inorganic elements such as Al, Si, Mg and P and had definite shapes with a flat surface that looked almost crystal-like. Fly ash is spherical and composed mainly of non-combustible inorganic material, but also contains some carbon left over from partial combustion [250]. The fly ash-like particles in this study were found to have similar content and structure.

3.2.2   Particle counter characterisation of particulates

Method overview

Size distribution analysis and quantification of particles from all sources were done by using an optical laser particle counter (Handheld 3016-IAQ, Graywolf). The test duct in 3.3.1 (Figure 69) was used for carrying out the analysis. However, a modification was done by blocking the downstream part by a plastic strip so that influent air was blocked and collected on the upstream section where the particle counter was connected.

Timepoint analysis (TPA) of particulate matters was done for incense and wood particles at 4 minutes intervals for up to 45 minutes using the particle counter data. The size distribution was calculated for particles of size 0.3, 0.5, 1, 2.5, 5 and 10 µm, expressed as percentage of total counts. The total number of PM2.5 particles was also calculated by totalling the counts in all size ranges, expressed as raw counts, and compared between incense and wood sources. TPA was only done for incense and wood smoke and not for diesel smoke because the filtration experiments for these two sources were designed to monitor the filtration efficiency over an extended period (up to 25 minutes). It provided an insight into the effect of particle size distribution on filtration efficiency at different time points. However, for diesel smoke experiments, filtration could only be done for 90 seconds (as a consequence of the size limitation of the collected particles) so TPA study was not important.

Results and interpretation

According to the size distribution analysis done at different time points of combustion of incense and wood particles, 0.3 µm particles were the most abundant (Figure 67). The percentage of particle count in the smoke decreased with the increase of particle size, for all size groups. It was also interesting to note that the number of 0.3 µm particles decreased with increase in time, whereas the number 0.5 µm particles increased with increase in time. This trend was similar in both incense and wood particles (Figure 67a, b). The curves were mirrors of each other, indicating a linked relationship. It could be a result of agglomeration of small particles giving rise to bigger particles with increasing time and with increasing time, there could be a possible increase of heat in the system causing unstable production of smoke particles.
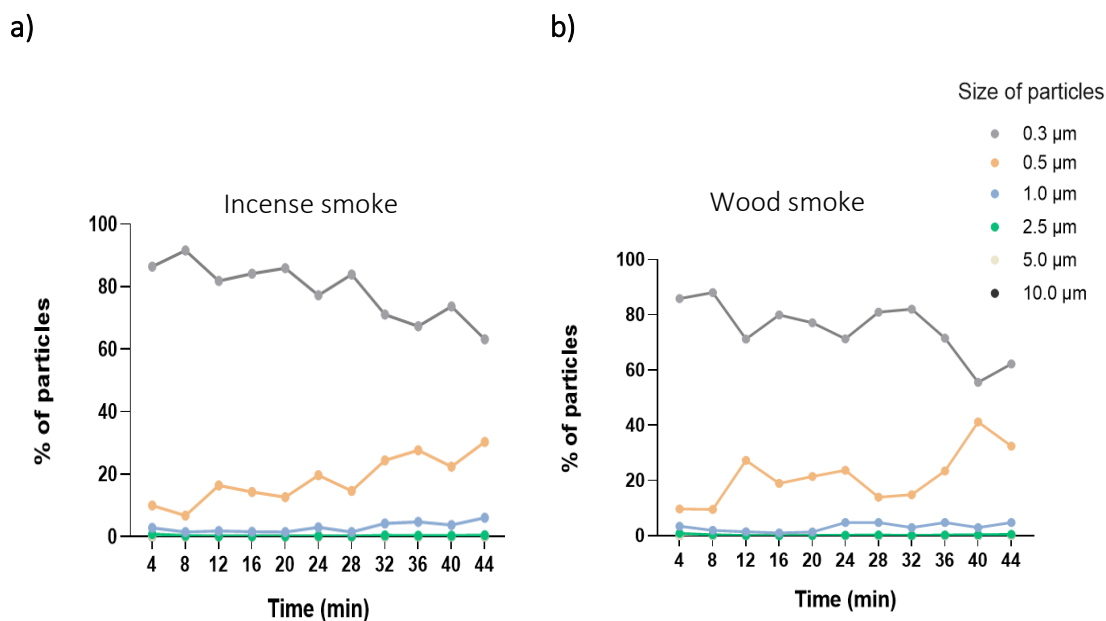
Figure 67: PM generation of different sizes at different time points. a) shows PM generation for incense smoke. b) shows PM generation for wood smoke. The sizes of 5.0 µm and 10 µm are not visible in both graphs of a) and b) because their count is too low. Total number of PM2.5 was calculated by adding up all particles equal to or below the size of 2.5 µm for both incense and wood particles and compared in Figure 65. Total count of PM2.5s increased with increasing time for both types and comparatively, wood smoke had a greater count of PM2.5 than incense smoke. Since two different sources and methods have been used for combustion, the difference in particle counts was predictable. Thus, it was proved that these sources generated particles of useful size range, particularly 0.5 µm and less and the particle counters could be efficiently used to quantify them.

Total number of PM2.5 was calculated by adding up all particles equal to or below the size of 2.5 µm for both incense and wood particles and compared (Figure 68). Total count of PM2.5s increased with increasing time for both types and comparatively, wood smoke had a greater count of PM2.5 than incense smoke. Since two different sources and methods have been used for combustion, the difference in total PM2.5 generation was expected. It was also noted that the production of particles is not stable as the total count dropped and increased at each time point, without following a specific trend. However, it was proved that the laser particle counters could efficiently count particles at range 0.3 µm-10.0 µm. Considering the unstable production of particles, quantitative methods were designed so that analysis could be done at each time points for up to 20 minutes and added and averaged to get a mean total count of particles. The method has been further described in forthcoming sections.
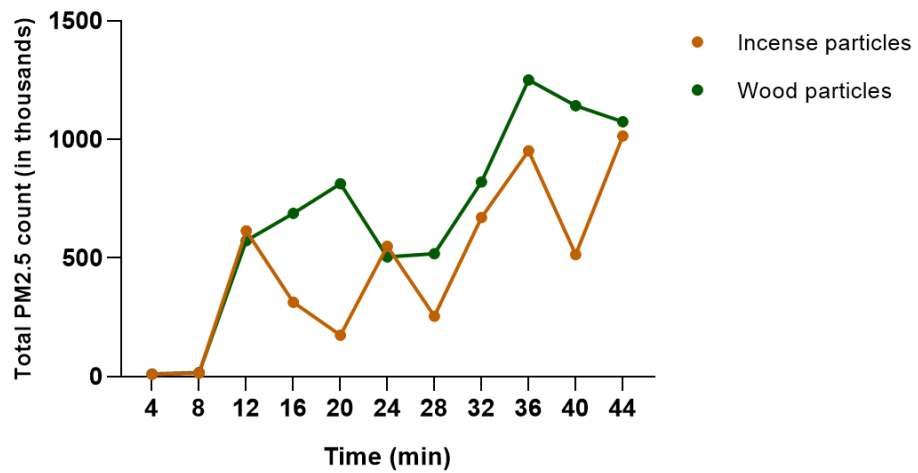
Figure 68: Total PM2.5 generation at each different time points using incense and wood combustion.

3.3 Filtration of particulate matters

3.3.1 Design of test duct

A rectangular test duct made of aluminium was designed with a cross-section of 50 mm x 50 mm and length of 300 mm (Figure 69). It had smooth interior finish and was divided into upstream and downstream sections. The desired filter of cross-section (60 mm x 60 mm) was then adjusted in between the cross-section of two ducts and sealed tightly by using clips to hold the ducts together.
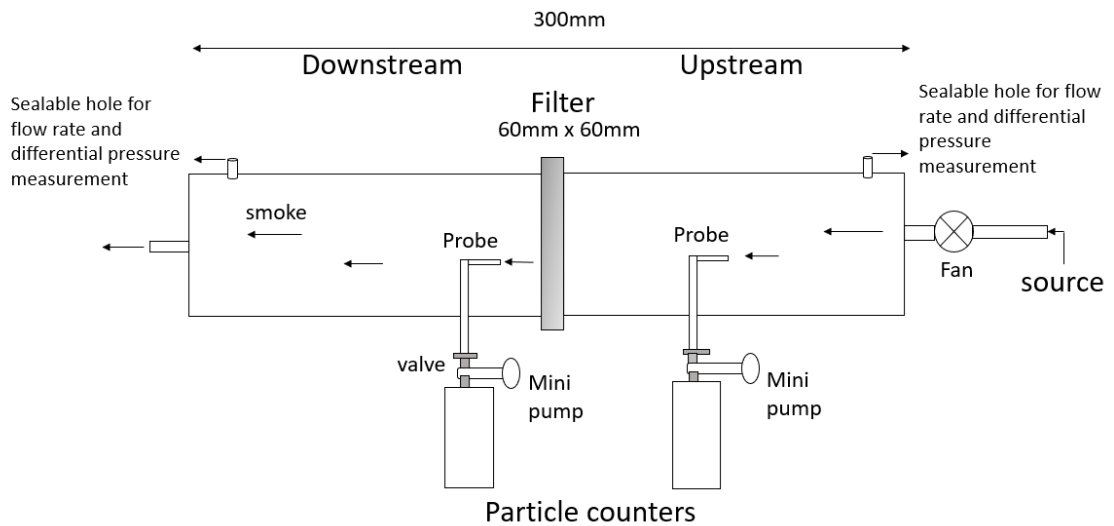
Figure 69: Test duct for measurement of filtration efficiency of coated nanofibres. The duct is divided into two sections-upstream and downstream. The filter is adjusted in between two sections and sealed tightly using clips. Probes of particle counters are inserted into each section to monitor the particles before and after filtration. Two mini pumps are used to sample air from duct to the counters.
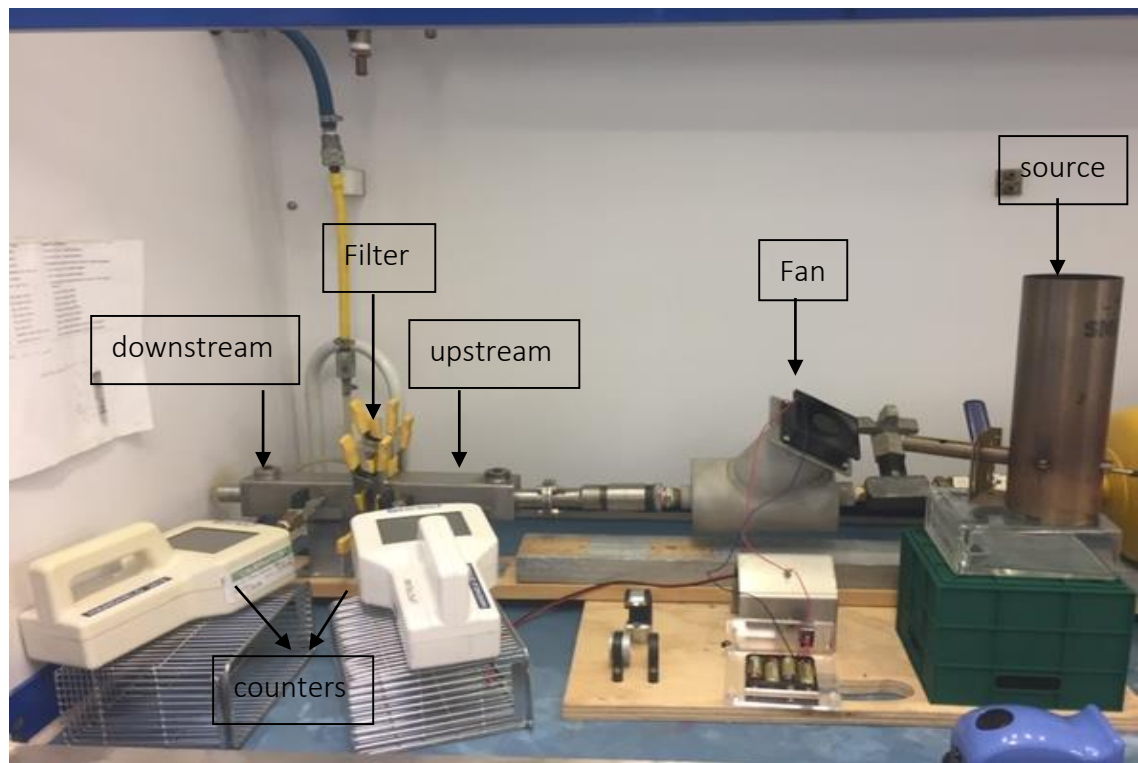
Figure 70: Test rig set-up inside a fume hood.

All experiments were conducted inside a fume hood, constantly filtering the surrounding air to avoid contamination (Figure 70). A 12v fan was used before the upstream section of duct to mix the smoke from the source with the ambient air in the hood for dilution. This was done to ensure that the particle counters are not overloaded and the flow velocity of test air remains consistent for all samples. The fan was used only in case of wood and incense smoke experiments as the filtration efficiency was monitored for a longer period of time and needed a large volume of test air. For diesel smoke experiment, the accumulator (a vessel that stored smoke from the diesel engine) was directly connected to the upstream section and filtration efficiency was calculated only for 90 seconds on a small volume of test air.

Two sealable holes were made on top of each section in the duct to insert an anemometer probe for measuring the velocity, flow rate and temperature of the air passing through the duct (Figure 69). The diameter of the holes was similar to that of anemometer probe so that duct was properly sealed even during measurements. The flow rate of incoming air was monitored on both sections before starting each experiment to check if it is constant throughout the duct. Using the same holes, differential pressures were also calculated using a differential pressure gauge.

When no filter was placed in the system, the difference in pressure on both sides had to be zero. Any deviation indicated a leak in the system. This was included as a part of the routine check before the start of each experiment. The pressure drop caused by the filter was also calculated before and after the FSL coatings to observe any significant increase in pressure drop caused by blocking of the filter due to FSL modification. It was noted that for all FSL-SPM coatings used, no significant pressure drop was observed. In all cases, the flow velocity in the duct was kept constant at 0.5 m/s.

Using the cross-section of duct (area of the filter surface used) and the flow velocity, flow rate of test air (R) was calculated to be 75 L/min (refer to equation i. below). Probes of upstream and downstream particle counters were inserted on each section through holes made on the wall that were joined with mini pumps on both sides. The mini pumps aided in pulling the air from inside the duct to the particle counters. The flow rate of mini pumps (2 L/min) was chosen to be significantly lower than the flow rate of test air so that they do not disturb the flow inside the duct.

$R = AV$ .... (equation i)

where,

R is flow rate

A is area of the cross section of the filter

V is velocity of air

3.3.2 Calculation of filtration efficiency

Background particle counting was performed before generating smoke. The valves of the mini pumps on both upstream and downstream sections were opened and both particle counters were run at the same time, thus measuring upstream background count (Ub) and downstream background counts (Db). After background particle counting, sample filter (filter to be tested) was inserted in the test duct and upstream count (Ut) and downstream count (Dt) were recorded at different sampling times.

For diesel smoke experiment, the upstream and downstream counts were recorded at the interval of 30 seconds for up to 90 seconds, giving three Ut readings for upstream section and three Dt readings for downstream section, where t is 30s, 60s or 90s.

For wood and incense smoke experiments, the counts were recorded at the interval of 5 minutes for up to 20 minutes for each sample. It gave four Ut and Dt readings, where t is 5 min, 10 min, 15 min or 20 min.

Background counts were subtracted from all Ut and Dt readings to get real particle counts UR,t and DR,t. All real counts at different time points were then added to get total no. of upstream or downstream particles ($URtotal$ and $DRtotal$). The particle counter was capable of counting particles at different diameters (0.3, 0.5, 1, 2.5, 5 and 10 μm). The same formula was applied to get the real counts for all particle size *(UR,t,d* and *DR,t,d)*.

$UR, t, d \quad = \quad Ut, d – Ub, d$

$DR, t, d \quad = \quad Dt, d – Db, d$

Where,

Ub, d is upstream background count for given particle size, before the sample filter is inserted

Db, d is downstream background count for given particle size, before the sample filter is inserted

UR, t, d is real upstream counts at a given time point for a given particle size

DR, t, d is real downstream counts at a given time point for a given particle size

t is 30, 60 *or* 90 *seconds in case of diesel and* 5, 10, 15 *or* 20 *minutes in case of wood and incense*

d is particle size of 0.3, 0.5, 1 *and* 2.5 μm

Again,

$URtotal, d \quad = \quad (UR, 30s, d \; + \; UR, 60s, d \; + \; UR, 90s, d \;) \; or \; (UR, 5min, d \; + \; UR, 10min, d$
$\qquad\qquad\qquad + \; UR, 15min, d \; + \; UR, 20min, d)$

$DRtotal, d \quad = \quad (DR, 30s, d \; + \; DR, 60s, d \; + \; DR, 90s, d) \; or \; (DR, 5min, d \; + \; DR, 10min, d$
$\qquad\qquad\qquad + \; DR, 15min, d \; + \; DR, 20min, d)$

$UPM2.5 \qquad = \quad URtotal, 0.3μm \; + \; URtotal, 0.5μm \; + \; URtotal, 1μm \; + \; URtotal, 2.5μm$

$DPM2.5 \qquad = \quad DRtotal, 0.3μm \; + \; DRtotal, 0.5μm \; + \; DRtotal, 1μm \; + \; DRtotal, 2.5μm$

Where,

$URtotal, d$ and $DRtotal, d$ are total upstream and downstream counts for given particle size

$UPM2.5$ and $DPM2.5$ are total PM2.5, calculated by adding URtotal and DRtotal of all particle size
less than or equal to 2.5μm.

The filtration efficiencies were calculated for different particle size range and different time points using the following formula

$$Filtration\ efficiency\ (FE\%) = \frac{Upstream\ count - downstream\ count}{Upstream\ count} \times 100 \qquad \text{(Equation 1)}$$

For example, the filtration efficiency of total PM2.5 is calculated as:

$$FEPM2.5 = \frac{UPM2.5 - DPM2.5}{UPM2.5} \times 100 \qquad \text{(Equation 2)}$$

3.3.3   Results of filtration experiment

The filtration efficiency of FSL-SPM treated nanofibre was observed to be better for all size range of particles and all sources analysed as shown in Figure 71. However, for higher size such as 1 and 2.5 µm, the standard deviation was higher. This could be due to an error in background counts. For counting of background particles, after recording data for each sample, the filter was removed and smoke generation was stopped. The fan was used to flush away any residual particle from previous run. However, it was noticed that the background counts at bigger particle was not consistent for every run, as compared with smaller size range.

The other reason could be the mechanism of filtration. It is well known that with increasing particle size, particles are captured due to inertial impaction rather than a diffusive deposition. Inertial impaction is highly dependent on the physical property of the filter. Therefore, even minor difference in surface morphology or structure of nanofibre surface could affect the process, resulting in deviated results.

It was expected that there would be a higher increase in efficiency of filtration for 0.3 µm particles as compared to bigger sizes based on the observation of authors who report that electrostatic attraction is the most preferred method of mechanism of filtration for smaller sized particles [251]. However, considering the standard deviations, there was no significant difference in the efficiencies based on the size of the particles but an overall enhancement of efficiency of filtration by coated sample as compared to the control was observed for all size groups included in the study.
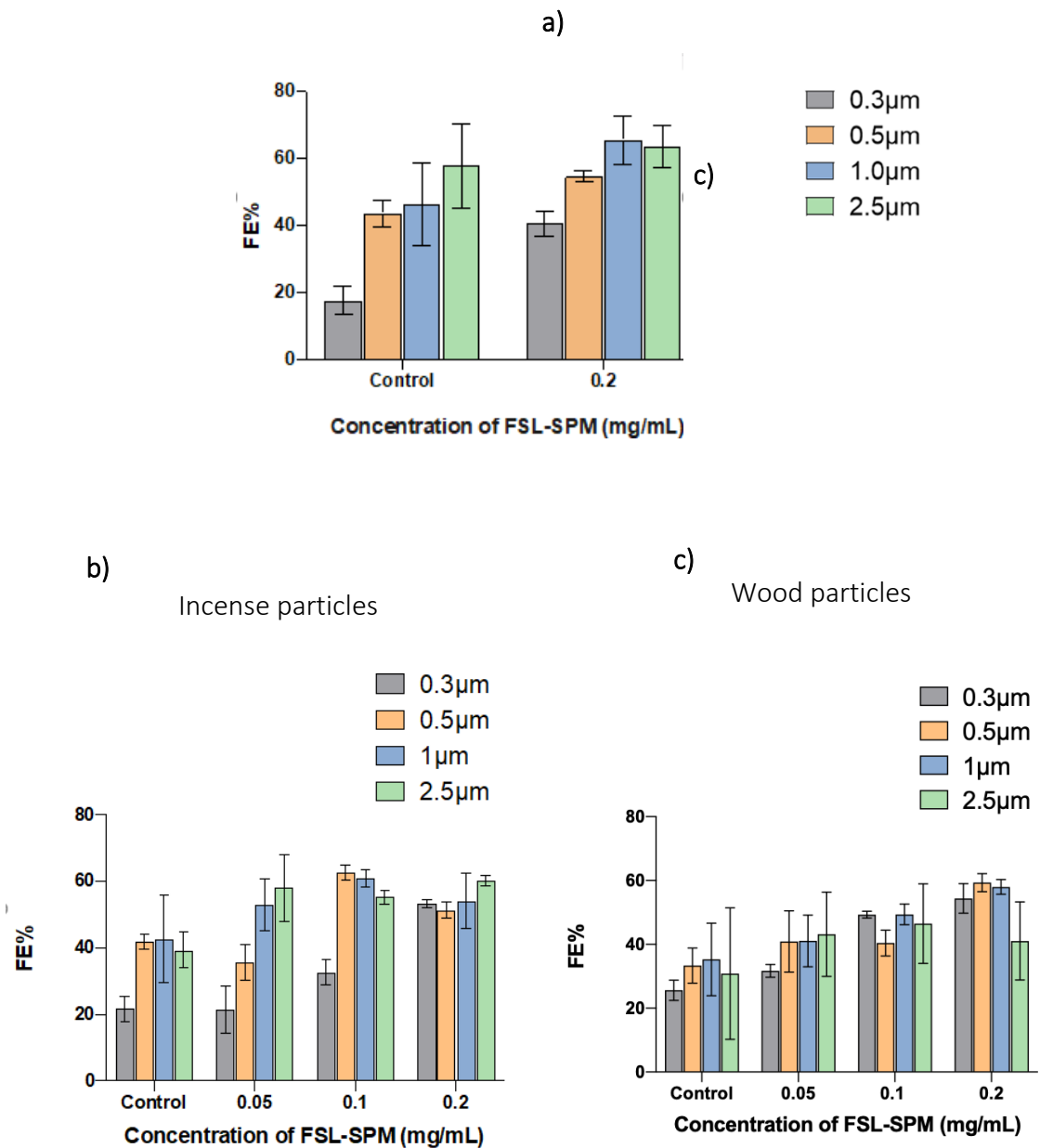
Figure 71: Filtration efficiency of FSL-SPM coated nanofibres for different particle size. a) shows diesel particles filtration efficiency of 0.2 mg/mL FSL-SPM coated filter against control nanofibre, b) shows incense particle filtration efficiency at different FSL-SPM concentrations, c) shows wood particles filtration efficiency at different FSL-SPM concentrations.

The trend of PM2.5 captured at different time points was almost different for different FSL-SPM concentrations and varied for incense and wood smoke particles as observed in Figure 72.

Figure 72: Filtration of PM2.5 at different time points and concentrations of FSL-SPM. a) shows filtration of incense particle filtration and b) shows wood particle filtration.

Filtration is dependent on several factors including background counts, upstream counts at a time point, the morphology of each nanofibre surface and morphology and chemical composition of particles at different time points of combustion. All these factors are important to control for each sample run. In addition, different methods were applied to generate PM from different sources. Therefore, discrepancies in the trends of PM2.5 were expected.

Calculation of overall PM2.5 and comparison of total PM2.5 filtration provided a wider view of the filtration process rather than comparing at each size range or at each time point as illustrated in Figure 73. From the results of PM2.5 capture obtained using different sources it can be concluded that treatment of nanofibre with FSL-SPM results in enhanced filtration of particulate matters as compared to uncoated ones. In figure 73b, the efficiency of 0.05 mg/mL coated PMMA is observed to have lower efficiency than that of control but considering the error bars, the difference is not significant and is therefore concluded to be a result of an experimental error. Table 8 summarises the results where it is showed that 22%, 21% and 27% filtration efficiency can be achieved at 0.2 mg/mL FSL-SPM coating for capture of diesel, incense and wood particles respectively.

Diesel PM2.5 filtration

a)
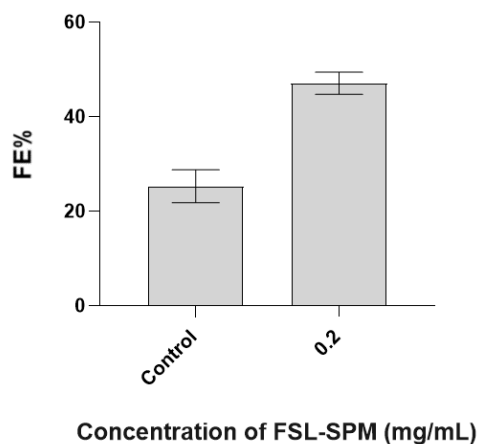
Incense PM2.5 filtration

b)
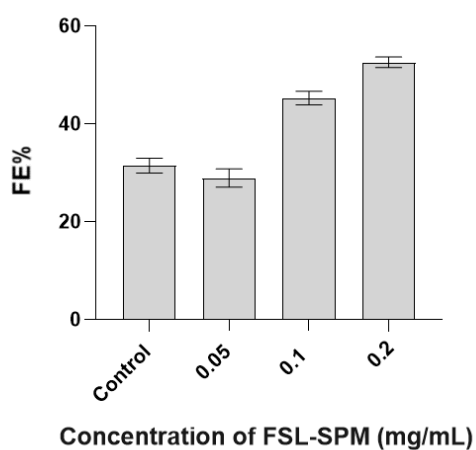
Wood PM2.5 filtration

c)
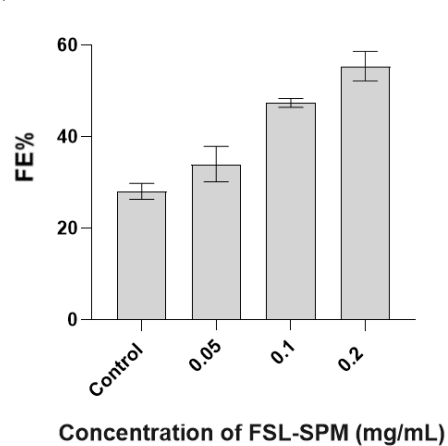
Figure 73: PM2.5 filtration by FSL-SPM coated nanofibre. a) PM2.5 filtration efficiency for diesel smoke particles, b) PM2.5 filtration efficiency for incense smoke particles, c) PM2.5 filtration efficiency of wood smoke particles. There is an increase in filtration with increasing concentration of FSL-SPM on fibres as illustrated by b) and c).

Table 8: Average PM2.5 filtration efficiencies of nanofibres FSL-SPM coated nanofibres compared with control nanofibre.

Source	Increase in PM2.5 filtration efficiency of coated PMMA at different FSL-SPM concentration with respect to uncoated PMMA		
	0.05 mg/mL	0.1 mg/mL	0.2 mg/mL
Diesel	-	-	22%
Incense	2%	14%	21%
Wood	6%	19%	27%

Conclusion

In this chapter, particulate matter in smoke from various sources such as diesel, wood and incense smoke were generated and characterised. FSL-SPM was used to modify PMMA nanofibres that were then used to capture the real air particulate matter from those sources using a test duct designed for the purpose. The smoke particles generated through various combustion methods were expected to be mostly charged as evidenced in the literature [143] where presence of polar functional groups on the surface of the air pollutants is discussed. It should however be considered that air particles are heterogenous in size and charge ranging from negative, positive to even neutral. The study was more focused on PM2.5 particles (particles equal to or less than 2.5 μm) as they are considered the most hazardous. Some important conclusions derived from this chapter are given below

- o The particles in smoke have various sizes, morphology, surface roughness and elemental compositions and thus it is a challenge to capture a range of these particles with Kode-modified nanofibres. However, FSL-SPM coated nanofibres showed up to 27% higher efficiency in the filtration of PM2.5 (in wood smoke) as compared to uncoated nanofibres.
- o Considering the reduction of pore size at 0.5 mg/mL of FSL-SPM coating, coating concentration up to 0.2 mg/mL was studied to capture air particles through filtration. However, use of higher concentrations could be investigated regarding the adsorption of particles.
- o For up to 0.2 mg/mL, the flow rate was uninhibited and thus shows that the increase in efficiency was not compromised by reduction in flow rate quality.
- o Multiple layers modified with oppositely charged Kode constructs could also be investigated for the efficacy in removing both positively and negatively charged particles.

Chapter 4: Biological particles capture – methods and results

4.1 Microbiological capture

Surface modified filter media are commonly used for the removal of pathogens from water. Most of them are treated by enhancing positive charge on the surface for capturing negatively charged microorganisms [252,253]. This experiment aimed to establish the principles for preparing modified nanofibre filter media remove microorganisms. After the successful application of FSL-SPM coated filters to capture charged particles, it was logical to investigate the ability to capture biological contaminants with charged surface. Therefore, this experiment was conducted as a proof of concept without extensive optimisation and standardisation of protocol.

In this experiment, *S.epidermidis* was used as a model pathogen to analyse the ability of FSL-SPM to attach microbes through electrostatic adsorption using the following protocol.

Method overview

1. A loopful of three different colonies were scraped from the surface of an agar plate and were transferred to a microcentrifuge tube containing 15 mL of 1× PBS as medium and vortexed for 10s.

2. 2 mL of the suspension was measured for its absorbance or optical density (OD) at 600 nm using a spectrophotometer.

3. The absorbance was monitored and the inoculum was adjusted by either adding more colonies or by diluting (in case of excessive OD reading) until an OD of 0.15 was reached. In this case, 10^8 CFUmL^{-1} (Colony Forming Unit per mL of suspension) gave an OD reading of 0.15.

4. Serial dilutions were then done in 1× PBS by using the 10^8 CFUmL^{-1} suspension as a stock solution.

5. 1mL syringe was used to filter bacterial suspension through 10 mm x 10 mm of 1 mg/mL FSL-SPM coated PCL nanofibres strip.

6. Two suspensions were chosen (10^8 and 10^5 CFUmL^{-1} of bacterial concentration) to be filtered separately through coated nanofibre and control nanofibre (without FSL-SPM coating)

7. Control suspension (1× PBS) was also filtered separately for comparison.

8. The filtration process was carried out manually by gently pushing the syringe by hand. It was made sure that the filtration rate remained as constant as possible for all samples.

9. All nanofibre surfaces were then washed once in 1 mL of DI water and incubated in 1mL of 2.5% glutaraldehyde (made up in 95% ethanol) for 10 minutes for fixing.

10. Crystal violet (CV) staining was used to analyse the attachment of bacteria. The surfaces were washed once again in 1 mL of DI water and were transferred to wells containing 1 mL of 0.4% crystal violet (made up in water). All washing and CV adsorption steps were done in 24 well plates for robustness.

11. After CV treatment, the surfaces were washed in DI water using 6 different wells.

12. The washed surfaces were then visually analysed for CV staining after drying at RT. Further, the surfaces were observed under SEM.

Results and interpretation

From Figure 74, it was apparent that no visible staining of surfaces was observed for nanofibres that were used to filter 10^5 CFUmL^{-1} suspensions. However, in the case of 10^8 suspension, both control and 1 mg/mL FSL-SPM coated surfaces showed staining by CV. There was a significant difference in the area and amount of staining in between control and FSL-SPM coated surface. It was clearly seen that the coated surfaces adsorbed more bacteria as compared to control surfaces as represented by the more CV staining of the surfaces. Both layers were analysed and it was found that the CV was stronger in layer beneath, indicating that bacteria passed through the upper layer but eventually were stuck in the interior during the process.
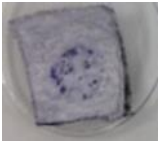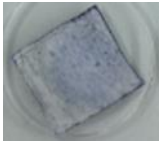
	Upper layer		Layer beneath	
Bacterial suspension	Control	FSL-SPM Coated	Control	FSL-SPM Coated
10^5				
10^8				

Figure 74: Crystal violet staining for the detection of *S.epidermidis*. Initial bacterial suspension of 10^8 was suitable for the staining method as compared to 10^5. 1 mg/mL FSL-SPM coated nanofibres showed stronger CV staining, indicating that it attached more bacteria than control nanofibre.

SEM images further supported the interpretation (Figure 75). More bacteria was observed on the surface of FSL-SPM coated nanofibres. It was also noted that the bacterial cells tend to pass through the filtering layer (the layer through which the suspension initially passes during filtration) and adhere beneath. The results were complementary to that of crystal violet staining when the opposite surface was analysed. In control nanofibre, the bacterial cells did not seem to attach in a consistent manner. They were observed as patches, which could be caused by the random adsorption caused by hydrophobic property of PCL nanofibre. Conversely, adsorption onto FSL-SPM coated was consistent throughout the surface, thus supporting the uniform coating and effect of electrostatic adsorption by FSL construct.

Nanofibre	Magnification	
	×1k	×3.50k
Control		
1mg/mL FSL-SPM coated		
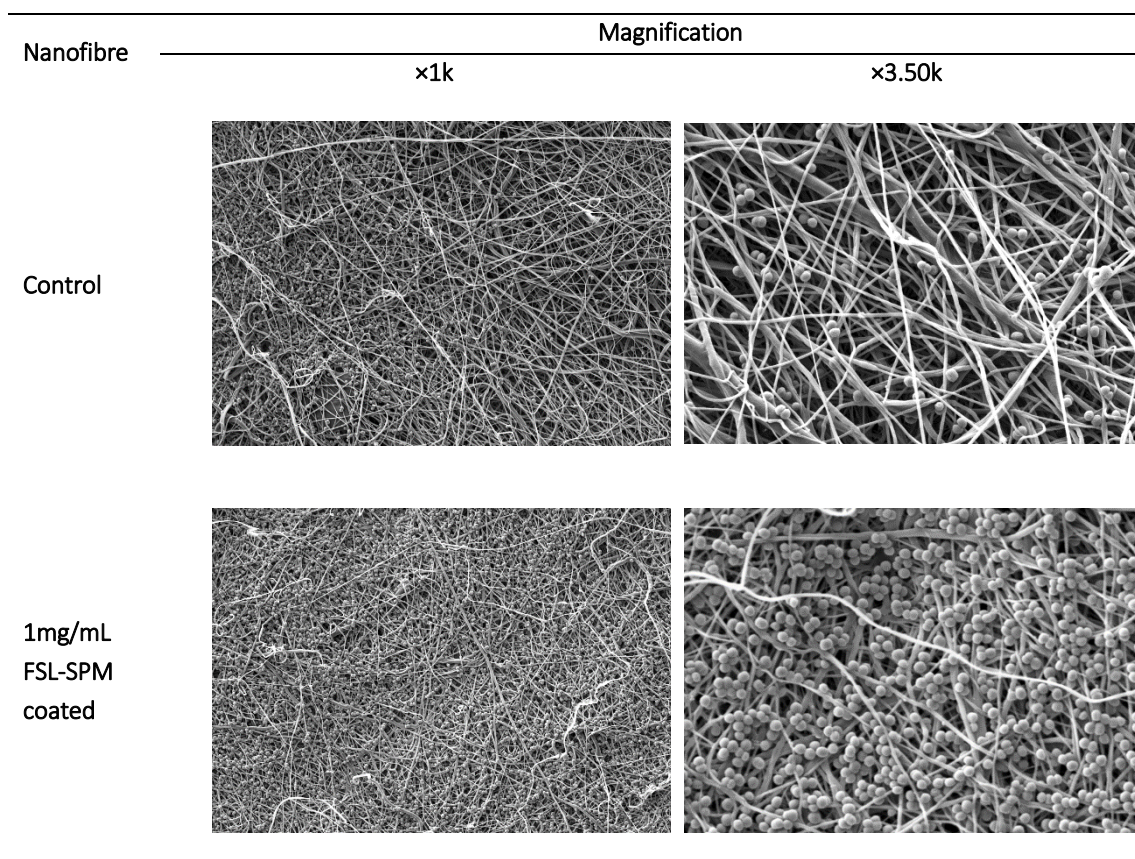
Figure 75: SEM observation of nanofibres after CV staining. It was observed that the 1 mg/mL FSL-SPM coated nanofibre was significantly better in capturing bacteria as compared to the control.

4.2 RBC capture

Method overview

Following protocol was used for RBC capture.

1. Human red blood cells (RBC) were washed 3 times by centrifugation, using 1× PBS and were diluted to 1%.

2. 200 µL of RBC was dropped on the PCL nanofibre surface (5 mm x 10.5 mm) coated with different concentrations of FSL-SPM (0.01, 0.5 and 0.1 mg/mL).

3. The cells were allowed to adsorb on the surfaces for 1 hour at room temperature (RT).

4. After 1 hour, the surfaces were gently washed with 1× PBS 3 times.

5. For washing, the fibres were transferred on a petri dish and enough PBS was added to soak the nanofibres. The dish was gently rocked for 5 seconds. The PBS solution was then discarded and fresh PBS was added for each wash.

6. For SEM observations, cells were fixed by immersing the fibres in 2.5% glutaraldehyde in 1× PBS for 30 minutes. The resulting fibres were then washed with MilliQ water and dried at RT before SEM observation.

Results and interpretation

FSL-SPM coated nanofibres were able to adsorb RBC efficiently (Figure 76). The increase of capture was directly proportional to an increase of FSL-SPM concentration on the surface. The possible reason for this phenomenon is the negative charge on the surface of RBCs due to which they are electrostatically filtered on the positively charged FSL-SPM coated nanofibres.

a) Control   b) 1 mg/mL FSL-SPM coated

c)   control   0.01 mg/mL

0.5 mg/mL   1 mg/mL
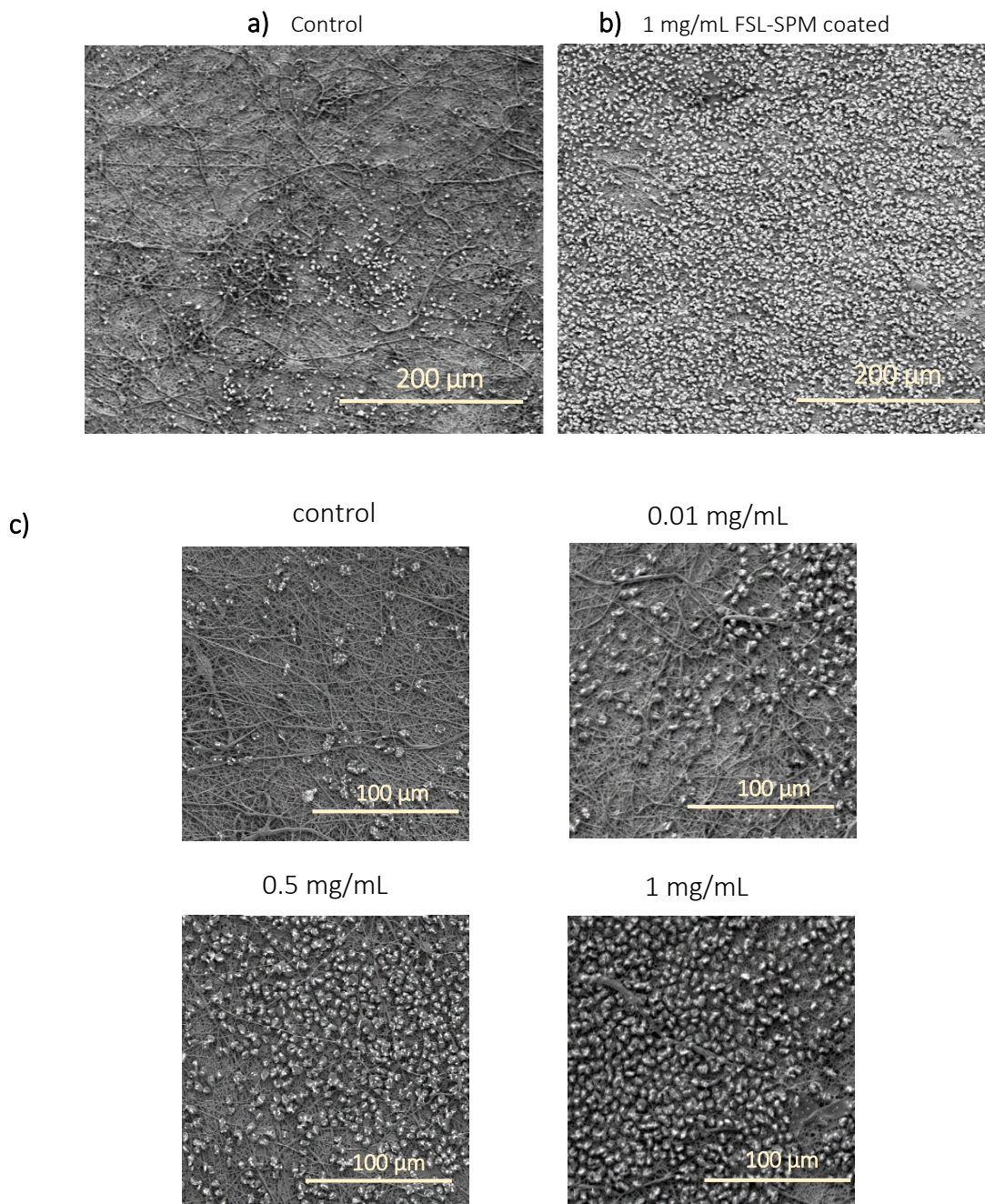
Figure 76: Adsorption of RBC on FSL-SPM coated nanofibre. a) shows RBC adsorption on control nanofibre, b) shows RBC adsorption on 1 mg/mL FSL-SPM coated nanofibre surface that is observed to greater than c) shows an increasing amount of RBC with increasing amount of FSL-SPM on the surface.

Conclusion

The FSL-SPM modified nanofibre was successfully applied to capture biological particles such as bacteria and RBCs that points towards the possibility of using Kode modification of nanofibres as a bio-compatible surface functionalisation technique for capture of cells and other biological materials.

Chapter 5: Discussion

Environmental pollution is one of the more serious global problems today. It is the contamination of physical and biological components of the earth to such an extent that environmental processes are affected adversely. The rise in air and water pollution demands for the development of advanced technologies for remediation. In the air, most contaminants originate from combustion [254,255]. Since the beginning of the industrial revolution, increasing use of fossil fuels has made the problems of air pollution more severe and specific emission regulations have been implemented against hazardous pollutants. The ideal method to protect air quality would be to reduce the emission of pollutants by changing to greener fuels. Similarly, for water pollution control, methods such as aeration, flocculation and chemical treatment have been used [256]. However, not all pollutants can be prevented and such pollutants should be trapped or captured in cleaning devices before they can enter the atmosphere.

Many filtration materials have been developed to trap air pollutants among which glass fibre has been applied extensively in cleaning devices as filtration media. Activated carbon filter has also received increasing attention and it is now considered a good air filtration material due to uniform pore size distribution, large adsorptive capacity and easy regeneration [257]. However, after the introduction of nanotechnology in the air filtration field, a wide range of capabilities and filtration technologies have become possible for the removal of both air and water pollutants [258]

Nanotechnology offers many advantages that can improve existing environmental technologies as they provide us with the ability to control the properties of materials at the nanoscale and produce materials with special functions [259]. Nanofibres have been gaining attention as advanced materials with very small diameters and large surface area. Due to their large surface area to volume ratio, they can be surface modified with specific functions resulting in a maximised functionalisation of filtration membranes [260]. Such membranes are advantageous as compared to commercial filtration media because conventionally, filtration media are based on size exclusion. In such membranes, filtration is dependent on physical aspects and membranes are usually made thick and compact so that large number of particles can be removed including the smaller ones that are more detrimental. However, such conventional filter membranes result in poor flow rate.

Therefore, the use of functionalised nanofibre membranes could potentially solve this problem and create filters where good capture and good flow are not compromised. The literature discusses existing surface modification techniques that are in use for air and water pollutants removal [137]. Many existing techniques rely on covalent attachment, toxic chemical and harsh reaction conditions. Such traditional techniques often result in damage of the surface being modified. Therefore, this study analysed the modification ability of a surface engineering technology called Kode Technology that is based on non-covalent attachment of biocompatible molecules called FSLs to surfaces. The resultant modified fibres were then assessed for their capacity to efficiently capture small particulate matter on nanofibres. This research was focused on the ability of surface modified nanofibres to capture small air and liquid particulate matter. However, to facilitate characterisation and validation, surrogates of particulate matter were first synthesised in the form of charged silver nanoparticles. The results from the nanoparticle capture experiments were then utilised to inform capture of real air particulates from a variety of sources including wood, incense and diesel combustion.

The results demonstrated a successful modification of nanofibres by Kode Technology and application of modified nanofibres for efficient removal of nanoparticles from water and smoke particles generated by combustion of sources. The specific aims of this study were to investigate the suitability of Kode Technology in modifying the surface of nanofibres, synthesis and characterisation of pollutants in air and water, assessing the ability of modified nanofibres to capture synthesised pollutants and biological particles.

Functionalisation/modification of nanofibre

The first aim of this research was to investigate the suitability of Kode Technology in functionalising nanofibres. There are many methods for fabricating nanofibres. However, electrospinning is the most widely used technique which is considered to be simpler with low start-up cost offering large scale production [21]. Nanofibres electrospun from various polymers types such as PCL, PMMA, PVB and PA66 were characterised. PCL nanofibre was used for most of the research conducted, including removal of nanoparticles using adsorption and filtration, standardisation of FSL coating, quantification of FSL on modified surface and comparison of modification before and after the fabrication of nanofibres. PCL was chosen primarily because of its extensive use in water filtration applications [261–

[263]. However, for air filtration study, PMMA of 0.5 gsm was used because this nanofibre was already in use for commercial facemasks (nanofibres traded by Revolution Fibres Ltd.). The use of PMMA as air filtration materials has been mentioned by various authors [263–265]. Moreover, considering the fact that melting temperature of PCL is around 60°C [266], it is not suitable for direct use in smoke filtration from high-temperature exhausts.

The nanofibres characterised in this study were found to have fibres less than 1000 nm and the morphologies and surface roughness were similar. The quality of the fibres was good with a smooth texture and no visible clumps or beads in the structure. The surface hydrophobicity of the nanofibres was also analysed by measuring the contact angle (CA) of water on the surface and the results indicated that the surfaces were hydrophobic which meant the surfaces resisted contact with water. It is also known that for any surface modifying agent to functionalise the surface perfectly, there needs to be a balance between the hydrophilic and hydrophobic properties of the surface [267] and it was expected that the amphiphilic nature of Kode construct could help in creating a balanced surface property required for proper modification.

Regarding the choice of FSL constructs, firstly, a variety of constructs were tested and compared for the ability to capture nanoparticles. Among the many constructs analysed, the functions of FSL-SPM and FSL-Z were studied more in detail. FSL-SPM is a positively charged constructs where the charge is provided by the presence of polyamine called spermine as the functional head. In contrast, FSL-Z is a negatively charged construct where the negative charge is provided by its spacer part (CMG). FSL-SPM was tested for its ability to capture negatively charged particles and FSL-Z was analysed for the capture of positively charged particles. FSL-SPM was observed to show significant removal of particles and thus it was hypothesized that FSL-SPM would be able to capture particles based on electrostatic affinity. It was then chosen as a primary construct to coat PCL nanofibre for testing various parameters in this study and was applied for the modification of PMMA nanofibre to capture air particulates.

Model nanoparticle adsorption experiments proved the efficiency of FSL-SPM to capture in house synthesised, negatively charged nanoparticles but nevertheless, it was expected that it would also be efficient in capturing smoke particles because of the fact that most particulates in the air are observed to be charged. These particulates could be potentially captured onto charge-modified filters through polar interactions [143,144]. Additionally, the

physical forces acting between spermine head of FSL-SPM and negatively charged particles such as hydrogen bonding and point-like hydrophobic interactions due to the –$(CH_2)_3$- and –$(CH_2)_4$- bridges between nitrogen atoms of spermine were expected which could potentially help in trapping particulate matter onto the modified membranes.

For immobilisation of Kode constructs on to the nanofibre membrane, a standard coating protocol involving dip-coating of fibres in FSL construct solution was used particularly in case of PCL modification. Wide variety of coating methods are available due to the diversity of applications and needs in different fields. Other deposition techniques such as spraying and vaporisation are in use for the treatment of surfaces. However, dip-coating or spraying is the most facile and economic technique used in many industrial fields to deposit onto metallic, ceramic or fibrous materials [268,269]. Nanofibres have been modified by various other researchers [270–272], utilising the dip-coating technique that is similar to the one applied in the thesis. For immobilisation of FSL-SPM on to PMMA nanofibres used for the air particulate capture study, the FSL-SPM solution was pipetted on one face of the nanofibre mat instead of dip-coating. This was done to ensure that a cost-effective quantity is utilised for the application as the surface area used for the air particles capture study was almost 70 times greater than that used for PCL (for nanoparticle capture). Dip-coating required relatively larger volume of construct solution and thus pipetting of constructs was done evenly on one side of the PMMA surface. Since the FSL-SPM solution was made in 70% methanol the surface was immediately wet and the coating spread evenly. However, this change in protocol should be accounted and possibly a better immobilisation strategy should be investigated for coating of larger surfaces. Based on the protocol developed for the study, a fixed volume (100 μL) of FSL solution was applied for 1 minute on each side of the membrane at room temperature. It should also be noted that more experiments including different contact times of FSL with the surface and different temperatures should also be analysed for optimum modification.

Surface modification generally introduces morphological changes including change in fibre diameter, surface roughness and pore diameter [273–275]. However, a good modification technique should not result in drastic changes in fibre diameters and pore dimensions, especially when used for filtration applications. Moreover, one of the objectives of this research was to create membranes that can provide a good flow rate,

which is why it is important that the nanofibre mats maintain their thin diameter and larger pore dimensions even after coating with FSL constructs. The SEM observation revealed that in the case of PCL modification, for up to 0.05 mg/mL of FSL-SPM coating, the fibre diameter was not significantly changed. The fibre diameter results were validated by size distribution analysis done by DiameterJ. However, at 0.5 and 1 mg/mL coating, the fibre diameters could not be calculated without error because of a web-like coating formed on the fibre surface. At these concentrations, pore-size also seemed to reduce because of the coating. Similarly, in the case of PMMA nanofibres at higher concentrations, FSL-SPM was observed to block the pores. Based on these observations, it was concluded that for filtration purpose, a lower concentration of FSL-SPM (less than 0.5 mg/ mL) would be suitable for modification. However, adsorption assays have been extensively used in this research to prove the charge affinity of FSL-SPM towards nanoparticles where change in fibre diameter and pore-blocking are not concerned. Therefore, higher concentrations have also been included for comparison.

Quantification of FSL-construct on the modified surface is important because the amount of FSL used to coat the surface does not represent the true amount remaining on the surface (after washing). After coating, the excess molecules are always washed with water. Therefore, the nanofibres have less molecule than what is initially applied. For quantification, a derivatisation method was used where the spermine in FSL-SPM was chemically derivatised with ninhydrin and quantified by using absorbance analysis. Thus, FSL-SPM was taken as a model construct to assess the amount of FSL on modified surfaces. This method was helpful in concluding that only 3.5% of FSL-constructs initially applied during the coating process are present on the surface after coating. However, more sensitive tools such as X-ray Photoelectron Spectroscopy (XPS) and Time-of-Flight Secondary Ion Mass Spectrometry (ToF-SIMS could provide more accurate measurements [276,277]. For qualitative determination of modification, FTIR was used and it showed that the FSL-SPM modified PCL membrane had specific peaks of amines and amides that indicated the presence of spermine on the surface. However, the FTIR instrument was not sensitive enough to quantify the amount of Kode constructs or show specific peaks relating to the lipid and spacer part of the constructs. More investigation using various other polymer surfaces and quantities of Kode constructs is required for better understanding of modification process.

An advantage of using FSL constructs is that the structure of the constructs could be changed using different functional heads, spacer and lipid groups, imparting diverse functionality and properties to the molecule. Therefore, the establishment of FSL-SPM coating on PCL nanofibre surface could open a wide range of opportunity to coat different nanofibres with a variety of FSL constructs in a similar fashion, which could be used for diverse array of applications.

Synthesis and characterisation of particulates

The second aim of the research was to synthesise and characterise particulates in liquid (water) and air. Silver nanoparticles were synthesised to be tested as surrogates for charged particles as they could be detected and characterised more easily than charged pollutants. However, the nanoparticles were in a liquid medium so the findings of the study were restricted to the solution. For air pollutants, smoke particles from diesel, wood and incense combustion were used to create air particulates. They have been described in detail below.

Water particulates (silver nanoparticles)

Silver nanoparticles (Agnp) were chosen as model pollutants because of two reasons. 1) They can be easily synthesized in the lab and the diameters can be controlled to be less than 200nm. 2) They can be prepared with either a negative or a positive charge and the particles are usually stable [216,278,279].

Silver nanoparticles (Agnp) with a positive and negative charge, namely [-]Agnp and [+]Agnp were synthesized separately using different precursors. Synthesis of Agnp using various methods has been mentioned in the literature. Synthesis of Agnp by chemical and physical methods using reduction methods have been widely used [280–283]. Over the last few years biosynthesis of nanoparticles using clean, non-toxic and environmentally friendly precursors have been reported as an alternative greener approach to synthesis [284,285]. However, it should be considered that each method has advantages and disadvantages with challenges such as cost of production, size of particles and scalability. Therefore, for this study, protocols described by Sharanova et al. [216] were followed as it described simple techniques that produce both negatively and positively charged Agnps

in a similar fashion and in the desired size range. The average diameter and size distribution of negative particles was close to those in the literature but for positively charged nanoparticle, the average diameter was larger than expected and the size distribution was slightly deviated from normal. This was interpreted to be due to a change in centrifugation protocol. The reference paper mentions the use of an ultra-centrifuge for purification but a regular centrifuge was used for this study. Moreover, multiple batches of nanoparticles were synthesised and mixed together to make a single stock solution enough for the entire experiment, which would have uniform heterogeneity among the particles. The stability of nanoparticles was confirmed by the regular SEM, EDS and UV vis characterisation of original Agnp solutions, included as controls in all experiments conducted.

UV-vis characterisation of the synthesised nanoparticles further confirmed the formation of silver ions based on the standard silver absorbance peaks mentioned in literature [224,279]. However, UV-vis spectra are quite sensitive as the plasmon peaks depend on the extent of colloid aggregation. Therefore, the maximum absorbance wavelength (λ_{max}) is dependent on the size of Agnp [286]. A mean value of λ_{max} was calculated and used for quantification. The zeta-sizer analysis was successful in providing accurate measurements of the charge and size of the particles at the original pH and over the range of pH 3 to 11. However, it should be noted that the analysis was done on a diluted sample as compared to what was actually used for particle capture because the zeta sizer can only analyse optically clear samples with low concentrated samples. The trend of change in charge of nanoparticles along with the pH and the phenomenon of particle aggregation at lower pH was mostly similar to the study by Lau et al. [287]. The addition of (H^+) or (OH^-) to the nanoparticle solution resulted in physio-chemical changes in the structure and surface charge of nanoparticles. Consequently, it was important to study the effect of pH in charge and size analysis because it is well known that pH could severely affect adsorption of particles [288,289] and thus zeta analysis was an important aspect of nanoparticle characterisation.

Air particulates (smoke particles)

Considering the fact that reference air particulate matter for purchase was very expensive (diesel particulate matter, https://www.sigmaaldrich.com/catalog), attempts

were made to generate similar particles in the lab, in a controlled manner. For preliminary experiments, a small diesel engine was modified to produce temperature-controlled smoke particles. However, due to ease of production and feasibility to be conducted inside a fume hood, a major part of the air particulate filtration study was done using wood and incense smoke. Aerosol generators that produce standard and reproducible monodisperse or polydisperse particles are used for most particle capture studies including the quality testing of high-efficiency particulate air (HEPA) filters [290,291]. However, such particles are not very close to real particulate samples in chemical content and might not have desired functional groups that might interact with Kode constructs. Filtration of atmospheric aerosols and health effects of ambient air particle have also been studied [292,293]. Therefore, in this study smoke samples were chosen because they contain higher number of small particles that are hazardous and would have expected functional groups required for interactions with Kode constructs.

SEM observation revealed the presence of various size of particles in all samples but the focus of this research was directed towards PM2.5 particles, considering their more hazardous nature [294,295]. Chemical composition derived from EDS was used to further correlate with the morphology and surface texture of particles and the conclusions indicated that most particulates in the smoke were carbonaceous and sticky in nature. The paper by Liu et al. [143] describes similar characteristics of PM and have further investigated their chemical compositions using XPS and FTIR. They report an important observation that is, PMs have polar functional groups such as C-C, C-O, and C=O and C-N present on their surface. This was helpful in laying a foundation for the hypothesis of this research that charged FSL constructs such as FSL-SPM could potentially capture PMs because of their interaction with functional groups on the surface of PM (additional to charge interactions). Additionally, the particles in air are heterogenous regarding size and charge including positive, negative and neutral. However, the air particles generated by combustion methods in this study were expected to be mostly charged due to presence of polar functional groups as mentioned in the literature [143].

Particulate capture

The third aim of the research was to investigate the ability of KodeTechnology modified nanofibres to capture air and water particulates.

Water particulates

Preliminary adsorption experiments demonstrated that FSL-SPM could remove [-]Agnp through adsorption. Different concentrations of FSL-SPM were diluted in water, coated on PCL nanofibres and were immersed in samples with various concentrations of [-]Agnp. Interestingly, it was observed that at some concentrations, the brown coloured nanoparticle solution became clear and the immersed nanofibres had become brown, indicating that the nanoparticles had stuck onto the fibres. This simple indicator system served as a basis for many studies that followed. The adsorption capacity of FSL-SPM was then utilised to analyse various other aspects of FSL constructs in general.

The first parameter studied was the effect of the solvent used for dilution of the FSL-SPM. Since PBS shows precipitation with FSL-SPM, two other solvents, 70% methanol and water were compared against each other and it was found that FSL-SPM in methanol worked better than in water for adsorption of nanoparticles. It gave an important insight about effect of solvent during modification/coating process. Further, it was also noticed that after the coating process (when the nanofibres were dried and ready to use for adsorption assay), nanofibres treated with methanol-diluted FSL-SPM could be immediately wetted when immersed in the nanoparticle solution while FSL-SPM diluted in water for coating showed some resistance in wetting. It was previously observed that FSL-SPM coating could enhance the hydrophilicity of nanofibres but the difference in the wetting property of nanofibres coated with methanol and water was important in understanding that FSL-SPM can modify surfaces better if used with appropriate solvents. Therefore, it is vital to assess the suitability of solvents when using FSL constructs. The same was observed for dilution of FSL-Z so it was decided that all FSL-constructs would be diluted in 70% methanol for this research. However, it should be noted that only 70% methanol was tested but it is predicted that concentration of solvents is also an important factor. More investigation needs to be done regarding the effect of methanol concentration in case of FSL-SPM dilution. Additionally, the use of methanol is not applicable to large scale processes due to its volatile nature.

Another important finding was the difference between the adsorption efficiency of spermine with FSL-SPM. The inefficiency of spermine in adsorption was crucial in

highlighting the importance of lipid and spacer of FSL construct. The lipid tail was clearly facilitating the attachment to the nanofibre surface and making it stable during washing.

In one of the adsorption experiments done with varying contact times, it was observed that the colour of nanoparticle solution changed to slightly pink colour after 12 hours contact with FSL-SPM modified nanofibre along with reduced adsorption efficiency. The SEM analysis of the solution indicated aggregation of nanoparticles and thus pointed towards change in physio-chemical properties of the solution. It was suspected that desorption of FSL-SPM could have caused the particles to aggregate. A similar experiment using spermine instead of FSL-SPM was conducted but the colour of nanoparticle solution did not change. Further, the SEM analysis of the solution showed no aggregation of particles, possibly indicating that spermine could have washed from the surface during coating unlike in case of FSL-SPM and thus not enough spermine was present on the surface to desorb into the nanoparticle solution. Another important study was done by directly mixing FSL-SPM and spermine into the nanoparticle solution and allowing to react for 12 hours. The results indicated that presence of spermine in the solution can cause colour change of nanoparticle solution at certain concentrations which further confirmed that FSL-SPM had desorbed from the surface with increasing contact time. However, at lower concentration of FSL-SPM, desorption is not observed which points towards the fact that FSL-construct can coat stably as mono or bilayers with strong attachment to the surface.

Various other parameters of adsorption were analysed including pH of nanoparticles, initial concentration of nanoparticles, time of adsorption, the concentration of FSL-SPM. Any change in these parameters affected the process significantly.

The adsorption results were compared with a similar study done by Dhandayuthapani [296] where PVA nanofibres were surface functionalised with gluten for adsorption of silver nanoparticles. They reported removal of 36 mg of silver per gram of nanofibre where adsorption was done for 90 min on an orbital shaker at 200 rpm at 30°C. Comparison of their results with our study showed that FSL-SPM coating was far more efficient in capturing the silver nanoparticles. The adsorption results of our study indicated that only 0.0003g of modified nanofibre was able to adsorb almost 1 mg of silver particles, which means that almost 3000 mg of silver could be theoretically captured per gram of

nanofibre. Moreover, the efficiency was achieved at only 60 min of contact time at room temperature.

Filtration results further validated the successful interaction of FSL-SPM with nanoparticles. The filtration efficiency was increased to 93% at just 30 s contact time as compared to adsorption which showed 64% efficiency at 60 minutes contact time. Further, FSL-SPM coated filters performed very efficiently at high flow rates. Higher capture efficiency by filtration was expected because a larger modified surface area is involved in the capture when the nanoparticle solution passes through the bulk of the nanofibre as compared to adsorption where only the exposed surfaces are involved in capture of nanoparticles.

The adsorption and filtration assays indicated successful removal of negatively charged particles by the positively charged FSL-SPM but in contrast, the negatively charged FSL-Z showed average efficiency in removal of positively charged particles.

It was hypothesised that a mix of FSL-SPM and FSL-Z might be able to remove a mixture of nanoparticles although expected more likely was that they might neutralise each other. Results demonstrated unsurprisingly that mixture of FSL-SPM and FSL-Z resulted in decrease in efficiency of adsorption. More experiments are needed to see if enhanced efficiency can be achieved by using separate layers of FSL-SPM and FSL-Z modified nanofibres to remove a mixture of negative and positive particles.

The adsorption assay was further utilised to compare the efficiency of FSL-SPM modification during electrospinning (that is FSL-SPM was added into the nanofibre polymer mix before spinning and allowed to assemble during manufacture) and after electrospinning (that is an addition to existing nanofibres). Firstly, it was observed that the FSL-SPM construct was compatible when added into the nanofibre mix and its activity was present on the surface of spun fibres. However, it was observed that the nanofibre coated with FSL-SPM after its fabrication/ electrospinning showed greater efficiency in adsorption of [-]Agnp than nanofibres that were electrospun with FSL-SPM. Although this variation in method worked, it was not optimised and when FSL-SPM is mixed together with the polymer solution during electrospinning, large amounts of constructs are potentially entrapped within the fibres. As there were many advantages of modification after electrospinning [297], the adding of FSL-SPM to the polymer mix was discontinued. Advantages of post-spinning modification include

1) Only the surface of the polymer nanofibre mat is expected to be modified. The bulk properties of the polymer usually remain unchanged [26,298].

2) Less FSL is required for modification, as only enough is needed for the available surface to be modified, and not for the full bulk of the nanofibre polymer [53].

3) Functional groups incompatible with the electrospinning process can be added.

4) The FSL will not be degraded by the acidic polymers used to make some fibres.

Lastly, the adsorption assay was also utilised to assess the stability of FSL-SPM coated nanofibres, which demonstrated that FSL-SPM coated filters remain stable up to 6 months if stored at 4°C. This means the modification is very suitable for product development and further work could establish better stabilisation.

Air particulates

Filtration experiments show better removal of the smallest size group of PMs (0.3μm) for all smoke samples tested (diesel, wood and incense smoke) by FSL-SPM modified nanofibres. This supports the findings from other studies [251,299] that surface functional groups are responsible for interacting with small-sized particles. Moreover, for particles less than 1 μm, electrostatic interaction is the preferred mechanism of capture [251,299,300]. Therefore, due to the possible electrostatic interaction caused by the positive charge of FSL-SPM with the polar groups on the surface of particulate matter, coating is observed to work better for small-sized particles rather than those of a large size.

Total PM2.5 removal efficiency increased by almost 20% when the fibres were FSL-SPM coated than uncoated fibres (average increase in efficiency calculated from all smoke samples). However, it should also be considered that only low concentrations of FSL-SPM up to 0.2 mg/mL were investigated for the capture of air particulates whereas, for silver nanoparticles, higher coating concentrations were also tested. Therefore, more investigation is required to optimise FSL coating on nanofibres by testing various other polymer types or charged FSL constructs for maximum filtration efficiency.

Biological capture

Contamination of water by micro-organisms and their health impacts are well documented [301,302]. Similarly, micro-organisms are also major contributors to air

pollution, especially in indoor settings [303]. Nanofibres are being functionalised with antimicrobial agents for application in wound healing and bio-medical implants [275]. On the other hand, modification of nanofibres to remove bioaerosols is also in advancement [304,305].

Many disinfection strategies including chlorination have been applied for remediation of microbes but most of the techniques use toxic chemicals that can react with organic compounds in water to form harmful by-products (as reviewed [306]). Therefore, there is a need for better microbial filtration technology and FSL construct modification of nanofibres could be a potential alternative. Moreover, ability to capture microorganisms onto nanofibres also finds its applications in bioremediation of PAH and VOCs (discussed in 1.4.2).

The efficiency of FSL-SPM in capturing of *S. epidermidis* was used to show that FSL-constructs have the ability to also capture bacteria and thus could be extended to capture other microbes because they have negatively charged lipopolysaccharide (LPS) in their bacterial cell walls. Similarly, FSL-SPM also demonstrated successful filtration of red blood cells (RBC) due to the negatively charged carboxyl group of sialic acids in the cell membrane [253]. Thus, these experiments show the potential to capture cellular materials.

Limitations of Kode constructs and research protocols

The main limitation of using Kode constructs for non-covalent modification of nanofibres is that the modification is temporary which means that although the constructs are stably attached to the fibres to some extent, they can be removed from the surface under certain conditions including temperature, force, solvents and contact time. All adsorption and filtration experiments were done at room temperature and therefore more investigation is required to observe how the changes in temperature with Agnp or smoke particulates could affect the efficiency of FSL modified membranes. Similarly, the modified nanofibres were washed only 3 times with water before being used for assays. It is thus important to know how strongly constructs remain attached to the surface with continuous exposure to water and for how long.

Stability tests indicated that the FSL-SPM modified membranes could capture Agnp with optimal efficiency for up to 4 months when stored at 4°C but it's efficacy relatively

145

reduced when stored at room temperature. This could indicate two possibilities 1) the FSL-SPM denatures over time at room temperature 2) the activity of spermine head of the FSL construct is compromised when stored at room temperature. However, it is of note that stability tests done on other non-biological surfaces with different types of FSL have shown the stability of FSL constructs on surfaces for up to 8 months and longer [192]. Nevertheless, decrease in efficiency of unprotected FSL-SPM modified membranes when stored at RT pose limitations for its applications in wider areas, although future development related to stability are needed to determine the cause and potentially mitigate the effect.

The ability of FSL constructs to form multiple layers is potentially an advantage in some situations and a disadvantage in others. The loss of the upper layers when in contact with solutions has the potential to add further functionality to a product such as anti-microbial activity. However, ability to form effective monolayers would ensure optimum attachment of molecules to the surface and economic use of constructs.

Kode constructs are known to coat everything including all biological and non-biological surfaces [193,197] and a variety of mechanisms are utilised to modify the surfaces depending on the structure of the construct and the nature of the surface. Therefore, detection of coating mechanism is complicated because construct could attach to surfaces by forming monolayer, bilayer, multilayer, self-assembly or aggregation. Moreover, detection of monolayer which is the most expected mechanism is generally difficult. More sensitive tools and standardised experiments are needed to investigate the exact coating mechanism for each specific construct.

Regeneration of used filters is another challenge that needs to be considered although it is probable that the FSL modified surfaces will not be suitable for regeneration unless they are reapplied to the surface. The different filtration mechanisms result in accumulation or fouling of pollutants at the surface of membranes and there are complex physical and chemical interactions between the pollutant particles and the surface that depend on the nature of pollutants, modifying molecule and the nature of the surface [307,308]. Eventually, fouling leads to increased resistance to flow, increased transmembrane pressure and saturation of the membranes. Regenerative methods such as backflushing, treatment with chemical reagents such as acids, alkalis, surfactants or chelating agents [309]. It is assumed that the non-covalent binding of FSL with the membrane surface does

not permanently modify the surface and thus would be easily removed with appropriate solvents or chemicals and that the pollutants particles attached with the functional head would also be easily removed in the process. However, proper protocols need to be designed and investigation is still required to assess the regenerative ability of the membranes after adsorption or filtration of particles.

It is of note that Agnps were synthesised to be used as surrogates of combustion particles because of their ease of validation and characterisation but there are differences between chemical contents of nanoparticles as compared to real samples of air particles in combustion smoke. The Agnps used in this study had either a negative or positive charge with relative uniform size and surface textures. However, the generated air particles in smoke from different combustion sources used in this study were found to be diverse in terms of surface roughness, size and organic content. Although the conclusions from nanoparticle capture have been utilised to design protocols for air particulate capture, it should be considered that there are some differences in nanoparticle and air particulate capture in this study in terms of samples analysed, types of polymer membrane and coating/capture protocols. Nevertheless, the nanoparticle capture study has provided important insights about nature and capture mechanisms of Kode constructs (primarily FSL-SPM).

It was observed that there was uneven production of particulate matter from wood and incense combustion smoke with time. Although the measurement of particulate capture efficiency accounts for the differences of amount of particles generated at certain time points by quantifying particles at various time points and calculating an average value, it is of note that the physical and chemical contents vary at each time point. It is difficult to control and standardise real smoke particles and thus more investigation is required to optimise the protocols. Various other parameters such as temperature, initial concentration, types of FSL constructs, types of polymer materials etc still need to be analysed. It is also of note that in case of diesel PM synthesis, parameters and variable would have been easier to control if the engine was set up with a variable dynamometer.

Future directions

The advantage of Kode construct lies in the ability to engineer diverse functional heads with the variation of spacer and lipid groups. It is possible to test a variety of other

constructs with different charge and chemical structure that can be optimised for capture of wider range of pollutants.

The successful demonstration of the capture of fine particulates by FSL-SPM coated nanofibres points towards the possibility to extend the project for gaseous capture. Amine-based adsorbents have already been used in the past for removal of CO_2 [310,311]. These papers have attributed the increased adsorption to be result of a quasi-chemisorption interaction between CO_2 and the functional amino groups. Therefore, there are opportunities to optimise the FSL protocols of particulate capture for gaseous capture.

Many studies show that functionalised nanofibres can efficiently adsorb harmful organic aerosols and VOCs [312,313]. Cyclodextrins functionalised nanofibres are gaining attention in the field VOC and harmful gases capture [314–316] due to their ability to form inclusion complexes with many molecules [317]. Kode constructs with cyclodextrins as functional heads have also been engineered. It is highly anticipated that Kode-cyclodextrins could be efficiently applied to remove a wide range of pollutants including polar, non-polar, organic and volatile compounds.

Further, the success of FSL-SPM in capturing biological particles can be potentially extended to capture viruses based on the studies that there is a significant role of electrostatic forces in governing virus-surface interactions [318,319]. Many studies show that the surface charge in the virus can be controlled by changing the pH of the viral suspension (similar to change in charge of Agnp suspensions, discussed in 2.3.3 [319,320]. Development of proper protocols and engineering of other similar constructs with optimised functions could be done in the future to assess the potential of Kode constructs in adsorption and filtration of viruses.

The successful modification of nanofibres by FSL-SPM thus serves as a proof-of-concept for exploring modification by different FSL constructs for other applications. FSL-Z did not perform as efficiently as FSL-SPM in capturing charged Agnps but their ability to attract positively charged Agnp to some extent shows that they can impart a negative charge to a surface and thus could be used to manipulate the surface charge of various other materials. Functional heads with stronger charge could be constructed and applied in similar manner for better activity against a wider range of pollutants and used in other areas such as antimicrobial drug-delivery, and purification of cellular materials.

Moreover, specific FSL constructs targeted towards a molecule based on lock and key concept could also be engineered to have a specific affinity.

Conclusion

This research successfully demonstrates the ability of the Kode or FSL constructs to modify nanofibre surfaces using a simple technique and shows how the modified surfaces could be utilised to capture a variety of particles such as charged nanoparticles, small air particulate matter and some biological materials. The conventional surface modification involves the use of harsh chemicals and includes complicated processes. However, FSL constructs are simple in design and are biocompatible and they were successful in coating nanofibre surfaces in a single step without complex procedures. This is the first time that polyamine spermine has been studied for their ability to capture pollutants and this is also the first time that FSL-SPM has been used to coat nanofibres for removing particles in air and water. The traditional filtration membranes must compromise in the quality of flux/flow to enhance the efficiency of capture because the filtration is dependent on the amount of filtration media used, which means filters must be made compact and thick to capture maximum particles especially the small-sized ones. However, the FSL modified nanofibres showed great increase in efficiency of removing nanoparticles through adsorption and filtration (even with a thin single layer) which could be applied to make very thin nanofibre membranes capable of providing a good capture without any compromise in the flow.

References

1.   Jirsak, O. & Dao, T. A. Production, Properties and End-Uses of Nanofibers. in *Nanotechnology in Construction 3* 95–99 (Springer, Berlin, Heidelberg, 2009). doi:https://doi.org/10.1007/978-3-642-00980-8_11.

2.   Wei, Q. *Functional Nanofibers and Their Applications*. (Woodhead Publishing, 2012).

3.   Nanalyze. Industrial Nanofiber Production with Elmarco. https://www.nanalyze.com/2014/02/industrial-nanofiber-production-with-elmarco/.

4.   Alghoraibi, I. & Alomari, S. Different Methods for Nanofiber Design and Fabrication. in *Handbook of Nanofibers* 1–46 (Springer International Publishing, 2018). doi:10.1007/978-3-319-42789-8.

5.   Choo, Y., Majewski, P. W., Fukuto, M., Osuji, C. O. & Yager, K. G. Pathway-engineering for highly-aligned block copolymer arrays. *Nanoscale* 10, 416–427 (2018).

6.   Liao, H. S. *et al.* Self-assembly mechanisms of nanofibers from peptide amphiphiles in solution and on substrate surfaces. *Nanoscale* 8, 14814–14820 (2016).

7.   George, M., John, P. & Christopher, T. Molecular Self-Assembly and Nanochemistry : A Chemical Strategy for the Synthesis of Nanoparticles. *Science (80-.).* 254, 1312 (1991).

8.   Cui, H., Webber, M. J. & Stupp, S. I. Self-Assembly of Peptide Amphiphiles: From Molecules to Nanostructures to Biomaterials. *Biopolymers* 94, 1–18 (2010).

9.   Dahlin, R. L., Kasper, F. K. & Mikos, A. G. Polymeric Nanofibers in Tissue Engineering. *Tissue Eng. Part B Rev.* 17, 349–364 (2011).

10. Kulkarni, A. A. & Rao, P. S. Synthesis of polymeric nanomaterials for biomedical applications. in *Nanomaterials in Tissue Engineering* 27–63 (Woodhead Publishing, 2013). doi:10.1533/9780857097231.1.27.

11. Rana, D., Ratheesh, G., Ramakrishna, S. & Ramalingam, M. Nanofiber composites in cartilage tissue engineering. in *Nanofiber Composites for Biomedical Applications* 325–344 (Woodhead Publishing, 2017). doi:10.1016/B978-0-08-100173-8.00013-2.

12. Blaker, J. J., Knowles, J. C. & Day, R. M. Novel fabrication techniques to produce microspheres by thermally induced phase separation for tissue engineering and drug delivery. *Acta Biomater.* 4, 264–272 (2008).

13. Xing, X. *et al.* Subwavelength and Nanometer Diameter Optical Polymer Fibers as Building Blocks for Miniaturized Photonics Integration. in *Optical Communication* (ed. Das, N.) (InTech, 2012). doi:10.5772/47822.

14. Liu, X. & Ma, P. X. The nanofibrous architecture of poly(L-lactic acid)-based functional copolymers. *Biomaterials* 31, 259–269 (2010).

15. Qin, W. *et al.* Fabrication of porous chitosan membranes composed of nanofibers by low temperature thermally induced phase separation, and their adsorption behavior for Cu2+. *Carbohydr. Polym.* 178, 338–346 (2017).

16. Xie, Y., Kocaefe, D., Chen, C. & Kocaefe, Y. Review of Research on Template Methods in Preparation of Nanomaterials. *J. Nanomater.* 8, 1–10 (2016).

17. Wen, L., Xu, R., Mi, Y. & Lei, Y. Multiple nanostructures based on anodized aluminium oxide templates. *Nat. Nanotechnol.* 12, 244–250 (2017).

18. Yang, F. *et al.* The precise preparation of anodic aluminum oxide template based on the current-controlled method. *Ferroelectrics* 523, 50–60 (2018).

19. Rossinyol, E. *et al.* Nanostructured metal oxides synthesized by hard template method for gas sensing applications. *Sensors Actuators, B Chem.* 109, 57–63 (2005).

20. Talwar, V., Singh, O. & Singh, R. C. ZnO assisted polyaniline nanofibers and its application as ammonia gas sensor. *Sensors Actuators, B Chem.* 191, 276–282 (2014).

21. Nayak, R., Padhye, R., Kyratzis, I. L., Truong, Y. B. & Arnold, L. Recent advances in nanofibre fabrication techniques. *Text. Res. J.* 82, 129–147 (2012).

22. Fong, H. *et al.* Beaded nano bers formed during electrospinning. *Polymer (Guildf).* 40, 4585–4592 (1999).

23. Doshi, J. & Reneker, D. H. Electrospinning Process and Applications of Electrospun Fibers. *J. Electrostat.* 35, 151–160 (1995).

24. Zhu, N. & Chen, X. Biofabrication of Tissue Scaffolds. in *Advances in Biomaterials Science and Biomedical Applications* 315–28 (2013). doi:http://dx.doi.org/10.5772/54125.

25. Abrigo, M., McArthur, S. L. & Kingshott, P. Electrospun nanofibers as dressings for chronic wound care: Advances, challenges, and future prospects. *Macromol. Biosci.* 14, 772–792 (2014).

26. Yoo, H. S., Kim, T. G. & Park, T. G. Surface-functionalized electrospun nanofibers for tissue engineering and drug delivery. *Adv. Drug Deliv. Rev.* 61, 1033–1042 (2009).

27. Haider, A., Haider, S. & Kang, I. K. *A comprehensive review summarizing the effect of electrospinning parameters and potential applications of nanofibers in biomedical and biotechnology*. *Arabian Journal of Chemistry* (2015). doi:10.1016/j.arabjc.2015.11.015.

28. Cooper, A., Oldinski, R., Ma, H., Bryers, J. D. & Zhang, M. Chitosan-based nanofibrous membranes for antibacterial filter applications. *Carbohydr. Polym.* 92, 254–259 (2013).

29. Guerrini, L. M., Branciforti, M. C., Canova, T. & Bretas, R. E. S. Electrospinning and Characterization of Polyamide 66 Nanofibers With Different Molecular Weights. *Mater. Res.* 12, 181–190 (2009).

30. Han Wang, Gaofeng Zheng & DaoHeng Sun. Electrospun nanofibrous membrane for air filtration. in *2007 7th IEEE Conference on Nanotechnology (IEEE NANO)* 1244–1247 (IEEE, 2007). doi:10.1109/NANO.2007.4601408.

31. Qin, X.-H. & Wang, S.-Y. Electrospun nanofibers from crosslinked poly(vinyl alcohol) and its filtration efficiency. *J. Appl. Polym. Sci.* 109, 951–956 (2008).

32. Marin, E., Rojas, J. & Ciro, Y. A review of polyvinilalcohol derivates: Promising materials for pharmaceutical and biomedical applications. *African J. Pharm. Pharmacol.* 8, 674–684 (2014).

33. Nasreen, S., Sundarrajan, S., Nizar, S., Balamurugan, R. & Ramakrishna, S. Advancement in Electrospun Nanofibrous Membranes Modification and Their Application in Water Treatment. *Membranes (Basel).* 3, 266–284 (2013).

34. Gibson, P., Schreuder-Gibson, H. & Schreuder-Gibson, H. Patterned Electrospray Fiber Structures. in *Nanomanufacturing Handbook* 351–365 (CRC Press, 2006). doi:10.1201/9781420004922-14.

35. Matulevicius, J., Kliucininkas, L., Prasauskas, T., Buivydiene, D. & Martuzevicius, D. The comparative study of aerosol filtration by electrospun polyamide, polyvinyl acetate, polyacrylonitrile and cellulose acetate nanofiber media. *J. Aerosol Sci.* 92, 27–37 (2016).

36. Homaeigohar, S. S., Buhr, K. & Ebert, K. Polyethersulfone electrospun nanofibrous composite membrane for liquid filtration. *J. Memb. Sci.* 365, 68–77 (2010).

37. Yun, K. M. *et al.* Morphology optimization of polymer nanofiber for applications in aerosol particle filtration. *Sep. Purif. Technol.* 75, 340–345 (2010).

38. Saeed, K., Haider, S., Oh, T.-J. & Park, S.-Y. Preparation of amidoxime-modified polyacrylonitrile (PAN-oxime) nanofibers and their applications to metal ions adsorption. *J. Memb. Sci.* 322, 400–405 (2008).

39. Pisignano, D. Structural and Surface Properties of Polymer Nanofibers and Their Applications. in *Polymer Nanofibers: Building Blocks for Nanotechnology* 189–235 (2013). doi:10.1039/9781849737746.

40. Fabbri, P. & Messori, M. *Surface Modification of Polymers: Chemical, Physical, and Biological Routes*. *Modification of Polymer Properties* (William Andrew Publishing, 2017). doi:10.1016/B978-0-323-44353-1.00005-1.

41. Ratner, B. D. Surface modification of polymers: chemical, biological and surface analytical challenges. *Biosens. Bioelectron.* 10, 797–804 (1995).

42. Mohamad, N. R., Marzuki, N. H. C., Buang, N. A., Huyop, F. & Wahab, R. A. An overview of technologies for immobilization of enzymes and surface analysis techniques for immobilized enzymes. *Biotechnol. Biotechnol. Equip.* 29, 205–220 (2015).

43. Thakur, M. K., Rana, A. K., Liping, Y., Singha, A. S. & Thakur, V. K. Surface modification of bio polymers: an overview. in *Surface modifaction of biopolymers* (eds. Singha, A. S. & Thakur, V. K.) 1–19 (2015).

44. Hegemann, D., Brunner, H. & Oehr, C. Plasma treatment of polymers for surface and adhesion improvement. *Nucl. Instruments Methods Phys. Res. Sect. B Beam Interact. with Mater. Atoms* 208, 281–286 (2003).

45. Friedrich, J. *et al.* Plasma-based introduction of monosort functional groups of different type and density onto polymer surfaces. Part 1: Behaviour of polymers exposed to oxygen plasma. *Compos. Interfaces* 10, 139–171 (2003).

46. Asadian, M. *et al.* [ASAP] Plasma Functionalization of Polycaprolactone Nanofibers Changes Protein Interactions with Cells, Resulting in Increased Cell Viability. *ACS Appl. Mater. Interfaces* 10, 41962–41977 (2018).

47. Liu, W. *et al.* Effects of plasma treatment to nanofibers on initial cell adhesion and cell morphology. *Colloids Surfaces B Biointerfaces* 113, 101–106 (2014).

48. Kolská, Z. *et al.* Properties of polyamide nanofibers treated by UV-A radiation. *Mater. Lett.* 214, 264–267 (2018).

49. Truica-Marasescu, F. & Wertheimer, M. R. Vacuum-ultraviolet photopolymerisation of amine-rich thin films. *Macromol. Chem. Phys.* 209, 1043–1049 (2008).

50. Stoyanov, O. V. *et al.* Surface treatment of polymers by an ultraviolet laser to improve adhesion quality. *Polym. Sci. Ser. D* 9, 5–12 (2016).

51. Baudrit, B. *et al.* Surface treatment with ultraviolet laser for adhesive bonding of polymeric materials. *J. Adhes.* 93, 204–215 (2015).

52. Ruckenstein, E. & Li, Z. F. Surface modification and functionalization through the self-assembled monolayer and graft polymerization. *Adv. Colloid Interface Sci.* 113, 43–63 (2005).

53. Yao, C., Li, X., Neoh, K. G., Shi, Z. & Kang, E. T. Surface modification and antibacterial activity of electrospun polyurethane fibrous membranes with quaternary ammonium moieties. *J. Memb. Sci.* 320, 259–267 (2008).

54. Ifuku, S., Iwasaki, M., Morimoto, M. & Saimoto, H. Graft polymerization of acrylic acid onto chitin nanofiber to improve dispersibility in basic water. *Carbohydr. Polym.* 90, 623–627 (2012).

55. Tsubokawa, N. Preparation and Properties of Polymer-grafted Carbon Nanotubes and Nanofibers. *Polym. J.* 37, 637–655 (2005).

56. Ma, Z., Kotaki, M., Yong, T., He, W. & Ramakrishna, S. Surface engineering of electrospun polyethylene terephthalate (PET) nanofibers towards development of a new material for blood vessel engineering. *Biomaterials* 26, 2527–2536 (2005).

57. Chen, G. & Lv, Y. Immobilization and Application of Electrospun Nanofiber Scaffold-based Growth Factor in Bone Tissue Engineering. *Curr. Pharm. Des.* 21, 1967–1978 (2015).

58. Xiao, S., Shen, M., Guo, R., Wang, S. & Shi, X. Immobilization of Zerovalent Iron Nanoparticles into Electrospun Polymer Nanofibers: Synthesis, Characterization, and Potential Environmental Applications. *J. Phys. Chem. C* 113, 18062–18068 (2009).

59.   Sassolas, A., Blum, L. J. & Leca-Bouvier, B. D. Immobilization strategies to develop enzymatic biosensors. *Biotechnol. Adv.* 30, 489–511 (2012).

60.   Sheldon, R. A. Enzyme immobilization: The quest for optimum performance. *Adv. Synth. Catal.* 349, 1289–1307 (2007).

61.   Johnson, E. R., Keinan, S., Mori-sánchez, P., Contreras-garcía, J. & Aron, J. Revealing Non-Covalent Interactions. *J. Am. Chem. Soc.* 132, 6498–6506 (2010).

62.   Yoo, H. S., Kim, T. G. & Park, T. G. Surface-functionalized electrospun nanofibers for tissue engineering and drug delivery. *Adv. Drug Deliv. Rev.* 61, 1033–1042 (2009).

63.   Zhang, J., Wang, X., Liu, T., Liu, S. & Jing, X. Antitumor activity of electrospun polylactide nanofibers loaded with 5-fluorouracil and oxaliplatin against colorectal cancer. *Drug Deliv.* 1–7 (2014) doi:10.3109/10717544.2014.916768.

64.   Ma, G. *et al.* Paclitaxel loaded electrospun porous nanofibers as mat potential application for chemotherapy against prostate cancer. *Carbohydr. Polym.* 86, 505–512 (2011).

65.   Goyal, R., Macri, L. K., Kaplan, H. M. & Kohn, J. Nanoparticles and nanofibers for topical drug delivery. *J Control Release* 240, 77–92 (2016).

66.   Kreuter, J. Nanoparticles and microparticles for drug and vaccine delivery. *J. Anat.* 189 (Pt 3, 503–505 (1996).

67.   Rujitanaroj, P. on, Pimpha, N. & Supaphol, P. Wound-dressing materials with antibacterial activity from electrospun gelatin fiber mats containing silver nanoparticles. *Polymer (Guildf).* 49, 4723–4732 (2008).

68.   Dong, H., Wang, D., Sun, G. & Hinestroza, J. P. Assembly of Metal Nanoparticles on Electrospun Nylon 6 Nanofibers.pdf. *Chem. Mater.* 20, 6627–6632 (2008).

69.   Watson, S., Nie, M., Wang, L. & Stokes, K. Challenges and developments of self-assembled monolayers and polymer brushes as a green lubrication solution for tribological applications. *RSC Adv.* 5, 89698–89730 (2015).

70.   Prashar, D. Self Assembled Monolayers. *Int. J. ChemTech Res.* 4, 258–265 (2012).

71.   Senaratne, W., Andruzzi, L. & Ober, C. K. Self-assembled monolayers and polymer brushes in biotechnology: Current applications and future perspectives. *Biomacromolecules* 6, 2427–2448 (2005).

72.   Zins, E. L., Silvi, B. & Alikhani, M. E. Activation of C-H and B-H bonds through agostic bonding: an ELF/QTAIM insight. *Phys. Chem. Chem. Phys.* 17, 9258–9281 (2015).

73.   Sonawane, M. D. & Nimse, S. B. Surface Modification Chemistries of Materials Used in Diagnostic Platforms with Biomolecules. *J. Chem.* 2016, 1–19 (2016).

74.   Hermanson, G. *Bioconjugate Techniques*. (Academic Press, 2013).

75.   Junka, R., Valmikinathan, C. M., Kalyon, D. M. & Yu, X. Laminin Functionalized Biomimetic Nanofibers for Nerve Tissue Engineering. *J. Biomater. Tissue Eng.* 3, 494–502 (2013).

76.   Chen, W. S. *et al.* The Effect of Laminin Surface Modification of Electrospun Silica Nanofiber Substrate on Neuronal Tissue Engineering. *Nanomater. (Basel, Switzerland)* 8, (2018).

77.   Rabolt, J. F., Sisson, K., Zhang, C., Farach-Carson, M. C. & Chase, D. B. Evaluation of Cross-Linking Methods for Electrospun Gelatin on Cell Growth and Viability. *Biomacromolecules* 10, 1675–1680 (2009).

78.   Qin, X., Dou, G., Jiang, G. & Zhang, S. Characterization of poly (vinyl alcohol) nanofiber mats cross-linked with glutaraldehyde. *J. Ind. Text.* 43, 34–44 (2013).

79.   Abd El-aziz, A. M., El-Maghraby, A. & Taha, N. A. Comparison between polyvinyl alcohol (PVA) nanofiber and polyvinyl alcohol (PVA) nanofiber/hydroxyapatite (HA) for removal of Zn2+ ions from wastewater. *Arab. J. Chem.* 10, 1052–1060 (2017).

80. Tang, C., Saquing, C. D., Harding, J. R. & Khan, S. A. *In Situ* Cross-Linking of Electrospun Poly(vinyl alcohol) Nanofibers. *Macromolecules* 43, 630–637 (2010).

81. Austero, M. S., Donius, A. E., Wegst, U. G. K. & Schauer, C. L. New crosslinkers for electrospun chitosan fibre mats. *J. R. Soc. Interface* 2551–2562 (2012).

82. Panzavolta, S. *et al.* Electrospun gelatin nanofibers: Optimization of genipin cross-linking to preserve fiber morphology after exposure to water. *Acta Biomater.* 7, 1702–1709 (2011).

83. Liu, Y. *et al.* Fabrication and Properties of High-Content Keratin/Poly (Ethylene Oxide) Blend Nanofibers Using Two-Step Cross-Linking Process. *J. Nanomater.* 2015, (2015).

84. Jassal, P. S., Raut, V. P. & Anand, N. Removal of copper (II) ions from aqueous solution onto chitosan and cross-linked chitosan beads. *Proc. Indian Natl. Sci. Acad.* 76, 1–6 (2010).

85. Meador, M. A. B. *et al.* Reinforcing polymer cross-linked aerogels with carbon nanofibers. *J. Mater. Chem.* 18, 1843–1852 (2008).

86. Kolb, H. C., Finn, M. G. & Sharpless, K. B. Click chemistry: Diverse chemical function from a few good reactions. *Angew. Chem. Int. Ed.* 40, 2004–2021 (2001).

87. Matyjewicz, J., Lesniewski, A. & Niedziolka-Jonsson, J. Click chemistry modification of glassy carbon electrode with gold nanoparticles for electroactive ion discrimination. *Electrochem. commun.* 48, 73–76 (2014).

88. Poonthiyil, V., Lindhorst, T. K., Golovko, V. B. & Fairbanks, A. J. Recent applications of click chemistry for the functionalization of gold nanoparticles and their conversion to glyco-gold nanoparticles. *Beilstein J. Org. Chem.* 14, 11–24 (2017).

89. Yi, G., Son, J., Yoo, J., Park, C. & Koo, H. Application of click chemistry in nanoparticle modification and its targeted delivery. *Biomater. Res.* 22, 1–8 (2018).

90. Barner-Kowollik, C. *et al.* 'Clicking' polymers or just efficient linking: What is the difference? *Angew. Chemie - Int. Ed.* 50, 60–62 (2011).

91. Lancuški, A., Fort, S. & Bossard, F. Electrospun azido-PCL nanofibers for enhanced surface functionalization by click chemistry. *ACS Appl. Mater. Interfaces* 4, 6499–6504 (2012).

92. Wang, W. xiang, Liu, Y., Wang, Y. xue, Chen, H. & Bai, L. jiu. A novel and convenient preparation of antibacterial polyacrylonitrile nanofibers via post-modification using nitrile click chemistry and electrospinning. *Chem. Pap.* 72, 191–200 (2018).

93. Wang, W. *et al.* Microwave-assisted rapid fabrication of antibacterial polyacrylonitrile microfibers/nanofibers via nitrile click chemistry and electrospinning. *J. Appl. Polym. Sci.* 134, (2017).

94. Nicholas J. Agard, Jennifer A. Prescher, A. & Bertozzi, C. R. A Strain-Promoted [3 + 2] Azide–Alkyne Cycloaddition for Covalent Modification of Biomolecules in Living Systems. *J. Am. Chem. Soc.* (2004) doi:10.1021/JA044996F.

95. Zhou, D. *et al.* Transport modelling for EAST with LHRF and NBI. *Plasma Sci. Technol.* 11, 417–421 (2009).

96. Ying, A. H. *et al.* Entrapment of cells within core-shell electrospun scaffold fibers Entrapment of Cells within Core-shell Electrospun Scaffold Fibers. 25–26 (2013).

97. Neisiany, R. E., Khorasani, S. N., Kong Yoong Lee, J. & Ramakrishna, S. Encapsulation of epoxy and amine curing agent in PAN nanofibers by coaxial electrospinning for self-healing purposes. *RSC Adv.* 6, 70056–70063 (2016).

98. Lee, M. W. *et al.* Hybrid Self-Healing Matrix Using Core–Shell Nanofibers and capsuleless microdroplets. *Appl. Mater. interfaces* 6, 10461–10468 (2014).

99. Kurtz, I. S. & Schiffman, J. D. Current and emerging approaches to engineer antibacterial and antifouling electrospun nanofibers. *Materials (Basel).* 11, (2018).

100. Klein, S. *et al.* Encapsulation of Bacterial Cells in Electrospun Microtubes. *Biomacromolecules* 10, 1751–1756 (2009).

101. Ang, H. Y. *et al.* Characterization of a bioactive fiber scaffold with entrapped HUVECs in coaxial electrospun core-shell fiber. *Biomatter* 4, e28238 (2014).

102. Song, Y., Miao, W., Liu, B., Dai, W. & Cai, X. Identifying anthropogenic and natural influences on extreme pollution of respirable suspended particulates in Beijing using backward trajectory analysis. *J. Hazard. Mater.* 154, 459–468 (2008).

103. Longo, B. M. & Longo, A. A. Volcanic ash in the air we breathe. *Multidiscip. Respir. Med.* 8, 1 (2013).

104. Liu, J. C. *et al.* Particulate Air Pollution from Wildfires in the Western US under Climate Change. *Clim. Chang.* 51, 195–212 (2017).

105. Appannagari, R. R. Environmental Pollution Causes and Consequences: A Study. *North Asian Int. Res. J. Soc. Sci. Humanit.* 3, (2017).

106. Oberdörster, G., Oberdörster, E. & Oberdörster, J. Nanotoxicology: An emerging discipline evolving from studies of ultrafine particles. *Environmental Health Perspectives* (2005) doi:10.1289/ehp.7339.

107. Karagulian, F. *et al.* Contributions to cities' ambient particulate matter (PM): A systematic review of local source contributions at global level. *Atmos. Environ.* 120, 475–483 (2015).

108. US EPA. Particulate Matter (PM) Basics. https://www.epa.gov/pm-pollution/particulate-matter-pm-basics.

109. WHO Regional Office to Europe. *Health effects of particulate matter*. http://www.euro.who.int/pubrequest (2013).

110. Dai, J. *et al.* Ambient air pollution, temperature and out-of-hospital coronary deaths in Shanghai, China. *Environ. Pollut.* 203, 116–121 (2015).

111. Kampa, M. & Castanas, E. Human health effects of air pollution. *Environ. Pollut.* 151, 362–367 (2008).

112. World Health Organization. Ambient (outdoor) air quality and health. https://www.who.int/news-room/fact-sheets/detail/ambient-(outdoor)-air-quality-and-health (2018).

113. Turpin, B. Characterising exposures to atmospheric carcinogens. in *Air pollution and cancer* 29–36 (IARC SCIENTIFIC PUBLICATION, 2009).

114. Ding, A. *et al.* Indoor PM2.5 exposure affects skin aging manifestation in a Chinese population. *Sci. Rep.* 7, 3–9 (2017).

115. Jeong, J. W. *et al.* Particulate matter 2.5 damages skin cells by inducing oxidative stress, subcellular organelle dysfunction, and apoptosis. *Arch. Toxicol.* 92, 2077–2091 (2018).

116. US geological survey. Volcanic Ash Impacts and Mitigation: Respiratory effects. https://volcanoes.usgs.gov/volcanic_ash/about_us.html.

117. Volcanic Ashfall Impacts Working Group. Volcanic Ash Impacts & Mitigation - Respiratory Effects. https://volcanoes.usgs.gov/volcanic_ash/respiratory_effects.html.

118. Shuai, J. *et al.* Health risk assessment of volatile organic compounds exposure near Daegu dyeing industrial complex in South Korea. *BMC Public Health* 18, 528 (2018).

119. Celebioglu, A., Sen, H. S., Durgun, E. & Uyar, T. Molecular entrapment of volatile organic compounds (VOCs) by electrospun cyclodextrin nanofibers. *Chemosphere* 144, 736–744 (2016).

120. Tobiszewski, M. & Namieśnik, J. PAH diagnostic ratios for the identification of pollution emission sources. *Environ. Pollut.* 162, 110–119 (2012).

121.   Boucher, O., Friedlingstein, P., Collins, B. & Shine, K. P. The indirect global warming potential and global temperature change potential due to methane oxidation. *Environ. Res. Lett.* 4, 044007 (2009).

122.   Rani, B., Singh, U., Chuhan, A., Sharma, D. & Maheshwari, R. Photochemical Smog Pollution and its mitigation Measures. *J. Adv. Sci. Res.* 2, 28–33 (2011).

123.   Rasalingam, S., Peng, R. & Koodali, R. T. Removal of hazardous pollutants from wastewaters: Applications of TiO2-SiO2 mixed oxide materials. *J. Nanomater.* 2014, (2014).

124.   WHO. Global Health Observatory Data. http://www.who.int/mediacentre/factsheets/fs391/en/ (2012).

125.   Vidmar, J. *et al.* Elements in water, suspended particulate matter and sediments of the Sava River. *J. Soils Sediments* 17, 1917–1927 (2017).

126.   Peters, R. J. B. *et al.* Nanomaterials for products and application in agriculture, feed and food. *Trends Food Sci. Technol.* 54, 155–164 (2016).

127.   Shi, L., Shan, J., Ju, Y., Aikens, P. & Prud'homme, R. K. Nanoparticles as delivery vehicles for sunscreen agents. *Colloids Surfaces A Physicochem. Eng. Asp.* 396, 122–129 (2012).

128.   Wu, M., Ma, B., Pan, T., Chen, S. & Sun, J. Silver-Nanoparticle-Colored Cotton Fabrics with Tunable Colors and Durable Antibacterial and Self-Healing Superhydrophobic Properties. *Adv. Funct. Mater.* 26, 569–576 (2016).

129.   Woo, K. J. *et al.* Antibacterial activity and mechanism of action of the silver ion in Staphylococcus aureus and Escherichia coli. *Appl. Environ. Microbiol.* 74, 2171–2178 (2008).

130.   Abbott Chalew, T. E., Ajmani, G. S., Huang, H. & Schwab, K. J. Evaluating nanoparticle breakthrough during drinking water treatment. *Environ. Health Perspect.* 121, 1161–1166 (2013).

131.   Amin, M. T., Alazba, a a & Manzoor, U. A review on removal of pollutants from water / wastewater using different types of nanomaterials. *Adv. Mater. Sci. Eng.* 2014, (2014).

132.   Puckett, L. J. Identifying the major sources of nutrient water pollution. *Environ. Sci. Technol.* 29, 408A-414A (1995).

133.   Aktar, M. W., Sengupta, D. & Chowdhury, A. Impact of pesticides use in agriculture: their benefits and hazards. *Interdiscip. Toxicol.* 2, 1–12 (2009).

134.   Jaishankar, M., Tseten, T., Anbalagan, N., Mathew, B. B. & Beeregowda, K. N. Toxicity, mechanism and health effects of some heavy metals. *Interdiscip. Toxicol.* 7, 60–72 (2014).

135.   Tchounwou, P. B., Yedjou, C. G., Patlolla, A. K. & Sutton, D. J. Heavy Metals Toxicity and the Environment. *EXS* 101, 1–30 (2012).

136.   Barhate, R. S. & Ramakrishna, S. Nanofibrous filtering media: Filtration problems and solutions from tiny materials. *J. Memb. Sci.* 296, 1–8 (2007).

137.   Poudyal, A. *et al.* Electrospun Nanofibre Filter Media: New Emergent Technologies and Market Perspectives. in *Filtering Media by Electrospinning: Next Generation Membranes for Separation Applications* 197–224 (Springer nature, 2018). doi:10.1007/978-3-319-78163-1_9.

138.   Ravindra, K., Sokhi, R. & Van Grieken, R. Atmospheric polycyclic aromatic hydrocarbons: Source attribution, emission factors and regulation. *Atmos. Environ.* 42, 2895–2921 (2008).

139.   Wania, F. & Mackay, D. Tracking the distribution of persistent organic pollutants. *Environ. Sci. Technol.* 30, 390A-396A (1996).

140.   Filatov, Y., Budyka, A. & Kirichenko, V. *Electrospinning of micro-and nanofibers : fundamentals and applications in separation and filtration processes*. (Begell House, 2007).

141.   Mukhopadhyay, A. Pulse-jet filtration: An effective way to control industrial pollution Part I: Theory, selection and design of pulse-jet filter. *Text. Prog.* 41, 195–315 (2009).

142. Yao, J., Bastiaansen, C. & Peijs, T. High Strength and High Modulus Electrospun Nanofibers. *Fibers* 2, 158–186 (2014).

143. Liu, C. *et al.* Transparent air filter for high-efficiency PM2.5 capture. *Nat. Commun.* 6, (2015).

144. Jing, L. *et al.* Electrospun Polyacrylonitrile-Ionic Liquid Nanofibers for Superior PM2.5 Capture Capacity. *ACS Appl. Mater. Interfaces* 8, 7030–7036 (2016).

145. Zhang, R. *et al.* Nanofiber air filters with high-temperature stability for efficient PM2.5 removal from the pollution sources. *Nano Lett.* 16, 3642–3649 (2016).

146. Wang, Y., Wang, S., Fang, J., Ding, L. X. & Wang, H. A nano-silica modified polyimide nanofiber separator with enhanced thermal and wetting properties for high safety lithium-ion batteries. *J. Memb. Sci.* 537, 248–254 (2017).

147. Szejtli, J. Introduction and General Overview of Cyclodextrin Chemistry. *Chem. Rev.* 98, 1743–1754 (1998).

148. Chen, P. *et al.* Carbonaceous nanofiber membrane functionalized by beta-cyclodextrins for molecular filtration. *ACS Nano* 5, 5928–5935 (2011).

149. Kayaci, F. & Uyar, T. Electrospun polyester/cyclodextrin nanofibers for entrapment of volatile organic compounds. *Polym. Eng. Sci.* 54, 2970–2978 (2014).

150. Uyar, T., Havelund, R., Hacaloglu, J., Besenbacher, Ḱ. F. & Kingshott, P. Cyclodextrins : Comparison of Molecular Filter Performance. 4, 5121–5130 (2010).

151. Celebioglu, A. & Uyar, T. Electrospinning of polymer-free nanofibers from cyclodextrin inclusion complexes. *Langmuir* 27, 6218–6226 (2011).

152. Celebioglu, A., Sen, H. S., Durgun, E. & Uyar, T. Molecular entrapment of volatile organic compounds (VOCs) by electrospun cyclodextrin nanofibers. *Chemosphere* 144, 736–744 (2016).

153. Zhang, Y. *et al.* Preparation of Nanofibrous Metal–Organic Framework Filters for Efficient Air Pollution Control. *J. Am. Chem. Soc.* 138, 5785–5788 (2016).

154. Qian, J. *et al.* A microporous MOF with open metal sites and Lewis basic sites for selective CO2 capture. *Dalt. Trans.* 46, 14102–14106 (2017).

155. Vellingiri, K. *et al.* Metal organic frameworks as sorption media for volatile and semi-volatile organic compounds at ambient conditions. *Sci. Rep.* 6, 27813 (2016).

156. Ge, J. & Choi, N. Fabrication of Functional Polyurethane/Rare Earth Nanocomposite Membranes by Electrospinning and Its VOCs Absorption Capacity from Air. *Nanomaterials* 7, 60 (2017).

157. Biswas, B., Sarkar, B., Rusmin, R. & Naidu, R. Bioremediation of PAHs and VOCs: Advances in clay mineral-microbial interaction. *Environ. Int.* 85, 168–181 (2015).

158. Blasi, B. *et al.* Pathogenic yet environmentally friendly? black fungal candidates for bioremediation of pollutants. *Geomicrobiol. J.* 33, 308–317 (2016).

159. Ma, H. & Hsiao, B. S. Current Advances on Nanofiber Membranes for Water Purification Applications. in *Filtering Media by Electrospinning* 25–46 (Springer International Publishing, 2018). doi:10.1007/978-3-319-78163-1_2.

160. Alkhudhiri, A., Darwish, N. & Hilal, N. Membrane distillation: A comprehensive review. *Desalination* 287, 2–18 (2012).

161. Sun, Z. & Chen, F. Hydrophilicity and antifouling property of membrane materials from cellulose acetate/polyethersulfone in DMAc. *Int. J. Biol. Macromol.* 91, 143–150 (2016).

162. Jeon, S. *et al.* The effect of membrane material and surface pore size on the fouling properties of submerged membranes. *Water (Switzerland)* 8, (2016).

163. Kandisa, R. V. & Saibaba KV, N. Dye Removal by Adsorption: A Review. *J. Bioremediation Biodegrad.* 07, (2016).

164. Gürses, A., Açıkyıldız, M., Güneş, K. & Gürses, M. S. Dyes and Pigments: Their structure and properties. in *Dyes and Pigments* (2016). doi:10.1007/978-3-319-33892-7.

165. Hou, C., Yang, H., Xu, Z. L. & Wei, Y. M. Preparation of PAN/PAMAM blend nanofiber mats as efficient adsorbent for dye removal. *Fibers Polym.* 16, 1917–1924 (2015).

166. Qureshi, U. A. *et al.* Highly efficient and robust electrospun nanofibers for selective removal of acid dye. *J. Mol. Liq.* 244, 478–488 (2017).

167. Mahmoodi, N. M., Mokhtari-Shourijeh, Z. & Ghane-Karade, A. *Synthesis of the modified nanofiber as a nanoadsorbent and its dye removal ability from water: Isotherm, kinetic and thermodynamic*. *Water Science & Technology* vol. 75 (2017).

168. Qureshi, U. A., Khatri, Z., Ahmed, F., Khatri, M. & Kim, I. S. Electrospun Zein Nanofiber as a Green and Recyclable Adsorbent for the Removal of Reactive Black 5 from the Aqueous Phase. *ACS Sustain. Chem. Eng.* 5, 4340–4351 (2017).

169. Stenstad, P., Andresen, M., Tanem, B. S. & Stenius, P. Chemical surface modifications of microfibrillated cellulose. *Cellulose* 15, 35–45 (2008).

170. Missoum, K., Belgacem, M. N. & Bras, J. Nanofibrillated cellulose surface modification: A review. *Materials (Basel).* 6, 1745–1766 (2013).

171. Gopakumar, D. A. *et al.* Meldrum's acid modified cellulose nanofiber-based polyvinylidene fluoride microfiltration membrane for dye water treatment and nanoparticle removal. *ACS Sustain. Chem. Eng.* 5, 2026–2033 (2017).

172. Aziz, S., Sabzi, M., Fattahi, A. & Arkan, E. Electrospun silk fibroin/PAN double-layer nanofibrous membranes containing polyaniline/TiO2 nanoparticles for anionic dye removal. *J. Polym. Res.* 24, 140 (2017).

173. Tahaei, P., Abdouss, M., Edrissi, M., Shoushtari, A. M. & Zargaran, M. Preparation of chelating fibrous polymer by different diamines and study on their physical and chemical properties. *Materwiss. Werksttech.* 39, 839–844 (2008).

174. Shen, X., Xu, C. & Ye, L. Molecularly Imprinted Polymers for Clean Water: Analysis and Purification. *Ind. Eng. Chem. Res.* 52, 13890–13899 (2013).

175. Vasapollo, G. *et al.* Molecularly imprinted polymers: Present and future prospective. *Int. J. Mol. Sci.* 12, 5908–5945 (2011).

176. Pan, G. *et al.* Controlled synthesis of water-compatible molecularly imprinted polymer microspheres with ultrathin hydrophilic polymer shells via surface-initiated reversible addition-fragmentation chain transfer polymerization. *Soft Matter* 7, 8428 (2011).

177. Luo, X. *et al.* Selective removal Pb(ii) ions form wastewater using Pb(ii) ion-imprinted polymers with bi-component polymer brushes. *RSC Adv.* 7, 25811–25820 (2017).

178. Mafu, L. D., Mamba, B. B. & Msagati, T. A. M. Synthesis and characterization of ion imprinted polymeric adsorbents for the selective recognition and removal of arsenic and selenium in wastewater samples. *J. Saudi Chem. Soc.* 20, 594–605 (2016).

179. Guo, X., Fei, G. T., Su, H. & De Zhang, L. High-performance and reproducible polyaniline nanowire/tubes for removal of Cr(VI) in aqueous solution. *J. Phys. Chem. C* 115, 1608–1613 (2011).

180. Ku, Y. & Jung, I. L. Photocatalytic reduction of Cr(VI) in aqueous solutions by UV irradiation with the presence of titanium dioxide. *Water Res.* 35, 135–142 (2001).

181. Mohamed, A. *et al.* Removal of chromium (VI) from aqueous solutions using surface modified composite nanofibers. *J. Colloid Interface Sci.* 505, 682–691 (2017).

182. Chitpong, N. & Husson, S. M. Nanofiber ion-exchange membranes for the rapid uptake and recovery of heavy metals from water. *Membranes (Basel).* 6, (2016).

183. Kumar, R., Barakat, M. A. & Alseroury, F. A. Oxidized g-C3N4/polyaniline nanofiber composite for the selective removal of hexavalent chromium. *Sci. Rep.* 7, 12850 (2017).

184. Hurk, R. van den & Evoy, S. A review of membrane-based biosensors for pathogen detection. *Sensors (Switzerland)* 15, 14045–14078 (2015).

185. Gao, Y., Truong, Y. B., Zhu, Y. & Louis Kyratzis, I. Electrospun antibacterial nanofibers: Production, activity, and in vivo applications. *J. Appl. Polym. Sci.* 131, 9041–9053 (2014).

186. Dubey, P. *et al.* Silver-nanoparticle-Incorporated composite nanofibers for potential wound-dressing applications. *J. Appl. Polym. Sci.* 132, n/a-n/a (2015).

187. Nthunya, L. N. *et al.* Greener Approach to Prepare Electrospun Antibacterial β-Cyclodextrin/Cellulose Acetate Nanofibers for Removal of Bacteria from Water. *ACS Sustain. Chem. Eng.* 5, 153–160 (2016).

188. Cheirsilp, B. & Rakmai, J. Inclusion complex formation of cyclodextrin with its guest and their applications. *Biol. Eng. Med.* 2, 1–6 (2017).

189. Yu, Z. *et al.* Preparation of a novel anti-fouling β-cyclodextrin–PVDF membrane. *RSC Adv.* 5, 51364–51370 (2015).

190. Henry, S. M. & Bovin, N. V. Kode Technology − a universal cell surface glycan modification technology. *J. R. Soc. New Zeal.* 49, 100–113 (2019).

191. Korchagina, E. Y. & Henry, S. M. Synthetic glycolipid-like constructs as tools for glycobiology research, diagnostics, and as potential therapeutics. *Biochem.* 80, 857–871 (2015).

192. Barr, K. Bio - Modification of Non - Biological Surfaces with Function - Spacer - Lipid Constructs by Methods Including Bioprinting. (Auckland University of Technology, 2013).

193. Williams, E. *et al.* Ultra-fast glyco-coating of non-biological surfaces. *Int. J. Mol. Sci.* 17, 1–18 (2016).

194. Henry, S. M., Komarraju, S., Heathcote, D. & Rodionov, I. L. Designing peptide-based FSL constructs to create Miltenberger kodecytes. *ISBT Sci. Ser.* 6, 306–312 (2011).

195. Henry, S. M., Barr, K. L. & Oliver, C. A. Modeling transfusion reactions with kodecytes and enabling ABO-incompatible transfusion with function-spacer-lipid constructs. *ISBT Sci. Ser.* 7, 106–111 (2012).

196. Barr, K. *et al.* Biofunctionalizing nanofibers with carbohydrate blood group antigens. *Biopolymers* 105, 787–794 (2016).

197. Henry, S. *et al.* Rapid one-step biotinylation of biological and non-biological surfaces. *Sci. Rep.* 3–8 (2018) doi:10.1038/s41598-018-21186-3.

198. Ramaseshan, R. *et al.* Functionalized polymer nanofibre membranes for protection from chemical warfare stimulants. *Nanotechnology* 17, 2947–2953 (2006).

199. Ramaseshan, R. *et al.* Functionalized polymer nanofibre membranes for protection from chemical warfare stimulants. *Nanotechnology* 17, 2947–2953 (2006).

200. Lockwood, D. J. & Bin Ding, J. yu. *Electrospun Nanofibers for Energy and Environmental Applications*. (Springer, 2015). doi:10.1007/978-3-642-54160-5.

201. Huang, F., Wei, Q., Cai, Y. & Wu, N. Surface Structures and Contact Angles of Electrospun Poly (vinylidene fluoride) Nanofiber Membranes Surface Structures and Contact Angles of. *Int. J. Polym. Anal. Charact.* 5341, (2009).

202. Yuan, Y. & Lee, T. R. Contact Angle and wetting properties. in *Surface Science Techniques* (Springer, 2013). doi:10.1007/978-3-642-34243-1.

203. Liu, C. *et al.* Transparent air filter for high-efficiency PM 2.5 capture. *Nat. Commun.* 6, (2015).

204. Votyakova, T. V., Wallace, H. M., Dunbar, B. & Wilson, S. B. The covalent attachment of polyamines to proteins in plant mitochondria. *Eur. J. Biochem.* 260, 250–257 (1999).

205. Li, M. *et al.* Spermine-modified Antheraea pernyi silk fibroin as a gene delivery carrier. *Int. J. Nanomedicine* Volume 11, 1013 (2016).

206. Shafi, Z. B., Martin, G. P., Olliff, C. J. & James, S. L. Surface modification of albumin microspheres. *J. Drug Target.* 3, 53–56 (1995).

207. Webspectra. IR Absorption Table. https://webspectra.chem.ucla.edu/irtable.html.

208. Seo, M. H. & Kim, H. Determination of electrospun fiber diameter distributions using image analysis processing Determination of Electrospun Fiber Diameter Distributions Using Image Analysis Processing. (2008) doi:10.1007/BF03218523.

209. Hotaling, N. A., Bharti, K., Kriel, H. & Simon, C. G. DiameterJ : A validated open source nano fi ber diameter measurement tool. *Biomaterials* 61, 327–338 (2015).

210. Friedman, M. Applications of the Ninhydrin Reaction for Analysis of Amino Acids, Peptides, and Proteins to Agricultural and Biomedical Sciences. *J. Agric. Food Chem.* 52, 385–406 (2004).

211. Fujita, K. *et al.* Improved analysis for urinary polyamines by use of high-voltage electrophoresis on paper. *Clin. Chem.* 26, 1577–1582 (1980).

212. Marton, L. J., Russell, D. H. & Levy, C. C. Measurement of putrescine, spermidine, and spermine in physiological fluids by use of an amino acid analyzer. *Clin. Chem.* 19, 923–926 (1973).

213. Parikh, S. J. & Chorover, J. FTIR spectroscopic study of biogenic Mn-oxide formation by Pseudomonas putida GB-1. *Geomicrobiol. J.* 22, 207–218 (2005).

214. Lopes, C. de C. A., Limirio, P. H. J. O., Novais, V. R. & Dechichi, P. Fourier transform infrared spectroscopy (FTIR) application chemical characterization of enamel, dentin and bone. *Appl. Spectrosc. Rev.* 53, 747–769 (2018).

215. Merlic, C. A. & Strouse, J. Problems in NMR and IR spectroscopy. *Web Spectra* https://webspectra.chem.ucla.edu/index.html.

216. Sharonova, A. *et al.* Synthesis of positively and negatively charged silver nanoparticles and their deposition on the surface of titanium. *IOP Conf. Ser. Mater. Sci. Eng.* 116, 012009 (2016).

217. Swinehart, D. F. The Beer-Lambert Law. *J. Chem. Educ.* 39, 333–335 (1962).

218. He, S. *et al.* Formation of Silver Nanoparticles and Self-Assembled.pdf. *Langmuir* 17, 1571–1575 (2001).

219. Xu, R. Progress in nanoparticles characterization : Sizing and zeta potential measurement. 6, 112–115 (2008).

220. Fatehah, M. O., Aziz, H. A. & Stoll, S. Stability of ZnO Nanoparticles in Solution. Influence of pH, Dissolution, Aggregation and Disaggregation Effects. *J. Colloid Sci. Biotechnol.* 3, 75–84 (2014).

221. Rashed, M. N. Adsorption Technique for the Removal of Organic Pollutants from Water and Wastewater. in *Organic Pollutants-Monitoring, Risk and Treatment* 167–194 (2013).

222. Chambers, B. A. *et al.* Effects of chloride and ionic strength on physical morphology, dissolution, and bacterial toxicity of silver nanoparticles. *Environ. Sci. Technol.* 48, 761–769 (2014).

223. Tejamaya, M., Römer, I., Merrifield, R. C. & Lead, J. R. Stability of citrate, PVP, and PEG coated silver nanoparticles in ecotoxicology media. *Environ. Sci. Technol.* 46, 7011–7017 (2012).

224. Babu, S., Claville, M. O. & Ghebreyessus, K. Rapid synthesis of highly stable silver nanoparticles and its application for colourimetric sensing of cysteine. *J. Exp. Nanosci.* 10, 1242–1255 (2015).

225. Wagers, K., Chui, T. & Adem, S. Effect of pH on the Stability of Gold Nanoparticles and Their Application for Melamine Detection in Infant Formula. *IOSR J. Appl. Chem.* 7, 15–20 (2014).

226. Xu, Y., Linares, K. A., Meehan, K., Love, B. J. & Love, N. G. pH Dependent Change in the Optical Properties of Surface Modified Gold Nanoparticles Using Bovine Serum Albumin. *NSTINanotech* 1, 15–18 (2004).

227. Kang, P. K. & Shah, D. O. Filtration of Nanoparticles with Dimethyldioctadecylammonium Bromide Treated Microporous Polypropylene Filters. *Langmuir* 13, 1820–1826 (1997).

228. Chattopadhyaya, M. C., Gautam, R. K., Sharma, Y. C., Dubey, S. & Banerjee, S. Adsorption characteristics of alumina nanoparticles for the removal of hazardous dye, Orange G from aqueous solutions. *Arab. J. Chem.* (2017) doi:10.1016/j.arabjc.2016.12.016.

229. Iglesias, M., Anticó, E. & Salvadó, V. The characterisation of silver sorption by chelating resins containing thiol and amine groups. *Solvent Extr. Ion Exch.* 19, 315–327 (2001).

230. Cassol, A. *et al.* Equilibrium measurements for silver(I) complexes with polyamines in dimethyl sulphoxide. *J. Chem. Soc. Dalt. Trans.* (1988) doi:10.1039/DT9880001781.

231. Yuan, C. G. *et al.* One-step fabrication and characterization of a poly(vinyl alcohol)/silver hybrid nanofiber mat by electrospinning for multifunctional applications. *RSC Adv.* 7, 4830–4839 (2017).

232. Momtazan, F. *et al.* Application of copper sulfide nanoparticles loaded activated carbon for simultaneous adsorption of ternary dyes: Response surface methodology. *Korean J. Chem. Eng.* 35, 1108–1118 (2018).

233. Hong-jian, G. A. O. & Xin, J. Effect of Initial Concentration on Adsorption-Desorption Characteristics and Desorption Hysteresis of Hexachlorobenzene in Soils. *Pedosph. An Int. J.* 20, 104–110 (2010).

234. Liu, L. L. *et al.* Incidence and risk factors for the prozone phenomenon in serologic testing for syphilis in a large cohort. *Clin. Infect. Dis.* 59, 384–389 (2014).

235. Gillet, P., Mori, M., Van Esbroeck, M., Van Den Ende, J. & Jacobs, J. Assessment of the prozone effect in malaria rapid diagnostic tests. *Malar. J.* 8, 1–7 (2009).

236. Nassif, N. The impact of air filter pressure drop on the performance of typical air-conditioning systems. *Build. Simul.* 5, 345–350 (2012).

237. Mei, Y., Wang, Z. & Li, X. Improving filtration performance of electrospun nanofiber mats by a bimodal method. *J. Appl. Polym. Sci.* 128, 1089–1094 (2013).

238. Ibupoto, A. S. *et al.* Reusable carbon nanofibers for efficient removal of methylene blue from aqueous solution. *Chem. Eng. Res. Des.* 136, 744–752 (2018).

239. Qureshi, U. A. *et al.* Removal of lead from aqueous solution using polyacrylonitrile/magnetite nanofibers. *Environ. Sci. Pollut. Res.* 25, 3557–3564 (2017).

240. Onur, A., Ng, A., Batchelor, W. & Garnier, G. Multi-Layer filters: adsorption and filtration mechanisms for improved separation. *Front. Chem.* 6, 1–11 (2018).

241. Barr, K. Bio - Modification of Non - Biological Surfaces with Function - Spacer - Lipid Constructs by Methods Including Bioprinting. (2013).

242. Asif, Z. & Chen, Z. Removal of arsenic from drinking water using rice husk. *Appl. Water Sci.* 7, 1449–1458 (2015).

243. Hou, J. *et al.* Transport and long-term release behavior of polymer-coated silver nanoparticles in saturated quartz sand: The impacts of input concentration, grain size and flow rate. *Water Res.* 127, 86–95 (2017).

244. Braun, A., Klumpp, E., Azzam, R. & Neukum, C. Transport and deposition of stabilized engineered silver nanoparticles in water saturated loamy sand and silty loam. *Sci. Total Environ.* 535, 102–112 (2015).

245. Han, R., Zou, W., Li, H., Li, Y. & Shi, J. Copper(II) and lead(II) removal from aqueous solution in fixed-bed columns by manganese oxide coated zeolite. *J. Hazard. Mater.* 137, 934–942 (2006).

246. Shi, Y. *et al.* Nanoscale characterization of PM 2.5 airborne pollutants reveals high adhesiveness and aggregation capability of soot particles. *Sci. Rep.* 5, (2015).

247. Zhang, R. *et al.* Morphology and property investigation of primary particulate matter particles from different sources. *Nano Res.* 1–11 (2017) doi:10.1007/s12274-017-1724-y.

248. Mico, S., Tsaousi, E., Deda, A. & Pomonis, P. Characterization of airborne particles and source identification using SEM/EDS. *Chem. Bull* 4, 224–229 (2015).

249. Chakrabarty, R. K. *et al.* Light scattering and absorption by fractal-like carbonaceous chain aggregates: comparison of theories and experiment. *Appl. Opt.* 46, 6990–7006 (2007).

250. Sundarrajan, S., Tan, K. L., Lim, S. H. & Ramakrishna, S. Electrospun nanofibers for air filtration applications. in *Procedia Engineering* (2014). doi:10.1016/j.proeng.2013.11.034.

251. Kadam, V. V, Wang, L. & Padhye, R. Electrospun nanofibre materials to filter air pollutants – A review. *J. Ind. Text.* 47, 2253–2280 (2018).

252. Gerba, C. P. & Hou, K. Endotoxin removal by charge-modified filters. *Appl. Environ. Microbiol.* 50, 1375–1377 (1985).

253. Ortolano, G., Canonica, F., McAlister, M., Howard, G. & Cervia, J. Bacterial lipopolysaccharide retention by a positively charged filter. *Appl. Environ. Microbiol.* 75, 1219 (2009).

254. Kelly, F. J. & Fussell, J. C. Air pollution and public health: emerging hazards and improved understanding of risk. *Environ. Geochem. Health* 37, 631–649 (2015).

255. Kelishadi, R. Environmental pollution: Health effects and operational implications for pollutants removal. *J. Environ. Public Health* 2012, 2012–2014 (2012).

256. Wang, J., Liu, X. D. & Lu, J. Urban River Pollution Control and Remediation. *Procedia Environ. Sci.* 13, 1856–1862 (2012).

257. Liu, G. *et al.* A review of air filtration technologies for sustainable and healthy building ventilation. *Sustain. Cities Soc.* 32, 375–396 (2017).

258. Yunus, I. S., Harwin, Kurniawan, A., Adityawarman, D. & Indarto, A. Nanotechnologies in water and air pollution treatment. *Environ. Technol. Rev.* 1, 136–148 (2012).

259. Yunus, I. S. *et al.* Nanotechnologies in water and air pollution treatment. *Environ. Technol. Rev.* 2515, (2012).

260. Hayes, T. R. & Hosie, I. C. Turning Nanofibres into Products: Electrospinning from a Manufacturer's Perspective. in *Electrospinning for High Performance Sensors* 305–329 (Springer, Cham, 2015). doi:https://doi.org/10.1007/978-3-319.

261. Qin, X. & Subianto, S. Electrospun nanofibers for filtration applications. *Electrospun Nanofibers* 75, 449–466 (2016).

262. Wang, N., Mao, X., Zhang, S., Yu, J. & Bin Ding. Electrospun Nanofibers for Air Filtration. in *Electrospun Nanofibers for Energy and Environmental Applications* 299–323 (Springer, 2014). doi:10.1007/978-3-642-54160-5 _12.

263. Kang, W. *et al.* Preparation and Properties of sc-PLA/PMMA Transparent Nanofiber Air Filter. *Polymers (Basel).* 10, 996 (2018).

264. Sundarrajan, S., Tan, K. L., Lim, S. H. & Ramakrishna, S. Electrospun Nanofibers for Air Filtration Applications. *Procedia Eng.* 75, 159–163 (2014).

265. Wang, C. Te *et al.* Experimental investigation of the filtration characteristics of charged porous fibers. *Aerosol Air Qual. Res.* 18, 1470–1482 (2018).

266. Speranza, V., Sorrentino, A., De Santis, F. & Pantani, R. Characterization of the Polycaprolactone Melt Crystallization: Complementary Optical Microscopy, DSC, and AFM Studies. *Sci. World J.* 2014, 1–9 (2014).

267. Kumar, N. & Kumar, R. Nanomedicine of gastrointestinal diseases. in *Nanotechnology and nanomaterials in the treatment of life-threatening diseases* 368–372 (Elsevier, 2014).

268. Tang, X. & Yan, X. Dip-coating for fibrous materials: mechanism, methods and applications. *J. Sol-Gel Sci. Technol.* 81, 378–404 (2017).

269. Fotovvati, B., Namdari, N. & Dehghanghadikolaei, A. On Coating Techniques for Surface Protection: A Review. *J. Manuf. Mater. Process.* 3, 28 (2019).

270. Bansal, M., Kumar, D., Chauhan, G. S. & Kaushik, A. Preparation, characterization and trifluralin degradation of laccase-modified cellulose nanofibers. *Mater. Sci. Energy Technol.* 1, 29–37 (2018).

271. Rathnayake, U. A. *et al.* Rice bran nanofiber composites for stabilization of phytase. *Chem. Cent. J.* 12, 1–7 (2018).

272. Ren, J., Tijing, L. D. & Shon, H. K. "Robbing behavior" and re-immobilization of nanoscale zero-valent iron (nZVI) onto electrospun polymeric nanofiber mats for trichloroethylene (TCE) remediation. *Sep. Purif. Technol.* 189, 375–381 (2017).

273. Kurusu, R. S. & Demarquette, N. R. Surface modification to control the water wettability of electrospun mats. *Int. Mater. Rev.* 0, 1–39 (2018).

274. Liu, X. Y. & Dai, G. C. Surface modification and micromechanical properties of jute fiber mat reinforced polypropylene composites. *Express Polym. Lett.* 1, 299–307 (2007).

275. Liu, X. *et al.* In vivo wound healing and antibacterial performances of electrospun nanofibre membranes. *J. Biomed. Mater. Res. - Part A* 94, 499–508 (2010).

276. Médard, N., Aouinti, M., Poncin-Epaillard, F. & Bertrand, P. ToF-SIMS ability to quantify surface chemical groups: Correlation with XPS analysis and spectrochemical titration. *Surf. Interface Anal.* 31, 1042–1047 (2001).

277. Chan, C. M. & Weng, L. T. Surface characterization of polymer blends by XPS and ToF-SIMS. *Materials (Basel).* 9, (2016).

278. Salvioni, L. *et al.* Negatively charged silver nanoparticles with potent antibacterial activity and reduced toxicity for pharmaceutical preparations. *Int. J. Nanomedicine* Volume 12, 2517–2530 (2017).

279. Ahila, N. K. *et al.* Synthesis of stable nanosilver particles (AgNPs) by the proteins of seagrass Syringodium isoetifolium and its biomedicinal properties. *Biomed. Pharmacother.* 84, 60–70 (2016).

280. Muzamil, M., Khalid, N., Aziz, M. D. & Abbas, S. A. Synthesis of silver nanoparticles by silver salt reduction and its characterization. *IOP Conf. Ser. Mater. Sci. Eng.* 60, (2014).

281. Suriati, G., Mariatti, M. & Azizan, A. Synthesis of silver nanoparticles by chemical reduction method: Effect of reducing agent and surfactant concentration. *Int. J. Automot. Mech. Eng.* 10, 1920–1927 (2014).

282. Gakiya-Teruya, M., Palomino-Marcelo, L. & Rodriguez-Reyes, J. Synthesis of Highly Concentrated Suspensions of Silver Nanoparticles by Two Versions of the Chemical Reduction Method. *Methods Protoc.* 2, 3 (2018).

283. Zhang, X. F., Liu, Z. G., Shen, W. & Gurunathan, S. Silver nanoparticles: Synthesis, characterization, properties, applications, and therapeutic approaches. *Int. J. Mol. Sci.* 17, (2016).

284. Behravan, M. *et al.* Facile green synthesis of silver nanoparticles using Berberis vulgaris leaf and root aqueous extract and its antibacterial activity. *Int. J. Biol. Macromol.* 124, 148–154 (2019).

285. Moodley, J. S., Krishna, S. B. N., Pillay, K., Sershen & Govender, P. Green synthesis of silver nanoparticles from Moringa oleifera leaf extracts and its antimicrobial potential. *Adv. Nat. Sci. Nanosci. Nanotechnol.* 9, (2018).

286. Agnihotri, S., Mukherji, S. & Mukherji, S. Size-controlled silver nanoparticles synthesized over the range 5-100 nm using the same protocol and their antibacterial efficacy. *RSC Adv.* 4, 3974–3983 (2014).

287. Lau, C. P., Abdul-Wahab, M. F., Jaafar, J., Chan, G. F. & Rashid, N. A. A. Effect of pH and biological media on polyvinylpyrrolidone-capped silver nanoparticles. in *AIP Conference Proceedings* (2016). doi:10.1063/1.4958781.

288. Chambers, B. A. *et al.* Effects of chloride and ionic strength on physical morphology, dissolution, and bacterial toxicity of silver nanoparticles. *Environ. Sci. Technol.* 48, 761–769 (2013).

289. Zhu, T., Fu, X., Wang, J., Liu, Z. & Mu, T. pH-Dependent Adsorption of Gold Nanoparticles on p -Aminothiophenol-Modified Gold Substrates . *Langmuir* 15, 5197–5199 (2002).

290. Arunkumar, R. *et al.* High-efficiency particulate air filter test stand and aerosol generator for particle loading studies. *Rev. Sci. Instrum.* 78, (2007).

291. Nelson, A. J., Page, M. A., Ginsberg, M. D. & Rood, M. J. Bench-scale aerosol filtration test system and evaluation of an acoustic bioaerosol removal device for indoor air streams. *Aerosol Sci. Technol.* 47, 1285–1292 (2013).

292. Bräuner, E. V. *et al.* Exposure to ultrafine particles from ambient air and oxidative stress-induced DNA damage. *Environ. Health Perspect.* 115, 1177–1182 (2007).

293. Li, J. *et al.* Filtration of fine particles in atmospheric aerosol with electrospinning nanofibers and its size distribution. *Sci. China Technol. Sci.* 57, 239–243 (2014).

294. Hartono, D., Lioe, B., Zhang, Y., Li, B. & Yu, J. Impacts of particulate matter (PM2.5) on the behavior of freshwater snail Parafossarulus striatulus. *Sci. Rep.* 7, 1–8 (2017).

295. WHO. Particulate matter. *Air Qual. Guidel.* 1–40 (2000) doi:10.1016/j.atmosenv.2.

296. Dhandayuthapani, B., Mallampati, R., Sriramulu, D., Dsouza, R. F. & Valiyaveettil, S. PVA/gluten hybrid nanofibers for removal of nanoparticles from water. *ACS Sustain. Chem. Eng.* 2, 1014–1021 (2014).

297. Cronje, L. & Klumperman, B. Modified electrospun polymer nanofibers as affinity membranes: The effect of pre-spinning modification versus post-spinning modification. *Eur. Polym. J.* 49, 3814–3824 (2013).

298. Greiner, A. & Wendorff, J. H. Electrospinning: A fascinating method for the preparation of ultrathin fibers. *Angew. Chemie - Int. Ed.* 46, 5670–5703 (2007).

299. Bi, H. *et al.* The Concentrations and Reduction of Airborne Particulate Matter (PM10, PM2.5, PM1) at Shelterbelt Site in Beijing. *Atmosphere (Basel).* 6, 650–676 (2015).

300. Zhu, M. *et al.* Electrospun Nanofibers Membranes for Effective Air Filtration. *Macromol. Mater. Eng.* 302, 1–36 (2017).

301. Cabral, J. P. S. Water microbiology. Bacterial pathogens and water. *Int. J. Environ. Res. Public Health* 7, 3657–3703 (2010).

302. Pandey, P. K., Kass, P. H., Soupir, M. L., Biswas, S. & Singh, V. P. Contamination of water resources by pathogenic bacteria. *AMB Express* 4, 1–16 (2014).

303. Schleibinger, H., Keller, R. & Rüden, H. Indoor Air Pollution by Microorganisms and Their Metabolites. in *Indoor air pollution* vol. 4F 149–177 (Springer, Berlin, Heidelberg, 2004).

304. Pyankov, O. V., Agranovski, I. E., Huang, R. & Mullins, B. J. Removal of biological aerosols by oil coated filters. *Clean - Soil, Air, Water* 36, 609–614 (2008).

305. Cresci, A., Orpianesi, C., Cecchini, C., Verdenelli, M. C. & Dadea, G. M. Efficacy of antimicrobial filter treatments on microbial colonization of air panel filters. *J. Appl. Microbiol.* 94, 9–15 (2003).

306. Wu, Q.-Y. *et al.* Formation and control of disinfection byproducts and toxicity during reclaimed water chlorination: A review. *J. Environ. Sci.* 58, 51–63 (2017).

307. Yan-jun, Z., Kai-fen, W., Zheng-jun, W., Liang, Z. & Shu-shen, L. Fouling and cleaning of membrane-a literature review. *J. Environ. Sci.* 12, 241–251 (2000).

308. Zielińska, A. Methods for regeneration and storage of ceramic membranes. *Acta Innov.* 72–81 (2018) doi:10.32933/actainnovations.28.7.

309. García-Fayos, B., Arnal, J. M. & Sancho, M. Cleaning of ultrafiltration membranes after the treatment of surface water: Static-dynamic test. *Desalin. Water Treat.* 51, 609–616 (2013).

310. Ethiraj, J. *et al.* Carbon dioxide adsorption in amine-functionalized mixed-ligand metal-organic frameworks of UiO-66 topology. *ChemSusChem* 7, 3382–3388 (2014).

311. Madden, D. G. *et al.* Flue-gas and direct-air capture of CO 2 by porous metal – organic materials Subject Areas : Authors for correspondence : *Philos. Trans. R. Soc. A Math. Phys. Eng. Sci.* 375, (2017).

312. Ge, J. & Choi, N. Fabrication of Functional Polyurethane/Rare Earth Nanocomposite Membranes by Electrospinning and Its VOCs Absorption Capacity from Air. *Nanomaterials* 7, 60 (2017).

313. Vellingiri, K. *et al.* Metal organic frameworks as sorption media for volatile and semi-volatile organic compounds at ambient conditions. *Sci. Rep.* 6, 27813 (2016).

314. Uyar, T. *et al.* Cyclodextrin functionalized poly(methyl methacrylate) (PMMA) electrospun nanofibers for organic vapors waste treatment. *J. Memb. Sci.* (2010) doi:10.1016/j.memsci.2010.09.037.

315. Kayaci, F. & Uyar, T. Encapsulation of vanillin/cyclodextrin inclusion complex in electrospun polyvinyl alcohol (PVA) nanowebs: Prolonged shelf-life and high temperature stability of vanillin. *Food Chem.* 133, 641–649 (2012).

316. Costoya, A., Concheiro, A. & Alvarez-Lorenzo, C. Electrospun fibers of cyclodextrins and poly(cyclodextrins). *Molecules* 22, (2017).

317. Cheirsilp, B. & Rakmai, J. Inclusion complex formation of cyclodextrin with its guest and their applications. *Biol. Eng. Med.* 2, 1–6 (2017).

318. Young, P. A. S., Klem, M. T., Douglas, T. & Young, M. Influence of Electrostatic Interactions on the Surface Adsorption of a Viral Protein Cage. *Langmuir* 21, 8686–8693 (2005).

319. Zerda, K. S., Gerba, C. P., Hou, K. C. & Goyal, S. M. Adsorption of viruses to charge-modified silica. *Appl. Environ. Microbiol.* 49, 91–5 (1985).

320. Michen, B. & Graule, T. Isoelectric points of viruses. *J. Appl. Microbiol.* 109, 388–397 (2010).